Engineering Design and Characterisation of Auxetic Yarns and Woven Fabrics

A thesis submitted to the University of Manchester for the degree of

Doctor of Philosophy

in the Faculty of Science and Engineering

2021

Yajie Gao

School of Natural Sciences

List of Contents

Word count: 51821

List of Figures

List of Tables

Abstract

Auxetic materials, including textiles, exhibit a negative Poisson's ratio (NPR), which is of interest for many applications. They expand laterally when stretched or shrink when compressed in contrast to conventional materials. In recent years, auxetic woven fabrics have gained much attention from researchers due to their special features, such as pore opening behaviour, impact resistance, energy absorption and clothing fit-ability. However, the development of woven fabrics made of auxetic yarns is still limited compared to other auxetic textiles because the auxeticity of the yarns cannot be fully transferred to the fabric due to the interlacement of the woven pattern. Therefore, this research aims to optimise the auxetic yarn and woven fabric manufacturing processes, establish the understanding of design principles and try to reduce the loss of auxeticity of the fabric inherited from the yarns.

A series of parametric study was carried out based on the experimental and numerical methods. The research reports on the improvement of helical auxetic yarn (HAY) quality and the yarn auxeticity through studying the factors of helical angles, yarn thickness and tensile moduli, as well as the binder feeding. The maximum negative Poisson's ratio of the optimised yarn was experimentally achieved as low as -9.6 and such optimised procedures enabled the making of high-quality auxetic yarns with a wider range of machine settings than before. The results showed lower initial helical angle, higher modulus ratio of the wrap ply to the core ply led to a higher auxetic behaviour of the yarn. A concave relationship between the yarn thickness and Poisson's ratio was revealed. In parallel, woven fabrics were produced with the selected HAYs in the weft direction and in both warp and weft directions. Tensile property, porosity and impact property were evaluated and the results indicated that the auxetic fabric displayed notable geometric changes compared to the non-auxetic fabric with the same structural parameters. The auxeticity of the fabric was measured in terms of fabric thickness and fabric dimension. Seven influential factors on Poisson's ratio were analysed and the results showed that the maximum NPR can be achieved as -3.57 in thickness direction and -1.17 in warp direction.

Declaration

No portion of the work referred to in the thesis has been submitted in support of an application for another degree or qualification of this or any other university or other institutes of learning.

Copyright Statement

i. The author of this thesis (including any appendices and/or schedules to this thesis) owns certain copyright or related rights in it (the "Copyright") and s/he has given The University of Manchester certain rights to use such Copyright, including for administrative purposes.

ii. Copies of this thesis, either in full or in extracts and whether in hard or electronic copy, may be made only in accordance with the Copyright, Designs and Patents Act 1988 (as amended) and regulations issued under it or, where appropriate, in accordance with licensing agreements which the University has from time to time. This page must form part of any such copies made.

iii. The ownership of certain Copyright, patents, designs, trademarks and other intellectual property (the "Intellectual Property") and any reproductions of copyright works in the thesis, for example graphs and tables ("Reproductions"), which may be described in this thesis, may not be owned by the author and may be owned by third parties. Such Intellectual Property and Reproductions cannot and must not be made available for use without the prior written permission of the owner(s) of the relevant Intellectual Property and/or Reproductions.

iv. Further information on the conditions under which disclosure, publication and commercialisation of this thesis, the Copyright and any Intellectual Property and/or Reproductions described in it may take place is available in the University IP Policy

(see http://documents.manchester.ac.uk/DocuInfo.aspx?DocID=24420), in any relevant Thesis restriction declarations deposited in the University Library, The University Library's regulations

(see http://www.library.manchester.ac.uk/about/regulations/) and in The University's policy on Presentation of Theses.

Acknowledgements

Foremost, I would like to express my deep gratitude to my supervisor, Dr Xiaogang Chen, for accepting me as one of his PhD students; for giving me support and professional guidance; for encouraging me to tackle problems in research. I would like to thank him for bringing me to the fascinating auxetic field and letting me know artist can be a scientist. Without him, I would not have had such academic achievements during my research period. I would like to thank my co-supervisor, Ms Rachel Studd, my internal and external examiners, Dr Anura Fernando and Professor Andrew Alderson, for providing valuable suggestions to my research.

I would like to acknowledge the support of staff at University of Manchester, Mr Peter Moroz, Mr Stephen Gillespie, Ms Elizabeth Carlton, Mr Stephen Cowling and Mr Adrian Handley for their kind help during this research. I wish to express my appreciation to my friends and colleagues in 'A27 family': Dr Zishun Yuan, Dr Haoxian Zeng, Dr Hang Zhou, Dr Jiawen Qiu, Dr Lei Zeng, Ms Ji Li, Ms Yazhen Liang, Mr Shihao Song, Ms Mengqi Yang, Dr Mengyu Lin, Mr Yinan Li and countless others. Particularly, I would like to express my thanks to Ms Ruihan Wang and Ms Ziyue Wei for their help and encourage during my time in Manchester. Many thanks to Ms Longxin Gu, Ms Miaobing Wu and Dr Sai Liu for kind help and discussion on auxetics. Thank you all for letting me experience an unforgettable life in the UK.

Last but not least, I would like to express my sincerest gratitude to my family, my dear parents, Mr He Gao and Ms Meijuan Shao, my grandparents, Ms Jueqing Liang, Mr Jinhan Gao and Ms Ayu Wang, for giving me endless love and unconditional support to pursue my dreams. Then, my special thanks go to my partner, Dr Jianlin Luan, for discussing technical issues and statistical methods to make the research more efficient. Lastly, thanks to my cat, Bangbang, for his company during the Covid-19 pandemic.

Publications

Parts of the thesis have been presented in the following publications.

Journal papers

1. **Gao Y** and Chen X (2021), 'A Study of Woven Fabrics Made of Helical Auxetic Yarns', *Applied Composite Materials*, 10.1007/s10443-021-09952-5.
2. **Gao Y**, Liu S, Wu M, Chen X and Studd R (2020), 'Manufacture and Evaluation of Auxetic Yarns and Woven Fabrics', *Physica Status Solidi (b)*, 257, 1900112.
3. **Gao Y**, Chen X and Studd R (2020), 'Experimental and Numerical Study of Helical Auxetic Yarns', *Textile Research Journal*, 91, 0040517520977194.
4. Liu S, **Gao Y**, Chen X and Du Z (2019), 'A Theoretical Study on the Effect of Structural Parameter on Tensile Properties of Helical Auxetic Yarns', *Fibers and Polymers*, 20, 1742-1748.

Conferences

5. **Gao Y** and Chen X, 'A Study of Microbiological Patterns Applied in Traditional Wall-hanging Designs', *The 91st Textile Institute World Conference*, 23rd-26th July, 2018, Leeds, United Kingdom.
6. **Gao Y**, Liu S, Wu M and Chen X, 'A Study of Manufacture and Characterisation of Auxetic Yarns and Fabrics', *Proceeding of 9th International Conference and 14th International Workshop- Auxetics and Related Systems with Negative Characteristics*, 10th-13th September, 2018, Sheffield, United Kingdom.
7. **Gao Y**, Chen X and Studd R, 'Auxetic Textile Materials and Structures for Technical Applications', *The Department of Materials PGR Conference*, 9th-10th May, 2019, Manchester, United Kingdom. (**Third Prize of Poster Competition**)
8. **Gao Y**, Chen X and Studd R, 'Engineering Design and Characterisation of Auxetic Yarns and Fabrics', *Proceeding of 10th International Conference and 15th International Workshop- Auxetics and Other Materials and Models with Negative Characteristics*, 2nd-6th September, 2019, Bedlewo near Poznan, Poland.
9. **Gao Y**, Chen X and Studd R, 'Manufacture and Evaluation of Auxetic Yarns and Woven Fabrics', *The Third International Forum on Textiles for Graduate Students (IFTGS)*, 28th-30th November, 2020, Tianjin, China. (**Third Prize Winner**)
10. **Gao Y** and Chen X, 'Development of Woven Fabrics Made of Helical Auxetic Yarns', *Proceeding to the 9th World Conference on 3D Fabrics and Their Applications*, 8th-9th April, 2021, Zhengzhou, China. (Online)

The Author

Yajie Gao is a PhD researcher of the Department of Materials, School of Natural Science in the University of Manchester. She was awarded her BA and MA degrees in textile design at Tsinghua University, Beijing, China in 2014 and 2017 respectively. After that, she decided to embark on her PhD study in the field of textile science and engineering at the University of Manchester, focusing on a study of auxetic textiles and applications. She has been a graduate teaching assistant in the Department of Materials from 2018 to 2021.

Chapter 1 Introduction

1.1 Background

In materials science, Poisson's ratio is used to describe the deformation of a material in a direction perpendicular to the direction of tensile loading, and it is defined as a ratio of the transverse strain to the axial strain of the material [1]. Based on the theory of elasticity, most of isotropic materials have Poisson's ratios ranging between 0 to 0.5. The Poisson's ratio of cork, for example, is close to 0, demonstrating little expansion when compressed. Glass, on the other hand, has the Poisson's ratio between 0.18 and 0.3 because it is less compressible. For most solid materials such as cast iron, steel, magnesium and aluminium-alloy, the Poisson's ratio is in the range of 0.2 to 0.35. For soft materials like rubber, the bulk modulus is much larger than the shear modulus and the Poisson's ratio is close to 0.5 [2]. In early 1848, the Poisson's ratio was first suggested to be negative and it may be larger than 0.5 for anisotropic materials [3]. Materials that can achieve a negative Poisson's ratio such as foams, polymers and fibres are referred to as auxetic materials [4].

Auxetic materials are a type of novel materials. They expand in the transverse direction under the longitudinal tensile loading, or contract when compressed, in contrast to the non-auxetic materials, as shown in Figure 1-1. In the late 19^{th} century, negative Poisson's ratio was reported in natural materials by Voigt [5]. Then, one of the first synthetically auxetic materials with diamond-fold structure was investigated by Pietsch in 1978 [6]. Although the term auxetics was not used in his work, he is considered as the inventor of the auxetic net because he reports the underlying lever mechanism and lateral expansion for the first time. In 1987, the first foam structure showing negative Poisson's ratio was produced successfully by Lakes [7]. Lakes' work has developed a new stage for artificial materials with negative Poisson's ratio. Later on, to avoid the cumbersome words, Evans et al. [4] suggested materials with negative Poisson's ratio be described by the term 'auxetic' which from the Greek word 'auxetos' meaning 'that may be increased'. Therefore, the term 'auxetic' has become an internationally accepted terminology and it is used by many researchers till now.

Auxetic materials are composed of two parts: natural auxetic materials and synthetic auxetic materials. Although the natural auxetic materials have been discovered for a

long time, the synthetic auxetic materials from nanoscale to macroscale are mainly used and developed in various applications. Auxetic textiles as one of the synthetic auxetic materials attracted many researchers in recent years due to their material adaptability and structural variability. An increasing number of researchers carried out the work of auxetic textiles, including auxetic polymers, auxetic fibres, auxetic yarns, auxetic fabrics and textile-reinforced composites. The unusual properties of auxetic textiles provide advantages for numerous potential applications including but not limited to medical textiles, military equipment, protective clothing, aerospace, automotive and filtration.

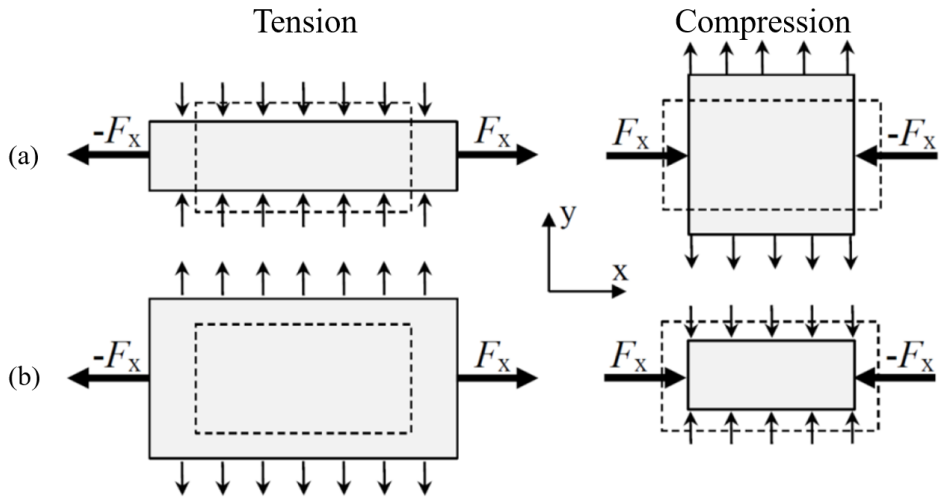

Figure 1-1 Materials under tensile loading: (a) non-auxetic material; (b) auxetic material [8]

1.2 Problems

In recent decades, auxetic textiles, as one category of auxetic materials and structures, have attracted much attention from researchers due to their special properties. The investigations of auxetic textile materials have been reported from polymers [9, 10], fibres [11-13], yarns [14, 15] to two-dimensional fabrics [16, 17] and three-dimensional fabrics [18, 19]. Compared to normal textile materials, the unusual properties of auxetic textile materials show advantages in various applications. One of the promising properties is the energy absorption property which can enhance the mechanical behaviour for the intended technical applications such as protective clothing, blast curtain, helmet and automotive equipment. Bending behaviour showing synclastic curvature is another property which can provide a better shape fitting of the garments, especially suitable for protective and flexible requirements of the fabric [20].

Additionally, adjustable porosity is an unique phenomenon of auxetic fabrics, which can release and block the liquid for medical textiles [21]. Thus, it is necessary to investigate the mechanical properties of auxetic fabrics and to analyse how they behave superior to non-auxetic fabrics.

Generally, auxetic fabrics can be made by two approaches. The first approach is to use conventional fibres or yarns, forming auxetic geometric structures of the fabrics. Another approach is to use auxetic fibres and yarns directly, so that auxetic behaviour of the fabrics can be inherited from the fibres and yarns. Although the auxetic fibres have been made, the majority of the fabrics are produced from the yarn level due to the easier production and lower cost of the auxetic yarns [3]. In the aspect of auxetic yarn production, structural stability, as one of the most important manufacturing factors, has been identified by researchers in recent years [22-24]. Even though some efforts have been done, the structural problem of the yarn still exists and this should be solved without adding a third material. By solving the structural problem of the yarn, it could highly enhance the auxetic property of the fabric [24, 25]. In order to use the auxetic yarns as the basic material for textile products, design principles for producing the yarns and fabrics should be drawn, so the manufacturer can select the proper parameters of the materials and suitable technology during the production. Based on the second approach of the fabric above, another problem is found that the auxetic behaviour of the auxetic yarns cannot be fully transferred to the woven fabric because the yarns are easily deformed during the weaving and the auxeticity is restricted by the interlacement of the woven pattern. Therefore, the auxetic yarns and woven fabrics should be designed detailly to reduce the loss of the auxeticity.

1.3 Aim and objectives

The aim of this research is to establish understanding of the design principles and behaviour of auxetic yarns and fabrics through investigating systematically the helical auxetic yarns and auxetic woven fabrics. The primary objectives are set as follows:

i. To manufacture helical auxetic yarns with better structural stability. To produce helical auxetic yarns with different machine settings and yarn parameters including cross-sectional shape, initial wrapping angles, yarn thickness and tensile moduli of the two plies;

ii. To establish and validate finite element models for auxetic yarns and fabrics to carry out numerical analysis of auxetic yarns and fabrics in parallel to the experimental investigation;
iii. To carry out the practical tensile test and simulation of the helical auxetic yarns to reveal the relationship between structural parameters of the yarns and their auxeticity;
iv. To design and produce woven fabrics from helical auxetic yarns with various fabric configurations;
v. To explore, experimentally and numerically, the effect of the key fabric factors on Poisson's ratio, such as yarn arrangement in the fabric, fabric density, helical angle of the auxetic yarn, thickness of the auxetic yarn, weave structures, warp yarn type, loading directions and the inter-yarn friction;
vi. To carry out a series of mechanical and physical tests for auxetic woven fabrics including tensile property test, porosity test and impact test. To measure the Poisson's ratios in fabric plane direction and fabric thickness direction.

1.4 Thesis layout

Followed by the introduction, the literature review in Chapter 2 is concentrated on the four aspects, which include applications of auxetic materials, nature of auxeticity, auxetic textiles and research areas for textiles. The most significant work is also discussed and the research gap is addressed afterwards.

In Chapter 3, the methodology of the research is proposed. Starting from the research strategy, it contains the idea and plan of the work. Secondly, two types of materials are selected in Section 3.2 for making auxetic yarns and fabrics. Then, the manufacturing approaches are presented in Section 3.3, followed by the characterisation methods of experiments in Section 3.4. After that, a parametric study is addressed by numerical simulations in Section 3.5. Finally, the results of auxeticity are given in Section 3.6.

In Chapter 4, the factorial analysis on Poisson's ratio of auxetic yarns is discussed, including the influencing factors of cross-sectional shape, initial helical angles, thickness of the yarn and tensile moduli of the two plies.

After achieving better understanding of auxetic yarns, the mechanical properties of auxetic woven fabrics are shown in Chapter 5. Tensile property, porosity and impact

property are specifically discussed in Section 5.1, 5.2 and 5.3, respectively, and the phenomenon of the auxetic woven fabric is summarised in Section 5.4.

In Chapter 6, factors that have influence on Poisson's ratio of auxetic woven fabrics are investigated, including auxetic yarn arrangements, fabric density, helical angle of the HAY, thickness of the HAY, weave structures, warp yarn types and loading directions. Then, a principle of how to increase the auxeticity of the woven fabric is provided in summary.

In Chapter 7, discussion and conclusions are made from all the work introduced in the research. Also, the limitations and future work are presented at the end.

Chapter 2 Literature Review

2.1 Introduction

Based on the nature of the work, the literature review is covered by four areas. The applications of auxetic materials are reviewed first because any development of auxetic materials and structures will be intended to be used in our daily life. Then, the nature of auxeticity is summarised including geometric structures, properties of auxetics and types of auxetic materials, which can provide a general understanding in the auxetic field. Following the nature of auxeticity, auxetic textiles are specifically reviewed from polymers, fibres and yarns to fabrics. After that, the research areas for auxetic textiles are presented, involving the manufacturing techniques, characterisation methods and mathematical modelling. These will highlight the motivation and gaps of the research.

2.2 Applications of auxetic materials

Auxetic materials and structures offer a great potential for many functional applications due to their special properties including negative Poisson's ratio, shear resistance, fracture resistance, hardness improvement, shape fitting and energy absorption. Prawoto [26] summarised various applications in different fields, such as aerospace, automotive, biomedical, composite, sensors and textiles [21, 27-32], as shown in Table 2-1. It is noted that the majority of them are classified as promising potential applications.

Table 2-1 Summary of the applications of the auxetic materials (in alphabetical order) [26]

Field	Application and rationale	
	Existing	Potential
Aerospace	n/a	Vanes for engine, thermal protection, aircraft nose-cones, wing panel, vibration absorber, rivet [29, 32]
Automotive	Tire [33]	Bumper, cushion, thermal protection, sounds and vibration absorber parts, fastener
Biomedical	Composites for medical ultrasound [34]	Bandage, wound pressure pad, dental floss, artificial blood vessel [35]
Composite	n/a	Fibre reinforcement (because it reduces the cracking between fibre and matrix)
Military (defence)	Helmet containing auxetic foam [36]	Helmet, bullet proof vest, knee pad, glove, protective gear (better impact property)
Sensors/actuators	piezoelectric sensor [30]	Hydrophone, various sensors (the low bulk modulus makes them more sensitive to hydrostatic pressure)
Textile Industry	Children's wear [37], maternity dress [38], smart bandage [39], garments [40], running shoes [41, 42]	Functional fabric, colour-change straps or fabrics, fibres, anti-inflammatory and anti-odour fabric [21]

In the aspect of textile applications, auxetic textiles become increasingly popular design ideas due to their fitting and protective performance. The auxetic fabrics can be used for children's wear, as shown in Figure 2-1 (a). Smithers [37] reported the creation of origami-inspired clothing designed by Yasin, which can grow with the children. The clothing can fit the same child from four months up to three years old, so their parents do not need to consider the size of the clothes. By using the auxetic feature for better fitting, it is also very useful for making maternity dress for pregnant women, as illustrated in Figure 2-1 (b). The auxetic clothing provides an enhanced fitting and comfort without adding too much pressure when stretched.

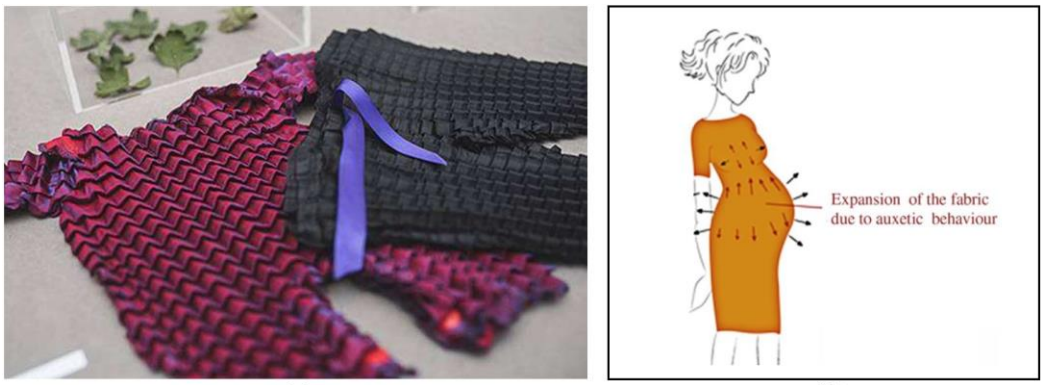

(a) (b)

Figure 2-1 Auxetic textiles for better fitting: (a) children's wear [37]; (b) maternity dress [38]

Auxetic textiles have been explored for developing applications for impact damping as the textiles offer auxeticity and comfort, making thinner or lighter components for energy absorption, such as protective helmet and clothes [36, 39]. Besides, auxetic textiles have been proposed for producing smart bandages [43], as shown in Figure 2-2. The auxetic filaments within the bandage can be utilised to carry medicine. When the wound swells, the pore area of the filaments will increase and release the drug. When the wound heals, the opening will decrease and the drug will stop migrating to the wound from the bandage [21, 43, 44].

Figure 2-2 The smart bandage [43]

Moreover, auxetic materials and structures could create new aesthetic and functional capabilities in many design fields, such as fashion design, product design and architecture [45]. When the auxetic structure is imposed on an inextensible leather fabric, the fabric can adapt to better shape fitting of the user's body [40], as shown in Figure 2-3 (a). This adaptability benefit for one-size-fit garments from the manufacturer provides a more comfortable fit for most customers. Auxetic materials are used for active clothing as well. For example, the temperature-active clothing is produced using composites of bilayer polymers, which allows for thermal mobility and controllable breathability, as shown in Figure 2-3 (b). The bilayer polymers

contain two differential thermal expansion, forcing the polymer from flat shape to curved shape. Therefore, the cellular structure of the clothing can expand at 40˚C and compress at 0˚C along one axis rather than two axis of other auxetic materials [41]. Sports company Nike produces running shoes with soles having auxetic behaviour [42] and Under Armour manufactures the auxetic layer for the upper part of the trainer [46] because the auxetic materials offer a good breathability and curvature control on footwear, as shown in Figure 2-3 (c) and (d), respectively. In the case of an auxetic sole of a shoe, the sole is expanded and compressed when it hits the ground due to the rotation of the triangular structure. In the case of an auxetic upper part of a shoe, the arrowhead structure responds to the movement of the foot and follows the deformation of the curvature. When a tension is applies by foot, the inward ribs of the fabric are pushed out leading to the expansion of the arrowhead structure.

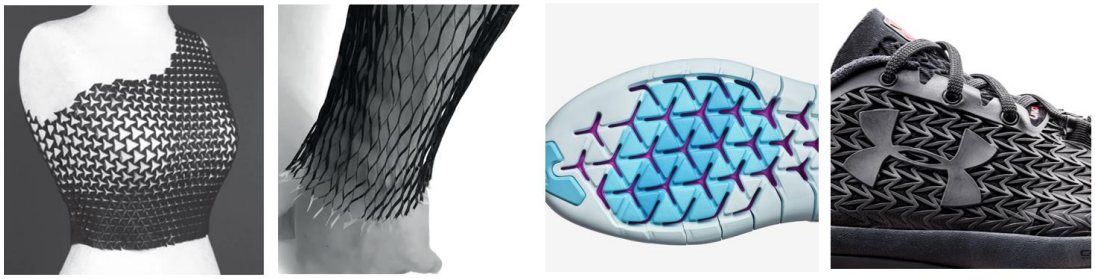

Figure 2-3 Auxetic materials and structures for garments and shoes: (a) fashion top with auxetic cuts [40]; (b) temperature-active clothing made of bilayer polymers [41]; (c) Nike shoes with auxetic soles; (d) Under Armour shoes with auxetic layer

In the field of product design, the chair is one of the most promising products using auxetic materials with chiral structure shown in Figure 2-4. It adapts to the user's weight and body shape under local expansion due to the rotation of rigid rods of the chiral units. When the user sits on the chair, the structure allows the seat to be swelled after the weight pressure and provides a better comfortability [47]. Another convenience for product design is the deployability of auxetic materials. For example, the furniture containing auxetic structures can be made in a compressed state and released to its full size later when delivered [45].

Figure 2-4 Chiral chair with auxetic behaviour [47]

As a type of material and structure, the auxetic behaviour could benefit applications in many areas. At this stage, it is vitally important to discover various ways the auxetic materials are engineered and manufactured, together with the understanding of the auxetic performance and applications. This research concentrates on the engineering design, manufacture and property assessment of textile based auxetic materials and structures, in view of different potential applications. As such, a systematic approach of understanding the structure and property relations need to be established based on a literature study.

2.3 Nature of auxeticity

2.3.1 Geometric structures for achieving auxetic behaviour

In order to achieve auxetic behaviour, different geometric structures have been engineered and studied including re-entrant structures [28], rotating polygons [48], sheets structures [49], chiral structures [50] and other structures [51-53]. Considering the geometrical features, these auxetic structures can be classified according to their spatial dimensions. It is important that the negative Poisson's ratio response relies on the deformation mechanism in combination with structural geometries.

2.3.1.1 2D-to-2D auxetic structures

If the original structure is two dimensional (2D) configuration, the auxeticity will be illustrated in the same 2D plane, which is termed 2D-to-2D auxeticity in this context.

Re-entrant structure is one of the auxetic structures. In 1982, Gibson et al. [54] reported the first example of the auxetic re-entrant structure derived from the conventional cellular material in the form of hexagonal honeycombs. The 2D re-entrant honeycomb deforming by hinging of the diagonal ribs under tensile loading is illustrated in Figure 2-5. The diagonal ribs will be pushed out when a tensile loading is applied along the horizontal direction of the re-entrant honeycomb network,

resulting in the auxetic behaviour. Flexure of the ribs also appears and also results in the auxeticity of the re-entrant honeycomb system [28, 35]. Based on the flexure, stretching and hinging of the ribs of the re-entrant honeycomb, a theoretical model was developed by Masters and Evans [55] for predicting the elastic constants of the structures, such as tensile moduli, shear moduli and Poisson's ratios.

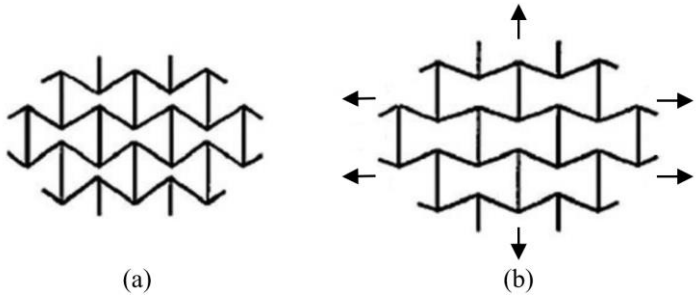

Figure 2-5 Illustration of 2D re-entrant honeycomb: (a) initial state; (b) under tensile loading [56]

Re-entrant cells take different forms which generate auxeticity. Larsen et al. [57] described a numerical topology optimisation method for compliant micro-mechanisms and structures with auxetic behaviour. A typical model is the 2D re-entrant triangular model or double-arrowhead model, as illustrated in Figure 2-6 (a). The auxeticity of the model can be adjusted by the angle between the ribs and the length of the ribs. Another notable work was reported by Grima et al. [58], where the star-shaped structures having the rational symmetry of order 3, 4 and 6, as shown in Figure 2-6 (b) to (d) respectively, would demonstrate auxeticity. The work is significant in two senses. The first is that the star-shape structures have a potential for auxetic effect and the stars with the rotational symmetry of order 4 and 6 exhibit lower Poisson's ratio values compared to those with the order of 3, where the magnitudes of the Poisson's ratio depend on the stiffness of the hinges and the adjacent ribs of the structure. The second is that the performance of periodic structures can be easily examined by using the force-field based methods, and to identify the systems between auxetic and non-auxetic. Lakes [50] conducted a hexagonal re-entrant honeycomb with structural symmetry shown in Figure 2-6 (e) and this structure could gain better planar isotropic property compared to the one in Figure 2-5. Figure 2-6 (f) and (g) illustrate another re-entrant structures based on lozenge and square grids, respectively. The structure shown in Figure 2-6 (g) demonstrates better auxetic behaviour than that of the structure shown in Figure 2-6 (f) due to the rotation of the unit cells in the initial state [59, 60].

Furthermore, Dolla et al. [61] developed a unique stent structure with sinusoidal ligaments, as illustrated in Figure 2-6 (h), claiming great circumferential strength under expansion and low flexural rigidity under the crimp. Compared to the conventional stent, Dolla's stent offers properties that are beneficial for drug diffusion and structural stiffness due to the auxetic response.

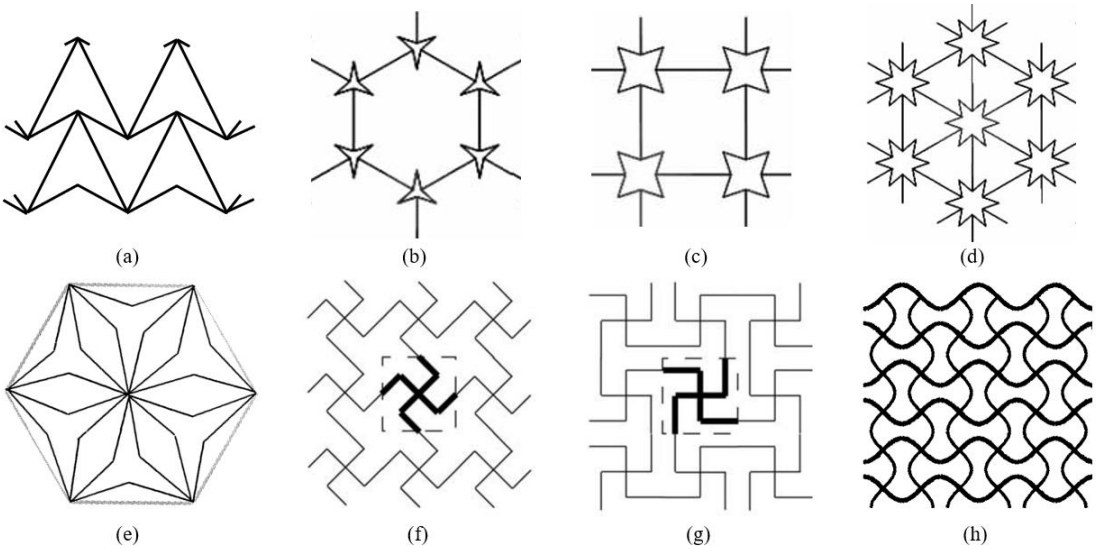

Figure 2-6 2D re-entrant triangular and star structures: (a) double arrowhead structure [62]; (b) re-entrant stars with rotational symmetry of order 3; (c) re-entrant stars with rotational symmetry of order 4; (d) re-entrant stars with rotational symmetry of order 6 [58]; (e) structurally hexagonal re-entrant honeycomb [50]; (f) structure based on lozenge grids [59]; (g) structure based on square grids [60]; (h) a sinusoidal ligament structure [61]

Rotating polygons are reported as one of the fundamental auxetic structures. Grima and Evans [48] demonstrated a new mechanism to achieve auxetic behaviour by involving the arrangement of rigid squares as shown in Figure 2-7. The squares are connected with each other at their vertices by hinges and this could be viewed as a projection of a specific plane of a 3D structure, such as inorganic crystalline materials. Also, they noted that auxetic behaviour can be achieved by more general cases including rotating parallelograms and rotating various sized squares, as illustrated in Figure 2-8 (a) and (b), respectively. The rotating squares are constrained not to shear and the isotropic in-plane Poisson's ratio value is close to -1.

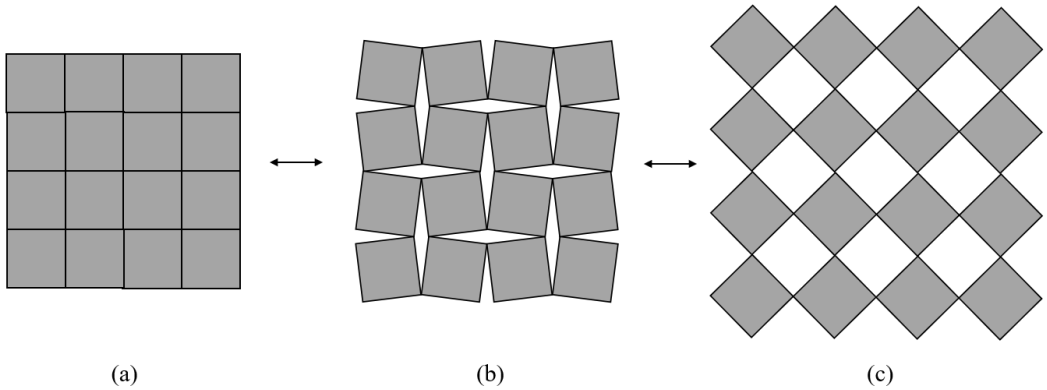

Figure 2-7 Rotating squares structure: (a) initial state; (b) under loaded; (c) fully loaded [48]

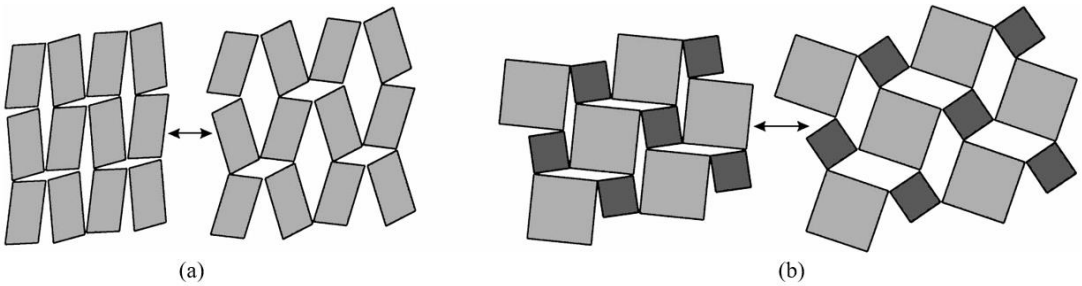

Figure 2-8 Variations of rotating geometry: (a) rotating parallelograms; (b) rotating different sized squares [48]

Later on, different types of rotating polygons are developed including rectangles, rhombi, triangles as well as tetrahedra, as shown in Figure 2-9. Grima et al. [63] proposed a new model exhibiting negative Poisson's ratio from rigid rotating rectangles shown in Figure 2-9 (a). This model offers advantages over the rotating squares because the rotating squares could only present negative Poisson's ratio, whereas the rotating rectangles can achieve both negative and positive Poisson's ratios. Therefore, by using the rectangles, it could be applied to a wider range of applications. As an extension to their work, Grima and his co-workers reported other rotating units which can be composed with either connected rhombi or parallelograms, as shown in Figure 2-9 (b). In Type α rhombi, the adjacent rhombi are connected between the small angle and the big angle attaining a space filling structure, whereas in Type β rhombi, they are connected with the same angle attaining a non-space filling structure. The magnitude of the auxetic behaviour depends on the shape of the rhombi and the loading direction [64]. Grima and Evans [65] conducted a theoretical investigation on rotating triangles, as shown in Figure 2-9 (c), and such mechanism illustrates a highly effective method for introducing negative Poisson's ratio in real materials.

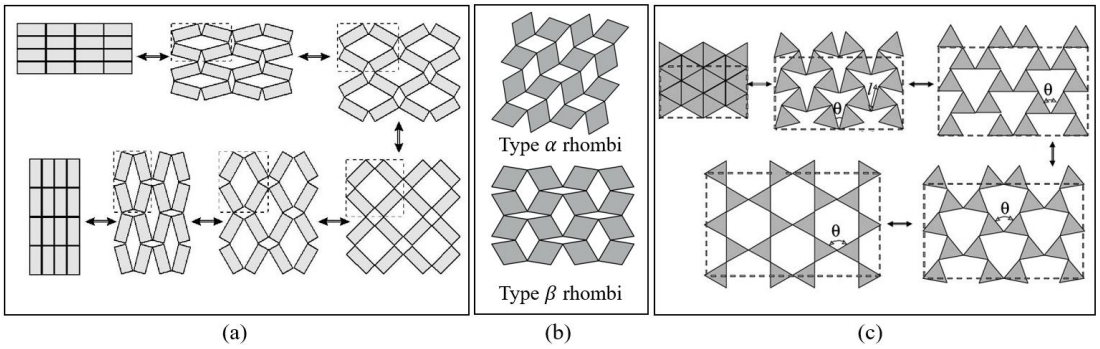

Figure 2-9 Different types of rotating polygons: (a) rotating rectangles [63]; (b) rotating rhombi [64]; (c) rotating triangles [65]

Sheets structure is a novel type of auxetic structure and it can be regarded as two forms, perforated sheets structure and crumpled sheets structure. Grima and Gatt [49] first proposed perforated sheets made from conventional materials involving diamond and star shapes which could exhibit auxetic behaviour in both extension and compression, as shown in Figure 2-10. These structures can be explained by the concept of rotating squares, rotating rectangles as well as rotating triangles. Meanwhile, they also investigated the perforated sheets containing star shapes through finite element models and it is noted one may control the magnitude and sign of the auxetic behaviour through the shape and density of the perforations [66].

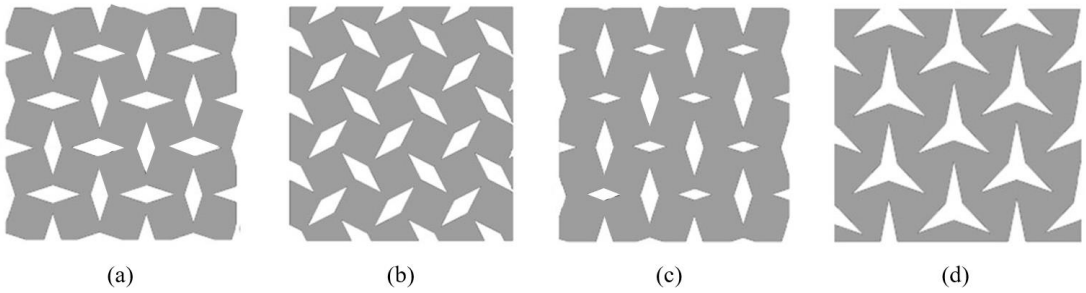

Figure 2-10 Perforated sheets structures: (a) diamond-shaped inclusions; (b) diamond-shaped inclusions having different orientation; (c) diamond-shaped inclusions with two different sizes; (d) star-shaped inclusions [49]

For the crumpled sheets structure, Grima et al. [67] presented their work on tailoring graphene sheet with vacancy defects. The sheet demonstrates in-plane auxetic behaviour through dewrinkling mechanism which is analogous to a crumpled sheet of paper, as shown in Figure 2-11.

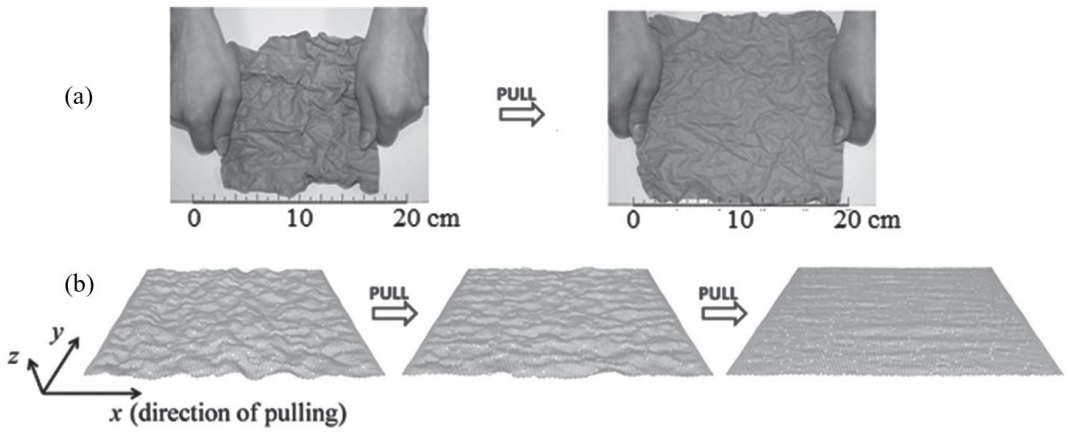

Figure 2-11 Typical images of crumpled sheets: (a) a crumpled sheet of paper at different levels of applied strain; (b) a graphene sheet containing 3% defects at different levels of applied strain [67]

Chiral structure is one of the most widely investigated structures in auxetic materials. Lakes [50] first reported a chiral hexagonal microstructure exhibiting negative Poisson's ratio. The structure lacks a centre of symmetry and it is formed by connecting straight ligaments (ribs) to the central nodes, as shown in Figure 2-12 (a). The auxetic behaviour can be achieved by the rotation of the nodes, leading to wrapping and unwrapping of the ribs under tensile loading. Based on the theoretical and experimental investigation, Prall and Lakes [68] conducted a study of a 2D chiral honeycomb which shows an in-plane Poisson's ratio of -1. This type of structure can offer a high negative Poisson's ratio value over a significant range of strains. Grima et al. [69] presented a novel class of structure coded as 'meta-chiral' which exhibits negative Poisson's ratio. Different chiral structures can be formed by connecting either symmetric units or chiral building blocks, as illustrated in Figure 2-12 (b). For chiral structures, the rigidity of the ligaments or rods is important. If soft materials are used for this type of structure, the ligaments are not rigid enough to push the structure out.

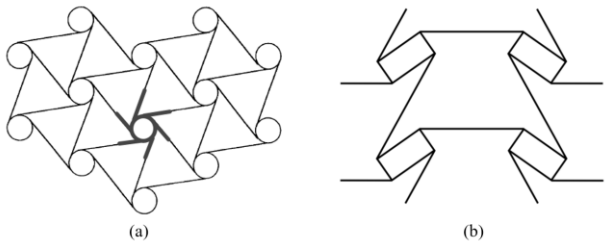

Figure 2-12 Chiral structures: (a) formed by chiral building blocks with highlighted unit in bold [68]; (b) formed by symmetric units [69]

Other structures can also achieve the auxetic behaviour based on 2D configuration. Alderson and Evans [51] developed a nodule-fibril model which effectively explain the deformation of auxetic microporous polytetrafluoroethylene (PTFE) and ultra-high molecular weight polyethylene (UHMWPE). The deformation depends on the fibril hinging, as shown in Figure 2-13.

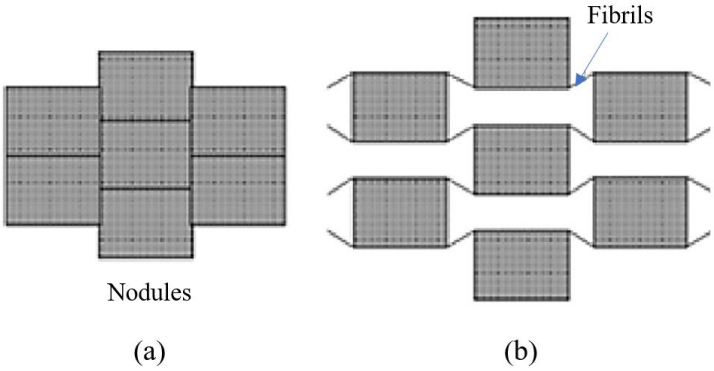

Figure 2-13 A nodule-fibril model showing auxetic microporous polymer: (a) without loading; (b) under tensile loading [35, 70]

Another 2D configuration is the molecular chain of liquid crystalline polymer [71], as illustrated in Figure 2-14. Because of the nematic field, the attached rods are parallel to the main chain. When a tensile stress is applied to the polymer chain axis, the chain is fully stretched, forcing the rods perpendicular to each other. Hence, the auxetic behaviour is shown due to the expansion normal to the main chain axis. It is noted that the rods should be long enough to increase the length between the chains and exhibit auxetic behaviour.

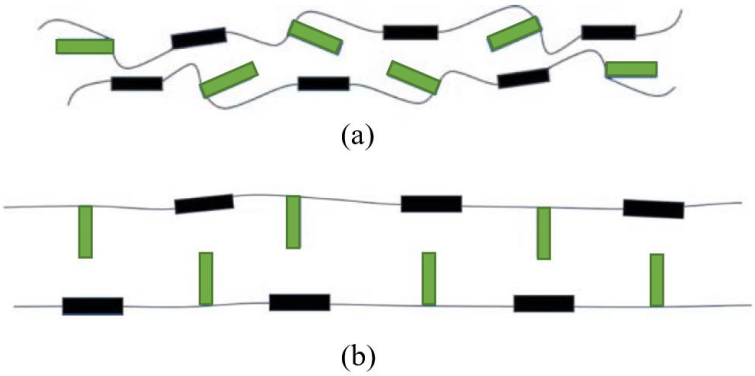

Figure 2-14 Liquid crystalline polymer chain: (a) initial; (b) full extended [71]

2.3.1.2 3D-to-3D auxetic structures

Compared to the 2D-to-2D auxetic structures, 3D-to-3D structures are featured by the three dimensional (3D) configuration and the auxetic behaviour will be generated in the same 3D space.

Based on the concept of 2D auxetic structures, 3D structures are patterned for achieving auxetic behaviour as well, including re-entrant structures, rotating polygons, chiral structures and sheets structures. By adopting the re-entrant structures, the earliest 3D auxetic structure was reported by Evans et al. [72] to verify the deformation of open-celled foams. The 3D re-entrant foam structure can be transformed by the conventional structure, as shown in Figure 2-15. Due to the inwardly protruded ribs in Figure 2-15 (b), it is easy to understand that the ribs tend to move out in the horizontal direction when the vertical tensile loading is applied. In contrast, the ribs tend to move further inward under the compression, leading to the contraction of the structure [73]. Another way to form the 3D re-entrant structure is using two 2D re-entrant structures with the rotating of 90˚ in X axis or Y axis, as illustrated in Figure 2-16 (a) and (b) respectively, and such made 3D structure can be presented by adopting direct laser writing [74, 75]. In Figure 2-16 (c), a structure comprising a pyramid-shaped unit cell was created by Ma [76] and the geometry, dimensions or composition can be varied to demonstrate different effective materials properties along different directions [76]. Recently, the 3D re-entrant structures are further developed, such as the analytical model of the 3D re-entrant honeycomb [77] and a cylindrical structure using 3D re-entrant triangles [78].

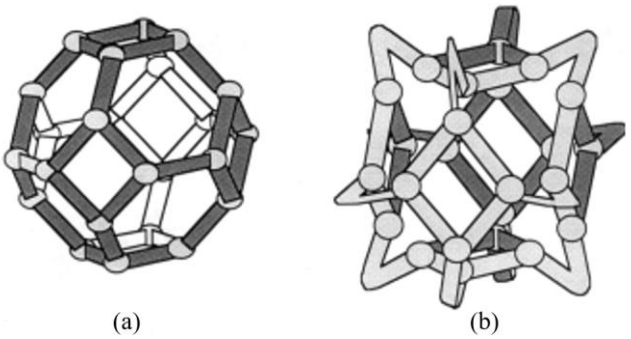

Figure 2-15 3D structure with tetrakaidecahedron cells: (a) conventional structure; (b) re-entrant structure [73]

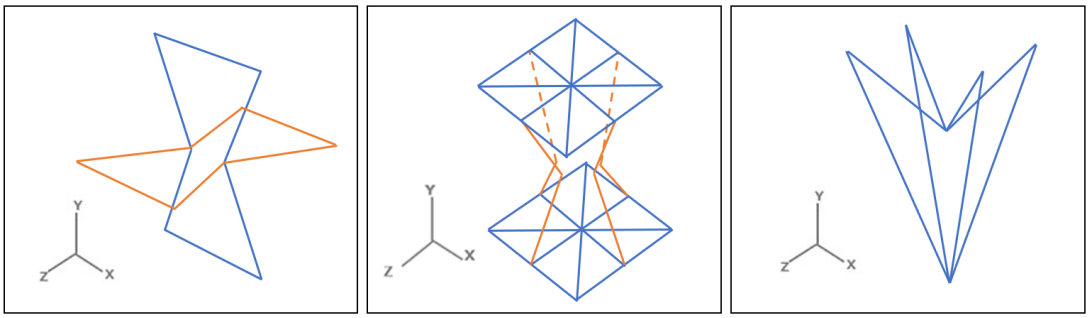

(a) (b) (c)

Figure 2-16 3D re-entrant structures: (a) structure formed by rotating the 2D structure 90˚ in X axis [74]; (b) structure formed by rotating the 2D structure 90˚ in Y axis [75]; (c) 3D re-entrant triangular [62]

By using the rotating polygons, Alderson and Evans [79] developed the rotation and dilation deformation mechanisms in the α-cristobalite tetrahedral framework structure exhibiting auxetic behaviour. The deformation of the structure is shown in Figure 2-17 including the fully densified state and the fully expanded state. In their study, three different models in a 3D tetrahedral network were analysed. The first one was the rotating tetrahedra model (RTM), in which each tetrahedron was assumed to be rigid and free to rotate. The behaviour of the auxeticity depends on the rotation of the unit. The second one was the dilating tetrahedra model (DTM), assuming each tetrahedron to be fixed in orientation but free to change size. The last one was called the concurrent tetrahedra model (CTM) and the response of the model was caused by the geometry and the combination of RTM and DTM to act in a concurrent manner. Also, the CTM offered a design route for achieving ultrahigh Young's moduli of the materials.

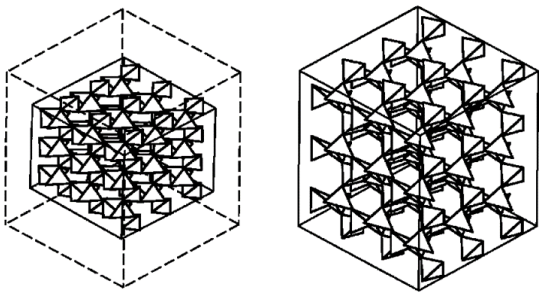

Figure 2-17 Rotating tetrahedral framework [79]

After that, chiral three-dimensional lattices were proposed by Ha et al. [80] with rigid cubical nodules, as shown in Figure 2-18. The 3D chiral lattices display stretch-twist coupling that increases with relative slenderness of ribs and the Poisson's ratio decreases from positive to negative with the increasing number of cells due to the

specific geometry. The lattices show significant size deformation and approach a factor of five in torsion rigidity [81]. Huang et al. [82] conducted a numerical and experimental analysis of a 3D anti-tetrachiral structure exhibiting negative Poisson's ratio. The structure shows isotropic behaviour in z-directional compression, but displays anisotropic behaviour in x-directional and y-directional compression. The relationship among the factors were discussed including Poisson's ratio, effective Young's modulus, porosity as well as the geometric structure.

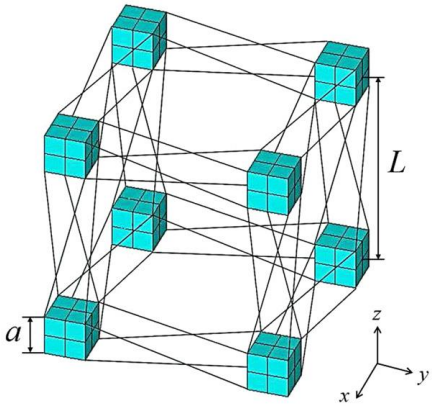

Figure 2-18 Unit cell of chiral 3D lattice structure. (The aspect ratio is defined to be L/a, where L/a > 1) [80]

According to the 2D crumpled sheets structure, Bouaziz et al. [83] developed crumpled aluminum thin foils shown in Figure 2-19. The crumpled foil can exhibit negative Poisson's ratio up to relative density of 15% as a result of the dewrinkling mechanism. A hybrid behaviour between foams and entangled fibrous materials is also presented. The entangled fibrous materials show a notable plasticity and a low hysteresis compared to the conventional foams, however, they have no plateau beyond the yield stress.

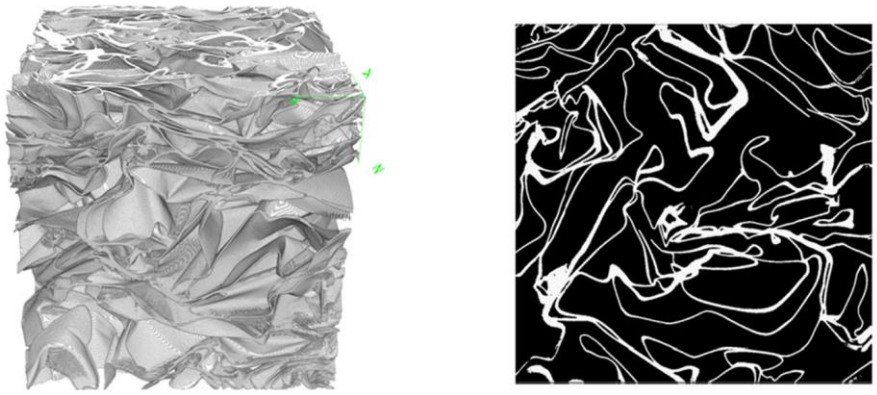

(a) (b)

Figure 2-19 A typical crumpled aluminum foil: (a) 3D image; (b) 2D segmented micrographs [83]

2.3.1.3 3D-to-2D auxetic structures

In this context, the original structure is formed by three dimensional (3D) configuration, containing x, y and z space. When the structure is stretched in x direction, the auxeticity can only show in y direction or in z direction. By demonstrating this feature, the structure is coded as 3D-to-2D auxetic structure.

Grima et al. [53] reported an analytical model of egg rack structure constructing from umbrella type sub-units, as shown in Figure 2-20. The structure is formed by rods through special three-dimensional hinges and such hinges can be treated as two 2D hinges. The on-axis auxeticity is achieved as -1 and the maximum non-auxetic behaviour is shown at ±45˚ off axis.

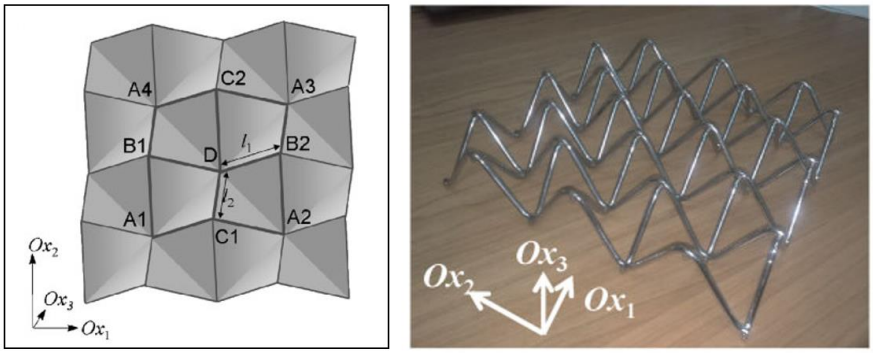

(a) (b)

Figure 2-20 Egg rack structure: (a) unite cell; (b) designed macrostructure [53]

In textiles, Ge and Hu [18] reported a 3D orthogonal structure which exhibits auxetic behaviour. As shown in Figure 2-21 (a), the warp and weft yarns are arranged in two orthogonal directions without interlacement and the stitch yarns are sewed through the

thickness direction, bounding the warp and weft yarns together. When compression is applied to the fabric in the thickness direction, the weft yarns will be crimped, leading to shrinkage in the weft direction, as shown in Figure 2-21 (b). Thus, the orthogonal structure allows the fabric to concentrate itself under the compression, resulting in a negative Poisson's ratio of the material. It should be pointed out that the materials used in the orthogonal structure must have the property which allows the structure to be deformed. Lacking anyone of these, the auxeticity would not be achieved.

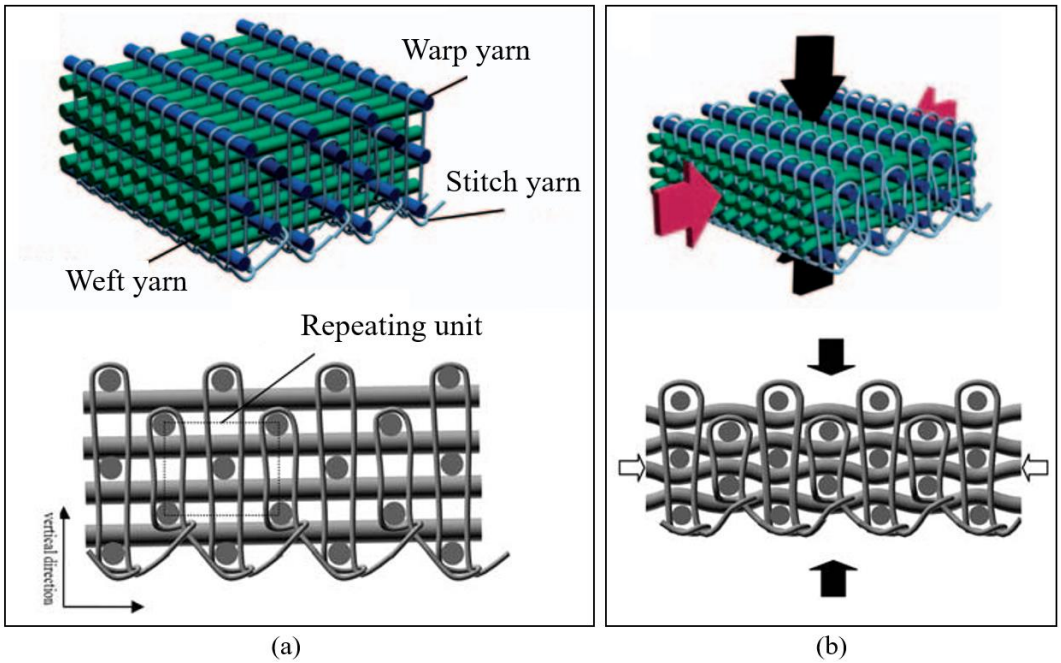

Figure 2-21 3D orthogonal woven structure: (a) without loading; (b) under compression [18]

2.3.1.4 1D-to-1D auxetic structures

1D-to-1D auxetic structures are featured by one dimensional (1D) configuration. When the structure is deformed, the auxeticity will be illustrated in the 1D configuration as well.

In textiles, auxetic behaviour can be achieved from 1D-to-1D by using the yarn with a helical structure, as illustrated in Figure 2-22. According to Hook [52], the auxeticity not only depends on the structure but also relates to the materials properties. The yarn was made of two plies with different diameters and with extremely different elastic moduli. These two plies were twisted together, with the thinner and stiffer yarn wrapping over the thicker and more elastic core ply. When stretched, the two types of plies would swap their roles, leading to a situation where the thinner and stiffer ply

became the straight core and the thicker and more elastic ply turned into the binder [84]. Therefore, the outer contour diameter of the yarn was larger and the auxetic behaviour was shown. In addition, the helical auxetic yarn can be made with more plies by using a different textile mechanism [23, 85] and the auxeticity is mainly contributed by the helical structure and the differential rigidity of the materials.

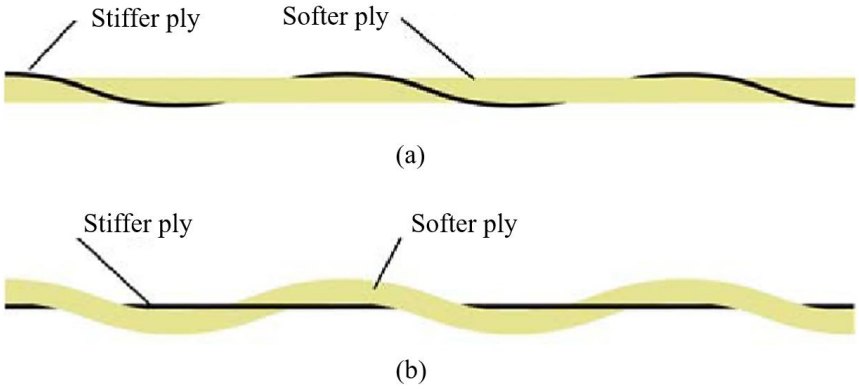

Figure 2-22 Helical structure of the auxetic yarn: (a) initial state; (b) under tensile loading [3]

2.3.1.5 1D-to-2D auxetic structure

When the original structure is one dimensional (1D) configuration, the auxeticity will be illustrated in the 2D plane, which is termed 1D-to-2D auxeticity in this context. Negative Poisson's ratio can be obtained from 1D-to-2D structures in textiles. For example, the helical auxetic yarns mentioned above can be used for making fabrics, so the auxeticity of the 2D fabric can be directly inherited from the yarns, as shown in Figure 2-23. The helical yarns are applied in the warp direction of the fabric. When stretched, the fabric expansion is observed along with the overlapping behaviour of the yarns, leading to the negative Poisson's ratio of the fabric. However, based on the work of Gao et al. [84], when this type of fabric is stretched in the warp direction, the dimensions in the weft and thickness directions could both be effected. In addition, it is important that the materials used in this structure are sufficiently soft in order to demonstrate the auxetic behaviour.

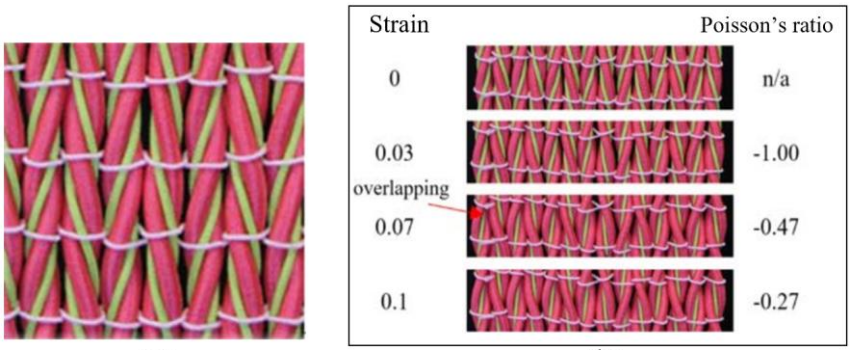

Figure 2-23 2D auxetic woven fabric made of auxetic yarns: (a) without tension; (b) under tension [86]

2.3.2 Properties of auxetic materials and structures

The elastic behaviour of the material is determined by four constants including the Young's modulus (E), the shear modulus (G), the bulk modulus (K) and the Poisson's ratio (v) [87]. The Poisson's ratio (v) represents the deformation of the material in the transverse direction when it is stretched in the axial direction. It can be calculated by using Equation (2-1).

$$v = -\frac{\varepsilon_{trans}}{\varepsilon_{axial}} \tag{2-1}$$

where ε_{trans} is the transverse strain and ε_{axial} is the axial strain [84].

The Poisson's ratio of a material influences the material properties, such as the shear modulus [27], fracture resistance [7], indentation resistance [9], out-of-plane bending behaviour [28], energy absorption ability [88] and variable permeability [89].

2.3.2.1 Shear modulus

Based on the elastic theory of isotropic materials, the shear modulus (G) is determined by two constants including the Poisson's ratio (v), Young's modulus (E) or the bulk modulus (K), as shown in Equations (2-2) and (2-3). The allowed range of Poisson's ratio values for isotropic materials is between -1 and 0.5 due to the requirement for Young's modulus, shear modulus and bulk modulus to be positive values. For conventional material with positive Poisson's ratio, shear modulus is always smaller than the Young's modulus, as indicated by Equation (2-2). However, if the Poisson's ratio becomes -1, the shear modulus tends to be infinitely high which is implied in Equation (2-2) and (2-3). Figure 2-24 shows the auxetic behaviour of a Magnox reactor core on a macroscopic level. The keyed brick structure can be freely

compressed and expanded in all radial directions under tensile loading, which makes the structure auxetic with the Poisson's ratio value of -1 in the horizontal plane. The value corresponds to an infinitely high shear modulus for isotropic materials [27].

$$G = \frac{E}{2(1+v)} \tag{2-2}$$

$$G = \frac{3K(1-2v)}{2(1+v)} \tag{2-3}$$

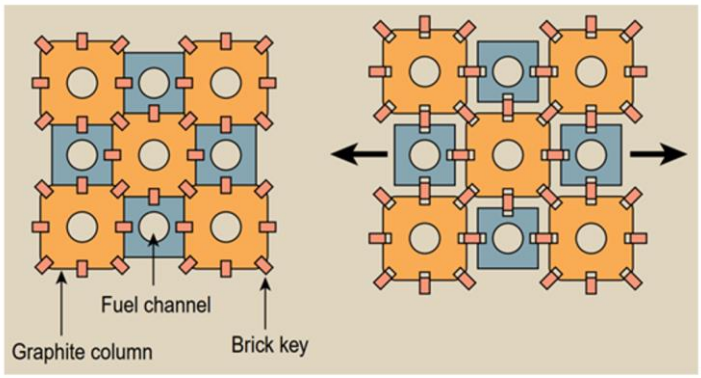

(a) (b)

Figure 2-24 Magnox nuclear reactor core: (a) fully compressed; (b) fully expanded [27]

2.3.2.2 Indentation resistance

For the indentation resistance of materials, as shown in Figure 2-25, when an indenter contacts the non-auxetic material, the material would spread perpendicular to the loading direction, resulting in the reduction of density and indentation resistance of the material. In contrast, the material flows into the vicinity of the loading area if the indentation is applied to an auxetic material. Thus, the material densifies and the indentation resistance or hardness increases [9]. The indentability of foam was reported by Lakes and Elms [90] using holographic interferometry. They found out that the novel re-entrant foams have higher yield strengths and energy absorption for dynamic impact than the conventional foams. Based on the theory of elasticity, the indentation resistance (H) of an isotropic material is associated with Young's modulus (E) and Poisson's ratio (v), as shown in Expression (2-4).

$$H \propto \left[\frac{E}{(1-v^2)}\right]^{\beta} \tag{2-4}$$

where β takes the value of 1 or 2/3 representing the situation of uniform pressure distribution or hertzian indentation respectively. It can be seen that the indentation resistance tends to be infinite, when the Poisson's ratio v approaches -1 [9].

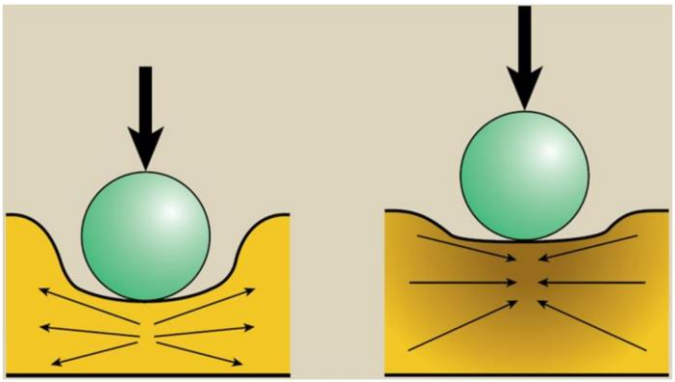

(a) (b)

Figure 2-25 Indentation resistance: (a) non-auxetic material; (b) auxetic material [27]

2.3.2.3 Bending behaviour

Auxetic materials are also reported to have an out-of-plane bending behaviour. Non-auxetic materials exhibit a saddle shape with anticlastic curvature when subject to out-of-plane bending, whereas auxetic materials display a dome shape or synclastic curvature without excessive forcing to achieve the desired shape [28, 73], as illustrated in Figure 2-26. This property allows better shape fitting onto doubly-curved surface for protection, such as knees and elbows.

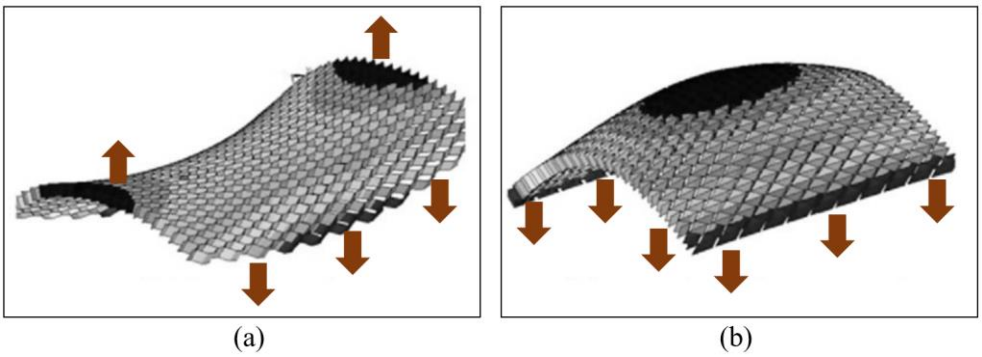

Figure 2-26 Deformation of non-auxetic material and auxetic material under out-of-plane bending: (a) anticlastic curvature (non-auxetic); (b) synclastic curvature (auxetic) [20]

2.3.2.4 Energy absorption

Auxetic materials show overall superior energy absorption ability compared with non-auxetic materials due to damping and the indentation effect, such as foams [91],

textiles and composites [92]. Scarpa et al. [93] reported the acoustic properties of auxetic polyurethane foam and they found the foam seeded with a magnetorheological fluid (then dried) has intrinsic higher acoustic absorption properties than normal open-cell foams. Yang et al. [94] conducted a numerical study on sandwich panels with aluminium foam and auxetic honeycomb cores. They found the panel with auxetic core is far superior to the panel with traditional aluminium foam in ballistic resistance due to the auxetic material concentration at the impact area. Hook [95] created a sample of auxetic fibres made into a porous material and it was used for explosion because the material is able to disperse blast energies [96]. Recently, Zhou et al. [97] investigated the low-velocity impact properties of 3D auxetic textile composite which has better protective performance than the non-auxetic textile composite due to the better transmitted force reduction and higher energy absorption.

2.3.2.5 Porosity variation

Due to the porosity variations of the auxetic materials under tension, auxetic materials are noted to have great potential for filtration applications. One of the first successful demonstrations, polymeric filter technology, was reported by Alderson et al. [89] in 2001. They showed how the auxetic material offers improved filter performance from the macro-scale to the nano-scale due to its unique pore-opening properties, as shown in Figure 2-27. For a conventional filter, the pores close up laterally when the filter is stretched. The particle is blocked and cannot be transmitted through the structure as illustrated in Figure 2-27 (a). However, for the auxetic filter, the pores shown in Figure 2-27 (b) open up with the same tensile loading and the particulate de-fouling is possible [89]. Based on that, they applied a glass bead transmission test for auxetic polyurethane foams and first confirmed the benefits of mass transport properties due to the persistence of auxetic behaviour in 3D macroscale filters. The auxetic benefits demonstrated in regular non-tortuous 2D auxetics remain even in 3D auxetics displaying tortuosity [98].

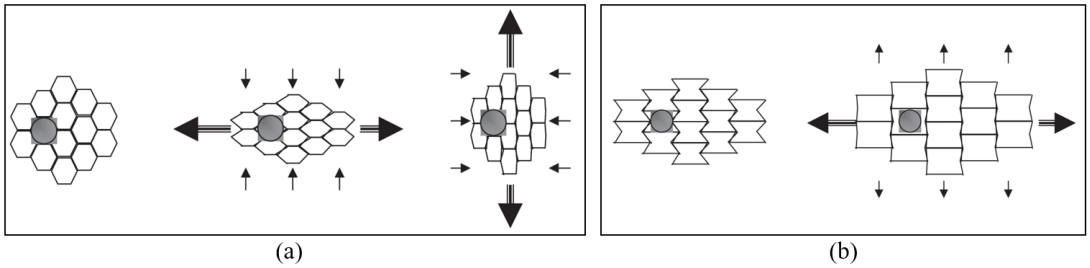

Figure 2-27 Schematic of enhanced particle transmission: (a) conventional filter; (b) auxetic filter [98]

2.3.2.6 Fracture resistance

Auxetic materials and structures exhibit a better fracture resistance and lower crack propagation compared to non-auxetic materials [99, 100]. Donoghue et al. [100] reported that the auxetic composite laminates have less notch sensitivity and they require more energy to propagate a crack. In the study of an auxetic plate by Bhullar et al. [101], the auxetic material exhibited around twice the crack resistance to fracture compared with the non-auxetic material.

Most of the mechanical formulae underpinning enhancements, such as those reviewed above, in auxetic materials, are based on assumptions like elastic range. The materials can be extended and recovered, whereas this is not always the case in textile materials. For conventional materials, such as metal, small scale deformation is considered in most cases, but for textiles the deformation is often larger-strain deformation including elastic deformation and plastic deformation. Therefore, textile deformation is not within the range above including the shear modulus and the hardness.

2.3.3 Types of auxetic materials

Auxetic materials can be classified into two types: natural auxetic materials and man-made auxetic materials. Auxetic materials have been discovered in nature for a long time, such as iron pyrites [102], pyrolytic graphite [103], cat skin [104], arsenic [105], cadmium [106], cancellous bone [107] and rocks with cracks [108, 109]. They did not attract significant attention to other researchers until the isotropic auxetic foam was created by Lakes [7] in 1987. After that, other auxetic materials were investigated in different fields to gain insight into how to make auxetic materials and how the auxeticity behaves in comparison to normal materials [35].

Foams are one of the most popular forms to achieve auxetic behaviour due to their low price and easy availability [110] using polymeric materials, including polyurethane

[31, 111], polytetrafluoroethylene (PTFE) [70, 112], polyethylene [113-116], ultra-high molecular weight polyethylene (UHMWPE) [117-120], polypropylene (PP) [121, 122], polyamide [120] and polyester [13]. Wang and Lakes [123] reported cushions made of auxetic foams which could provide more comfort and reduce the pressure especially for patients. There are two different methods for auxetic foams converted from conventional foams: one for polymeric foams and another for metallic foams. Generally, for polymeric materials, the auxetic behaviour of the foam structure is achieved by the three-step process in which the foam structure is tri-axially compressed, heated and cooled. The process changes the shape of the open cell structure, and then the materials soften and fix in a new position after heating and cooling, as shown in Figure 2-28 [7, 87, 124]. In addition to this, multi-phase fabrications are developed by several researchers such as solvent-based fabrication by Grima et al. [125], vac-bag method by Bianchi et al. [126] and dual density fabrication by Bianchi et al. [127]. For metallic materials, the foam can be compressed in three perpendicular directions at the temperature between 18˚C to 23˚C exhibiting auxetic behaviour [7]. Also, the thermal transformation method can be applied to metallic foams but it may be difficult due to the higher melting point of the materials [31].

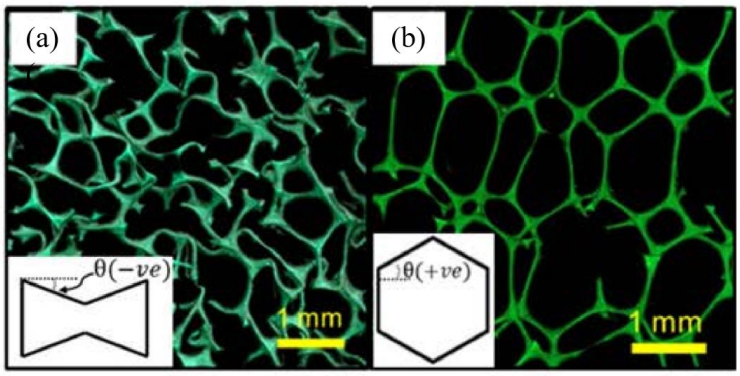

Figure 2-28 Auxetic foam structure: (a) auxetic foam showing re-entrant cells; (b) conventional foam showing polyhedral cells [128]

For textiles, fibres and yarns can be manufactured using natural materials or synthetic materials. The principle of the auxetic textiles, such as the helical auxetic yarn, is totally different from the foams. The yarn consists of two components, a thicker soft ply and the thinner stiff ply. When the yarn is in the free state, the stiff ply wraps the soft ply helically. When the yarn is stretched in the axial direction, the stiff ply will force the soft ply to a helical shape, leading to the increased outer contour diameter of

the yarn. Therefore, the auxetic behaviour is achieved and the deformation depends on the stiffness of the materials.

Additionally, ceramic, metal, composites, laminates and inorganic materials with auxetic behaviour have also been manufactured [28, 87] and these auxetic materials are summarised by Critchley et al. [110], shown in Figure 2-29.

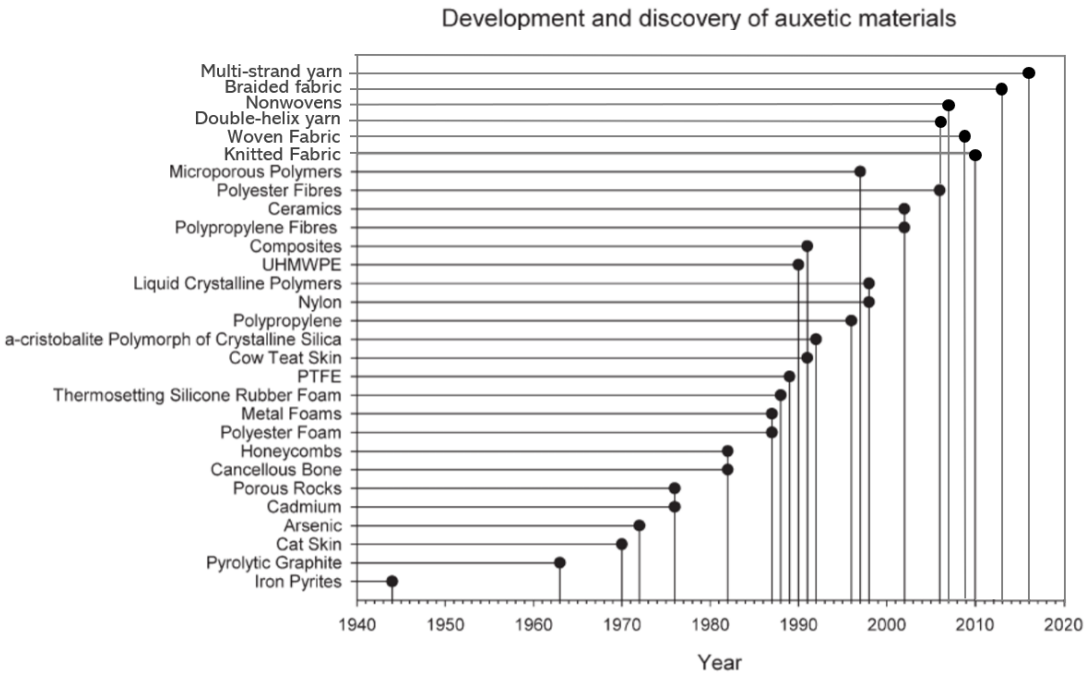

Figure 2-29 Timeline for discovery of auxetic materials [110]

2.4 Auxetic textiles

Textile materials refer to fibres, yarns, fabrics or various types of textile-reinforced composites. Fibres and yarns are the basic materials for manufacturing textile fabrics and they generally exhibit positive Poisson's ratio. Auxetic fibres made from polymers expand the potential applications of polymeric materials, but the applications are limited because of their size and shape [10, 11, 129]. In most cases, auxetic yarns are made of non-auxetic plies using different helical arrangements. Such auxetic yarns can be directly manufactured into a fabric because the auxeticity can be achieved by stretching the interlaced yarns in woven fabrics. However, the auxetic yarns cannot be directly used for knitted fabrics due to the loop structure and the yarns cannot be straightened during the stretching [3].

Auxetic fabric can be manufactured by all the existing textile technologies including weaving, knitting, braiding as well as nonwoven [3], and the auxetic behaviour of the

fabrics can be achieved by two general approaches. The first one is to use auxetic fibres and yarns directly fabricating the fabrics. The second approach is by the use of non-auxetic materials with specially designed fabric structures so that the structure displays auxeticity.

2.4.1 Fibres and polymers

Auxetic fibres as one of the polymeric materials provide the advantages not only in textile materials but also in auxetic polymers. The first auxetic microporous material was found by Caddock and Evans [70]. They reported that the anisotropic form of polytetrafluoroethylene (PTFE) demonstrates a large negative Poisson's ratio of -12 arising from a nodule-fibril structure shown in Figure 2-30. The work revealed that other polymers can be produced in such a manner as well for auxeticity and the auxetic behaviour depends on the microstructural deformation with nodule translation and rotation. Auxetic polymers were fabricated in the form of cylinders and rods by Evans and Ainsworth [130]. They reported a patent which covers a production route for polymers with microstructural nodules and fibrils. Based on the three-stage processing route of auxetic ultra-high molecular weight polyethylene (UHMWPE), an auxetic polyethylene was fabricated with up to -0.22 of negative Poisson's ratio at 1.6% strain [121]. Subsequently, the works of auxetic filaments and fibres occurred, such as polypropylene fibres [11, 12], polyester and polyamide fibres [13].

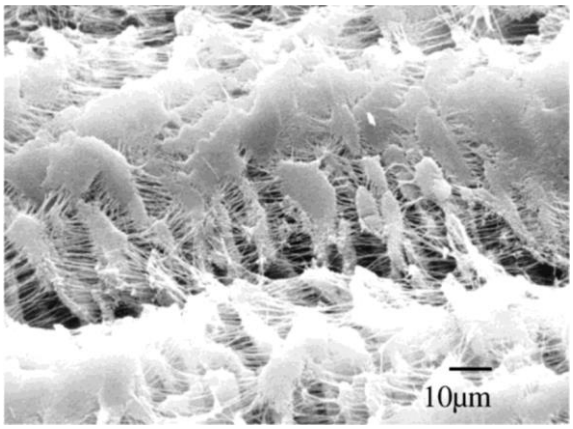

Figure 2-30 Auxetic expanded polytetrafluoroethylene (PTFE) structure [9]

To date, the typical auxetic fibres are polypropylene fibres, polyamide fibres and polyester fibres. Alderson et al. [11] first produced auxetic polypropylene fibres using a novel modification of melt spinning technique in 2002. This is the first time that the auxetic polypropylene fibres are made with diameters less than 1 mm. As shown in

Figure 2-31, the extruder containing an Archimedian screw mechanism has five temperature zones and each zone has thermostatic control, compression ratio of 3:1, diameter screw of 1 in. and 24:1 length/diameter ratio. The polypropylene powder is fed through the hopper into the barrel marked as 1 and 2. Then the filaments are collected and guided to the cooling roller after the powder is pushed through the three barrel zones, adapter zone and die zone, marked as 4 to 8. The molten polypropylene is reshaped and extruded through a 40 hole spinneret plate having around 0.55 mm hole diameters. After that, the auxetic polypropylene fibre is produced successfully shown in Figure 2-32.

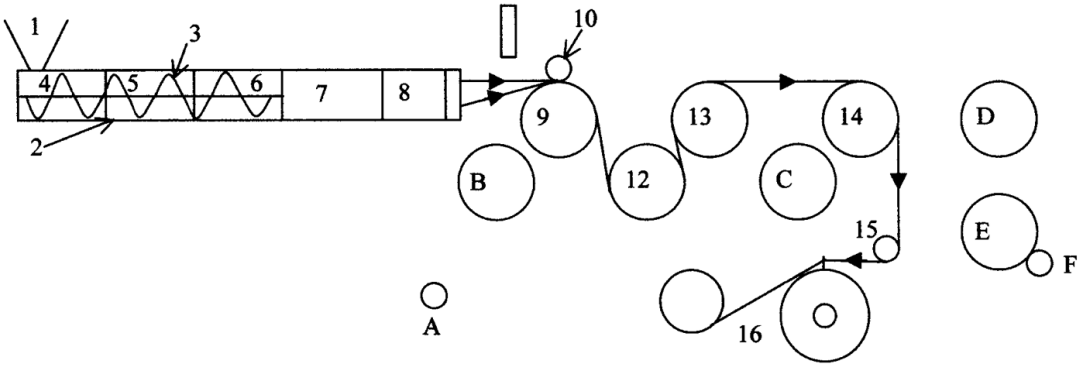

1, polymer hopper; 2, barrel; 3, Archimedean feed screw; 4, screw feed zone; 5, screw compression zone; 6 screw metering zone; 7, cavity transfer mixing zone (adaptor zone); 8, die zone; 9, cooling roller; 10, nip roller; 11, air knife; 12, 13, 14, rollers; 15, guide rail; 16 windup unit; A, B, C, D, E, F, unused rollers

Figure 2-31 Schematic diagram for producing auxetic polypropylene fibres [11]

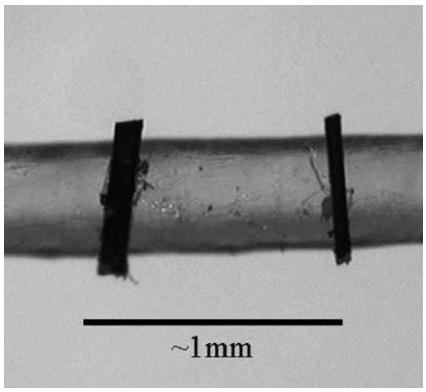

Figure 2-32 Auxetic polypropylene fibre with markers in microtensile test [11]

Meanwhile, Alderson et al. [11] measured the Poisson's ratio value of the auxetic polypropylene fibre compared to the non-auxetic polypropylene fibre, as shown in Figure 2-33. The curves for non-auxetic fibres are out of phase representing thinning of the fibre when stretched, whereas for auxetic fibres, the curves are in phase

indicating thickening of the fibre under tensile loading. The Poisson's ratio of the fibre is reported as -0.6±0.05 but the manufacturing process is limited to the laboratory scale.

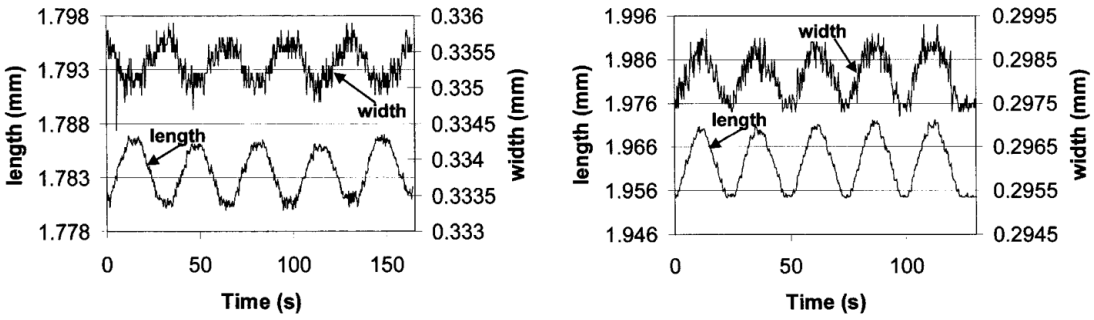

(a) (b)

Figure 2-33 The length and width variations against time for polypropylene fibre: (a) non-auxetic; (b) auxetic [11]

To overcome the limitation of the manufacturing process for auxetic polypropylene fibres, the effect of the processing factors are investigated such as screw speed, take-off speed, die geometry, temperature and the extruder [131]. Then, Alderson's group conducted a large-scale production of them and they found that the fibres show auxetic response over a larger strain than before [132]. To develop the mechanical properties of the auxetic polypropylene fibres, Simkins et al. [122] conducted a study into the effect of different thermal post-production processing conditions. The mechanical properties of the fibres are enhanced by annealing and the auxeticity is more uniformly delivered.

Polyamide fibre is another synthetic fibre exhibiting negative Poisson's ratio. Ravirala et al. [133] produced the auxetic polyamide fibres using the nylon powder with 43 μm average size of particles. By using different heating temperatures including 230˚C, 200˚C, 195˚and 190˚C, it was found that the auxetic behaviour is achieved between -0.15 to -0.25 when the fibres were fabricated at 195˚C only with 1.05 rad/s screw speed and 0.03 m/s take-up speed.

Besides, auxetic polyester fibre was manufactured and characterised by Ravirala et al. [13, 133]. The manufacturing method of the auxetic polyester fibre was derived from that of the polypropylene fibre, using the screw speed of 0.525 rad/s and the take-up speed of 0.075 m/s. The auxeticity was found when the fibre produced at 225˚C exhibiting the Poisson's ratio of -0.72±0.05. Such auxetic fibres have great potential

in various applications, such as biomedical materials, protective garments and fibre reinforced composites [13].

Although the specially designed polymers and fibres would demonstrate a negative Poisson's ratio of the materials, the auxeticity is achieved by making use of normal materials to form special structures in most of the cases.

2.4.2 Yarns

Up to now, auxetic yarns are made in two major methods. One is the yarn directly produced from auxetic polymers and fibres; another one is combining different non-auxetic yarns based on the textile technology, so the auxetic behaviour purely depends on the yarn structure. The concept of helical auxetic yarn (HAY) was proposed by Hook and Evans [134] and the yarn is composed of two filaments: a thicker soft core filament and a thinner stiff wrap filament. The thinner filament wraps around the soft filament helically. When a tensile load is applied in the axial direction, the core filament is pushed into a helical shape around the wrap filament as the wrap filament moves inward, leading to an increase of the outer contour diameter of the yarn. After that, the HAY has been studied, analysed and improved by using different methods and materials.

2.4.2.1 Two-ply helical structure

Based on the second method, the helical auxetic yarn was first designed by Hook [52] and then the theory of the yarn was also proposed by Alderson and Alderson [21] in 2005. A multifilament construction is manufactured by a stiffer filament wrapping around a softer filament helically and it can be made by using conventional textile machinery. Miller et al. [16] produced a novel double-helix yarn exhibiting the negative Poisson's ratio of -2.1. A stiffer fibre with 0.32 mm diameter, 6 GPa Young's modulus and 0.5 Poisson's ratio, was helically wrapped around a elastomeric cylinder with 0.64 mm diameter, 53 MPa Young's modulus and 0.48 Poisson's ratio. When the yarn was stretched in axial direction, the stiffer fibre became straight and forced the cylinder as a helix around it, leading to the auxetic behaviour of the yarn. In their study, it was noted that arranging two yarns out of register can maximize the auxetic behaviour because the yarns were pushed with each other resulting in the overall expansion, as illustrated in Figure 2-34.

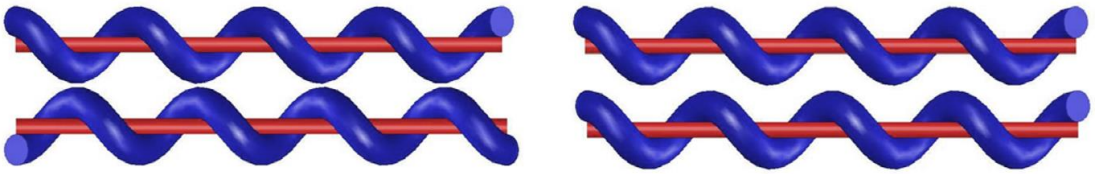

(a) (b)

Figure 2-34 Double-helix yarn with different arrangement: (a) out of register; (b) in register [16]

Meanwhile, Miller et al. [135] produced the auxetic double-helix yarn by using a higher modulus carbon fibre and a lower modulus nylon fibre. The carbon fibre was wound around the nylon fibre helically with different angles of 10˚, 20˚ and 30˚ demonstrating the Poisson's ratio of -5.8, -2.3 and -1.1, respectively. Based on the two-ply structure of the auxetic yarn, different materials were investigated and the details of them are summarised in Table 2-2. It can be seen that the two components of the helical auxetic yarn should possess differential stiffness and thickness for auxeticity. The maximum negative Poisson's ratio of the two-ply helix yarn can be achieved as low as -13.5 by using the combination of the elastomeric polyester and UHMWPE, however, the value is obtained by the resin embedding under specific load and it may be different when measured without adding the third material. The large negative Poisson's ratio value can also be explained by the less cross-sectional deformation of the monofilament core.

Table 2-2 Summary of different materials used for the helical auxetic yarn in experiments

Year	Author(s)	Wrap ply of the yarn	Core ply of the yarn	Maximum NPR
2009	Miller et al. [16]	Ultra-high molecular weight polyethylene (UHMWPE) fibre	Polyurethane fibre	-2.1
2010	Wright et al. [14]	Polyamide	Polyurethane	-5
2011	Sloan et al. [15]	Co-polymer polyamide (Trade name Platil)	Polyurethane elastomer (Trade name TROFIL)	-2.7
2012	Miller et al. [135]	Carbon fibre (Toray T300-1K)	Nylon fibre	-5.8
2012	Wright et al. [136]	Textured nylon	Covered rubber	-1.55
2013	Zhou and Du [137]	Nylon filaments	Spandex filaments	-4.31
2014	Bhattacharya et al. [138]	Multifilament UHMWPE; Monofilament Co-polymer polyamide (CPPA)	Monofilament: Polyurethane; Polyamide 12; Polyethylene; Polyester	-13.5
2015	Du et al. [139]	Nylon filaments	Spandex filaments	-2.01
2015	Sibal and Rawal [140]	Carbon multi-filaments	Nylon	-5.8
2016	Zhang et al. [141], [142]	Multifilament UHMWPE; Monofilament stainless steel wire	Thermoplastic polyurethane (TPU)	-7.5 (Instantaneous value is around -14)
2018	Zhang et al. [143]	Nylon 6 and polypropylene for monofilament fibre	Monofilament TPU	-0.5 (Instantaneous value is around -5.5)
2020	Chen and Du [144]	Stainless steel monofilament	Spandex	-2.55
2020	Liu et al. [145]	Polyester	Polyurethane	-0.88

According to the literatures, different factors of the yarn parameters can influence the auxetic behaviour, such as diameters, wrapping angles and tensile moduli. Sloan et al. [15] investigated the starting angle of the helical auxetic yarn, which can dominate the magnitude of the auxeticity. They also pointed out that the auxetic behaviour is influenced by the diameter ratio of the wrap ply to the core ply. Based on analytical calculations and finite element analysis, three main factors were addressed by McAfee and Faisal [146] including Poisson's ratio, diameter ratio of the wrap to the core as well as the starting angle. It was shown that increasing diameter ratio and reducing starting angle result in a higher auxetic behaviour. Du and co-workers discussed the

effect of wrapping angle, Young's modulus and core/wrap diameter ratio of helical auxetic yarns [139, 147]. They manufactured the yarn samples with different wrapping angles (25˚, 30˚ and 35˚), core/wrap linear density ratios (93.3tex/16.7tex, 124.4tex/16.7tex and 186.7tex/16.7tex) corresponding to the diameter ratio and tensile moduli (0.34 GPa, 0.93 GPa and 1.72 GPa). It was found that lower wrapping angle, higher diameter ratio and lager tensile modulus of the wrap lead to a higher negative Poisson's ratio value. However, the ranges of the investigated angles, diameter ratios and tensile moduli are rather small and limited, which could be further explored in the study of auxetic yarns.

2.4.2.2 Multi-strand helical structure

Multi-strand structure is another structure for producing the helical auxetic yarn as the yarn consist of several plies with different structural parameters. Ge et al. [23] first introduced a novel plied yarn which made of two soft yarns and two stiff yarns exhibiting the maximum negative Poisson's ratio around -4.5. The two types of yarns are placed in the same direction alternately, as illustrated in Figure 2-35. Then, the yarns are twisted together forming the four-ply structure at point A and the produced yarns are carefully collected by the rotating bobbin. In Figure 2-36, the two stiff yarns are placed outside of the two soft yarns and they migrate to the centre position slowly with the increasing tensile loading. Therefore, the auxetic behaviour is achieved by the increased cross-sectional size of the yarn. Additionally, the multi-strand structure is one of the effective structure to improve the structural problem of the two-ply yarns and the structural problem will be discussed in detail, in Section 2.4.2.4.

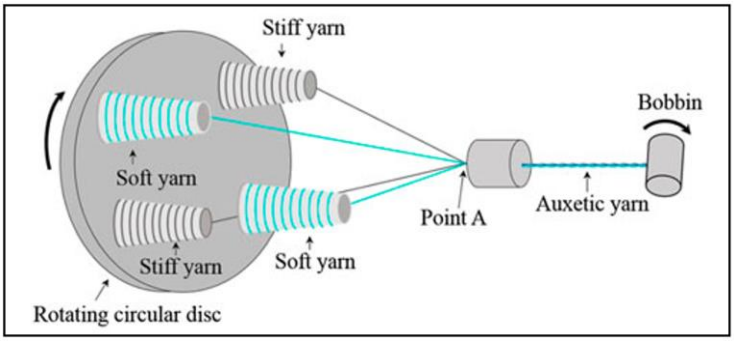

Figure 2-35 Illustration of the manufacturing process for the auxetic plied yarn [23]

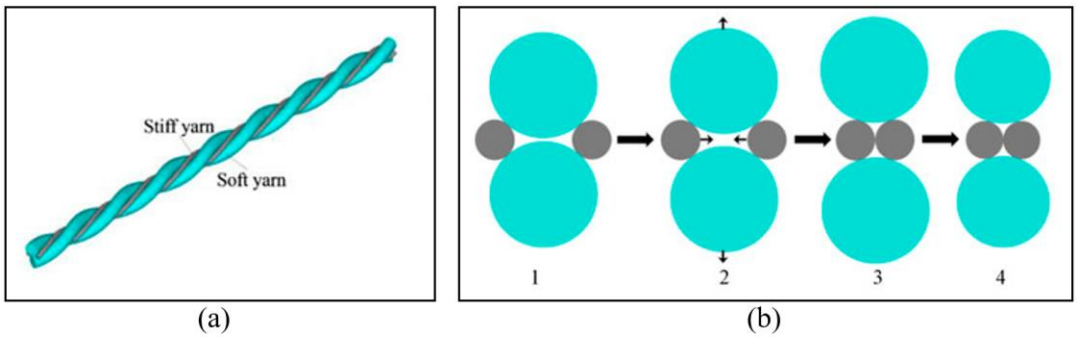

Figure 2-36 Auxetic yarn with four-ply structure: (a) 3D view; (b) cross-sectional changes under different tensile loading [23]

Based on the four-ply structure of the auxetic yarn, Ng and Hu [148] produced a six-ply auxetic yarn, as show in Figure 2-37. Similarly, the stiff yarns are moved to the centre of the yarn leading to the cross-sectional expansion of the auxetic yarn. Key parameters of the yarn were discussed including the soft yarn diameter, tensile modulus of the stiff yarn, twist level, cross-sectional deformation and helical structure. It was confirmed that the yarn with four-ply structure exhibits auxetic behaviour during the whole tensile process and smaller soft yarn diameter, higher stiff yarn modulus, lower twist level result in a larger negative Poisson's ratio value.

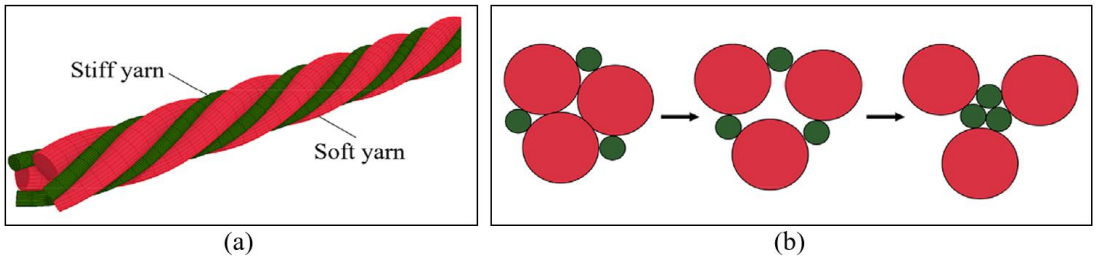

Figure 2-37 Auxetic yarn with six-ply structure: (a) 3D view; (b) cross-sectional changes under different tensile loading [148]

2.4.2.3 Structural problem of auxetic yarns

According to the auxetic yarns reviewed above, it was found that the helical yarns have a structural problem during the production. The stiffer ply is too loose when it wraps around the soft ply, leading to the slippage or torque problems in the auxetic yarn. In order to overcome this problem, several achievements have been reported by adopting sewing, coating, braiding and heating. Lim [149] explored a semi-auxetic yarn by sewing a thin cord in a triangular pattern through an elastic fat cord, as illustrated in Figure 2-38. The side view and the top view of the yarn are marked as the auxetic plane and the conventional plane, respectively. The Poisson's ratio of the

semi-auxetic yarn is mainly influenced by the initial half angle of the thin cord in the auxetic plane and the Poisson's ratio of the fat cord in conventional plane. This type of yarn can achieve very high Poisson's ratio both in negative and positive signs, such as 0.906 in conventional plane and -4.82 in auxetic plane. However, sewing a yarn into another yarn is difficult in textiles and it may not be suitable for large scale production.

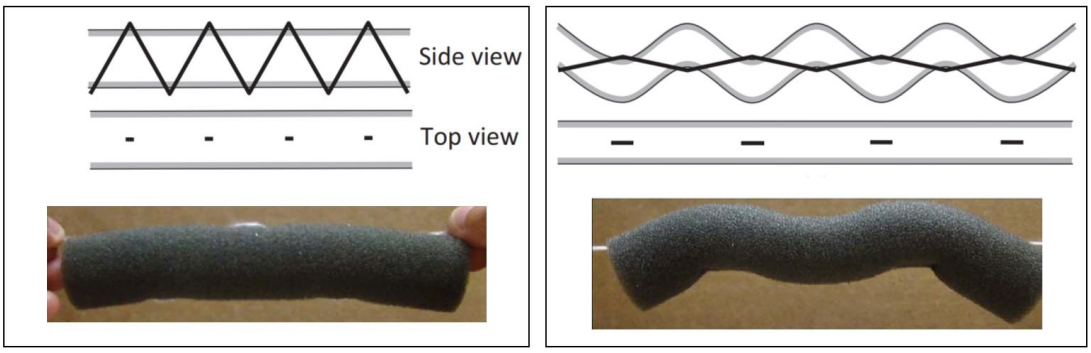

(a) (b)

Figure 2-38 Side and top views of a semi-auxetic yarn: (a) initial state; (b) under loading [149]

Zhang et al. [22] fabricated a 3-component auxetic yarn coated by silicone rubber gel as a sheath shown in Figure 2-39. The idea of the yarn was generated from the auxetic yarn with two-ply structure and the maximum negative Poisson's ratio of the new yarn was exhibited around -1.5. It was noted that the coating thickness of the sheath influence the yarn auxeticity and it can be seen as the new factor for exploring the yarn. Although the 3-component auxetic yarn offered a good binding between the core ply and the wrap ply, the yarn structure is restricted by the sheath and the auxetic behaviour is decreased with the increasing coating thickness.

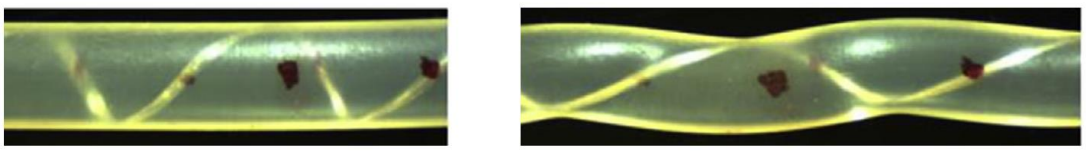

(a) (b)

Figure 2-39 Deformation of the 3-component (a stiff wrap fibre, an elastomeric core fibre and a rubber gel sheath) auxetic yarn: (a) initial state; (b) under tensile loading [22]

Another study proposed by Jiang and Hu [150] is the use of circular braiding technology where the wrap ply is directly braided with the elastic core ply, as shown

in Figure 2-40. Three components are used to form the yarn including elastic core yarn, stiff wrap yarn and elastic wrap yarn. It was shown that the stiff yarn wraps uniformly around the core yarn without slippage and the maximum negative Poisson's ratio is achieved as around -5.2 [85]. Lower wrapping angle, higher braiding angle and braiding yarn diameter leads to a better auxetic performance and the effect of new parameters on Poisson's ratio is reported as well, such as the number and position of the stiff yarn.

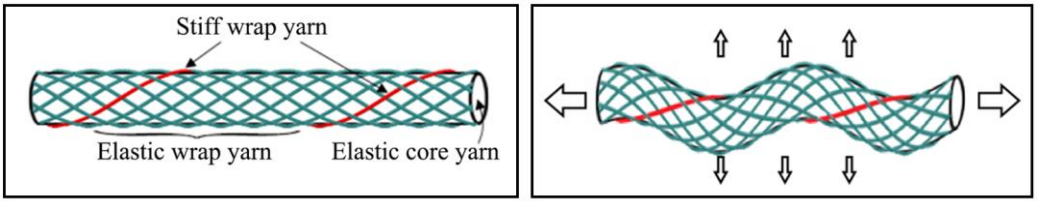

Figure 2-40 Braided auxetic yarn structure: (a) initial state; (b) under tensile loading [150]

Recently, Liu et al. [24] proposed a heat treatment for helical auxetic yarns, where a polyamide filament with a melting point of 80˚C together with the wrap ply were wrapped around the core ply. Then after the 120˚C heat treatment in oven, the melted polyamide improved the contact state between the two plies without tension. However, the melted polyamide can be used for once under tensile loading and the complex manufacturing process was not suitable for a large-scale production. The auxetic yarns produced in this study exhibited a maximum negative Poisson's ratio of -1.12. Based on the existing literature, the auxeticity of the helical auxetic yarn still needs to be maximized and the quality of the yarn calls for further investigation for the large-scale production.

2.4.3 Two-dimensional fabrics

Auxetic fabric can be made by two general approaches. One is using auxetic yarns to fabricate the fabric, so the auxetic behaviour can be inherited from the yarns. Another is by the use of non-auxetic yarns with special designed structures, so the auxeticity is obtained by the structures. In this section, auxetic fabrics are classified based on the textile technologies, including woven, knitted and braided.

2.4.3.1 Woven fabrics

A woven fabric is formed by interlacing two sets of yarns, i.e. warp and weft. The woven fabrics are more stable than the other types of fabrics due to more frequent yarn interlacements. As mentioned earlier, auxetic woven fabrics can be produced by using either auxetic yarns or non-auxetic yarns with special structures.

Auxetic woven fabrics made of auxetic yarns are manufactured and the summary of them is shown in Table 2-3. Herein, the helical auxetic yarn is referred to the two-ply structure of the auxetic yarn or the double-helix yarn. Miller et al. [16] first explored the auxetic woven fabric containing double helix yarns and the fabric was used for reinforced composite by coating with silicone rubber matrix, as shown in Figure 2-41 (a). The adjacent yarns were placed out of register to maximise the negative Poisson's ratio and the out-of-plane auxetic behaviour was obtained by the overlapping yarns under tensile loading shown in Figure 2-41 (b). In order to avoid overlapping of the yarns, two glass plates were set up to prevent the yarns going out-of-plane. Thus, the in-plane Poisson's ratio of the fabric was changed from positive 0.06 to negative -0.1 by using the double helix yarn which has the maximum negative Poisson's ratio around -2.1.

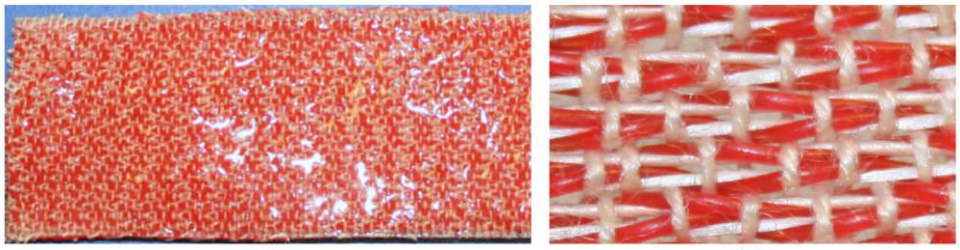

Figure 2-41 Auxetic woven fabric using double helix yarns: (a) coating with silicone rubber; (b) close-up image under tension [16]

Table 2-3 Summary of auxetic woven fabrics made of auxetic yarns

Year	Author(s)	Weave structure	Warp yarn	Weft yarn
2009	Miller et al. [16]	Plain	Meta-aramid	Double helix yarn (core: polyurethane; wrap: UHMWPE)
2012	Wright et al. [136]	Plain	Helical auxetic yarn (core: covered rubber; wrap: PET)	Multifilament polyethylene terephthalate (PET)
2013	Monika and Petra [151]	Plain, 2/2 twill, 3/5(3) satin	Polypropylene	Helical auxetic yarn (core: polyester; wrap: multifilament polypropylene)
2018	Ng and Hu [86]	Plain, 2/1 twill, 3/1 twill, 5-end satin	Auxetic plied yarn (four-ply yarns and six-ply yarns)	Elastic materials
2018	Liu et al. [152]	Plain, pointed twill (waved), diamond twill	UHMWPE	Helical auxetic yarn (core: polyurethane; wrap: polyester)
2019	Nazir et al. [153]	Plain, 3/1 twill, 2/2 matt, 2/2 twill	Helical auxetic yarn (core: multifilament polypropylene; wrap: multifilament Kevlar)	Kevlar
2020	Lolaki and Shanbeh [154]	Plain, 3/3 basket, weft-backed satin 6	Polyester	Helical auxetic yarn (core: rubber; wrap: nylon 66)
2020	Chen et al. [155]	Plain, basket, derivative	Aramid	Helical auxetic yarn (core: spandex; wrap: polyester)
2020	Gao et al. [84]	Plain	Helical auxetic yarn (core: polyurethane; wrap: polyamide)	Helical auxetic yarn (core: polyurethane; wrap: polyamide)

Wright et al. [136] conducted a bandage-like fabric by using the low stiffness helical auxetic yarns, which offers various potential applications such as garments, bandages and medical devices. The pore opening, colour changes and auxetic behaviour of the fabric were analysed and it was revealed that the strain-dependent variation in Poisson's ratio and tensile modulus are possible by adopting auxetic yarns with different structural parameters. The maximum negative in-plane Poisson's ratio of the fabric was achieved as -0.1 and that of the auxetic yarn was around -1.5.

By adopting the same method, Monika and Petra [151] first reported the investigation of auxetic woven fabrics using helical auxetic yarns with various weave structures including plain, 2/2 twill and 3/5 (3) satin, as shown in Figure 2-42. The auxetic yarns were selected in the weft direction for making the fabric with the density of 9

threads/cm and polypropylene multifilament yarns were selected in the warp direction with the sett of 2 threads/cm. It was found that satin structure behaves less auxetic, and the plain and twill structures are more auxetic. Also, less auxetic behaviour leads to less porosity of the fabric.

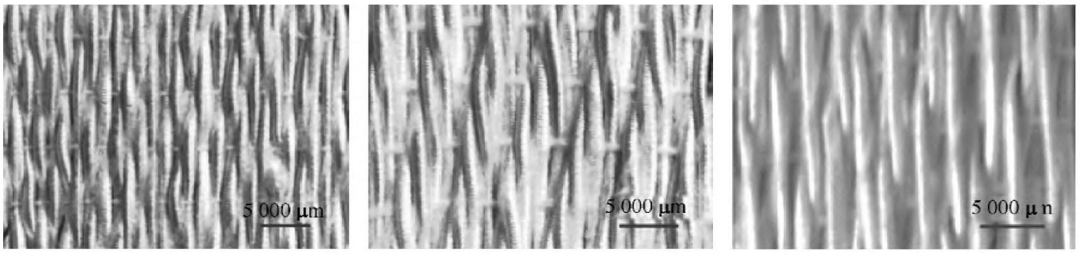

(a) (b) (c)

Figure 2-42 Auxetic woven fabrics with different weave structures: (a) plain; (b) 2/2 twill; (c) 3/5 (3) satin [151]

After that, different weave structures of the fabric are investigated such as diamond, basket and derivative. Most of the researchers reported that the structural performance of the auxetic yarn can be easily controlled by arranging them in the weft direction. Du's group conducted pointed twill structure and diamond twill structure of the auxetic woven fabric compared to the plain structure [152]. The maximum negative Poisson's ratio was achieved as -0.3 under the diagonal tensile loading with the strain of 200% and the fabric exhibited self-curling and self-folding behaviour without tension, as shown in Figure 2-43. It was found that the weave structure and the yarn twist can influence the performance of auxetic fabrics. Recently, Du's group reported an experimental analysis of auxetic woven fabrics with basket weave structure and derivative weave structure. The elastic recovery of the fabric, weave structures and wrap density of the auxetic yarn were analysed, which revealed that the derivative structure arranging the yarns in a series of zigzags can reach the maximum negative Poisson's ratio of -0.585 [155].

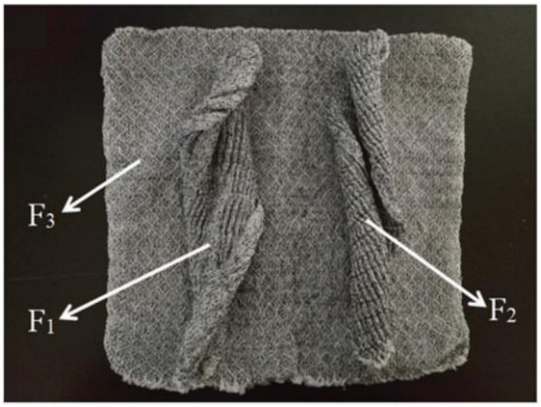

Figure 2-43 Auxetic woven fabric with diamond twill structure: (F1) Z twist of auxetic yarns; (F2) S twist of auxetic yarns; (F3) Z/S twist of auxetic yarns [152]

To investigate the influence of fabric thread densities and warp count, Lolaki and Shanbeh [154] fabricated 30 samples containing two warp counts and three weave structures including plain, 3/3 basket and weft-backed satin 6, as illustrated in Figure 2-44. The auxetic yarns were set as the weft and polyester was set as the warp with two different linear densities, 29.5 tex and 59 tex respectively. The calculation of the Poisson's ratio was based on the recorded images in MATLAB software. Among the samples they produced, it was found that increasing thread density and warp yarn fineness of the plain structure and basket structure result in lower auxetic behaviour. However, the weft-backed satin structure with increased weft density exhibits a slightly higher auxetic behaviour from the Poisson's ratio of -0.33 to -0.54. Thus, the influence of increase in thread density cannot be drawn firmly on auxetic behaviour.

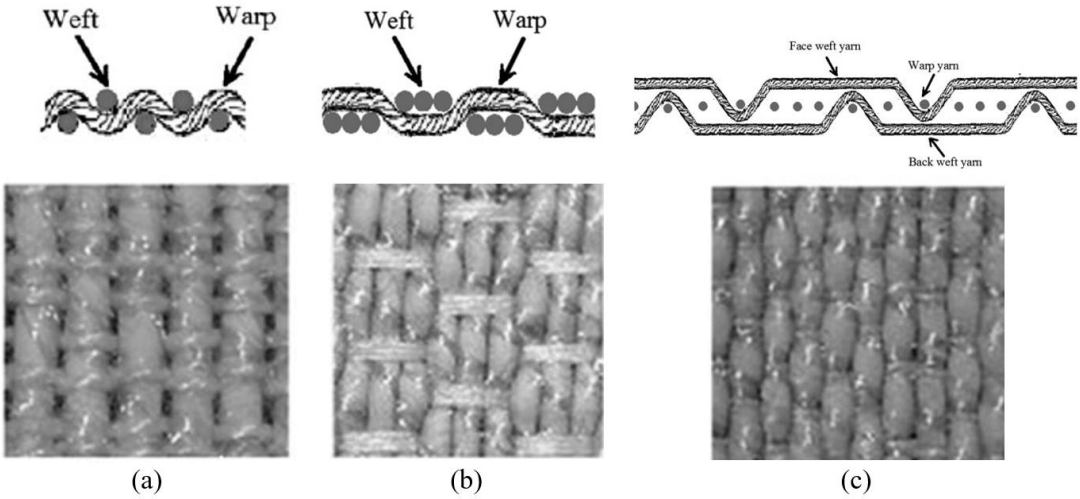

Figure 2-44 Three structures of auxetic woven fabrics: (a) plain; (b) 3/3 basket; (c) weft-backed satin 6 [154]

Apart from the auxetic yarns used in the weft direction of the fabric, the auxetic plied yarns produced by Ng and Hu [86] are arranged in the warp direction because the structural stability of the plied yarn is better than that of the helical auxetic yarn with two-ply structure. The auxetic yarn arrangement, properties of the yarn components, weft yarns and weave structures on Poisson's ratio were evaluated. It was shown that the woven fabric containing four-ply auxetic yarns generates higher auxetic behaviour and percent open area by arranging S twist and Z twist of auxetic yarns alternatively. Low modulus and short float of the weft yarns were favourable for increasing auxetic behaviour. Additionally, stiffer ply of the auxetic yarn led to higher auxetic behaviour, but finer soft ply did not contribute such behaviour in terms of the early onset of the fabric construction.

Auxetic woven fabrics made of non-auxetic yarns with special structures have attracted may researchers in recent years. The structures are formed by the shrinkage behaviour of the non-auxetic elastic yarns and non-elastic yarns. The details of the structures and yarn combinations are summarised in Table 2-4. Ali et al. [156] fabricated a 2D woven fabric by orienting yarns in a honeycomb geometry, which exhibits auxetic behaviour. Cotton yarn and elastic cotton yarn were selected in warp and weft directions respectively and the honeycomb geometry was formed by the shrinkage behaviour of the weave structures due to the differential float length of them. As shown in Figure 2-45, the plain weave is the highly interlaced weave, which is expanded because the intersections occupy more space after weaving. The high float weave is shrunk as the single interlacement occupy less space and the satin weave is defined as the medium interlaced weave. It was found that the maximum negative Poisson's ratio of the fabric was achieved as -0.77 and -0.17 in warp and weft directions, respectively. Such fabric was suggested for protective applications due to its superior cut resistance, bursting resistance and energy absorption.

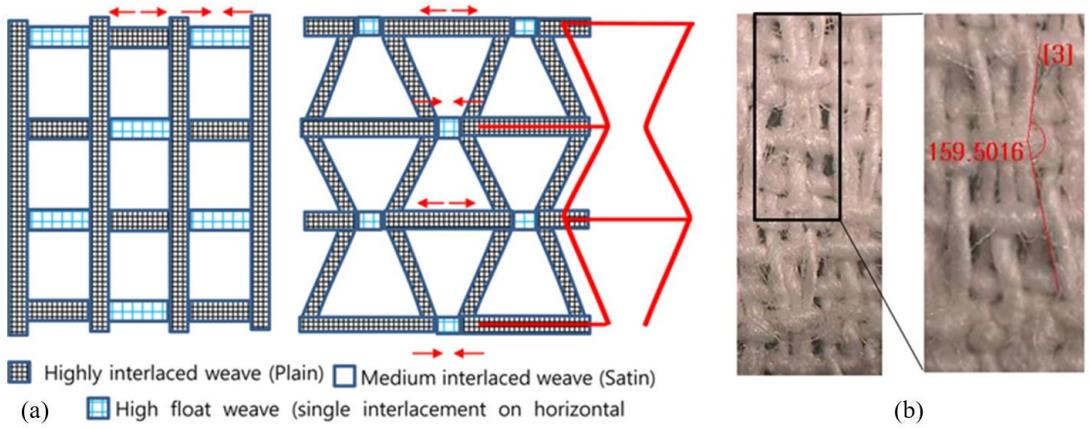

Figure 2-45 Auxetic woven fabric with honeycomb geometry: (a) arrangement of different weaves before (left) and after (right) de-sizing; (b) arrangement of yarns in fabric [156]

Table 2-4 Summary of auxetic woven fabrics made of non-auxetic yarns

Year	Author(s)	Geometric structure	Warp yarn	Weft yarn
2018	Ali et al. [156], [157]	Honeycomb geometry	Cotton yarn	Elastane cotton yarn
2018	Zulifqar et al. [158]	Foldable geometries; rotating rectangle geometry; re-entrant hexagonal geometry	Non-elastic yarn	Elastic yarn
2019, 2020	Zulifqar and Hu [159] Kamrul et al. [160]	Re-entrant hexagonal geometry	Cotton spun yarn; core spun cotton spandex yarn	Core spun cotton spandex yarn
2019	Cao et al. [161]	Foldable geometry	Elastic yarn; non-elastic yarn	Elastic yarn

By adopting auxetic geometries, a series of investigations was reported by Hu's group using experimental analysis [158] and geometric analysis [162]. Foldable geometry, rotating rectangle geometry and re-entrant hexagonal geometry were developed for making uni-stretch woven fabrics, as shown in Figure 2-46. The foldable geometry can be unfolded under tensile loading resulting in zero or negative Poisson's ratio and the maximum negative Poisson's ratio achieved was -0.17 with parallel in-phase zig-zag stripes along weft direction. The rotating rectangle structure generated smaller auxetic behaviour with Poisson's ratio of -0.05 due to the absence of the elastic warp yarn, unstable rectangular units and restricted rotation of the rectangles. The re-entrant hexagonal geometry was formed by the combination of the loose weave and tight

weave, where the longer ribs can be made to bend and then translate into straight position under tension, exhibiting negative Poisson's ratio of -0.1.

After a year, Hu's group further developed the bi-stretch auxetic woven fabrics based on the foldable geometry [161] and the re-entrant hexagonal geometry [159]. For foldable geometry, different parameters were discussed including yarn float length, weave arrangement and the placement of yarns. The result shows the designed fabric exhibiting negative Poisson's ratio of -0.36 and -0.27 along the warp and weft tensile loading, respectively. By adopting re-entrant hexagonal geometry, the auxetic behaviour of the bi-stretch woven fabric in the warp direction was higher than that in the weft direction, which demonstrated maximum negative Poisson's ratio around -0.35 and -0.15 respectively.

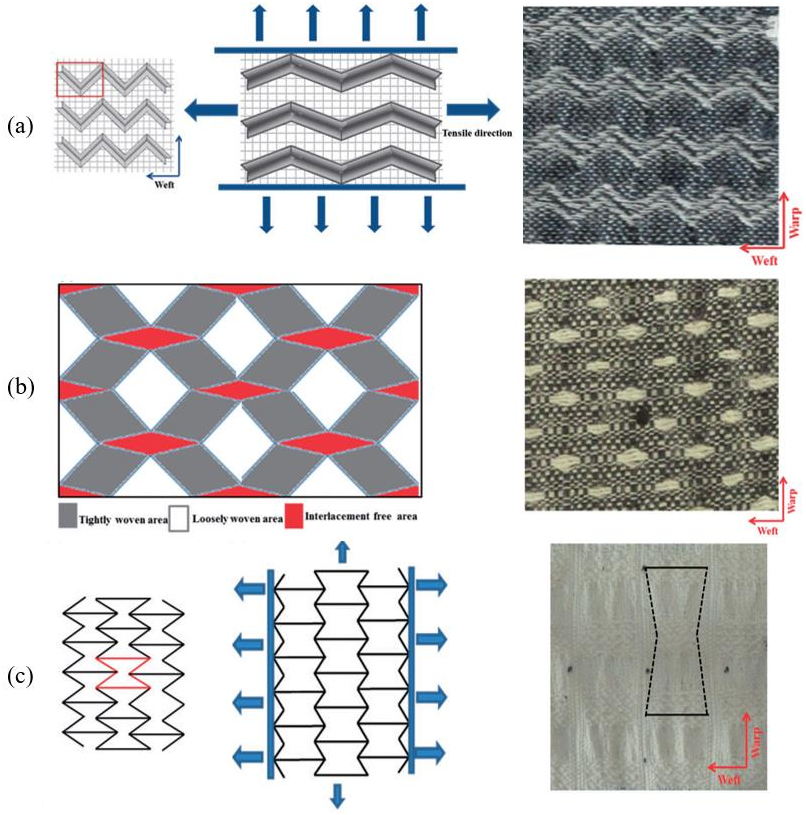

Figure 2-46 Auxetic woven fabrics with different geometries: (a) foldable geometry containing parallel in-phase zig-zag stripes along the weft direction; (b) rotating rectangle geometry; (c) re-entrant hexagonal geometry [158]

2.4.3.2 Knitted fabrics

Knitted fabric is formed by loop structures which make the fabric more stretchable and breathable. Based on the textile technology, auxetic knitted fabrics can be classified into two parts, weft knitted and warp-knitted fabrics. The auxetic behaviour

is mainly contributed by the geometric structures in knitting, however, the auxeticity is not achieved by knitting with auxetic yarns directly because the auxetic yarns cannot be straightened in the loop structure.

Weft-knitted auxetic fabrics are investigated based on three structures, including foldable structure, rotating rectangle structure and re-entrant hexagonal structure. According to the literature, most of the investigations are based on flat knitting technology because it is efficient, flexible and able to produce various geometric structures compared to circular and warp knitting technologies. The development of weft-knitted auxetic fabric was started by Liu et al. [163] in 2010. They first fabricated auxetic knitted fabrics with foldable structure based on the Miura-origami geometry. 100% wool 2/28 Nm yarns were selected for making the fabric, and the auxetic behaviour was achieved by arranging face loops and reverse loops in a zigzag shape. As shown in Figure 2-47, the fabric is folded in the relaxed state, then each parallelogram changes its position relative to the surface plane under tensile loading either in the horizontal or vertical direction. It was found that the opening angle θ has great influence on the auxetic effect and a smaller initial opening angle results in a higher negative Poisson's ratio. The opening of the whole structure was demonstrated with the maximum negative Poisson's ratio of -0.5.

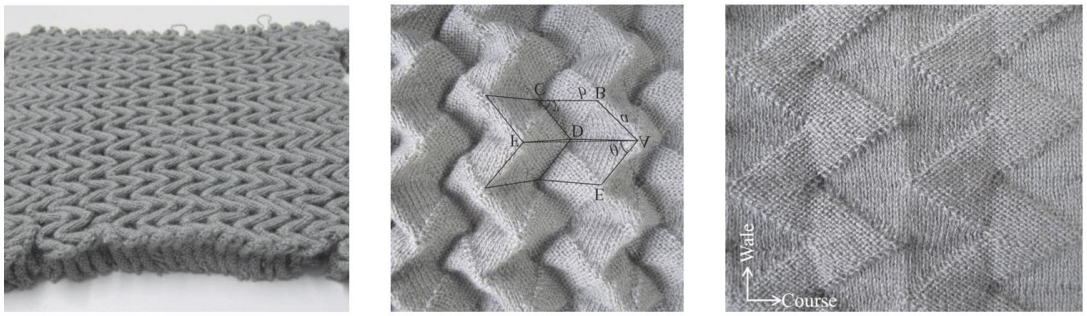

(a) (b) (c)

Figure 2-47 Weft-knitted fabric with foldable structure at different states: (a) relaxed state; (b) stretched state; (c) fully opened state [163]

By using the same principle of arranging face loops and reverse loops, Hu et al. [17] reported the other two arrangements of the foldable structure shown in Figure 2-48. The first fabric is formed by arranging loops in rectangles and it is folded without tensile loading, however, the auxetic behaviour is only found in the course direction. They also pointed out the different number of the courses and wales in a unit cell and these should be considered for affecting the auxetic behaviour of the fabric. The

second fabric is made by arranging loops in vertical and horizontal stripes. Compared to the first fabric, the second fabric has less folded performance and the auxetic behaviour rapidly decreases with increasing tensile strain because the opening behaviour of the structure is not larger than the fabric deformation.

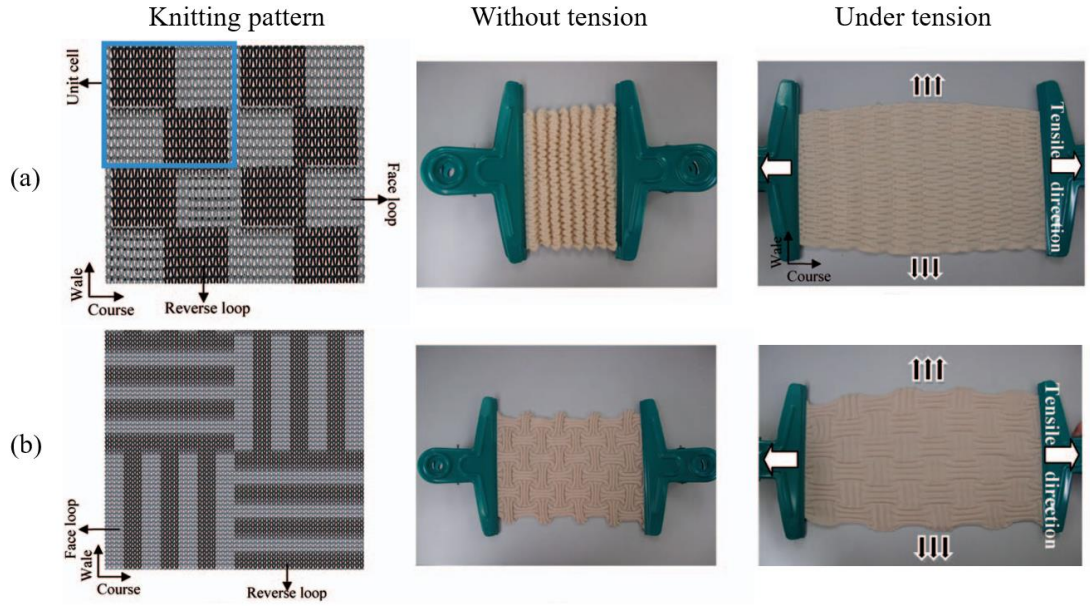

Figure 2-48 Foldable structures of the weft-knitted fabrics: (a) arrangement in rectangle forms; (b) arrangement in vertical and horizontal stripes [17]

Besides, rotating rectangles and re-entrant hexagonal structure were used for making weft-knitted auxetic fabrics by Hu et al. [17], as shown in Figure 2-49. For the fabric formed with rotating rectangles, the Poisson's ratio of the experiments increased with the increasing strain, however, the calculated value decreased with the increasing strain. This can be explained by the rotating model which assumed rigid rectangles and each rectangles can be rotated freely under tension. In the knitted fabric, the rectangles can be deformed as parallelograms and the rotation of them is limited by the connected yarn between the rectangles. For the fabric based on the re-entrant hexagonal structure, similar behaviour was observed, that is, opposite trends between the experiment and calculated value. Therefore, the calculated model was not suitable for predicting auxetic behaviour of the fabrics based on rotating units and re-entrant structure.

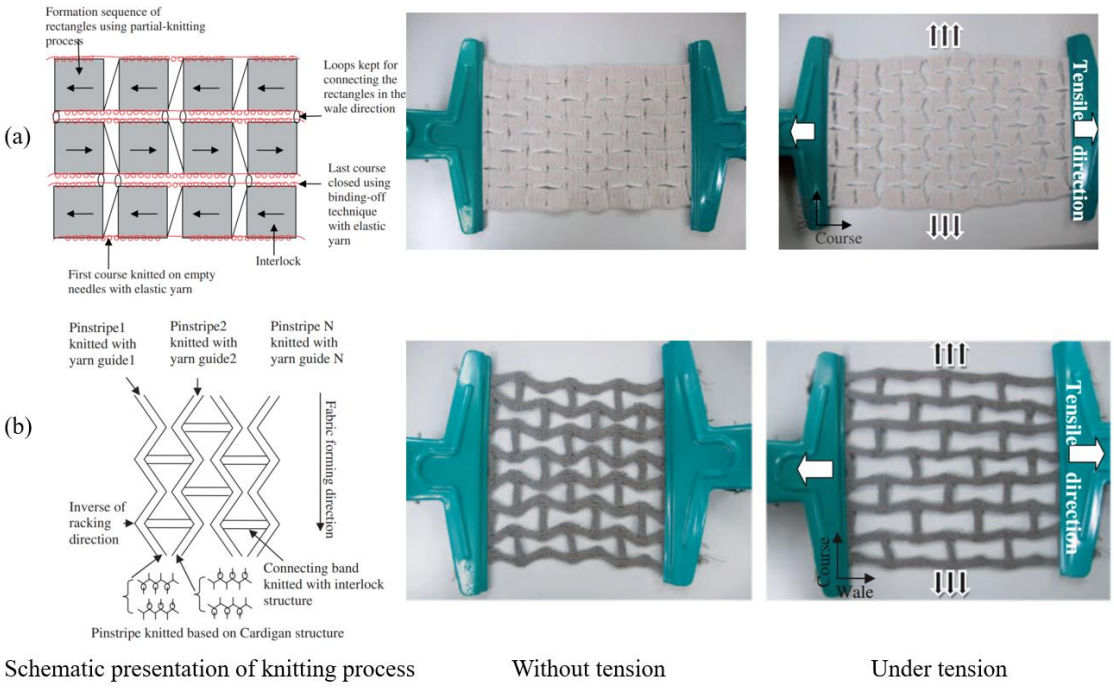

Figure 2-49 Weft-knitted auxetic fabrics: (a) formed with rotating rectangles; (b) formed with re-entrant hexagonal structure [17]

Warp-knitted auxetic fabrics can be made using various structures either single or double faced, such as chain stitches [164], double arrowhead structure [165] and rotating structures [166]. Ugbolue et al. [164] studied warp knitted fabrics with several geometrical configurations by using filling yarn inlays. The base structure was formed by the wales of chain and the fabric was produced by the minimum of two guide bars to the maximum of six guide bars. The wales were constructed from open loops with soft thicker filaments and the stiffer filament was inlaid shown in Figure 2-50 (a). When a tensile loading is applied, the auxetic behaviour is achieved by the straightening of the stiffer filament and the combination of the wales in an appropriate manner, shown in Figure 2-50 (b) and (c). Such inlay auxetic knit structure is similar to the geometrical model reported by Gaspar et al. [60] and Smith et al. [59]. Besides, Ugbolue et al. [167] further developed the warp-knitted auxetic fabric based on a re-entrant hexagonal structure. The structure was formed by combining inlay yarn and hexagonal nets and different parameters on Poisson's ratio were also discussed, such as yarn type, strain level and number of chain courses. It was noted that the stiffness of the yarn is the most important parameter, which can determine the Poisson's ratio being negative or positive.

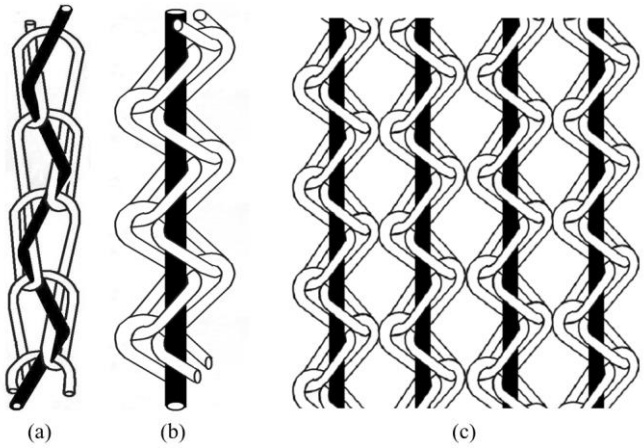

Figure 2-50 Warp-knitted structure formed by wales of chain and inlay yarns [164]

Double arrowhead structure is another structure that can be used for warp-knitted auxetic fabric. Alderson et al. [165] produced four textile structures based on the double arrowhead structure exhibiting negative Poisson's ratio. The main concept of the fabric is to form the double arrowhead structure consisting of two components. One is the auxetic component using open loop stitches and the other is the stabilizing component. It was confirmed that the auxeticity of the fabric is shown at ±45˚ to the warp direction, with negative Poisson's ratio value up to -0.22±0.03.

Ma et al. [166] conducted four similar warp-knitted structures based on a rotational hexagonal structure, as illustrated in Figure 2-51. The fabrics were manufactured by two components. The first component was called basic component, which can balance the hexagonal structure. The second component was called deforming component, which can provide unevenness of the basic component causing rotation of the structure. When the fabric is stretched laterally or longitudinally, the hexagons will recover to the original shape, leading to the expansion of the fabric. Structures of the front bar and let-off values of front bar chain stitches were investigated. It can be concluded that the less needles the front bar traverses across and the larger let-off values, the more auxetic behaviour achieved.

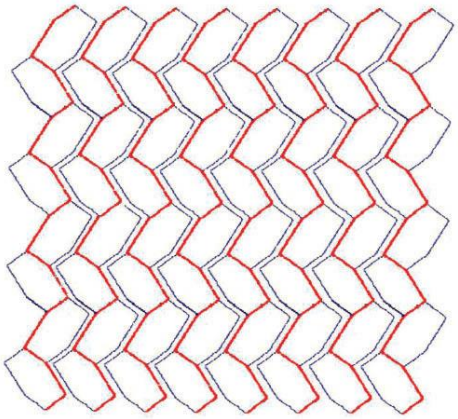

Figure 2-51 Rotational hexagonal structure of warp-knitted fabric [166]

2.4.3.3 Nonwoven fabrics

Nonwoven technology is used to produce a fabric directly from fibres, so the spinning process of the yarn is omitted. The nonwoven fabrics have been made for various applications, such as medical textile, automotive and civil engineering industry, due to their low price and short fabricating period. Based on the literature, auxetic nonwoven fabrics are mainly manufactured by using two methods, including heat-compression treatment and laser cutting.

By adopting the heat-compression treatment, Verma's group produced needle-punched nonwoven fabrics exhibiting out-of-plane auxetic behaviour [168, 169]. PET crimped staple fibres were used for making the nonwoven fabrics and fabric samples were compressed at 2.45 MPa pressure with 20 hours heating temperature of 70˚C, coded as heat-compressed samples. Then, additional samples were prepared using the same compression route without heating for comparison purpose, coded as compressed samples. All samples were subjected to the thickness recovery test and the auxetic behaviour measurement. It was found that both heat-compression and compression samples demonstrated out-of-plane auxetic behaviour. Especially, the magnitude of auxetic behaviour was larger in heat-compressed samples due to the tilted and buckled vertical fibre bundles after the heat-compression treatment, as shown in Figure 2-52. The angle of the buckled bundles was opened up with the increasing strain, leading to the increased thickness of the nonwoven. Recently, Verma et al. [170] produced heat-compressed wool nonwovens which exhibited the maximum negative Poisson's ratio of -8.3±0.8. The nature of the deformation is

similar to the polyester nonwovens above and the auxetic behaviour is more obvious with the increasing temperature of the treatment.

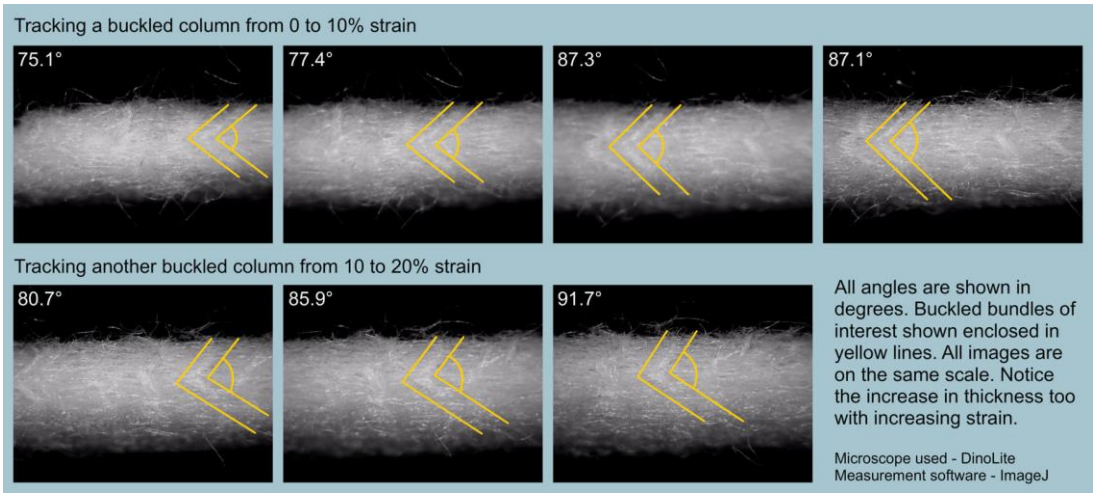

Figure 2-52 Thickness view of the treated nonwoven sample [169]

By using the laser cutting method, Bhullar et al. [171] fabricated a nonwoven auxetic polymer stent which can improve the biocompatibility and the drug reservoir capacity in biomaterials. Polycaprolactone (PCL) microfibre and PCL auxetic sheet were produced using femtosecond laser machine, containing the auxetic structure of rotating squares, as shown in Figure 2-53. It was found that the stenting performance was improved by the auxetic structure and the maximum negative Poisson's ratio of the PCL machined sheet and PCL microfibre sheet was -1.105 and -1.0208, respectively. With the same auxetic structure of rotating squares, Dobnik Dubrovski et al. [172] reported a modified nonwoven Silon fabric by using laser cutting, exhibiting in-plane auxetic behaviour. The nonwoven fabric with smaller rotating squares demonstrated higher auxetic behaviour. Also, equal distribution and orientation of the fibres can exhibit a better auxetic performance with a smaller out-of-plane rotation of the squares.

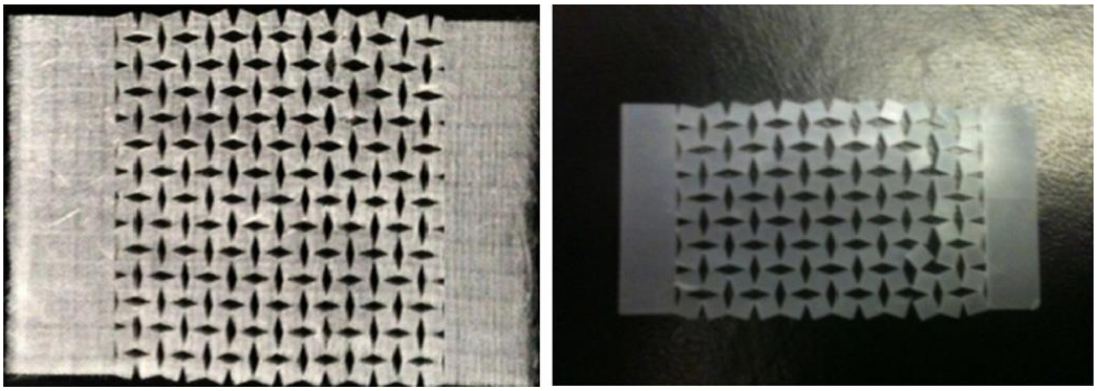

Figure 2-53 Micromachined-polycaprolactone (PCL) microfibre and machined PCL auxetic sheet [171]

2.4.4 Three-dimensional fabrics

Auxetic three dimensional fabrics can be made using conventional textile technologies, such as weaving, knitting and braiding. They can also be used as textile reinforced composites, which could provide enhanced property of the materials.

2.4.4.1 Woven fabrics

Ahmed et al. [173] reported 3D auxetic woven fabrics made of para-aramid and ultra-high molecular weight polyethylene (UHMWPE) yarns by using traditional weaving machines. Different orthogonal structures were produced and one of the samples is shown in Figure 2-54. When the 3D fabric is stretched in the horizontal direction, the binder yarn tends to be straightened, forcing the other yarns out-of-plane. The results showed that the float length of warp and binder yarns significantly influenced the Poisson's ratio and the Poisson's ratio decreases with the increasing float length. By using the 3D orthogonal structure, the woven fabric is used for textile reinforced composites for technical applications and these will be reviewed in Section 2.4.4.4.

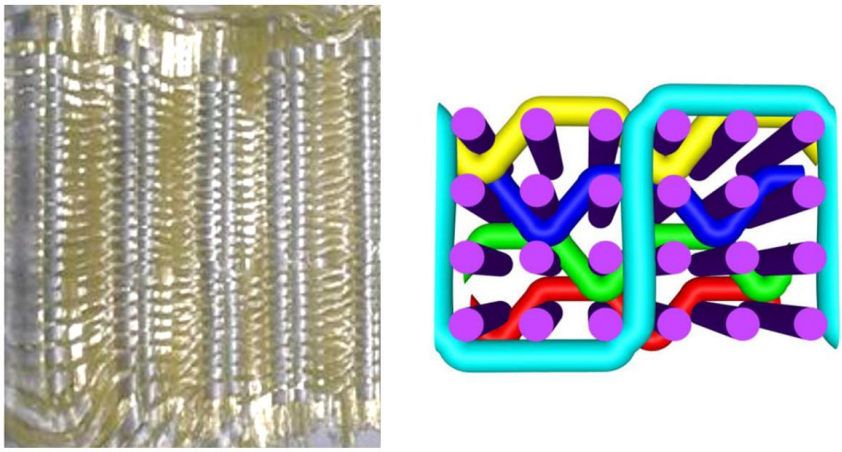

(a) (b)

Figure 2-54 3D auxetic woven fabric with orthogonal structure: (a) real fabric with warp pattern 2/1 and binder pattern 3/3; (b) weft wise cross-sectional view [173]

2.4.4.2 Knitted fabrics

Spacer fabrics are unique forms of three dimensional fabrics as they consist of two fabric layers jointed but kept apart by spacer yarns [174]. According to the literature, the majority of the 3D and spacer fabrics are based on the warp knitted technology and the properties of the fabrics are not only focused on the auxeticity but also concentrated on the improvement of stiffness and energy absorption [19, 173-185]. Liu et al. fabricated a series of auxetic warp-knitted spacer fabrics with different structural parameters, such as fabric thickness, surface layer structure, spacer monofilament inclination and fineness [175]. To achieve better energy absorption capacity with high efficiency, the spacer fabric was suggested to be set with a higher inclination angle of the spacer yarn, lower fabric thickness, thicker spacer yarn and smaller size mesh of the outer layers [176]. Such auxetic spacer fabric can be used for cushioning applications due to its easily tailored, similar performance but better moisture transmission compared to the conventional cushioning materials.

2.4.4.3 Braided fabrics

Braiding technology is a unique textile preforming process to form a narrow strip of the fabric, combining the features of woven and near-net capability of yarn winding [186]. Braided fabrics provide many advantages due to their great dimensional stability, strength and ability to construct various shapes, but the investigation of the auxetic fabrics using braided structures are still limited so far [3]. According to the literatures, the auxetic braided fabric can be made by two different methods. One is

using auxetic yarns braided into a fabric and the other is using conventional yarns in braided fabric, mimicking the helical structure of the auxetic yarn.

By the use of helical auxetic yarns, Shen [187] fabricated a tubular braiding fabric made of helical auxetic yarns and a finite element model was built for analysing the auxetic behaviour of the structure. Two polyester yarns with different stiffness and diameters were selected for making helical auxetic yarns, and such auxetic yarns were used as the components to produce the tubular braided fabric, as shown in Figure 2-55 (a). The open area of the braided fabric is decreased at first and then gradually increased after 250 N of axial force, as shown in Figure 2-55 (b). This can be explained by the fact that the auxetic behaviour of the yarn components and the decreasing cross angle under axial force. Most importantly, the increasing width of the auxetic yarn reduces the open area of the braided fabric and the decreasing cross angle shows the opposite effect.

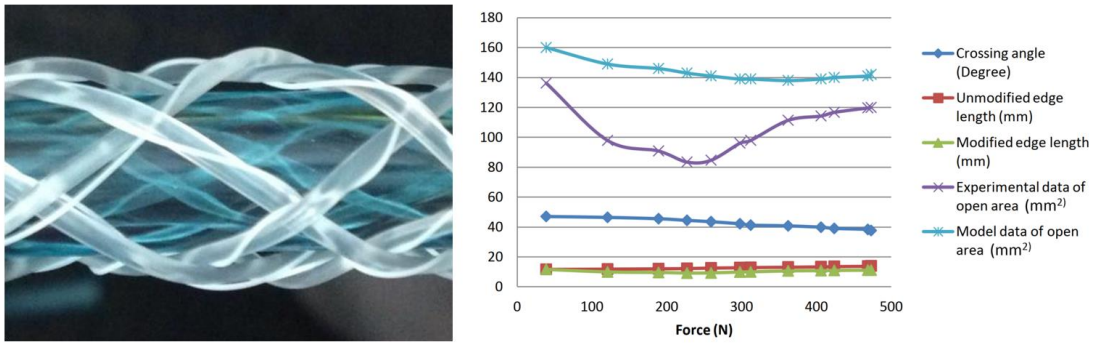

(a) (b)

Figure 2-55 Braided fabric made of helical auxetic yarns: (a) biaxial tubular structure; (b) experimental and simulation results [187]

Afterwards, Shen and Adanur [188] further developed the auxetic braided fabric based on the same method. They conducted a mechanical analysis by combining experimental results and a multi-scale finite element model. It was confirmed that the open area in biaxial structure is decreased under tension because of the local auxetic behaviour of the yarn. Two major factors on fabric permeability were addressed including the auxeticity of the yarn and the decreasing cross angle under tension.

By the use of conventional yarns, a novel type of auxetic braided structure was reported by Jiang and Hu [85] and the structure was based on the helical structural arrangement. This type of structure can also be used for overcoming the structural problem of the double helix yarn. As shown in Figure 2-56, the structure is formed by

the fine stiff wrap yarn and the tubular braided yarn, where the wrap yarn is wound around the braided structure and fixed by four evenly spaced points. Then the wrap yarn straightens under tension, forcing the braided structure into a wave shape. Therefore, the cross-sectional contour diameter of the structure is increased, leading to the auxetic behaviour of the whole braid. Additionally, three structural parameters on Poisson's ratio were discussed, including initial wrapping angle, initial braiding angle and the diameter of the braiding yarn. They pointed out that the lower wrapping angle, higher braiding angle and larger diameter of the braiding yarn lead to better auxetic behaviour. Such novel braided structure was suggested for solid knots which can be used in medical sutures, secure threads and shoelaces.

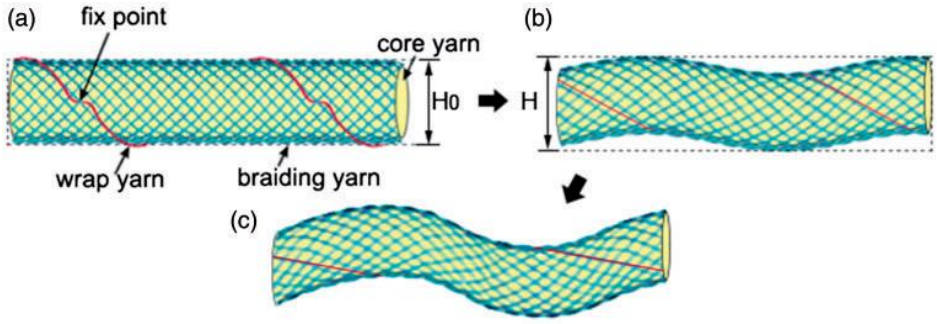

Figure 2-56 Auxetic braided structure using conventional yarns: (a) without tension; (b) under tension; (c) maximum contour size [85]

2.4.4.4 Textile reinforced composites

Auxetic textile reinforced composite has become a popular research area in textiles due to its superior properties compared to conventional textile composites. According to Alderson et al. [189], textile reinforced composites can be made from conventional materials or auxetic components. By using the conventional materials, the auxetic behaviour is achieved by the angle ply structure of the assembling sequences, whereas by the use of auxetic components, the auxeticity is directly inherited from the component, such as the auxetic fibres.

Based on the conventional materials, Herakovich [190] first reported the composite laminates with negative Poisson's ratio in thickness direction by using the theory of two-dimensional lamination. The auxetic behaviour highly depends on the fibre alignment in each ply of the composite, resulting in the range of Poisson's ratio from 0.49 to -0.21.

Zhou et al. [191] investigated 3D auxetic textile composites containing polyurethane foam, as shown in Figure 2-57. The warp, weft and stitch yarns were selected for making the 3D orthogonal structure and the auxetic behaviour was achieved by the different placements of the warp yarns. Then, the 3D structure was fixed by the designed mold and the polyurethane foam was fabricated as matrix by the injection and foaming process. It was found that the auxetic composites contract in lateral direction under compression in contrast to the non-auxetic composites. Apart from the weaving technology [16, 18, 135, 191-196], auxetic composites can be made using other textile technologies, such as knitting [197-201] and braiding [202].

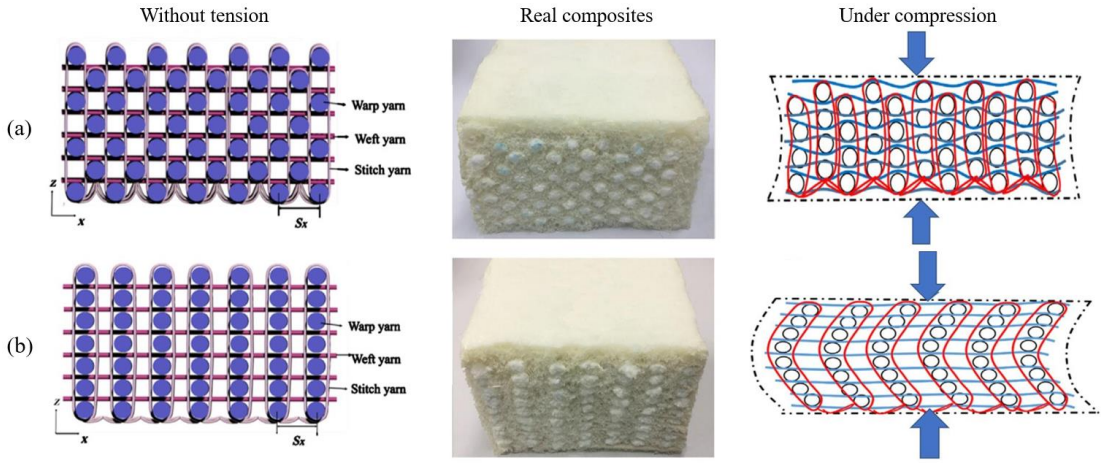

Figure 2-57 3D auxetic composites: (a) auxetic; (b) non-auxetic [97]

By using auxetic materials, Miller et al. [135] first manufactured a carbon fibre composite containing auxetic yarns, as shown in Figure 2-58. Carbon fibre and nylon monofilament were selected for making the auxetic double helix yarn and polyester resin was used as the matrix material of the composite. In order to maximise the auxeticity of the yarns, they were arranged and placed parallel in a mould in the form of out-of-register. Compared to other auxetic composites, the unidirectional textile composite exhibited both high stiffness of 4 GPa and negative Poisson's ratio of -6.8, which has great potential for various engineering applications.

Figure 2-58 Carbon fibre composite sample during tensile test [135]

Recently, Moshtaghian et al. [199] developed 3D composites with newly-designed multi-cell flat-knitted spacer fabrics, exhibiting a high negative Poisson's ratio between -6 and -1 under compression. It was noted that the 3D re-entrant composite demonstrates the highest auxetic behaviour due to the rapid bulking and concentration of stress of the cell walls, getting the unit cells closer together. The developed 3D composites offered a high resistance under compression and high energy absorption which could be seen as a candidate for sandwich panels.

2.5 Research areas for auxetic textiles

After the literature reviews, it was found that the research area related to auxetic textiles are in three perspectives, including development of manufacturing techniques, characterisation methods, mathematical modelling and design. Some of the researchers are working on the manufacturing techniques of auxetic yarns and fabrics, utilising the experimental methods to get the auxetic structures manufactured. The existing textile machinery is used, but the new developed or modified machinery is also necessary if the structure is very complicated. Some researchers focus on the mathematical modelling and design, such as the re-entrant and hexagonal structure design. The others concentrate on the characterisation of the auxetic textiles, such as impact resistance and energy absorption, which could provide a reference for many potential applications.

2.5.1 Manufacturing techniques

To achieve auxetic behaviour of the yarns and fabrics, manufacturing techniques have attracted many textile researchers especially exploring how to combine the conventional materials together. For helical auxetic yarns, different machineries were

used, such as the machine with ring-spinning system [139], the bespoke spinner [142], two-head braiding machine with a bobbin [151] and locally developed wrapping machine [153]. It was reported that majority of the auxetic yarns can be produced by the existing spinning machinery, however, some researchers also built a small-scale machinery which was convenient for lab investigation [148]. As shown in Figure 2-59, the yarn spinning device is created for manufacturing lab-scale lengths of helical yarns. Different numbers of strands are fed through the guiding board and the twisted strands are held in the clamp which is controlled with a moveable board on the left and a rotating handle. During the process, the handle can rotate and move backward manually, drawing free ends of strands in the yarn forming zone. By using the device, the yarn twist is established by the feeding length of the strands and it is suitable for making multi-strand auxetic yarns because the industry machines are not easily controlled.

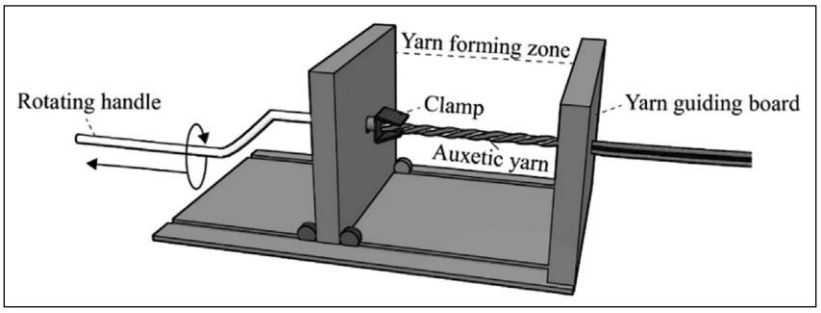

Figure 2-59 Schematic diagram of yarn spinning device [148]

Due to the elasticity of the yarn materials, the woven fabric made of auxetic yarns is mainly produced on a hand loom [86, 151], so the yarns can be controlled and reorganised during the fabrication. Whereas for the woven fabric made of non-auxetic yarns, the electronic machinery is used, such as air-jet loom with dobby shedding system [156], a rapier weaving machine [160] and Jacquard loom [158], because the auxeticity of the fabric comes from the shrinkage behaviour of different weave structures rather than the helical structure of the yarns. Compared to warp knitting and circular knitting technologies, flat knitting technology is a preferred used method for producing auxetic knitted fabrics due to its great process flexibility. The flat knitting machine offers individual needled selection, binding-off technique, knitting different stitches in the same course and easily adjustment of knitting parameters, so it can realize various auxetic geometries including foldable geometry, rotating rectangles and re-entrant hexagons [17]. For auxetic nonwoven fabrics, the auxetic behaviour is

determined by the other treatments of the needle-punched fabrics, such as heat-compression [169, 170] and laser cutting [171, 172, 203]. Then, by using tubular braiding technology, the auxetic braided fabrics can be made as well. Similar to the construction of the helical auxetic yarn, the auxeticity of the braided fabric comes from the arrangement of the stiff yarn and the soft yarns, as the stiff yarn is helically braided into the structure [85]. Additionally, helical auxetic yarns can be directly used for the tubular braided fabric, leading to the reduced open area of the structure [188].

2.5.2 Characterisation methods

The purpose of manufacturing auxetic textiles is to have a better understanding on the mechanical properties so the materials can be used for technical applications in real life. Different characterisation methods have been reported, such as tensile testing, Poisson's ratio measurement, compressive testing, puncture resistance test [157], impact examination and air permeability check.

To observe the deformation of the auxetic yarns and fabrics, the measurement is highly relied on the video recording or snapshots of the testing machine. For example, the auxetic yarn was subjected to the Shimadzu AGS-10KN D testing machine with a video extensometer system [16], so the deformation of the yarn can be captured in specific strain. Similar to the yarn measurement, the deformation of the auxetic fabric was recorded by a camera during the tensile test as well [19] shown in Figure 2-60. The auxetic behaviour and open areas among the structures can be captured at 2-second intervals corresponded to the 1.1% interval tensile strain of the fabric [86]. Then, the images were exported to the image processing software, such as ImageJ, Digimizer and Matlab, for further investigation. However, some of the auxetic fabrics are not deformed along the fabric plane but in the thickness direction. For example, to measure the thickness of the auxetic nonwoven fabrics, a digital micrometer containing a flat circular platen was used. The platen could compensate the heterogeneity of the nonwoven surface and add a pressure helping to define the thickness uniformly [170].

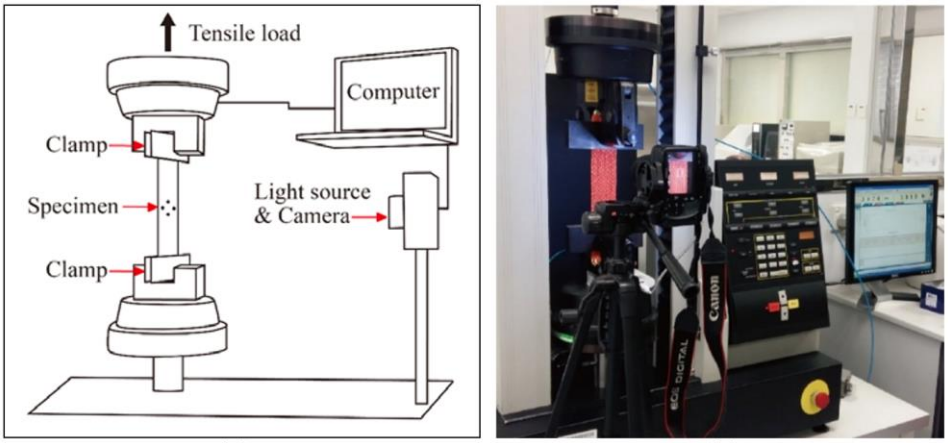

Figure 2-60 Tensile testing system with a camera: (a) schematic diagram; (b) photograph of the real machine [86]

Apart from the tensile testing and measurement of auxetic behaviour, the properties of the auxetic fabric have been evaluated using different mechanical tests. One of the promising property is the impact resistance or energy absorption. Charpy impact test method with the standard ASTM D6110 was adopted in which a pendulum is released from a measured height and then allows to fall. The swinging pendulum impacts and breaks the fabric, rising to a new height. Therefore, the difference of the height and the energy lost can be directly given due to the fracture of the fabric [194]. Generally, the designed auxetic fabrics or textile composites are compared with the conventional one in most of the studies, exhibiting better impact property and energy absorption for resistance applications.

The characterisation of auxetic textiles is not only concentrated on the mechanical properties but also focused on the variation of structural parameters. In the aspect of auxetic yarns, the helical angle is the most studied parameter in the literature, followed by the yarn dimension and stiffness. In the aspect of auxetic fabrics, the structural parameters are more complexed due to the involvement of the fabric structures. For instance, the manufacturing parameters of the auxetic woven fabric are evaluated including the auxetic yarns used in the fabric, the warp yarn [86], weave structures [155] and auxetic yarn arrangements.

2.5.3 Mathematical modelling and design

2.5.3.1 Yarns

Finite element (FE) modelling is a popular method in textiles for engineering and mathematical design. Setting up a mathematical model will help researchers to predict the properties of the materials and structures, however, the model is inevitably too idealised.

Wright et al. [14] first conducted a numerical study of helical auxetic yarns by using the commercial software ABAQUS V6.8-3, as shown in Figure 2-61. The geometric yarn model was created by SolidWorks software before inputted for FE analysis and all models were set as C3D10M element with default tolerances. Based on the yarn properties shown in Table 2-5, effects on Poisson's ratio were investigated including boundary conditions, mesh density, core/wrap diameter ratio, wrapping angle and core/wrap tensile modulus. Among the different cycles (3, 5, 10, 20 and 50 cycles) of the yarn model, the 10-cycle model was selected for investigation because the result of it lies within 1.5% of the model with the largest cycle. Wright et al. [14] pointed out that the combination of the diameter and modulus should be considered at the same time for optimising auxetic behaviour. However, the limitation in practical situations still existed due to the finite positive Poisson's ratio of the two plies.

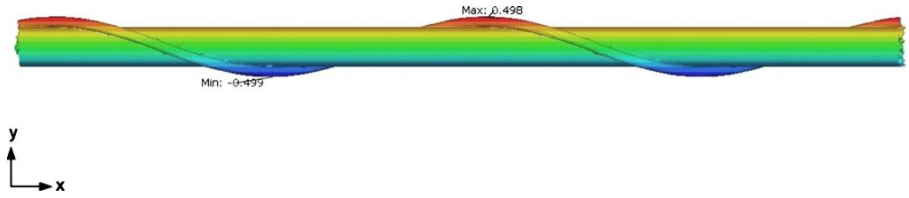

Figure 2-61 Helical auxetic yarn model [14]

Table 2-5 Properties of the yarn model [14]

	Material	**Diameter (μm)**	**Tensile modulus (MPa)**	**Poisson's ratio**
Core ply	Polyurethane	648.5	150	0.45
Wrap ply A	Polyamide	97.4	10000	0.45
Wrap ply B	Polyamide	174.5	10000	0.45

Du et al. [147] adopted the FE analysis of the helical auxetic yarn under tension using ABAQUS software. Their work manifests four key variables on Poisson's ratio, including mesh size, diameter ratio of the two plies, helical angle and tensile modulus

of the wrap ply. Firstly, three mesh sizes of the core were determined as 0.06 mm, 0.08 mm and 0.1 mm, while the mesh size of the wrap was 5 times larger than that of the core. With the wrap/core diameter ratio of 1:4, the yarn model met the accuracy of the theoretical result when the mesh size of the core and wrap were set as 0.06 mm and 0.3 mm, respectively. It was revealed that the finer mesh size leads to the closer theoretical result, however, it was time consuming for making calculations if the mesh size was infinitely small. Secondly, with the same mesh size, three different wrap/core diameter ratios were determined including 0.3:0.6, 0.15:0.6 and 0.1:0.6, respectively. It was noted that a larger diameter ratio of the auxetic yarn has a better auxetic effect or a lower Poisson's ratio value. This can be explained that in order to keep the same helical angle of the yarn, the length of the wrap in one cycle is shorter when the diameter of the core decreases. Thirdly, initial helical angles of 20°, 30° and 40° were tried with the wrap/core mesh size ratio of 0.3:0.06 and the wrap/core diameter ratio of 0.15:0.6. It was shown that the helical angle of 20° expresses the best auxetic behaviour of the yarn, demonstrating the maximum negative Poisson's ratio of -3.52. Thus, the auxetic behaviour increases with the decreasing initial helical angles in terms of the reducing length of the wrap in one unit and the expansion of the core. Finally, tensile modulus of the wrap was set to the yarn model with the value of 0.93 GPa, 1.80 GPa and 3.00 GPa, respectively. With the same mesh size and diameter ratio above, it was found that the higher modulus of the wrap demonstrates a higher auxetic behaviour of the yarn. In their study, the FE method was suggested for analysing theoretical parameters of the yarn and it was helpful to design the yarn in practical situation.

Meanwhile, Sibal and Rawal [140] reported a theoretical study of dual helix yarn and the yarn system was further developed by McAfee and Faisal [146] using ANSYS® Workbench. The yarn model was set as two components which contained the material properties of carbon fibre and nylon 66, respectively. Initial length of the yarn, helical angles, Poisson's ratio and diameter of the yarn were analysed. It was found that the auxetic behaviour is more obvious with the decreasing helical angle and the angle of 7° gives the maximum negative Poisson's ratio of -12.04 as the angle of 6° stops the analysis of the model. Additionally, increasing core/wrap diameter ratio causes higher auxetic behaviour as well. Focused on the core tension of the helical auxetic yarn, Kwietniewski and Miedzińska [204] conducted a finite element analysis by using the

LS-Dyna software. It was found that the numerical model exhibits good compatibility with the experimental result and the true stress-true strain curves indicates the hardness of the material under tension.

For multi-strand auxetic yarn, Zeng et al. [205] conducted a finite element analysis of auxetic plied yarn by using the ANSYS 15.0. software shown in Figure 2-62 and the parameters on Poisson's ratio were further investigated including the tilt angle of the stiff ply, tensile modulus and friction. It was revealed that avoiding de-twisting trend of the stiff ply can improve the yarn structure. Lower friction and higher modulus of the stiff yarn can provide more significant auxetic behaviour. These can provide a guidance for designing and fabricating the auxetic yarn with plied structure.

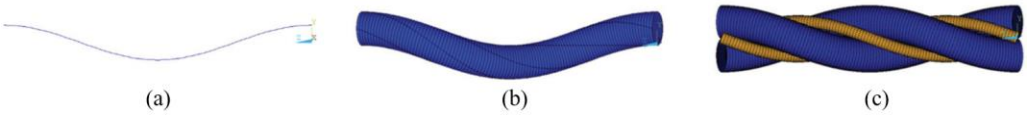

Figure 2-62 Finite element model of auxetic plied yarn: (a) one helical path of the soft ply; (b) one soft ply; (c) finite element model [205]

Geometric calculation is another wildly used method for investigating the yarn structural parameters. Generally, the deformation process of the auxetic yarn can be classified into three stages. In the first stage, the wrap ply stays on the core ply helically without tension. The outer contour of the auxetic yarn contracts during stretching initially. In the second stage, the helical radius of the wrap ply is decreased and the core ply is extended along the helical path under tension. The core ply replaces the wrap ply during the elongation of the yarn, that is, the core ply is pushed out and the wrap ply become straight in the centre of the auxetic yarn. As a result, the outer contour of the yarn is expanded. In the third stage, the wrap ply keeps the straight position, however, the radius of the wrap ply and the core ply continuously decreases until the auxetic yarn is broken.

Based on the three stages of the yarn deformation, the geometry of the helical auxetic yarn was introduced by Sloan et al. [15] and Du et al. [147]. As shown in Figure 2-63 (a), the wrap ply twines around the core ply without tension and the initial helical angle α is represented by the core length per helical cycle λ. The helical cycle of the yarn can be rolled out on a surface and a trigonometric relationship is formed in Figure 2-63 (b). Then, the initial helical angle α can be calculated by using any combination

between the λ and the diameters of the two plies, as shown in Equation (2-5). The initial diameter of the yarn D_0 is expressed in Equation (2-6).

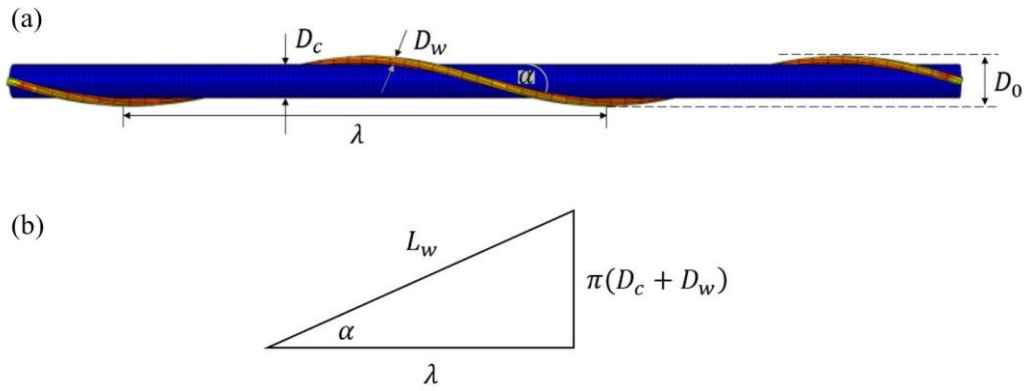

Figure 2-63 Helical auxetic yarn in the first stage: (a) geometric definitions; (b) trigonometric relationship [15]

$$\alpha = \arctan\left[\frac{\pi(D_c+D_w)}{\lambda}\right] \tag{2-5}$$

$$D_0 = D_c + 2D_w \tag{2-6}$$

In the second stage, the two plies swap their position when the load applied in the longitudinal direction is large enough, as shown in Figure 2-64. From the initial state to the fully loaded state, the helical radius of the wrap ply decreases and the wrap ply becomes in the centre of the auxetic yarn. In addition, the radius of the core ply R is changed as well during the stretching and it is given by Equation (2-7). The axial strain of the core ply can be calculated from the axial strain of the auxetic yarn, as shown in Equation (2-8). Figure 2-65 illustrates the cross-sectional graph of the helical auxetic yarn. The distance between the centre of the cross-sectional core ply and the centre of the auxetic yarn is r and it can be calculated using Equation (2-9). From the initial state to the fully loaded state, the outer contour diameter of the yarn D is the larger value of D_1 or D_2, as shown in Equation (2-10). The values of D_1 and D_2 depend on the crimp shape of the core ply and that of the wrap ply, respectively.

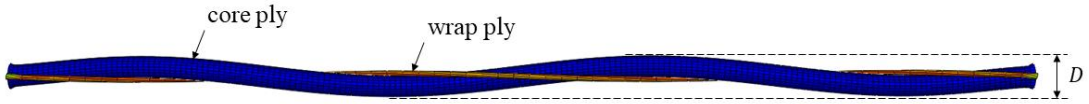

Figure 2-64 Helical auxetic yarn in the second stage (fully loaded stage) [147]

$$R = R_0 - v_c\varepsilon_c R_0 \tag{2-7}$$

where R_0 is the initial radius of the core ply. v_c and ε_c are the Poisson's ratio and axial strain of the core ply, respectively.

$$\varepsilon_c = \frac{\sqrt{(2\pi r)^2+\lambda_0^2(1+\varepsilon_t)^2}-\lambda_0}{\lambda_0} \tag{2-8}$$

where λ_0 is the initial core length of one helical cycle and ε_t is the axial strain of the auxetic yarn.

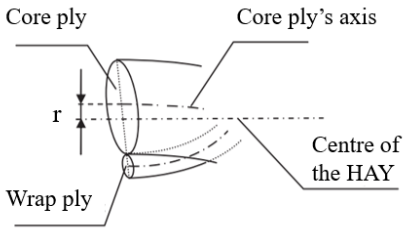

Figure 2-65 The expanded graph of the helical auxetic yarn [147]

$$r = \left(R + \frac{D_w}{2}\right) - \frac{L_w \sin\alpha'}{4\pi}$$

$$= \left[R_0\left(1 - v_c\frac{\sqrt{(2\pi r)^2+\lambda_0^2(1+\varepsilon_t)^2}-\lambda_0}{\lambda_0}\right) + \frac{D_w}{2}\right] - \frac{L_w \sin\alpha'}{4\pi} \tag{2-9}$$

where α' is the helical angle of the auxetic yarn during the deformation.

$$D_1 = 2(R + r)$$

$$D_2 = D_w + \frac{L_w \sin\alpha'}{2\pi}\ , \alpha' \in (\alpha, 0) \tag{2-10}$$

After the wrap ply is straightened, further loading makes the auxetic yarn thinner until the wrap ply is broken. So, in the third stage, the outer contour diameter of the yarn depends on the period of the helical shape of the core ply and the helical radius of the core ply axis r is expressed in Equation (2-11).

$$r = R + \frac{D_w'}{2} \tag{2-11}$$

where R is the radius of the core ply under tensile loading and D_w' is the diameter of the wrap ply under tensile loading.

By using Equation (2-11), the outer contour diameter of the yarn D is calculated as follow:

$$D = 2(R + r) \tag{2-12}$$

Recently, Liu et al. [206] proposed a mechanical model of helical auxetic yarn based on the previous geometric model which was reported without interaction force between the two plies. The mechanical property and deformation in radial direction should both consider in the model and the model of the core is formed as an elliptical shape in the second stage mentioned above. Additionally, 5% lag of radial strain was applied in the calculation for achieving better accordance with the experiments of the Poisson's ratio.

Zeng and Hu [207] conducted a theoretical analysis of auxetic plied yarn based on their previous study on the plied structure. Similar to the two-ply structure of the yarn, the deformation of the four-ply yarn was classified into three stages as well. The radial strain ε_r and the Poisson's ratio of the yarn v are expressed in Equation (2-13) and (2-14), respectively. Also, the tilt angle model and the diameter ratio between the soft ply and stiff ply were developed, which provide better understanding of the auxetic plied yarns under tension.

$$\varepsilon_r = \left(\frac{H}{H_0} - 1\right) \times 100\% \tag{2-13}$$

$$v = -\varepsilon_r / \varepsilon_{axial} \tag{2-14}$$

where H and H_0 are the initial state and stretched state of the maximal thickness of the plied yarn.

Consequently, the parameters of the auxetic yarn can be analysed by using the geometric calculation, such as the initial helical angle (tilt angle), the outer contour diameter and Poisson's ratio of the yarn. The method was also conducted by Wright et al. [136], Ge et al. [23] and Zhang et al. [208] for auxetic yarns and the assumption of them provide a clue on yarn production.

2.5.3.2 Fabrics

Finite element analysis is the most popular numerical method which could assist the experimental analysis for further investigation. If the finite element model is validated, it would give more detailed information for researchers because some of the data

cannot be achieved for the experiments due to the sensor of the testing machine. Through the investigation of auxetic fabrics, the simulated model could dive into the process and get more data out, helping researchers to fully understand the nature of the auxetic behaviour.

Ge et al. [192] conduced a finite element analysis of the auxetic 3D fabric after their experimental work [18]. The model was established by ANSYS software and the front view of the unit cell under compression is shown in Figure 2-66. It was confirmed that the auxetic behaviour of the fabric structure is increased with the increasing compression level. Most importantly, the simulated model can provide a better understanding on auxeticity and the structural parameters of the fabric were drawn. It was found that the increased ratios of radii and moduli between the warp and weft, and decreased spacing between the adjacent warps could generate a higher auxetic behaviour.

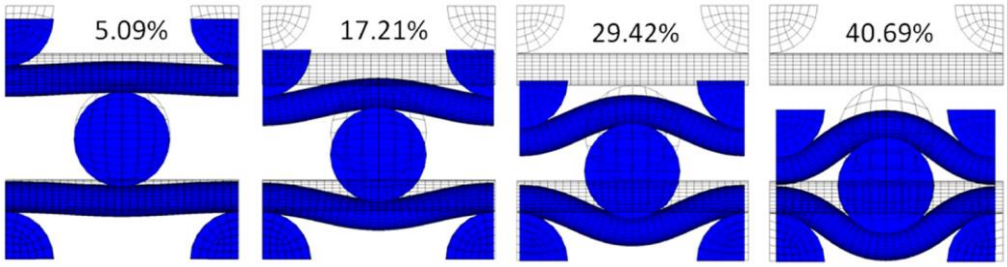

Figure 2-66 Front view of the 3D fabric model under different compression strain [192]

In order to observe the details of the auxetic structure, the simulated model can be created for knitted fabrics [179], 3D woven fabrics [209] and braided fabrics [187, 188]. Luan et al. [210] presented a finite element model for a weft-knitted Miura-ori fold fabric which was referred to the auxetic foldable structure, as shown in Figure 2-67. They found that the fabric thickness, knit patterns and the angle between the neighbouring edges shown in Figure 2-67 (c) are the key parameters for achieving better auxetic behaviour. However, the simulated results of the force were slightly higher than the experimental results as the yarn interactions and slippages were neglected in the model.

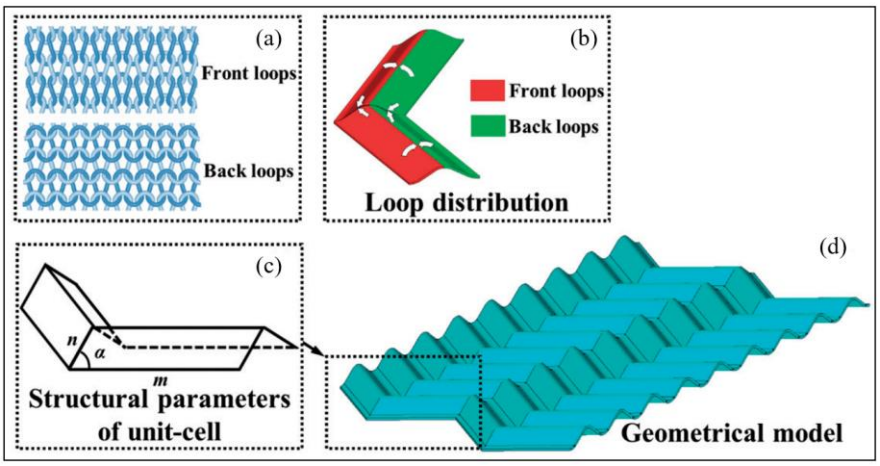

Figure 2-67 Finite element model of the foldable knitted fabric: (a) micro-scale knit loops; (b) meso-scale unit cell; (c) constructive parameters; (d) macro-scale geometrical model [210]

Geometrical analysis can also provide a better understanding in a theoretical way. Recently, Kamrul et al. [211] reported a geometrical model of auxetic woven fabric containing foldable geometry. The model was analysed when stretched in warp and weft directions, as illustrated in Figure 2-68. Then, two semi-empirical equations between the tensile strain and Poisson's ratio are established in each direction shown in Equations (2-15) and (2-16), respectively. The equations are useful for predicting and designing the auxetic woven fabrics made with foldable geometry.

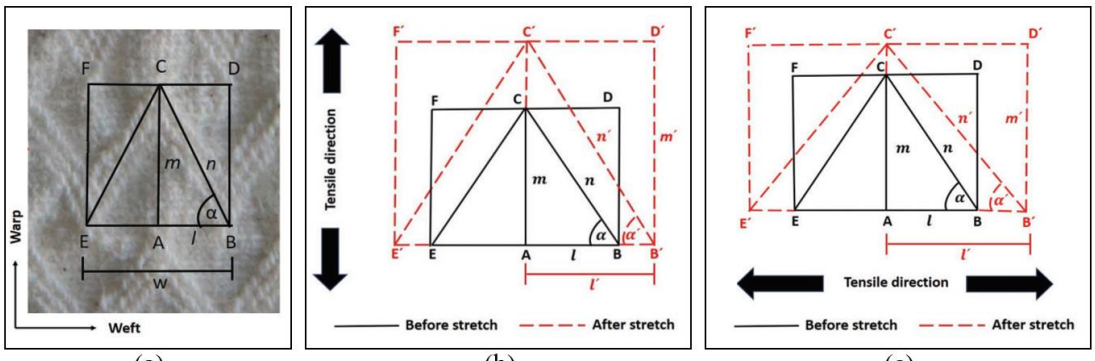

(a) (b) (c)

Figure 2-68 Geometrical model: (a) unit cell without stretching; (b) deformation of the unit cell when stretched in the warp direction; (c) deformation of the unit cell when stretched in the weft direction [211]

$$v_{warp} = -\left[\frac{\sqrt{(0.9089\varepsilon_k+1.0151)^2-\{(\varepsilon_k+1)\sin\alpha\}^2}-\cos\alpha}{\varepsilon_k\cos\alpha}\right] \quad (2\text{-}15)$$

$$v_{weft} = -\left[\frac{\sqrt{\left(-0.28\times10^{-5}\varepsilon_k^2+0.412\varepsilon_k+1.128\right)^2-\{(\varepsilon_k+1)\cos\alpha\}^2}-\sin\alpha}{\varepsilon_k\sin\alpha}\right] \quad (2\text{-}16)$$

where v_{warp} and v_{weft} are the Poisson's ratio when the fabric stretched in warp and weft directions, respectively. ε_k is the tensile strain of the fabric and α is the angle of the structure shown in Figure 2-68 (a).

2.6 Summary and research gaps

In this Chapter, the literature on auxetic materials and structures has been reviewed thoroughly, including various geometric structures, superior properties, different types of materials and applications. Especially, auxetic textiles with focused research areas are presented in details. In the past three decades, auxetic textiles, including fibres, yarns and fabrics, have been made and developed by using experimental analysis, geometric calculation and finite element modelling. Although many remarkable achievements have been reported, there still exist some interesting problems and gaps which need further investigation.

For the aspect of auxetic yarns, the double helix structure is the most common structure of the yarn for achieving auxetic behaviour. Based on the literatures of auxetic yarns, it was found that producing a stable two-ply structure of the yarns remains to be a challenge, with matched lengths of the two components, that influences the auxeticity of yarns to a great extent. One of the serious concern of the helical auxetic yarn is the poor structural stability problem. As mentioned in Section 2.4.2, the double helix yarn consists of two components, a thicker soft core ply and the finer stiff wrap ply. When the two plies twist together, the wrap ply would have some loops, that is, the wrap ply cannot firmly wrap around the core ply, leading to the torque and slippage problem of the auxetic yarn. In order to fix the problem, several methods are reported, such as silicone rubber gel coating and adding a polyamide filament for heat treatment. They are all based on the use of the third materials and the auxetic behaviour is reduced by using this kind of method. Another group of researchers focused on changing the manufactured form of the yarn based on helical structure, such as sewing and braiding, so the wrap ply can be fixed by some connected points. In this study, the structural problem of the double helix yarn is investigated based on the machinery settings, rooted in the control of tension applied to the two plies, which has not been studied in

the literatures so far. In addition, according to the literatures of auxetic yarns, the key parameters on Poisson's ratio have been reported, including wrapping angle, diameter ratio and tensile modulus. However, the range of each parameter still needs further expansion for general principles and the yarn cross-sectional shape should also be considered.

For the aspect of auxetic fabrics, auxetic yarns can be directly used for making a woven fabric, so the fabric exhibits auxetic behaviour. However, the major drawback of the woven fabric is that the auxetic behaviour cannot be fully inherited from the auxetic yarns due to the interlacement of the weave structure. Although some effects of auxetic plied yarn for woven fabrics have been investigated, including yarn arrangement, component properties, weave structure and weft yarn type, the mechanical properties of auxetic woven fabric made of double helix yarns still need to be developed systematically by using experimental method and numerical simulation. According to the literatures, the auxetic woven fabrics are produced by adopting helical auxetic yarns either in the warp direction or in the weft direction. Therefore, it is necessary to further investigate the auxetic yarns used in both warp and weft directions.

Considering all the research gaps of auxetic yarns and woven fabrics, a series of methodology will be proposed and the principles for maximising auxetic behaviour of the yarns and woven fabrics will be presented in the following sections, using experimental analysis and numerical simulation.

Chapter 3 Research Methodology

3.1 Research strategy

The purpose of this research is to find out the best mechanical principles for producing auxetic yarns and woven fabrics. Polyurethane multifilament yarn and polyamide 6,6 yarn are used for this research because they are easy to obtain and widely applied in various textile applications. The research strategy contains auxetic yarn level and auxetic woven fabric level.

As explained in the previous Chapter, the helical auxetic yarn (HAY) has a structural problem during the spinning process, rooted in the control of tension in the two comprising plies. As such, solving the structural problem is the first priority for yarn manufacture. After the successful making of HAYs with acceptable quality, a wide range of yarns is developed with different parameters, including the cross-sectional shapes, initial helical angles, thickness of the yarn and the tensile moduli of the two plies. A series of tensile testing is carried out to understand the variation of the auxetic behaviour influenced by these four parameters and the results are analysed in Chapter 4.

Based on the understanding of HAYs, the yarns are selected for making woven fabrics, in order to examine the influence of auxetic HAYs on the auxetic behaviour of the resulting fabrics. According to the variations in HAY arrangement in the fabric, fabric density, helical angles and thickness of the HAYs, weave structures, warp yarn types and loading directions, different types of woven fabrics are designed and fabricated. Such made auxetic woven fabrics are investigated for auxeticity as well as their tensile property, porosity and impact property, followed by the parametrical analysis and discussion on the roles of key factors on the Poisson's ratio of the fabrics. It is anticipated that general principles for making auxetic woven fabrics are to be established, providing guidance for fabricating woven fabrics with meaningful auxeticity.

The combination of experimental research and numerical simulation is used for characterising the yarns and woven fabrics for auxeticity. The reason for using experimental and finite element (FE) methods is that the experiments produce real data and the responses of the materials, but sensors that pick up the experimental data

cannot be placed in all the locations preferred. The FE method is advantageous in obtaining more detailed responsive technical information of the materials.

3.2 Materials selection

According to the literature review, the auxeticity of helical yarns is rooted in the different linear densities and Young's moduli of two types of materials. In this research, the polyurethane (PU) multifilament yarn and the polyamide (PA) 6,6 yarn are used, which were purchased from HYOSUNG TNC (Korea). The basic information of the yarns are summarised in Table 3-1.

Table 3-1 The PU and PA 6,6 yarns specification

	Polyurethane (PU) multifilament yarn	Polyamide (PA) 6,6 yarn
Linear density	241.1 tex	16.5 tex
Volume density	1.54 g/cm^3	1.14 g/cm^3
Poisson's ratio	0.48	0.42
Young's modulus	30 MPa	1850 MPa

For the yarn property point of view, the superelastic polyurethane multifilament yarn has a low stiffness and a large linear density, which is favourable for selection as the core ply of the helical auxetic yarn. The polyamide 6,6 yarn has higher modulus and finer diameter. Therefore, it is the best option for the wrap ply of the helical auxetic yarn. Then, for the purely academic point of view, PU and PA 6,6 materials are widely used in textiles and they are the most studied materials in the area of auxetic yarns. At last, for the practical point of view, these two types of yarns are easy to obtain and they are not expensive for the lab-scale research.

3.3 Manufacture of auxetic yarns and fabrics

3.3.1 Auxetic yarns

To produce helical auxetic yarns (HAYs), a highly elastic polyurethane multifilament yarn of 241.1 tex and a conventional Polyamide 6,6 of 16.5 tex multifilament yarns were selected as the core ply and the wrap ply, respectively. A hollow spindle fancy-yarn machine (model GDM/MK2/M manufactured by Gemmill & Dunsmore Ltd) was used for yarn production, where the core and the wrap can be twisted together with

different parameters by changing the yarn delivery speed and the twisting speed, as shown in Figure 3-1 (a). Two methods were used for the manufacture of HAYs as indicated in Figure 3-1 (b). One was to use two delivery rollers (two pairs roller system), where the core ply was delivered by the upper pair of delivery rollers and before it went through the middle of the hollow spindle. The wrap ply was wound on the hollow spindle and it also entered the middle of the hollow spindle wrapping around the core ply. Then the yarn was directed out from the lower pair of delivery rollers and it was finally collected onto the yarn package. Another method was to use one pair of delivery rollers (one pair roller system) which was the lower delivery rollers after the hollow spindle, and it led the wrapped core ply into the middle of the spindle and delivered the wrapped yarn to the yarn winding unit during the production. The differences between the two methods are the matching and stretching of the two components. By using the two types of roller system, the combination of the tension and twisting speed for each ply can be investigated. All the produced yarns are listed in Table 3-2 and the yarn wrapping quality was examined under the Projectina microscope using 10× magnification.

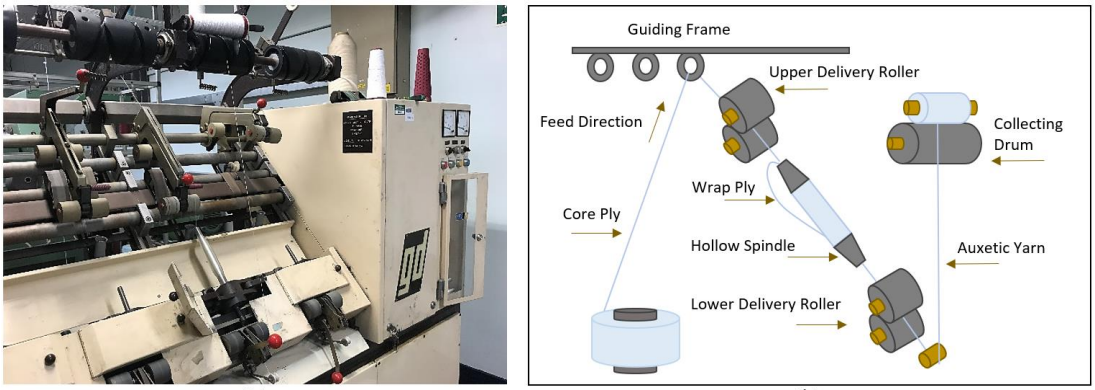

Figure 3-1 Spinning machine for auxetic yarns: (a) real machine; (b) schematic diagram

Table 3-2 Manufacturing parameters of the yarns [84]

Yarn code	Core ply thickness	Twisting speed (rpm*)	Upper delivery speed(m/min)	Lower delivery speed(m/min)	Avg helical angle (°)	Feeding format
S1	Single-core	5000	12.5	14.2	39.0	Under feeding
S2		4500	12.5	14.2	37.8	
S3		4000	12.5	14.2	36.4	
S4		3500	12.5	14.2	34.0	
S5		3000	12.5	14.2	29.9	
S6		2500	12.5	14.2	26.7	
S7		2000	12.5	14.2	25.2	
S4’	Single-core	3500	n/a	14.2	34.5	Equal feeding
S5’		3000	n/a	14.2	29.3	
S6’		2500	n/a	14.2	26.4	
S7’		2000	n/a	14.2	18.1	
S5”	Single-core	3000	16.8	14.2	28.2	Over feeding
S6”		2500	16.8	14.2	23.2	
S7”		2000	16.8	14.2	19.9	
S8”		1500	16.8	14.2	14.0	
D1	Double-core	3500	n/a	14.2	39.9	Equal feeding
D2		3000	n/a	14.2	35.0	
D3		2500	n/a	14.2	32.8	
D4		2000	n/a	14.2	23.9	
D5		1500	n/a	14.2	19.0	
T1	Triple-core	3500	n/a	14.2	40.4	Equal feeding
T2		3000	n/a	14.2	36.9	
T3		2500	n/a	14.2	31.7	
T4		2000	n/a	14.2	26.3	
T5		1500	n/a	14.2	23.0	
S9	Single-core	n/a	n/a	n/a	0	n/a

*rpm: rounds per minutes

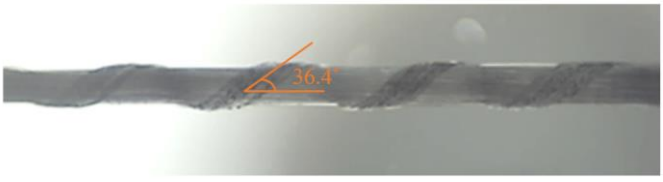

Figure 3-2 Measurement of initial helical angle (S3)

The initial helical angle of the yarn was measured by ImageJ software, as shown in Figure 3-2. Ten yarn samples of each type were measured and the average helical angles are listed in Table 3-2.

During the production, the wrapping quality of the HAY was found to be a main concern. A high-quality helical yarn is one where the wrapping ply wraps firmly around the core ply without any structural problems. Because of the compressibility of the real textile yarns, the actual wrapping length of the yarn is flexible. More extension of the core ply results in more recovery of it and a longer length of the wrap ply. The length of the wrapping ply per cycle L_w can be calculated using Equation (3-1), and the measured length, according to experimental observations, should not exceed 5% of the calculated one to guarantee the yarn quality.

$$L_w = \frac{\pi(D_c + D_w)}{\sin \alpha} \tag{3-1}$$

where D_c and D_w are the diameter of the core ply and the wrap ply, respectively. α is the initial wrapping angle of the wrap ply [15].

Seven types of yarn, coded as S1-S7, were created for the investigation on the effect of different twisting speeds from 5000 rpm to 2000 rpm on the yarn wrapping quality, keeping the same delivery speed, as the helical angle of the yarn is not controllable and the twisting speed can be changed by every interval 500 rpm. It was found that the wrap ply is too loose when the twisting speed lower than 3500 rpm corresponding to the helical angle around 34˚, as shown in Figure 3-3 (a). This could be explained that the two pairs of delivery rollers showed less feeding and there existed some stretch of the core ply during the production. Then, four types of yarn, coded as S4'-S7', were produced by one pair roller system representing the equal feeding of the yarn with the same delivery speed of 14.2 m/min. The quality of the yarn was slightly improved because of the decreased tension of the core ply. Therefore, yarns from S5" to S8" were manufactured using the two pairs roller system with 34.4% increased speed of upper delivery roller corresponding to the over feeding format, which works to achieve the best quality of the yarn, as shown in Figure 3-3 (b). By adopting the over feeding procedure, high-quality auxetic yarns were produced with a wider range of machine settings than before and the range of the helical angles for stable yarns was expanded from 34˚ to around 14.0°. In addition, to explore the relationship between the auxetic effect and the diameter ratio of the two plies, double-core yarns (D1-D5) and triple-core yarns (T1-T5) were manufactured using equal feeding, as listed in Table 3-2.

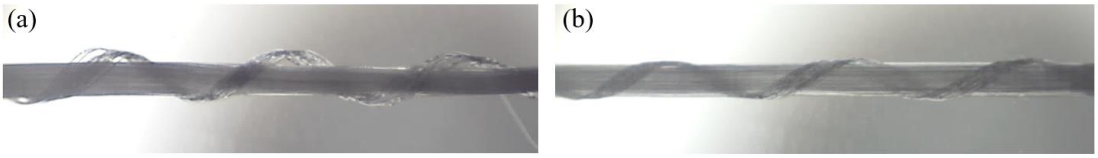

Figure 3-3 Different feeding format of the auxetic yarn: (a) under feeding; (b) over feeding [25]

3.3.2 Woven fabrics

The woven fabric was produced on the ARM AG CH-3507 BIGLEN semi-automatic weaving machine, as shown in Figure 3-4 (a). Helical auxetic yarn S5" of 264.4 tex was selected as the warp and weft yarns for weaving the plain woven fabric due to its structural stability and reasonable NPR, denoted as AF, with the warp and weft densities being 11 × 9 threads/cm, having the areal density of 526.2 g/m². For comparison purposes, another woven fabric, coded NF indicating non-auxetic fabric, was made from yarn S9, a yarn with the same filaments, but with a parallel yarn structure, instead of helical. The warp and weft densities of fabric NF was also 11 × 9 threads/cm but the areal density is 502.3 g/m². The photographs of the two fabrics are shown in Figure 3-4 (b) and (c). During the weaving process, the warp yarn sheet was given a 5% pre-stretch in order to meet the requirement for weaving. A constant basic warp tension level was maintained during the production process by controlling the let-off and take-up. The reed with 7.7 dents/cm was used and 1 warp end was drawn into one dent in order to avoid yarn entanglement during weaving. The fabric density increased when the fabric was taken off loom, which is due to the property of the elastic materials and the tension applied in warp and weft yarn during weaving.

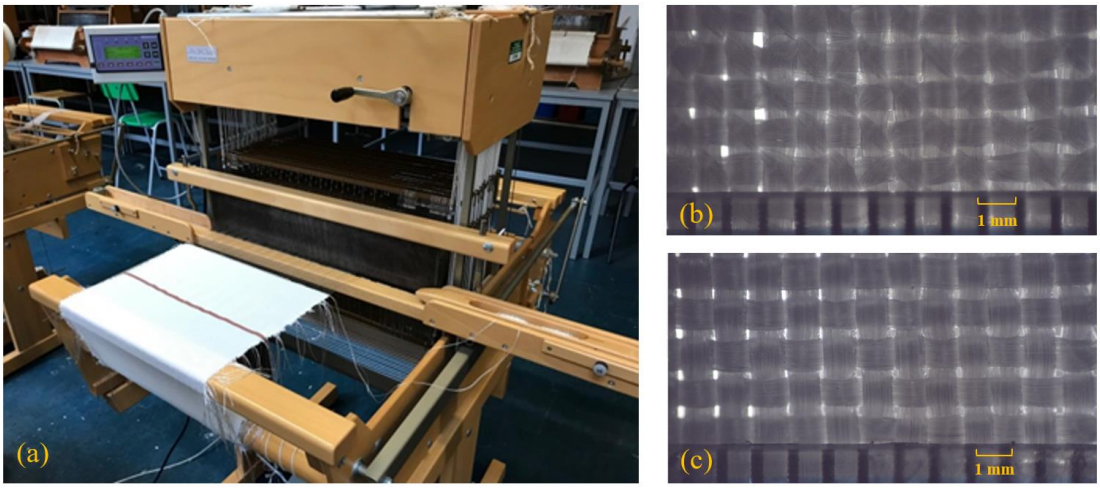

Figure 3-4 Woven fabrics: (a) semi-automatic hand weaving machine; (b) auxetic woven fabric (AF); (c) non-auxetic woven fabric (NF) [84]

Then, another group of woven fabrics were fabricated using the same manufacturing process but with different yarn combinations. Due to the low efficiency of the warp preparation during the weaving, the auxetic yarns were only applied in the weft direction of the fabric afterwards. Yarn S5" of 263.8 tex was selected as weft and polyamide 6,6 which is the binder of the helical auxetic yarn was selected as warp for weaving a plain woven fabric. Then a plain woven fabric coded as SWF-5 (referring to single weft fabric) and a 2/2 warp rib fabric coded as DWF-5 (representing double weft fabric) have been made with the same density of 5×10 threads/cm, as shown in Figure 3-5. In order to find the relationship between the yarns and fabrics, the auxetic yarns S1, S4 and S7" were selected as the weft yarns for making plain woven fabrics as well coded as SWF-1, SWF-4 and SWF-7, respectively. All of the produced woven fabrics are summarised in Table 3-3.

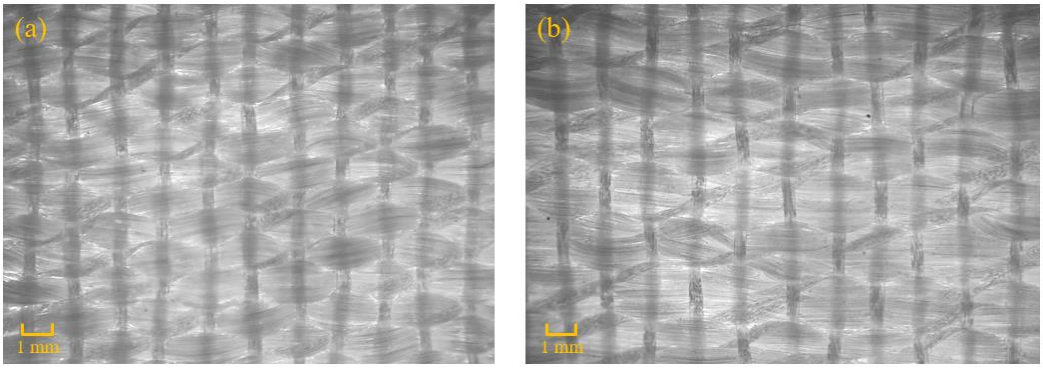

Figure 3-5 Auxetic woven fabrics with different structures: (a) plain (SWF-5); (b) 2/2 warp rib (DWF-5)

Table 3-3 Manufacturing parameters of woven fabrics

Fabric code	Warp	Weft	Weave structure	Fabric density (threads/cm)
AF	Yarn S5”	Yarn S5”	Plain	11×9
NF	Parallel PU and PA 6,6 yarns	Parallel PU and PA 6,6 yarns	Plain	11×9
PUF	PU yarn	PU yarn	Plain	11×9
SWF-1	PA 6,6	Yarn S1	Plain	5×10
SWF-4	PA 6,6	Yarn S4	Plain	5×10
SWF-5	PA 6,6	Yarn S5”	Plain	5×10
SWF-7	PA 6,6	Yarn S7”	Plain	5×10
DWF-5	PA 6,6	Yarn S5”	2/2 Warp rib	5×10

3.4 Experimental work

3.4.1 Tensile test

Tensile tests were carried out on INSTRON 2519-107 together with the Instron Bluehill software. To test the auxetic woven fabrics, the fabric sample was fixed by the top and bottom clamps, as illustrated in Figure 3-6 (a). A microfocus camera (Jiusion 1000× USB Digital Microscope, China) was used and placed in front of the fabric during the tensile test to capture and record the fabric deformation. In order to avoid a loose structure at the edge, the fabric sample was cut into a width of 100 mm, carefully, after being clamped on the machine. Three tensile test fabric specimens for each AF and NF were tested in both warp and weft directions with a crosshead speed of 60 mm/min and a gauge length of 100 mm. With the same machine settings, the samples for SWF-1, SWF-4, SWF-5, SWF-7 and DWF-5 were tested along the weft direction three times as well. To test the auxetic yarns, the crosshead of the machine was changed, as illustrated in Figure 3-6 (b). The yarn sample was wound around the top and bottom grips and clamped tightly, following the standard ASTM D3822 [212]. Ten specimens for each type of yarns were tested with a crosshead speed of 60 mm/min and a gauge length of 50 mm, recording by the camera on the side.

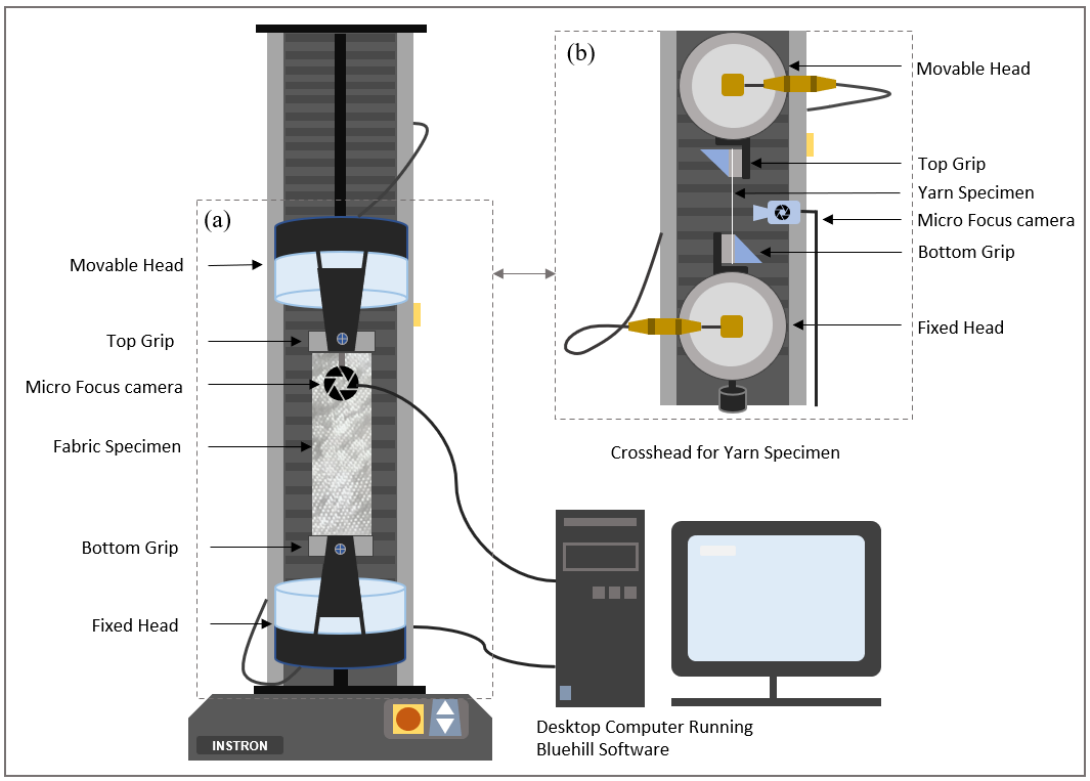

Figure 3-6 Tensile test machine with a micro focus camera: (a) for woven fabrics; (b) for auxetic yarns

Before the measurement of the yarn deformation, the tensile property of each of the specimens were examined, including the HAY, the wrap ply (PA 6,6), the core ply (PU) and non-auxetic yarn. As shown in Figure 3-7 (a), compared with PA 6,6, the auxetic yarn displays larger tensile strain and slightly higher load bearing due to the involvement of the PU core ply. Yarn S9 made from parallel polyamide and polyurethane filament plies, of non-auxetic nature, was tested for tensile behavior too for comparison purposes. The tensile behaviour of helical auxetic yarn and that of the non-auxetic yarn are shown in Figure 3-7 (b). The curve for the auxetic yarn demonstrated low initial tensile modulus because of the helical structural feature of the yarn, where the elastic polyurethane ply was extended easily and the wrapping polyamide ply did not constrain the extension as it straightened when the whole yarn was loaded. The modulus of the yarn became higher gradually after the strain reached 20%. Further loading to the yarn made the polyamide ply more straightened and the polyurethane more helical until the two completely swapped positions. The auxetic yarn broke when the straightened polyamide ply failed. In the case of the non-auxetic yarn where the two plies were parallel, the tensile behavior exhibited in Figure 3-7 (b) mainly came from the polyamide ply because it offered higher tensile rigidity. It is

noted that the peak shapes for the two yarns are almost identical. Hence, with the same components of the yarn, helical structure displayed a higher axial strain compared to the parallel structure and these two structures showed no significant difference in the value of breaking stress.

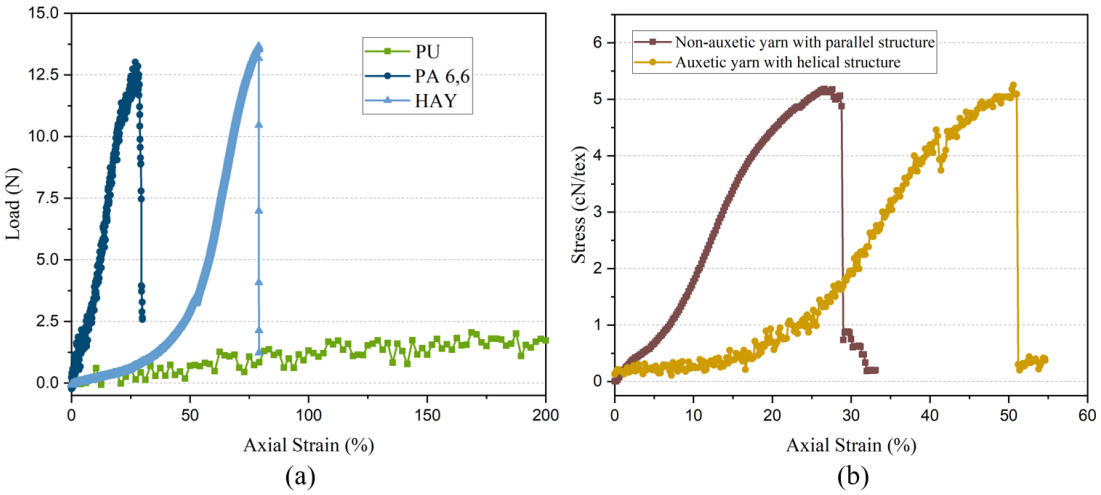

Figure 3-7 Tensile property of different yarns: (a) polyurethane (PU) yarn, polyamide (PA) 6,6 yarn and helical auxetic yarn (HAY); (b) auxetic yarn versus non-auxetic yarn

When the auxetic yarns were fabricated adopting different twisting speeds, different wrapping angles were formed, which could influence the tensile property of the yarn. As shown in Figure 3-8, yarn S1, S3, S5 and S7 were selected for comparison as they produced by the twisting speed of 5000 rpm, 4000 rpm, 3000 rpm and 2000 rpm, respectively, with the same delivery speed of 14.2 m/min. It can be seen that the higher twisting speed of the yarn results in a larger axial strain because the generated yarn has a lower wrapping angle as the twisting speed decreased. Therefore, the low angle of the wrap ply offers less space for the core ply to be deformed and the extension of the yarn is shorter until the wrap ply straightened.

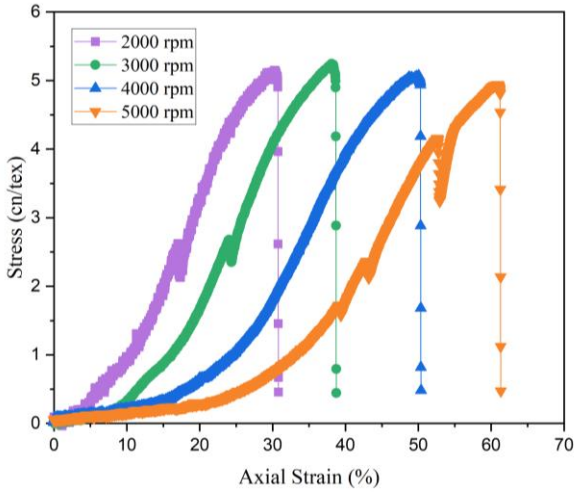

Figure 3-8 Tensile property of auxetic yarns with different twisting speed

3.4.2 NPR measurement

3.4.2.1 Yarns

To measure the change of the outer contour diameter of the yarn in experiments, a micro-focus camera (Jiusion 1000X USB Digital Microscope) was used during the tensile test. The camera was placed to the side of the testing machine focusing on the testing specimen, capturing 48 pictures per minute corresponding to a 2.5% interval axial strain of the yarns. In order to set up the benchmark for comparison, the camera was kept the same magnification and distance to each specimen. Then, the pictures were imported to an image analysis software Digimizer for measuring the diameter change of the auxetic yarns, as shown in Figure 3-9. The outer contour diameter was measured from the selected helical unit from the highest point to the lowest point among each picture representing the different tensile level.

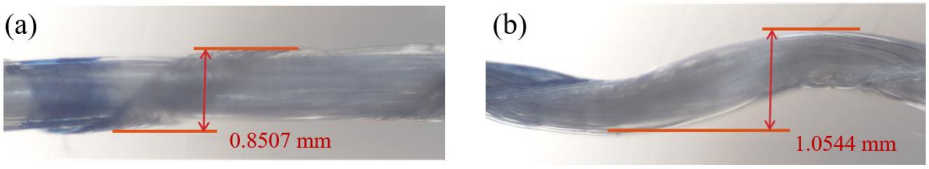

Figure 3-9 Outer contour diameter of the yarn measured by Digimizer software: (a) initial state; (b) under tension

3.4.2.2 Fabrics

To determine the auxetic behaviour of the woven fabrics in warp/weft direction, the microfocus camera was fixed on the top grid of the tensile testing machine so the camera could focus on basically the same area of the fabric specimen. The dimensional

changes of the fabric were measured involving the same number of interlaced warp and weft yarns.

To observe the thickness of the fabric, the camera was set up to the side of the machine capturing 48 pictures per minute corresponding to a 1.25% interval strain of the fabric. This is different compared to the interval strain of the yarn because the length of the fabric specimen was 100 mm and that of the yarn specimen was 50 mm. According to the ASTM standard D1777-96, a blackboard was placed on the one side of the fabric for measuring the thickness of the fabric and keeping the fabric perpendicular to the micro-focus camera, as shown in Figure 3-10. It is obvious that the fabric was thicker under tension.

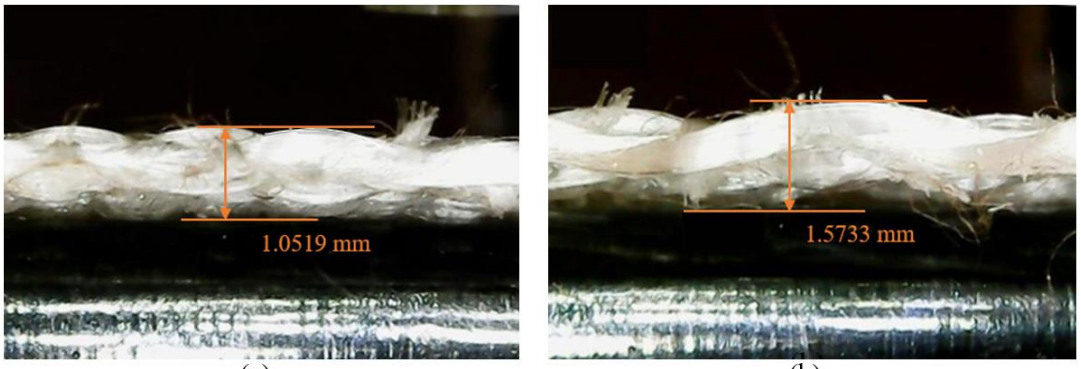

(a) (b)

Figure 3-10 Thickness of the fabric: (a) initial state; (b) under tension

Upon achieving the yarn strains in the axial and transverse directions and the fabric strains in the weft and warp/thickness directions, the Poisson's ratio v_{yarn}, v_{fab} and v'_{fab} were calculated using Equations (3-1), (3-2) and (3-3) as follows. According to the equations, the measurement that goes increased is always positive and that goes decreased is always negative. In the calculation, the positive and negative signs are also included in the equations.

$$v_{yarn} = -\frac{\varepsilon_{\text{trans}}}{\varepsilon_{\text{axial}}} \tag{3-1}$$

$$v_{fab} = -\frac{\varepsilon_{\text{warp}}}{\varepsilon_{\text{weft}}} \tag{3-2}$$

$$v'_{fab} = -\frac{\varepsilon_{thick}}{\varepsilon_{\text{weft}}} \tag{3-3}$$

where ε_{trans} is the transverse strain of the yarn, which was calculated as the ratio of the transverse changes to the original transverse length. ε_{axial} is the axial strain of the yarn. ε_{weft} is the strain of the fabric in the weft direction, which was calculated as the ratio of length changes in the weft direction to the original weft length. ε_{warp} and ε_{thick} are the strain of the fabric in the warp and thickness directions, respectively.

In order to achieve a representative value of Poisson's ratios, a mean absolute deviation (MAD) test was involved [213] and all the selected data were followed by the MAD method. The MAD can be calculated by Equation (3-4) as follow:

$$MAD = \frac{\sum_{i=1}^{n} |NPR_i - M_e|}{n} \tag{3-4}$$

where NPR_i is the maximum NPR of auxetic yarn or fabric during the tensile test and M_e is the median value of the maximum NPRs for total tested times. n is the number of tests for the same type of yarn or fabric.

Therefore, each yarn and fabric sample were tested ten times and three times respectively, and the median value of them was used for the parametric study.

3.4.3 Porosity and air permeability

To measure the porosity, a micro-focus USB video class (UVC) camera was set up on the top crosshead of the tensile machine in front of the fabric sample, as shown in Figure 3-11. Timed shots of the fabric sample were captured every 4 seconds during the tensile loading, which corresponded to a 6.67% strain interval shots due to the length of the specimen being 60 mm. Images, containing 640×480 pixels, were exported and measured by the ImageJ software. The pore areas of each image were processed in the binary section of the ImageJ software, as shown in Figure 3-12. Then, Equation (3-5) was used for calculating the fabric porosity based on the ImageJ measurements.

$$\varphi = \frac{p_o}{p_t} \times 100 \tag{3-5}$$

where φ is the porosity of the fabric, p_o is the total number of pixels of all pores and p_t is the total number of pixels of whole image.

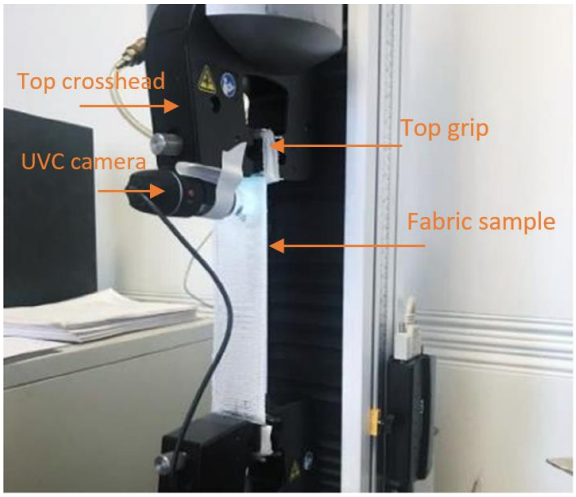

Figure 3-11 Settings for measuring porosity of the fabric

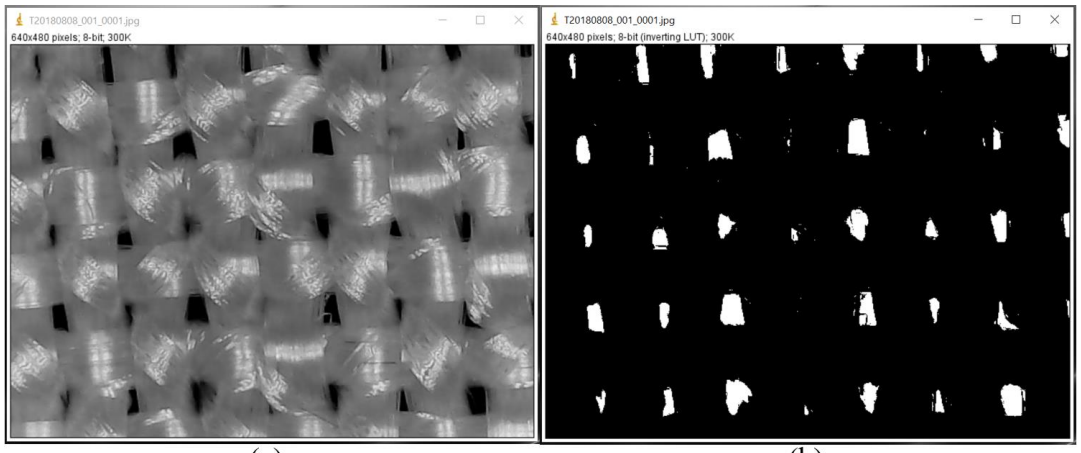

(a) (b)

Figure 3-12 Pore area measurement of the fabric (640×480): (a) real fabric image; (b) binary image after processing

Associated to the porosity analysis earlier, the air permeability test was carried out to confirm the pore opening effect of the auxetic woven fabrics using the SDL ATLAS Tester, as shown in Figure 3-13. The tester could measure the flow of air through the fabric sample under a specific pressure level. Each fabric sample was cut to an area of 20 cm^2 and placed on the black plate by pressing the arm against the fabric sample to start the test.

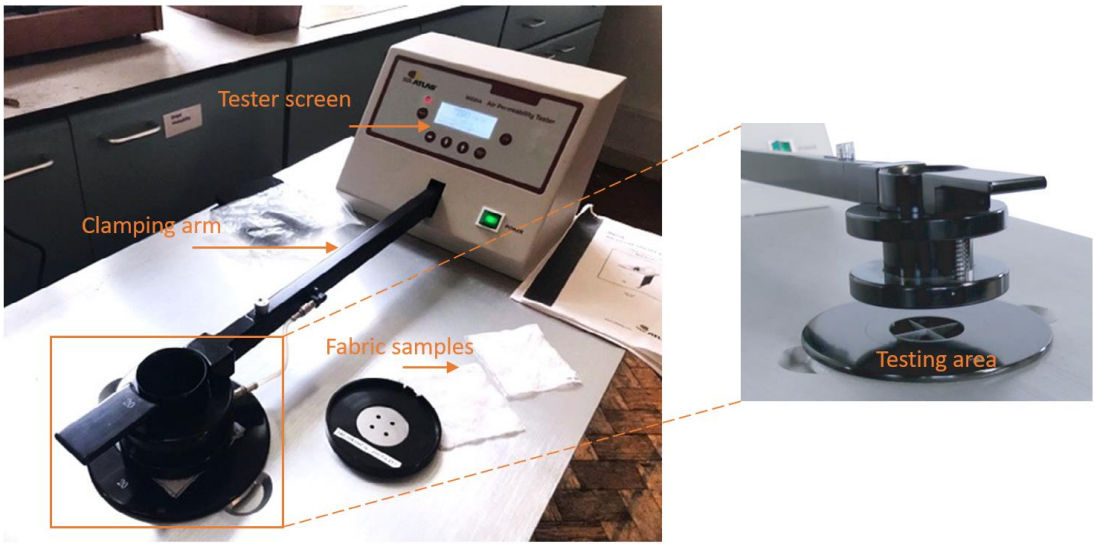

Figure 3-13 Air permeability tester

3.4.4 Impact test

Low velocity impact testing was conducted on Dynatup Model 8200 Instrumented falling weight impact machine, as shown in Figure 3-14 (a). The machine is able to test the fabric sample with a maximum velocity of 4.4 m/s and a maximum dropping height of 1.2 metres [214]. As illustrated in Figure 3-14 (b), the drop weight assembly contains three parts, including drop weight, tup and flag bracket. The value of the impact force is determined by the drop weight (4 kg of drop mass) and tup assembly, which consists of a flat head impactor made from Tecamid 66 having good toughness and rigidity. Then, the impactor was guided by the rails and released manually against the fabric sample from a specific height, such as 5.1 mm, 11.5 mm and 20.4 mm used in this research corresponding to the velocity of 1 m/s, 1.5m/s and 2m/s, respectively. During the falling, the velocity flag which is located on the right side of the drop weight passed through the detector. Therefore, the velocity and the load was detected by different sensors. In order to fix the sample under the impact loading, the fabric was clamped by a special specimen holder, as shown in Figure 3-14 (c). The velocity V could be adjusted by setting the weight height based on the principle demonstrated by Equation (3-6) and the impact energy E could be calculated from Equation (3-7) as follows.

$$V = \sqrt{2gh} \tag{3-6}$$

$$E = mgh \tag{3-7}$$

where g is 9.8 m/s^2 which is the constant value of gravity acceleration, h is the height in metres and m is the mass in kilograms.

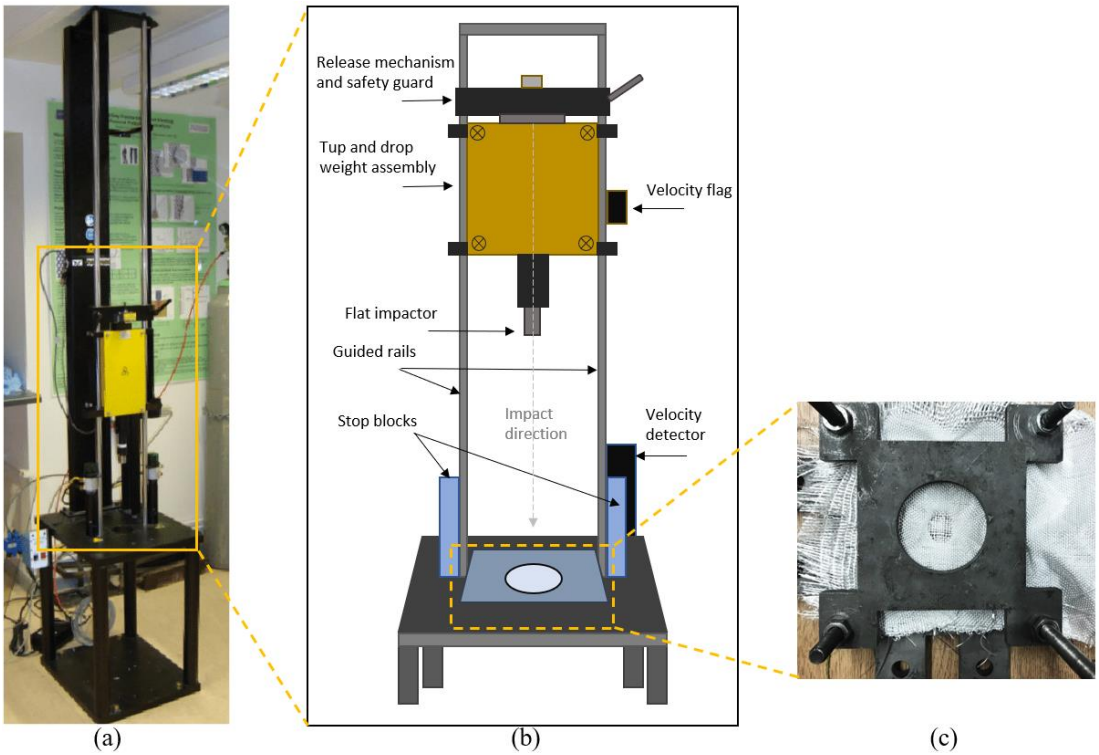

Figure 3-14 Impact testing machine: (a) impact testing instrument; (b) schematic diagram of the machine; (c) tested fabric sample with clamps

3.5 Numerical simulation

3.5.1 Modelling of auxetic yarns and fabrics

3.5.1.1 Pre-processing geometric models

Based on the experimental results of the helical auxetic yarn (HAY), the geometric model was created using ABAQUS 6.14 software, which consists of two parts. One is a cylinder with the diameter of 0.68 mm representing the core ply of the HAY; the other is a helix with the thickness of 0.17 mm corresponding to the wrap ply of the HAY. The helical angle of the wrap ply is determined by the length of the core and wrap plies per helical cycle and these two values can be calculated by Equations (3-8) and (3-1) respectively. The cross-section of the two plies was assumed as a circular first shown in Figure 3-15 (a) in order to have better measurement of the thickness under tension. Then, another yarn model with the cross-sectional shape of ellipse for both core and wrap plies was generated as well, as shown in Figure 3-15 (b). The

aspect ratios of the diameter for both core and wrap plies were 0.56:0.82 and 0.11:0.26, respectively, so the cross-sectional area of the yarn for circular model and elliptical model was the same. Thus, the yarn model was generated with three helical cycles shown in Figure 3-15 (c) and the deformation was measured from the middle cycle of the model.

$$\lambda = \frac{\pi(D_c + D_w)}{\tan \alpha} \tag{3-8}$$

where λ is the length of the core ply per helical cycle. D_c, D_w and α are the diameter of the core, diameter of the wrap and helical angle of the wrap, respectively.

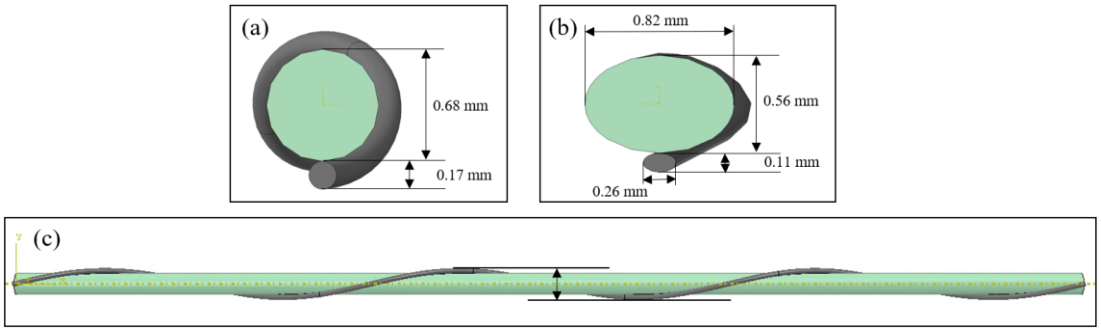

Figure 3-15 Geometric model of HAY: (a) cross-sectional shape of circular; (b) cross-sectional shape of ellipse; (c) three helical cycles of the model

Due to the complexity of the fabric model, Solidworks 2020 software was used and the cross-section of the yarn within the fabric is assumed as an ellipse. Based on the experimental parameters of the woven fabric SWF-5, the auxetic yarns were set as the weft yarns with crimped and helical geometry. The non-auxetic yarns with structural parameters of PA 6,6 were modelled as the warp yarns. Then, the two setts of yarns were interlaced together with the fabric density of 5×10 threads/cm, forming a plain weave structure, as shown in Figure 3-16.

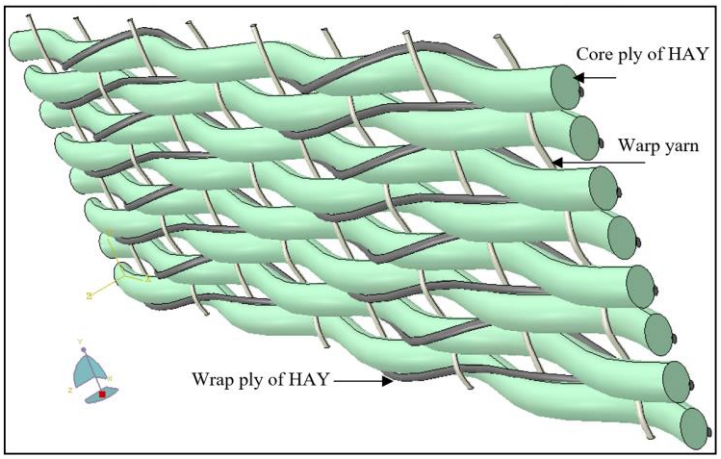

Figure 3-16 Fabric model of SWF-5

3.5.1.2 Mechanical modelling

After the geometric models were created successfully, ABAQUS 2019 software was adopted for the mechanical investigation. There are five main steps for the yarn modelling. Firstly, the geometric model is imported with two separate parts. Secondly, a super elastic property is assigned to the core ply with the Young's modulus of 30 MPa and the Poisson's ratio of 0.48. An elastic property is applied to the wrap ply with the Young's modulus of 1850 MPa and the Poisson's ratio of 0.42 following the data in the experiments above (Table 3-1). Thirdly, a tensile loading is applied to one end of the HAY with the speed of 1 mm/s assigned, and a fixed constraint applied to other ends. During the tensile loading, a hard contact property between the two plies is applied in the model along with the master surface of the wrap ply and slave surface of the core ply. Then, the mesh size of the core ply is set as 0.075 which is three times smaller than that of the wrap ply. The fully integrated linear 3D element type C3D8 with hexahedral element shape and 8-nodes is adopted for the model. In the study of mesh, different sizes and types of the mesh were experimented and these will be discussed in the next Section. Finally, the job is created for running until the wrap ply of the HAY is broken. An experimental strain-stress data of the wrap ply is input to identify the failure of the yarn.

For the mechanical modelling of the auxetic woven fabric, the material property of the HAY model is applied to the weft yarn. An elastic property is applied to the warp yarns with the Young's modulus of 1850 MPa and the Poisson's ratio of 0.42

corresponding to the property of PA 6,6. Then, a tensile loading with the speed of 1 mm/s is applied to the one end of the weft yarns and a fixed constraint applied to the opposite end because the auxetic yarns are arranged in the weft direction only. The interaction between the parts is set as 'all with self' along with a tie constraint between the warp yarns and the wrap plies, meaning that the interfacial reaction is identical between any pairs of yarns. In order to overcome the overlap problem of each part, the quadratic tetrahedral element shape with 3D 10-node modified element type (C3D10M) is adopted for the model, because it offers a good convergence rate and mitigates the problems associated with linear elements [215]. At last, the fabric model is submitted for running until the wrap ply of the weft yarn is broken.

3.5.2 Validation of models

In order to achieve reasonable accuracy of the yarn model, five different mesh sizes were experimented with the same initial helical angle of 28° and the diameter ratio of 4:1, as shown in Table 3-4. Based on the numerical work of Du et al. [147] and Liu et al. [216], the mesh size of the wrap ply was set as three times larger than that of the core ply. Then, a non-linear relationship between the Poisson's ratio and the mesh sizes is generated in Figure 3-17. The denser mesh size results in higher auxetic behaviour of the yarn and it is closer to the geometric calculation and the experimental result. In ABAQUS, it is too time consuming when the mesh size of the model is set as infinitely small. Therefore, the lowest mesh size of M1 is used for the HAY model, which can provide the accuracy and efficiency. The comparison between the experiments and the Finite element (FE) results with the mesh size of M1 is shown in Figure 3-18. It was found that the two curves has a good agreement with each other. They exhibited positive Poisson's ratio first and subsequently decreased with the increasing strain. It is evident that with 0 to 2.5% strain, the highest Poisson's ratio from FE simulation is much larger than that from the experiment, because it was not possible to have denser strain interval in experiments. As a result, the Poisson's ratio data between 0 and 2.5% axial strain could not be collected in experiments with the equipment used.

Table 3-4 Input parameters of the mesh size (mm)

	M1	**M2**	**M3**	**M4**	**M5**
Core ply	0.075	0.08	0.09	0.1	0.125
Wrap ply	0.225	0.24	0.27	0.3	0.375

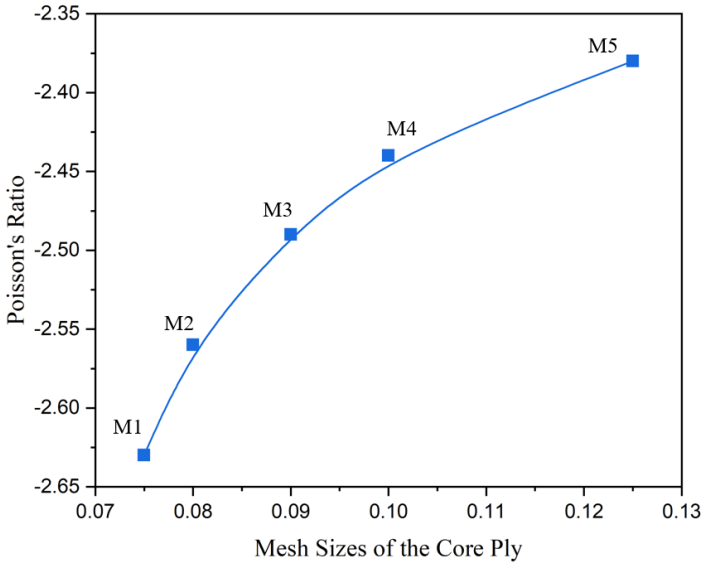

Figure 3-17 Relationship between the Poisson's ratio and the mesh size for the core ply

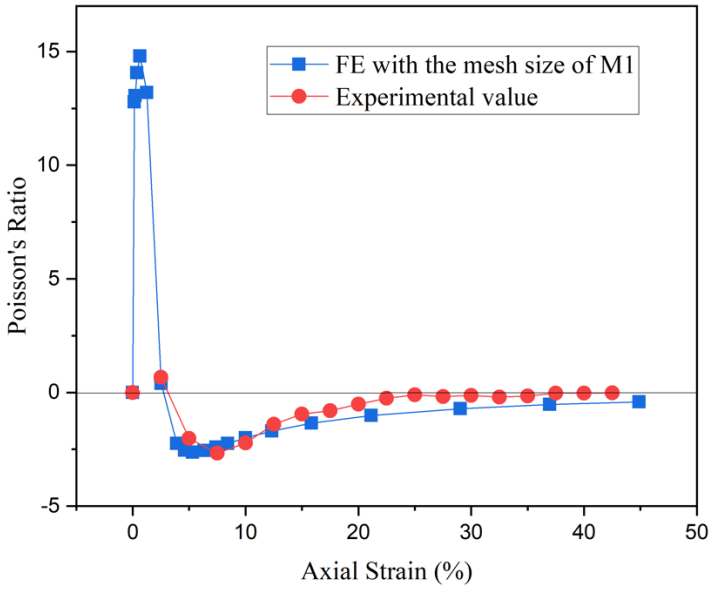

Figure 3-18 Comparison between the experiments and the FE values of the yarn

In the study of mesh sizes, three types of mesh were experimented as well. It was found that the tetrahedral and the wedge elements have the problem of being overly stiff and this finding is supported by Sadowski and Rotter [217]. Thus, the hexahedral

element shape with the C3D8 model is adopted for the yarn model. Finally, the job was created for running until the wrap ply of the HAY was broken.

In the establishment of the yarn model, there was hardly any relative movement between the two plies, so the coefficient of friction was less important and it was not considered in the model. However, the coefficient of friction between the polyurethane and polyamide yarns demonstrated high effect on the deformation of the woven fabric due to more contact area between the warp and weft yarns, so it was considered for all fabric models. In practical situations, the rigidity of the two materials is pretty different and the polyamide ply may cut into the polyurethane ply, so the interactive relationship between them could be very complicated. The nominal frictional coefficient between the two materials may not reflect the real frictional situation and it may be smaller than the real frictional value. Therefore, different frictional coefficient levels were investigated using fabric model F-A28 corresponded to the fabric SWF-5 and the results at 17.5% strain level are illustrated in Figure 3-19. It can be seen that the Poisson's ratio is decreased with the decreasing frictional coefficient corresponding to higher auxetic behaviour of the fabric. Based on the results, the frictional coefficient of 0.2 was used in the fabric model as it demonstrated a closer simulated result compared to the experimental result, exhibiting a low average percentage error of 11%.

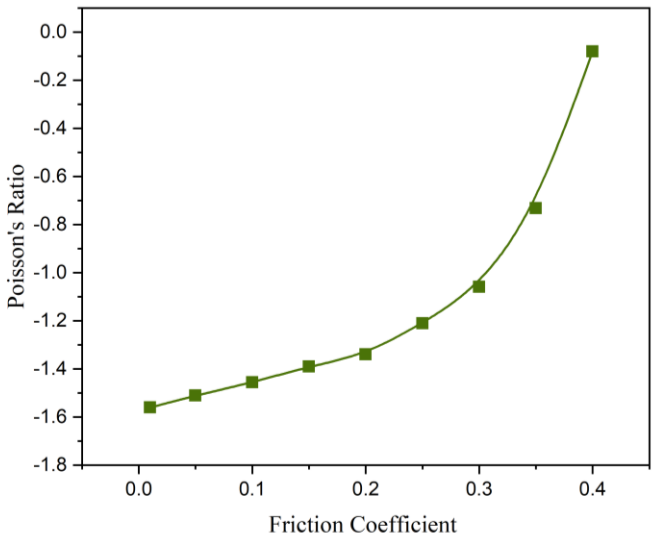

Figure 3-19 Relationship between the Poisson's ratio and the frictional coefficient

To validate the fabric model, SWF-5 and DWF-5 were selected for comparison, as shown in Figure 3-20. It was found that the experimental and FE results had good

accordance with each other for both SWF-5 and DWF-5. An initial increase in positive Poisson's ratio at the lowest strains was observed and the Poisson's ratio subsequently decreased with the increasing strain. The highest Poisson's ratio value of the FE result was higher than that of the experimental result from strain 2.5% to 10% due to the sensitivity of the FE model under the low strain level. It is also attributed to the same phenomenon for the yarns, showing differential Poisson's ratio from strain 0 to 2.5%. Then, the Poisson's ratio of the FE model matched with the experimental result after 12.5% of strain within 15% of average percentage error. The maximum negative Poisson's ratios between the experimental and the FE results were shown at 17.5% of strain for SWF-5 with the values of -1.1 and -1.35, respectively. Meanwhile, the two values for DWF-5 were -1.47 and -1.56 respectively, exhibiting at 15% of strain.

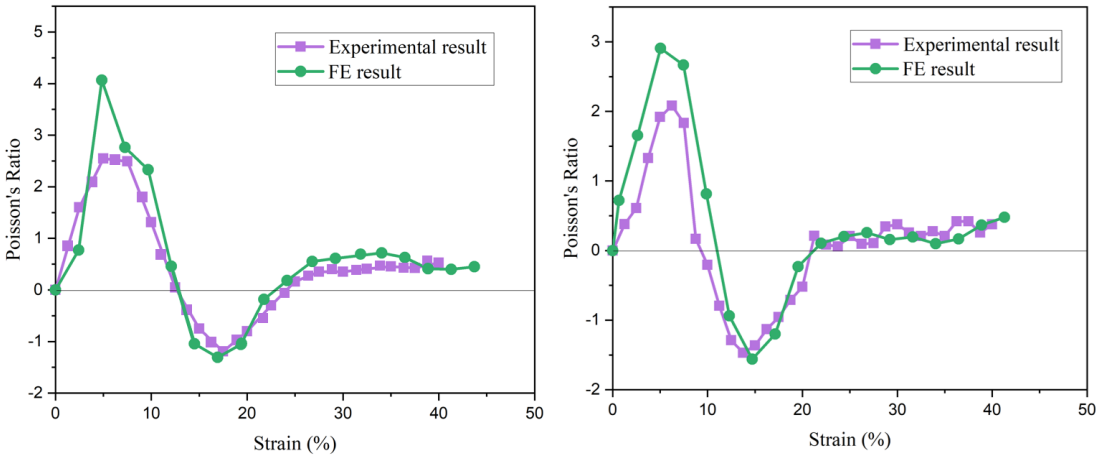

Figure 3-20 Comparison between the experimental and FE results of fabrics: (a) SWF-5; (b) DWF-5

In addition, to validate the results of the yarn and fabric models, a method of the mean absolute percentage error (MAPE) was used [218], as shown in Equation (3-9). The MAPEs of the FE results were all lower than 10% compared with the experimental results.

$$M = \frac{1}{n}\sum_{t=1}^{n}\left|\frac{A_t - F_t}{A_t}\right| \quad (3\text{-}9)$$

where A_t is the value of the experiments and F_t is the value of the FE modelling.

3.5.3 Parametric study of auxetic yarns and fabrics

Based on the validated models of auxetic yarns and woven fabrics, parametric studies were designed and carried out to identify the key parameters on Poisson's ratio of the

yarns and fabrics. Table 3-5 lists the three variable parameters of concern, which are helical angles of the wrap ply, thickness of the yarn and tensile moduli of the two plies.

To carry out the parametric analysis in association with yarn helical angles, different helical angles in the yarn models were created from 14˚ to 39˚, corresponding to the angle of the experimental measurements. Then, the angle range of the validated model was expanded to the lowest 10˚ and highest 50˚ for further investigation and the other parameters were kept constant including the yarn thickness and modulus. From angle 10˚ to 15˚, the incremental interval was 1˚ because the yarn is more sensitive when the angle is small. Angles 43˚ and 50˚ were selected based on the calculated angle from the twisting speed and delivery speed in Appendix 1.

The thickness of the yarn was selected as the second parameter for investigation. Because the auxetic behaviour of the yarn was demonstrated by the deformation of the two plies, the change of the thickness was represented by the diameter ratio of the core ply to the wrap ply. Herein, the investigation of the yarn thickness focused on the adjustment of the core and wrap plies, respectively. Based on the experimental measurement, the core ply thickness was 0.68 mm. The range of the thickness of the core ply in this parametric analysis was assigned to be from 0.34 mm to 1.36 mm, coded from Y-R2 to Y-R8, corresponding to the diameter ratio 2:1 to 8:1. The code 'R' is the abbreviation of 'ratio' and the following number represents the integer of the diameter ratio of the core ply to the wrap ply. In this analysis, the thickness of the wrap ply was adjusted from 0.17mm to 0.68 mm, keeping the core ply thickness as 0.68 mm. For the yarn code Y-R4, Y-R2', Y-R1.3 and Y-R1, the thickness of the wrap ply was increased by an incremental interval of 0.17 mm, corresponding to the diameter ratio of 4:1, 2:1, 4:3 and 1:1, respectively. In order to a deep investigation, the diameter ratio of 8:5 was designed, which is between the diameter ratios of 2:1 and 4:3 with an incremental interval of 0.085 mm.

To investigate the influence of the tensile moduli of the two plies on the yarn auxeticity, the tensile modulus of the wrap ply was set to 500 to 4000 MPa and that of the core ply was applied to 15 MPa to 120 MPa, coded as Y-M1 to Y-M5 and Y-M1' to Y-M5', respectively. As the benchmarks, tensile moduli of the core ply and the wrap ply were experimentally measured, and they were 30 MPa and 1850 MPa, respectively.

Structural details of the yarn models are listed in Table 3-5, where Y-A28 yarn model was used for analysis from different perspectives.

Table 3-5 Models of auxetic yarns

Yarn code	Parameters				
	Helical angle (°)	Ply thickness (mm)		Tensile moduli (MPa)	
		Core ply	Wrap ply	Core ply	Wrap ply
Y-A50	50	0.68	0.17	30	1850
Y-A43	43				
Y-A39	39				
Y-A38	38				
Y-A36	36				
Y-A34	34				
Y-A28	28				
Y-A23	23				
Y-A20	20				
Y-A15	15				
Y-A14	14				
Y-A13	13				
Y-A12	12				
Y-A11	11				
Y-A10	10				
Y-R2	28	0.34	0.17	30	1850
Y-R3		0.51			
Y-R4 (Y-A28)		0.68			
Y-R5		0.85			
Y-R6		1.02			
Y-R8		1.36			
Y-R4 (Y-A28)	28	0.68	0.17	30	1850
Y-R2’			0.34		
Y-R1.6			0.425		
Y-R1.3			0.51		
Y-R1			0.68		
Y-M1	28	0.68	0.17	30	500
Y-M2					1000
Y-M3 (Y-A28)					1850
Y-M4					3000
Y-M5					4000
Y-M1’	28	0.68	0.17	15	1850
Y-M2’ (Y-A28)				30	
Y-M3’				60	
Y-M4’				90	
Y-M5’				120	

Woven fabric models established for parametric studies are summarised in Table 3-6. Seven variable parameters were designed. Firstly, three types of yarn arrangements were created, including in-phase, out-of-phase and hybrid phase. Each arrangement was used to two fabric types. The fabric type A is to use auxetic yarns in the weft

direction and non-auxetic yarns in the warp direction. The fabric type B is to apply auxetic yarns in both warp and weft directions. To save calculation time, the fabric type A was used for investigating the factors, including fabric density, helical angle of the HAY, thickness of the HAY, weave structure and warp yarn type. Secondly, two types of fabric density were designed including 5×6 threads/cm and 5×8 threads/cm, compared to the fabric density of 5×10 threads/cm from the experiments. Thirdly, auxetic yarns with helical angles of 20˚, 28˚, 34˚ and 39˚ were created in the weft direction of the fabric model, corresponding to the yarns used in experiments. Fourthly, because the auxetic behaviour was mainly contributed in the thickness direction of the fabric, the vertical thickness of HAY was designed by every 0.28 mm interval value, keeping the same aspect ratio of the core ply and the parameter of the wrap ply. The fabric density was set as 5×5 threads/cm because the auxetic yarns with higher thickness were overlapped initially and it was difficult to model if the density was set as 5×10 threads/cm. Therefore, the fabric density of 5×5 threads/cm was used in this factorial investigation, keeping the thickest yarns side by side without any overlapping. Fifthly, three types of weave structures were created, such as plain, 2/2 warp rib and 3/3 warp rib. Sixthly, based on the non-auxetic behaviour of the material, the warp yarn type was demonstrated with different modulus, Poisson's ratio and thickness. After that, in order to investigate the factor of loading directions, the fabric model was created by adopting the HAYs in both warp and weft directions. Four types of uniaxial loading and two types of biaxial loading were designed with the stretching along weft direction, warp direction and both. The details of them are listed in the following table.

Table 3-6 Parametric study of auxetic woven fabrics

Code	Variable parameters								
	Yarn arrangement	Fabric density (threads/cm)	Helical angle of the HAY (˚)	Vertical thickness of HAY (mm)	Weave structure	Warp yarn type			Loading direction
						Modulus (MPa)	PR*	Vertical thickness	
F-P1 (F-A28)	In-phase	5×10	28	0.56	Plain	1850	0.42	0.11	Uniaxial
F-P2	Out-of-phase								
F-P3	Hybrid phase								
F-P1'	In-phase	5×10	28	0.56	Plain	HAY(Y-A28)			Biaxial
F-P2'	Out-of-phase								

F-P3’	Hybrid phase								
F-N1	In-phase	5×6	28	0.56	Plain	1850	0.42	0.11	Uniaxial
F-N2	Out-of-phase								
F-N3	Hybrid phase								
F-N4	In-phase	5×8	28	0.56	Plain	1850	0.42	0.11	Uniaxial
F-N5	Out-of-phase								
F-N6	Hybrid phase								
F-A39	In-phase	5×10	39	0.56	Plain	1850	0.42	0.11	Uniaxial
F-A34			34						
F-A28			28						
F-A20			20						
F-T1	In-phase	5×5	28	0.28	Plain	1850	0.42	0.11	Uniaxial
F-T2				0.56					
F-T3				0.84					
F-T4				1.12					
F-T5				1.4					
F-W1 (F-A28)	In-phase	5×10	28	0.56	Plain	1850	0.42	0.11	Uniaxial
F-W2					2/2 warp rib				
F-W3					3/3 warp rib				
F-M1	In-phase	5×10	28	0.56	Plain	1000	0.42	0.11	Uniaxial
F-M2 (F-A28)						1850			
F-M3						3000			
F-M4						4000			
F-M5						5000			
F-R1	In-phase	5×10	28	0.56	Plain	1850	0.3	0.11	Uniaxial
F-R2							0.35		
F-R3 (F-A28)							0.42		
F-R4							0.45		
F-R5							0.48		
F-F1 (F-A28)	In-phase	5×10	28	0.56	Plain	1850	0.42	0.11	Uniaxial
F-F2								0.22	
F-F3								0.33	
F-F4								0.44	
F-D1	In-phase	5×10	28	0.56	Plain	HAY(Y-A28)			Uniaxial-weft1
F-D2									Uniaxial-weft2
F-D3									Uniaxial-warp1
F-D4									Uniaxial-warp2
F-D5	In-phase	5×10	28	0.56	Plain	HAY(Y-A28)			Biaxial 1
F-D6 (F-P1’)									Biaxial 2

*PR: Poisson’s ratio

3.6 Experimental and simulation results

The characterisation of the auxetic yarns and woven fabrics were carried out by combining the experimental work and finite element simulation together. Table 3-7 shows the results of auxetic yarns with corresponding parameters and minimum Poisson's ratios. The brackets in sample code represent the yarn or fabric samples with the same parameters.

Table 3-7 Minimum Poisson's ratios of auxetic yarns

Sample code	Corresponding parameter	Minimum Poisson's ratio	Method
Y-A50	Angle 50˚	-0.82	FE
Y-A43	Angle 43˚	-1.18	
Y-A39	Angle 39˚	-1.35	
Y-A38	Angle 38˚	-1.45	
Y-A36	Angle 36˚	-1.56	
Y-A34	Angle 34˚	-1.78	
Y-A28	Angle 28˚	-2.63	
Y-A23	Angle 23˚	-4.03	
Y-A20	Angle 20˚	-5.27	
Y-A15	Angle 15˚	-9.40	
Y-A14	Angle 14˚	-10.8	
Y-A13	Angle 13˚	-11.65	
Y-A12	Angle 12˚	-13.92	
Y-A11	Angle 11˚	-16.16	
Y-A10	Angle 10˚	-20.94	
S1	Angle 39.0˚	-0.42	Experiment
S2	Angle 37.8˚	-0.69	
S3	Angle 36.4˚	-0.76	
S4	Angle 34˚	-1.50	
S5	Angle 29.9˚	-2.30	
S6	Angle 26.7˚	-3.58	
S7	Angle 25.2˚	-5.62	
S4'	Angle 34.5˚	-2.03	
S5'	Angle 29.3˚	-2.99	
S6'	Angle 26.4˚	-4.21	
S7'	Angle 18.1˚	-5.43	
S5"	Angle 28.2˚	-2.78	
S6"	Angle 23.2˚	-4.08	
S7"	Angle 19.9˚	-5.63	
S8"	Angle 14.0˚	-9.60	
Y-R1	Diameter ratio 1:1-wrap	0.37	FE
Y-R1.3	Diameter ratio 4:3-wrap	0.03	
Y-R1.6	Diameter ratio 8:5-wrap	-0.38	
Y-R2	Diameter ratio 2:1	-1.25	
Y-R2'	Diameter ratio 2:1-wrap	-1.20	
Y-R3	Diameter ratio 3:1	-2.41	
Y-R4 (Y-A28)	Diameter ratio 4:1	-2.63	
Y-R5	Diameter ratio 5:1	-2.47	
Y-R6	Diameter ratio 6:1	-2.18	
Y-R8	Diameter ratio 8:1	-1.44	
D1	Double-core; angle 39.9˚	-0.33	Experiment

D2	Double-core; angle 35.0˚	-0.64	
D3	Double-core; angle 32.8˚	-0.93	
D4	Double-core; angle 23.9˚	-1.80	
D5	Double-core; angle 19.0˚	-3.70	
T1	Triple-core; angle 40.4˚	-0.12	
T2	Triple-core; angle 36.9˚	-0.23	
T3	Triple-core; angle 31.7˚	-0.35	
T4	Triple-core; angle 26.3˚	-0.80	
T5	Triple-core; angle 23.0˚	-1.29	
Y-M1	Wrap modulus 500 MPa	0.05	FE
Y-M2	Wrap modulus 1000 MPa	-1.08	
Y-M3 (Y-A28)	Wrap modulus 1850 MPa	-2.63	
Y-M4	Wrap modulus 3000 MPa	-4.04	
Y-M5	Wrap modulus 4000 MPa	-4.9	
Y-M1’	Core modulus 15 MPa	-4.71	
Y-M2’ (Y-A28)	Core modulus 30 MPa	-2.63	
Y-M3’	Core modulus 60 MPa	-0.88	
Y-M4’	Core modulus 90 MPa	-0.18	
Y-M5’	Core modulus 120 MPa	0.09	

Table 3-8 demonstrates the minimum Poisson’s ratio of auxetic woven fabrics in experiments. For AF, the load was applied to the warp and weft directions, respectively. The corresponding auxeticity was measured in the weft and warp directions. For SWF-1, SWF-4, SWF-5, SWF-7 and DWF-5, the load was applied to the weft direction of the fabric and the auxetic behaviour was tested in the thickness direction.

Table 3-8 Minimum Poisson’s ratios of auxetic woven fabrics in experiments

Sample code	**Corresponding parameter**	**Minimum Poisson’s ratio**	**Method**
AF	HAYs applied in warp and weft	-0.052 (weft direction); -0.025 (warp direction)	Experiment
SWF-1	HAY 39˚	-0.30	
SWF-4	HAY 34˚	-0.43	
SWF-5	HAY 28˚	-1.29	
SWF-7	HAY 20˚	-3.32	
DWF-5	2/2 warp rib	-1.47	

Table 3-9 shows the minimum Poisson’s ratio of auxetic woven fabrics in FE simulation. Apart from F-D3 and F-D4, the auxetic behaviour of each sample was tested in the thickness direction and the warp direction when the load was applied to the weft direction of the fabric. The deformation of F-D3 and F-D4 was measured in the thickness direction and the weft direction when the load was applied to the warp

direction of the fabric. With the table of results, it will be analysed and discussed in the following Chapters with different concentrations.

Table 3-9 Minimum Poisson's ratios of auxetic woven fabrics in FE simulation

Sample code	Corresponding parameter	Minimum Poisson's ratio in the thickness direction	Minimum Poisson's ratio in the warp direction
F-P1 (F-A28)	In-phase HAY(weft only)	-1.35	-0.35
F-P2	Out-of-phase HAY(weft only)	-0.85	-0.63
F-P3	Hybrid phase HAY(weft only)	-0.92	-0.51
F-P1'	In-phase HAY	-0.62	-0.99
F-P2'	Out-of-phase HAY	-0.35	-1.17
F-P3'	Hybrid phase HAY	-0.45	-1.06
F-N1	Density 5×6, In-phase	-1.23	-0.18
F-N2	Density 5×6, Out-of-phase	-1.1	-0.32
F-N3	Density 5×6, Hybrid phase	-1.21	-0.25
F-N4	Density 5×8, In-phase	-1.29	-0.28
F-N5	Density 5×8, Out-of-phase	-1.07	-0.47
F-N6	Density 5×8, Hybrid phase	-1.19	-0.31
F-A39	39˚ angle of HAY	-0.38	-0.11
F-A34	34˚ angle of HAY	-0.53	-0.25
F-A28	28˚ angle of HAY	-1.35	-0.35
F-A20	20˚ angle of HAY	-3.57	-0.73
F-T1	HAY thickness 0.28 mm	-2.67	-0.36
F-T2	HAY thickness 0.56 mm	-1.1	-0.32
F-T3	HAY thickness 0.84 mm	-0.99	-0.28
F-T4	HAY thickness 1.12 mm	-0.78	-0.15
F-T5	HAY thickness 1.4 mm	-0.14	-0.08
F-W1 (F-A28)	Plain	-1.35	-0.35
F-W2	2/2 warp rib	-1.56	-0.46
F-W3	3/3 warp rib	-1.85	-0.59
F-M1	Warp modulus 1000 MPa	-1.39	-0.41
F-M2 (F-A28)	Warp modulus 1850 MPa	-1.35	-0.35
F-M3	Warp modulus 3000 MPa	-1.32	-0.33
F-M4	Warp modulus 4000 MPa	-1.28	-0.30
F-M5	Warp modulus 5000 MPa	-1.27	-0.28
F-R1	0.3 Poisson's ratio of the warp	-1.42	-0.41
F-R2	0.35 Poisson's ratio of the warp	-1.39	-0.37
F-R3 (F-A28)	0.42 Poisson's ratio of the warp	-1.35	-0.35
F-R4	0.45 Poisson's ratio of the warp	-1.37	-0.36
F-R5	0.48 Poisson's ratio of the warp	-1.39	-0.40
F-F1 (F-A28)	Warp thickness 0.11 mm	-1.35	-0.35
F-F2	Warp thickness 0.22 mm	-1.20	-0.21
F-F3	Warp thickness 0.33 mm	-1.08	-0.13

F-F4	Warp thickness 0.44 mm	-0.85	-0.05
F-D1	Uniaxial- weft1	-0.58	-0.70
F-D2	Uniaxial- weft2	-0.80	-1.16
F-D3	Uniaxial- warp1	-0.56	-0.06 (in the weft direction)
F-D4	Uniaxial- warp2	-1.09	-0.09 (in the weft direction)
F-D5	Biaxial 1 (orthogonal stretch)	-0.70	-0.76
F-D6 (F-P1')	Biaxial 2 (four sides stretch)	-0.62	-0.99

Chapter 4 Factorial Analysis on Poisson's Ratio of Auxetic Yarns

4.1 Cross-sectional shape of yarns

The cross-sectional shapes of circular and ellipse were used to construct the yarn models. In reality, the cross-section of the multifilament yarn in a woven fabric or even on its own would never be perfectly circular and it would be flattened to some extent as could be observed in experimental measurement. Therefore, it is necessary to consider the cross-sectional shape assumed in the yarn model before it is subjected to further investigation. Two yarn models were created in this research with circular and elliptical cross-sectional shapes respectively, keeping the same yarn linear density and the constant helical angle of 28˚, as shown in Figure 4-1.

Under tensile loading, the deformation of the auxetic yarn can be summarised in four stages according the experimental and FE results. In the first stage, the wrap ply twines around the core ply without tension. In the second stage, the two plies swaps their position when the load is large enough applied in the longitudinal direction. Then, in the third stage, the wrap ply is fully stretched and locates in the axis of the auxetic yarn, forcing the core ply helically wrapped around it. In the final step, the wrap ply is straightened and further loading makes the auxetic yarn thinner until the wrap ply breaks. During the four stages, the deformation of the yarn is measured in the defined vertical direction of the cross-sectional plane, as illustrated in Figure 4-1. Due to the symmetry for the circular cross-section yarn model, the vertical and horizontal dimensional changes over one full helix period would be the same. The maximum negative Poisson's ratios achieved for the circular model and the elliptical model are -2.68 and -2.57, respectively. Because of the asymmetry of the elliptical model, the maximum negative Poisson's ratio achieved in the defined horizontal direction of the cross-sectional plane is -1.49, which is around 42% smaller than that in the defined vertical direction.

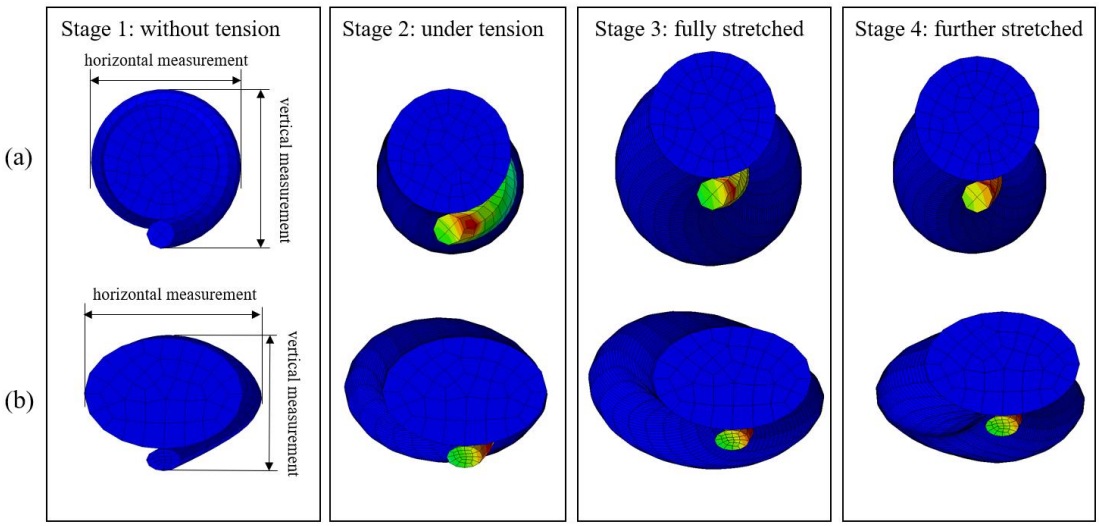

Figure 4-1 Cross-sectional deformation of the yarn: (a) circular model; (b) elliptical model

Figure 4-2 demonstrates the Poisson's ratio of the yarn models with different cross-sectional shapes measured in the defined vertical direction. It can be seen that the trend of the two models have a good accordance with each other and they demonstrate a low average percentage error of 4.1%. Some of the points in the figure are not perfectly matched due to the irregular cross-sectional shape of the elliptical model under tension. Therefore, in order to have a good efficiency and a better measurement of the finite element simulation, the cross-sectional shape of the yarn models are assumed as a circular and the deformation of them are measured in the defined vertical direction of the cross-sectional plane for the following sections.

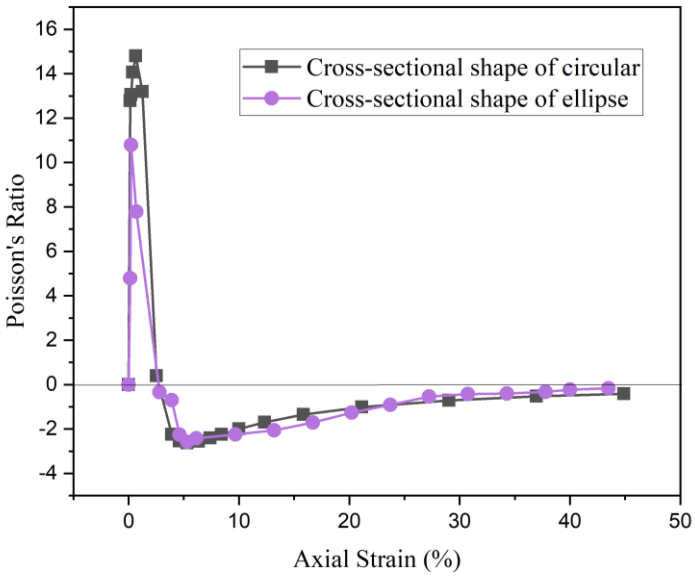

Figure 4-2 Poisson's ratio of the yarn models with different cross-sectional shapes measured in the defined vertical direction

4.2 Initial helical angles

Figure 4-3 demonstrates the Poisson's ratio of single-core auxetic yarns produced in experiments with different helical angles. The Poisson's ratio has become smaller with the decreasing twisting speed from S1-39.0° to S8''-14.0°, which indicated that the core filament has more space to be deformed with less wraps or a smaller helical angle. Then, the maximum negative Poisson's ratio (NPR) values of each yarn are summarised in Figure 4-4, which illustrates the relationship between the Poisson's ratio and the helical angles. The Poisson's ratio is gradually reduced as the helical angle decreases, corresponding to the principle that a lower helical angle leads to a higher auxetic behaviour [139]. The geometric model reported by Du et al. [147] is also adopted and the calculated results are shown in Figure 4-4. The maximum NPR can be achieved as -9.6 with the helical angle of approximately 14.0° based on the experiments, however, with the same parameters, the values achieved from the geometric calculation and the FE modelling are -9.3 and -10.8 respectively because the shape of the yarn is assumed as a cylinder with a hard contact of the binder and the friction of the two plies is not considered in the simulated model.

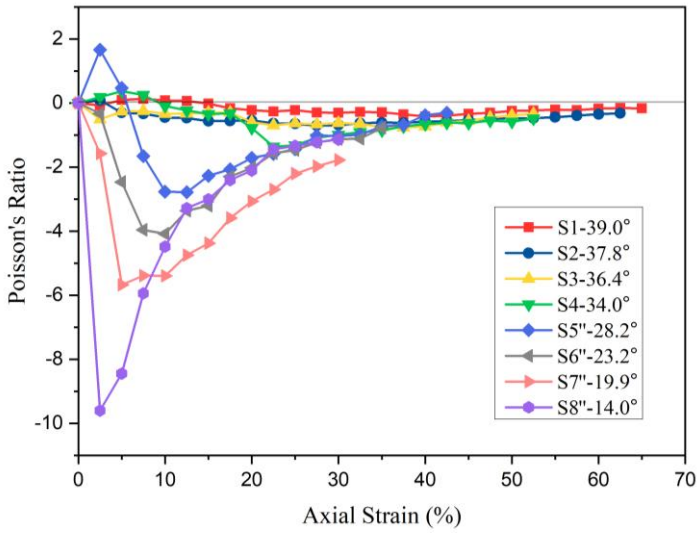

Figure 4-3 Poisson's ratio of single-core auxetic yarns in experiments

In Figure 4-4**,** the trends between the experiments and the theoretical results are almost identical with a low mean absolute percentage error (MAPE) of 9.29%. Then, based on the experimental values, the helical angles can be extended from 50° to 10° in the FE model. The relationship between the helical angles and the Poisson's ratio has two regions. From the helical angle 10° to around 20°, the HAY is more sensitive as the Poisson' ratio dropped quickly by changing a small value of the angle. From the helical angle 20° to 50°, the gradient of the auxetic effect decreased with the increasing helical angles and the HAY is not as sensitive as the first region. The maximum NPR of the yarn could be further explored and reached to the value of -20.94 with the angle of 10° in simulation.

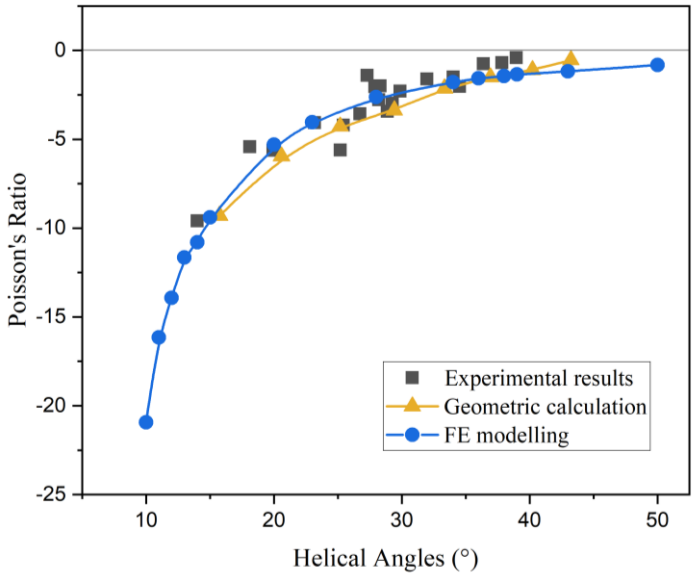

Figure 4-4 Relationship between the Poisson's ratio and the helical angles

During the simulation of the yarn model, the cross-sectional deformation of the yarn can be seen clearly, as shown in Figure 4-5. The model Y-A11 with helical angle of 11˚ exhibits a high sensibility under tensile loading. The diameter of the yarn is 1.02 mm initially and it reaches the minimum value of 0.85 mm under 0.23% axial strain shown in Figure 4-5 (b). Then, the soft core ply is extruded helically by the stiffer wrap ply under 0.44% axial strain, leading to the increased diameter back to initial around 1.03 mm, as shown in Figure 4-5 (c). When the tension further applied and reached to 0.78% axial strain, the HAY exhibits the maximum negative Poisson's ratio of -16.16. However, the wrap ply is not placed in the central axis of the yarn until the strain reached to 4.87% shown in Figure 4-5 (e). This can be explained by the fact that the Poisson's ratio is determined by both the transverse strain and the axial strain. Even though the transverse strain in Figure 4-5 (e) is slightly larger than that in Figure 4-5 (d), the axial strain of 4.87% is more than six times higher than the strain of 0.78%. Therefore, the maximum negative Poisson's ratio of the yarn is not exhibited when the yarn reaches the largest outer contour diameter. When the helical angle of the yarn is getting smaller, the yarn is deformed much earlier under a lower axial strain as the diameter range from 0.85 mm to 1.29 mm is kept the same.

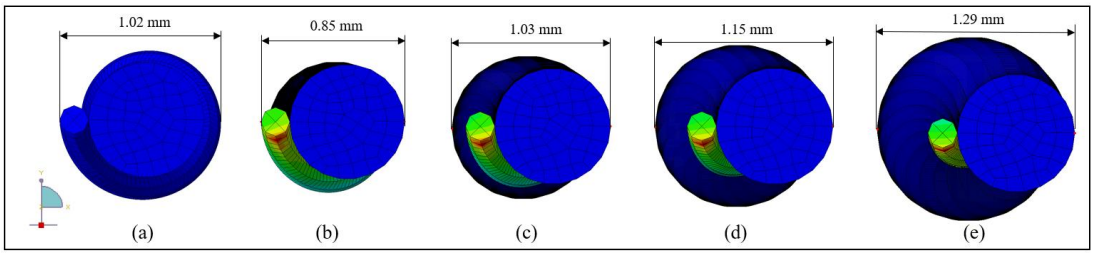

Figure 4-5 Cross-sectional deformation of the yarn model (Y-A11): (a) 0 axial strain; (b) 0.23% axial strain; (c) 0.44% axial strain; (d) 0.78% axial strain; (e) 4.87% axial strain

4.3 Thickness of the yarn

4.3.1 The influence of the core ply thickness

In order to investigate the influence of the core ply thickness on Poisson's ratio, three types of yarn were spun, i.e. including single-core, double-core and triple-core. The details of these yarns are shown in Table 4-1. With the same twisting speed and the delivery speed applied to making the single-core and double-core yarns, the triple-core yarns generated higher Poisson's ratios among all five samples due to the contraction within the multi-core filaments. The helical angles were slightly increased as the core filament became thicker. Figure 4-6 (a) shows the comparison between the single-core, double-core and triple-core yarns with the same twisting speed of 3000 rpm. It is noted that thicker cores lead to higher helical angles because the yarn length becomes shorter for one helical cycle of the binder. Moreover, with the same helical angle of the yarn, a thicker core results in a lower value of NPR, as indicated in Figure 4-6 (b), where the single-core and triple-core yarns with the same helical angle around 26° are compared. In this figure, the triple-core yarn T4 starts to be extruded at approximately 5% axial strain, but the single-core yarn S6 shows a later extrusion at around 7.5% axial strain. The maximum NPR of yarn T4 and S6 are achieved when the axial strain increases to 12.5% and 15%, respectively. Yarn T4 exhibits a much lower negative Poisson's ratio of -0.8 than yarn S6 which has a value of -3.58. This phenomenon shows that larger diameter ratio leads to lower auxetic effect and there are two reasons can explain it. Firstly, the auxetic effect is decreased because the space within the multi-core ply leads to a large initial diameter of the yarn and the space can easily be contracted with each other. Secondly, the thicker core ply is too soft that the wrap ply is a kind of eaten by the core ply when it is straightened during the stretching, that is, the core ply cannot be fully deformed as a helical shape.

Table 4-1 Parameters of the single-core, double-core and triple-core yarns using the equal feeding process

Yarn code	Twisting speed (rpm)	Delivery speed (m/min)	Avg helical angle (°)	Linear Density(tex)	Maximum NPR
S4’	3500	14.2	34.5	264.4	-1.5
S5’	3000	14.2	29.3	263.8	-2.3
S6’	2500	14.2	26.4	263	-3.58
S7’	2000	14.2	18.1	261.8	-5.62
D1	3500	14.2	39.9	508	-0.33
D2	3000	14.2	35.0	504	-0.64
D3	2500	14.2	32.8	502	-0.93
D4	2000	14.2	23.9	501	-1.8
D5	1500	14.2	19.0	499	-3.7
T1	3500	14.2	40.4	768	-0.12
T2	3000	14.2	36.9	761	-0.23
T3	2500	14.2	31.7	757	-0.35
T4	2000	14.2	26.3	755	-0.8
T5	1500	14.2	23.0	749	-1.29

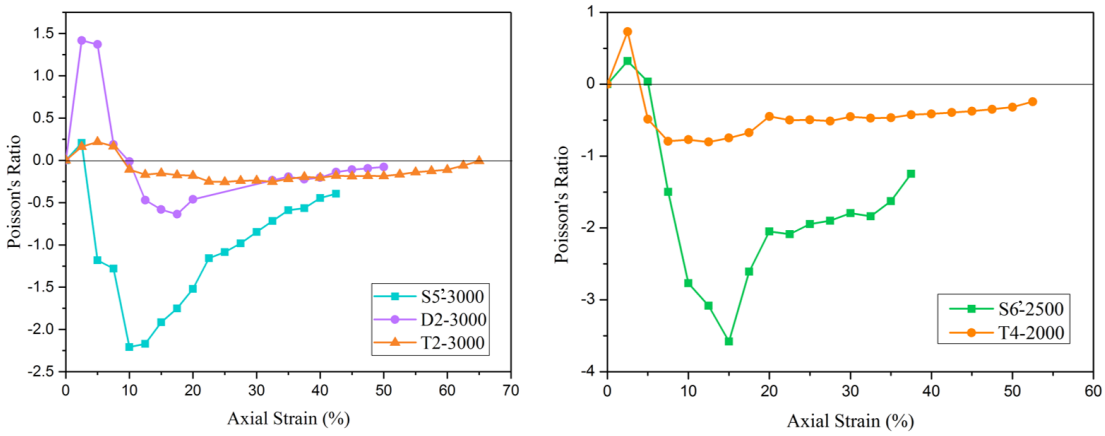

Figure 4-6 Poisson’s ratio of the HAYs with different core diameters: (a) the yarns with the same twisting speed of 3000 rpm; (b) the yarns with the same helical angle of 26˚

To verify the above phenomenon, geometric models of six types of the HAYs were set up using ABAQUS 6.14 with different diameter ratios of the core ply to the wrap ply, the details of which are listed in Table 4-2. All the models were generated having the same initial helical angle of 28° and the relationship between the NPR and the diameter ratio is illustrated in Figure 4-7. Because 1 is taken for the wrap ply in the diameter ratio, the integer numbers 2 to 8 are used in the figure to represent the ratio. It reveals an NPR peak at the diameter ratios of 4:1, indicating the biggest auxetic

effect. This result coincides with the experimental finding that the increasing diameter of the core ply leads to less obvious effect. This could be explained that the diameter ratio of the double-core yarn and the triple-core yarn are much larger than the peak point of 4:1. Thus, a concave relationship is discovered. The auxetic effect is larger with the increasing diameter ratio from 2:1 to 4:1. When the ratio reaches to 4:1, further ascending ratio makes the auxetic effect smaller. Figure 4-8 demonstrates the influence of the helical angle on the NPR for the yarns with the three different diameter ratios numbers of the core plies obtained experimentally representing the single-core, double-core and triple-core yarns. It is noted that the triple-core yarn exhibited the lowest auxetic effect and the single-core the highest.

Table 4-2 Input parameters of the core ply

Yarn code	Y-R2	Y-R3	Y-R4	Y-R5	Y-R6	Y-R8
Diameter Ratio	2:1	3:1	4:1	5:1	6:1	8:1
Core ply (mm)	0.34	0.51	0.68	0.85	1.02	1.36
Wrap ply (mm)	0.17	0.17	0.17	0.17	0.17	0.17

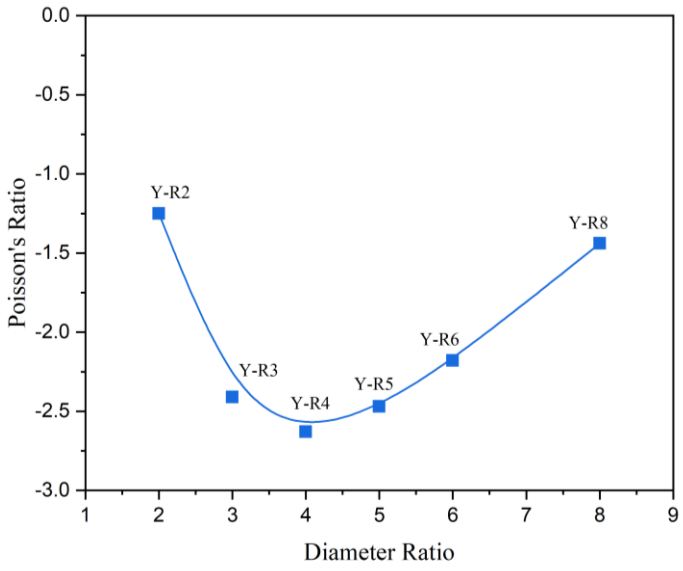

Figure 4-7 Relationship between the Poisson's ratio and the diameter ratio in FE simulation

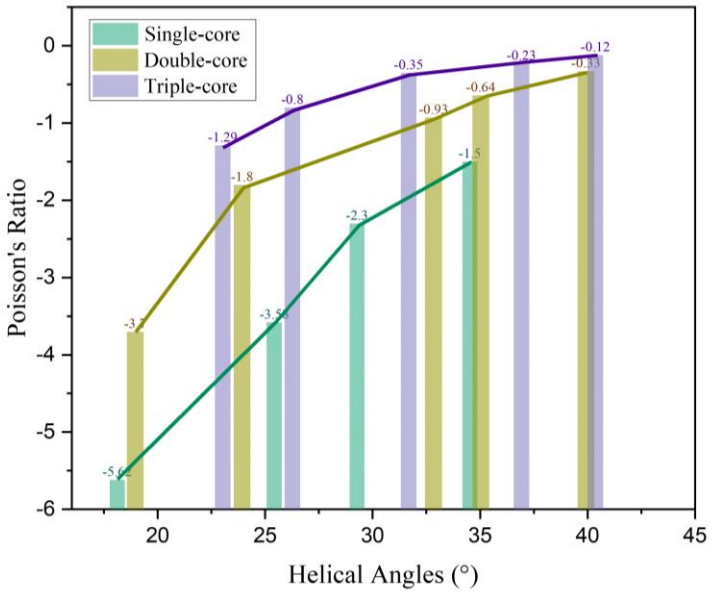

Figure 4-8 The NPR of the yarns with different numbers of the core plies in experiments

4.3.2 The effect of the wrap ply thickness

Moreover, different parameters of the wrap ply were carried out for further investigation. By keeping the helical angle of 28˚, core tensile modulus of 30 MPa and wrap tensile modulus of 1850 MPa as the constant values, the thickness of the wrap ply was set as 0.34 mm, 0.425 mm, 0.51 mm and 0.68 mm corresponding to the diameter ratio of 2:1, 8:5, 4:3 and 1:1, respectively. Then, the diameter ratios are represented by the calculated numbers of 2, 1.6, 1.3 and 1 and the relationship between the diameter ratio and Poisson's ratio is illustrated in Figure 4-9. When the diameter ratio was set as 2:1, it was confirmed that yarns Y-R2 and Y-R2' exhibit the same value of negative Poisson's ratio which is around -1.2. This revealed that by keeping the same diameter ratio, the thickness changes of the yarn cannot influence on the Poisson's ratio. With the decreasing diameter ratio of the yarn, the Poisson's ratio is increased and it is close to zero when the diameter ratio is around 4:3. Then, the minimum Poisson's ratio of the yarn is achieved as 0.37 when the diameter of the core ply and that of the wrap ply are set as the same. It is noted that the diameters of the two plies should be designed in a specific range or a ratio in order to demonstrate the auxetic behaviour.

Table 4-3 Input parameters of the wrap ply

Yarn code	Y-R4	Y-R2’	Y-R1.6	Y-R1.3	Y-R1
Diameter Ratio	4:1	2:1	8:5	4:3	1:1
Core ply (mm)	0.68	0.68	0.68	0.68	0.68
Wrap ply (mm)	0.17	0.34	0.425	0.51	0.68

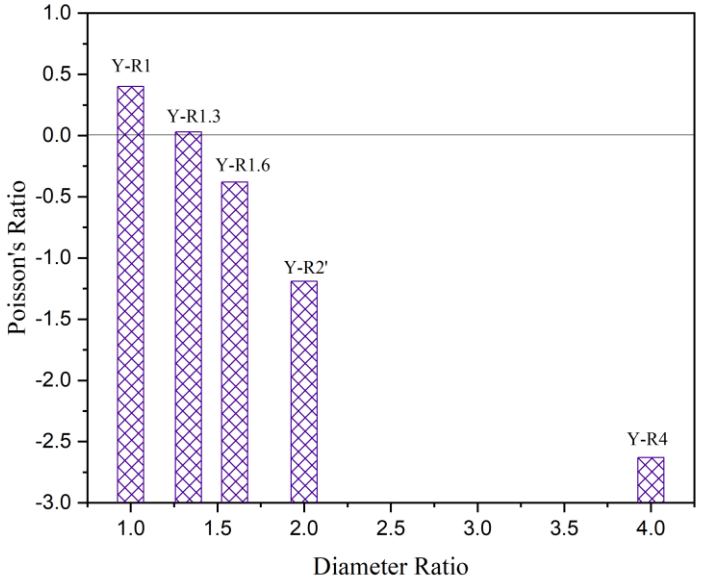

Figure 4-9 Relationship between the Poisson’s ratio and the diameter ratio by changing parameters of the wrap ply

4.3.3 Discussion

Combining the effects of the core ply thickness and the wrap ply thickness, it is necessary to find the boundary of the diameter ratio of the core ply to the wrap ply for achieving auxetic behaviour of the yarn. As shown in Figure 4-10, the relationship between the diameter ratio and Poisson’s ratio has two regions. From the diameter ratio of 1:1 to 3:1, the results show a linear trend between the two values. From the diameter ratio of 3:1 to 8:1, the nonlinear curve is demonstrated and the point with diameter ratio of 4:1 shows the lowest Poisson’s ratio value. It can be seen that from the ratio number 1.3 to 1.7, the Poisson’s ratio reduces from positive to negative, which is 0.03 and -0.38 respectively. In order to predict the diameter ratio when the Poisson’s ratio becomes zero, the results were analysed by to OriginPro 2019 software and a regression equation was set up with the diameter ratio range from 1:1 to 3:1, and

this is shown in Equation (4-1). By substituting the Poisson's ratio value of zero, the predicted range of the diameter ratio number is from 1.09 to 1.5. Therefore, the diameter ratio of the core ply to the wrap ply should be at least 3:2 to demonstrate negative Poisson's ratio.

$$v_d = a_d + b_d D_r, \quad D_r \in [1,3] \tag{4-1}$$

where v_d is the Poisson's ratio influenced by the diameter ratio, D_r is the diameter ratio with the range from 1 to 3, and a_d and b_d take the values of 1.87±0.18 and -1.45±0.10, respectively.

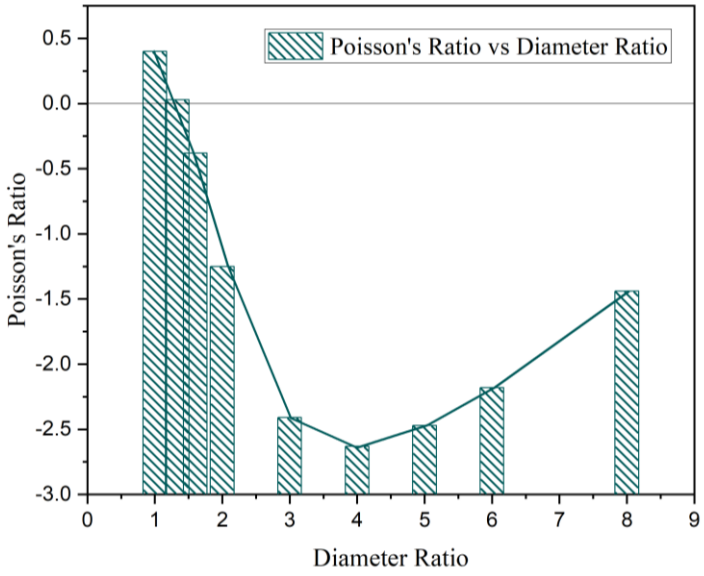

Figure 4-10 Poisson's ratio influenced by the diameter ratio of the two plies

4.4 Tensile moduli of the two plies

4.4.1 Material consideration of the wrap ply

To explore the effect of tensile modulus on yarn auxeticity, wrap plies with different tensile moduli were used for the FE modelling. The moduli of the two plies were obtained from experiments, with the moduli of the core ply and the wrap ply being 30 MPa and 1850 MPa, respectively. Then, the tensile modulus of the wrap ply was assumed to be 500, 1000, 1850, 3000 and 4000 MPa for numerical investigation, as shown in Table 4-4. The other parameters of the model, including the modulus for the core ply, were kept constant with the initial helical angle of 28°, the diameter ratio of

4:1 and the mesh size of M1. Figure 4-11 demonstrates the results of the HAYs with different tensile moduli for the wrap ply, and the relationship between the NPR and the axial strain, shown in Figure 4-11 (a), resembles that from the experiment. When the tensile moduli of Y-M1 is used for simulation, no auxetic effect is apparent for the corresponding HAY, and the Poisson's ratio is 0.05 while the Poisson's ratio became negative by increasing the wrap modulus from 500 MPa to 600 MPa. It is revealed that the auxetic effect is more obvious and the gradient of the curve becomes lower with the ascending tensile modulus of the wrap ply, as illustrated in Figure 4-11 (b). In the yarn simulation, Y-M5 exhibits the lowest Poisson's ratio of -4.9 with the wrap ply modulus being 4000 MPa. It is indicated when the modulus of the wrap ply is close to 4000 MPa, such as the glass fibre [219], the yarn could be produced with the same level of auxeticity. This obviously provides a reference for selecting ply materials, and it suggests that the tensile modulus of the wrap ply should be at least 20 times larger than that of the core ply for achieving any yarn auxeticity.

Table 4-4 Assumed tensile moduli of the core and wrap plies

Yarn code	Y-M1	Y-M2	Y-M3	Y-M4	Y-M5
Core ply (MPa)	30	30	30	30	30
Wrap ply (MPa)	500	1000	1850	3000	4000

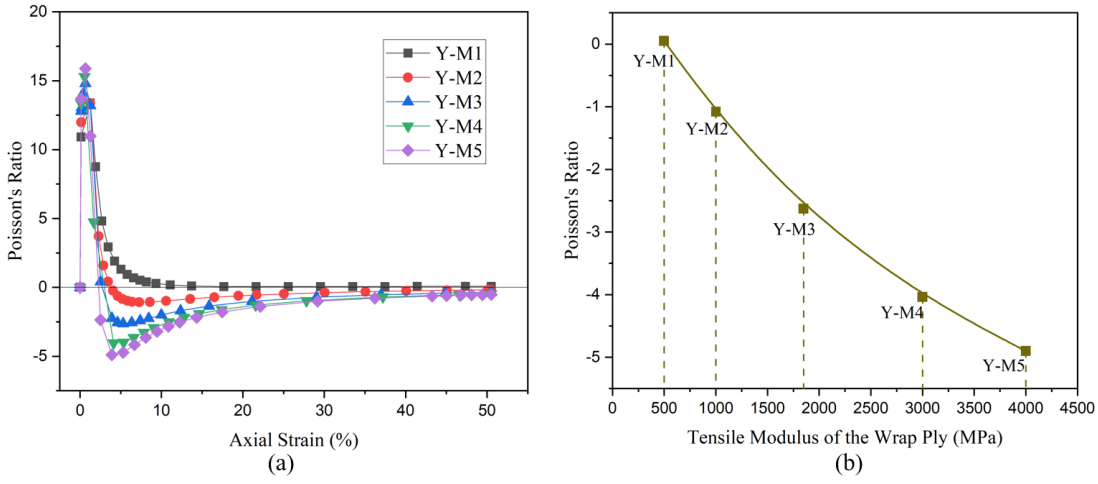

Figure 4-11 The Poisson's ratio of the HAYs with different tensile moduli of the wrap ply: (a) Poisson's ratio vs axial strain; (b) Poisson's ratio vs tensile modulus

4.4.2 Material consideration of the core ply

Different tensile moduli of the core ply were experimented on in the simulation, which are listed in Table 4-5. For this investigation, the tensile modulus of the wrap ply was kept constant at 1850 MPa and that of the core ply was changed from 15 MPa to 120 MPa, which is coded Y-M1' to Y-M5' respectively. During the simulation of the core ply, Y-M1' exhibited the highest auxetic behaviour with the core ply modulus being 15 MPa, which indicated the corresponding rubber-like materials for the core ply could generate the same level of auxeticity with the maximum negative Poisson's ratio around -4.71. In Figure 4-12 (a), when the tensile modulus of the core ply is sufficiently high, the HAYs would not show auxeticity, and the lower the core ply modulus, the more obvious is the yarn auxeticity. Figure 4-12 (b) plots the relationship between the NPR and the modulus of the core ply, which shows that as the tensile modulus of the core ply is decreased the yarn auxeticity becomes more sensitive such as in the case of Y-M1' to Y-M3'. This also indicates that the tensile modulus of the wrap ply should be at least 20 times larger than that of the core ply as the Poisson's ratio of Y-M4' is negative and the Poisson's ratio of Y-M5' is positive.

Table 4-5 Input parameters of the tensile moduli of the core ply

	Y-M1' (MPa)	Y-M2' (MPa)	Y-M3' (MPa)	Y-M4' (MPa)	Y-M5' (MPa)
Core ply	15	30	60	90	120
Wrap ply	1850	1850	1850	1850	1850

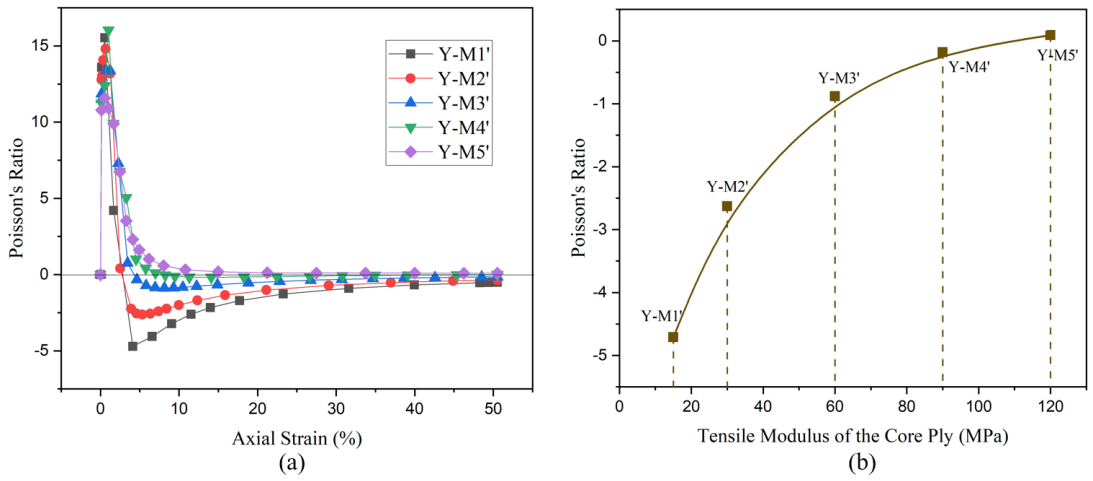

Figure 4-12 The Poisson's ratio of the HAYs with different tensile moduli of the core ply: (a) Poisson's ratio vs axial strain; (b) Poisson's ratio vs tensile modulus

4.4.3 Discussion

Based on the results above, the modulus ratio between the wrap ply to the core ply was demonstrated and the ratio number was calculated by using the wrap modulus divided by the core modulus. As illustrated in Figure 4-13, the Poisson's ratio is decreased as the modulus ratio increased, which shows that higher differential tensile modulus between the wrap ply and the core ply results in higher auxetic behaviour of the yarn. But the sensitivity of the yarn on Poisson's ratio becomes smaller after the modulus ratio of 120. In order to predict the modulus ratio in a statistic way when the Poisson's ratio becomes zero, a polynomial fit is generated by OriginPro 2019 software, which has a good accordance with the FE results. The fitted regression is yielded in Equation (4-2). Substituting the Poisson's ratio of zero into the quadratic equation, the predicted range of the modulus ratio number can be calculated as 17.9 to 19.4. Therefore, by using the integer of the modulus ratio, the tensile modulus of the wrap ply should be at least 20 times larger than that of the core ply in order to achieve negative Poisson's ratio.

$$v_m = a_m + b_m M_r + c_m M_r^2,\ M_r \in [15,133] \tag{4-2}$$

where v_m is the Poisson's ratio influenced by the modulus ratio. M_r is the modulus ratio of the wrap ply to the core ply with the range from 15 to 133. a_m, b_m and c_m are the value of 1.23±0.045, -0.07±0.002 and 2.23E-4±1.25E-5, respectively.

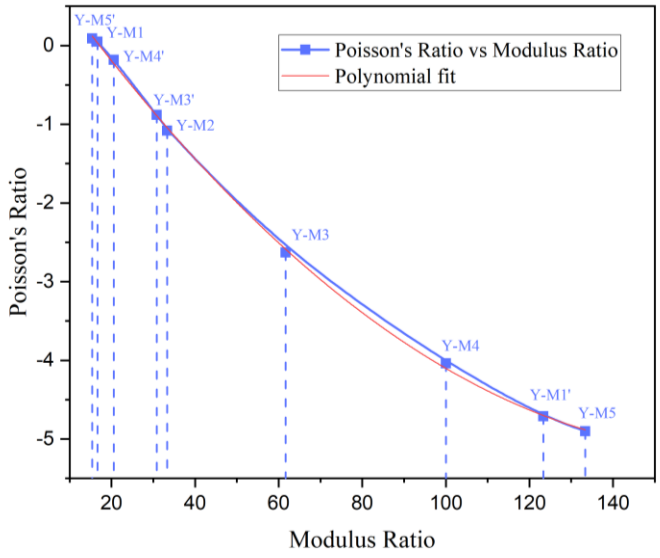

Figure 4-13 Summary of Poisson's ratio versus tensile modulus ratio

4.5 Summary

This Chapter reported the experimental and numerical analyses of the HAYs systematically. The properties of the HAY have been investigated and the factors of the key parameters on Poisson's ratio were discussed. The summaries can be drawn as follows.

(1) Based on the designed yarn models, the auxetic behaviour of the circular model and that of the elliptical model show a good accordance with a low average percentage error of 4.1%. Therefore, in order to have a good efficiency during the simulation, the circular model can be used instead of the elliptical model to predict the yarn properties.

(2) The research results reveal that lower initial helical angle of the HAY leads to higher auxetic effect and the yarn is more sensitive when the angle is smaller especially within the range between 10˚ to 20˚. For a given core and a given binder, both experimental and numerical studies suggested the existence of a smallest helical angle.

(3) A concaved relationship between the diameter ratio and the NPR is discovered through the numerical analysis which is a new finding not reported yet in literatures. This was supported by the experimental results. Additionally, it can be claimed that the diameter ratio of the core ply to the wrap ply should be at least 3:2 to demonstrate negative Poisson's ratio.

(4) The combination of the tensile moduli of the two plies has been found to have great influence on the NPR. The auxetic behaviour is increased with the increasing tensile modulus of the wrap ply or the decreasing tensile modulus of the core ply. This provides a reference for choosing the best ply material for the highest auxeticity. Based on the numerical analysis, it is indicated that the tensile modulus of the wrap ply should be at least 20 times larger than that of the core ply to achieve the auxetic effect.

In summary, the auxetic behaviour of the HAY indicates great potential for many technical applications. The HAYs can be used for making functional fabrics and composites. The performance of auxetic fabrics made from the HAYs will be discussed in the following Chapters. The reported findings in this Chapter can be used by researchers to determine the best structural parameters for the yarn auxeticity, which has not been reported systematically in the existing literature. Even though the

work was investigated through a systematic route, the details of influential factors on Poisson's ratio need to be further explored. For example, the auxeticity increases as the helical angle comes down and there is no auxeticity when the angle is 0, showing it would be theoretically interesting to find out the turning point of the angle on auxeticity. This could be planed as a part of the future work.

Chapter 5 Mechanical Properties of Auxetic Woven Fabrics

5.1 Tensile property

Tensile tests were carried out for the auxetic fabric (AF) and the non-auxetic fabric (NF). Three specimens for each AF and NF fabrics were tested three times in both warp and weft directions, and the median value of the results are shown in Figure 5-1. As shown, the load-extension curves of NF under the load in the weft direction is larger than that of NF in the warp direction, because the tension and the density of the fabric in the warp direction were controlled by the machine during weaving, while these parameters in the weft direction were controlled manually. It can be seen that AF exhibited a low initial modulus and a big extension (≈70%). After the helical polyamide yarn plies were straightened, they took the load applied to the fabric specimen. The polyamide yarns of AF started to break when the fabric were extended to around 70 mm, whereas the specimens of NF started to break at around 35 mm elongation. NF undertook notably higher load than the AF, as the two components of the parallel yarn used in NF took on the load from the beginning of the test. Comparing the difference between the warp and weft directions, as shown in Figure 5-1, the specimen of NF could bear more loads (around 400 N) than that of AF. The difference in load bearing of AF between the warp and weft directions may be associated with the fact that the warp yarns were repeatedly loaded during weaving by the beat-up motion, whereas the weft yarns were hardly loaded in hand weaving. The pretension of the warp yarns could also influence the result.

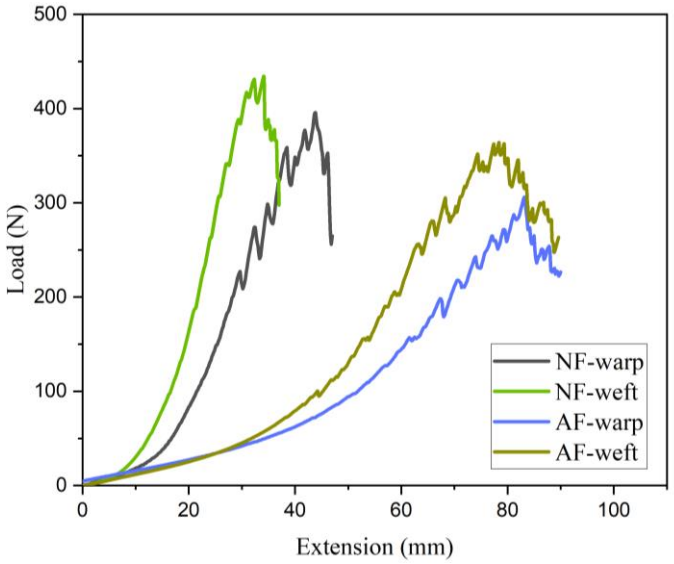

Figure 5-1 Tensile properties of auxetic fabric (AF) and non-auxetic fabric (NF)

5.2 Porosity

5.2.1 Auxetic fabrics versus non-auxetic fabrics

To measure the porosity of the auxetic fabric (AF) and the non-auxetic fabric (NF), the deformation of the fabric surface was recorded and captured by the microfocus USB video class (UVC) camera which has been introduced in Section 3.4.3. After analyse the timed shots for each specimens, the changes of porosity of AF and NF under tensile loading in both warp and weft directions are shown in Figure 5-2. It is noted that AF had a higher porosity than that of NF at all levels of strains, and the difference increases as the strain became higher. This is believed to be associated with the mechanical properties of the yarns used for AF and NF fabrics. Figure 5-3 shows the different configurations of the yarns in fabrics under loading tension. When stretched in a warp direction, the yarns were deformed to either synclastic form or symmetrical form, and it is apparent that the pores were larger formed among auxetic yarns compared with that among parallel yarns. The reason for synclastic form and symmetrical form appeared in the fabric is that the auxetic yarns were arranged randomly during the weaving. This finding is suggested that the yarn arrangement of the woven fabric on Poisson's ratio should be studied and it will be discussed in the following Chapter. In Figure 5-2, the initial porosity of AF was slightly higher than that of NF due to the fact that the HAYs ended up with larger thread spacing. In

addition, the porosity of AF was demonstrated around 3 times as large as that of NF just when the fabrics started to fail.

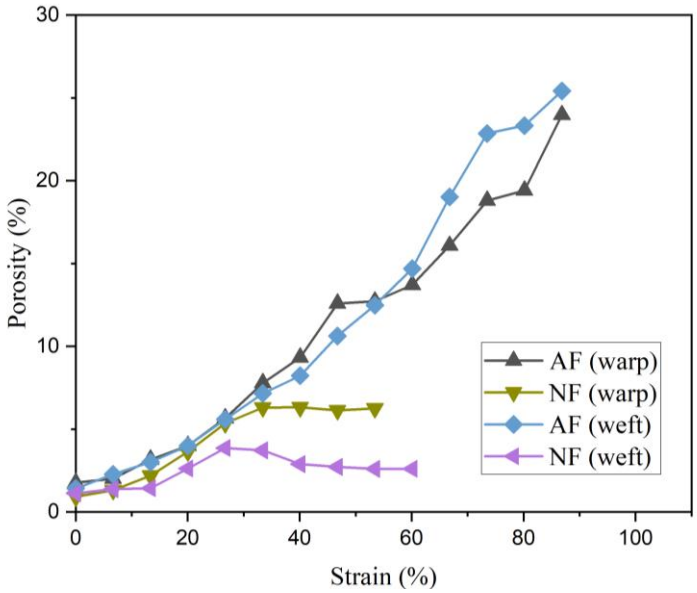

Figure 5-2 Porosities of auxetic fabric (AF) and non-auxetic fabric (NF)

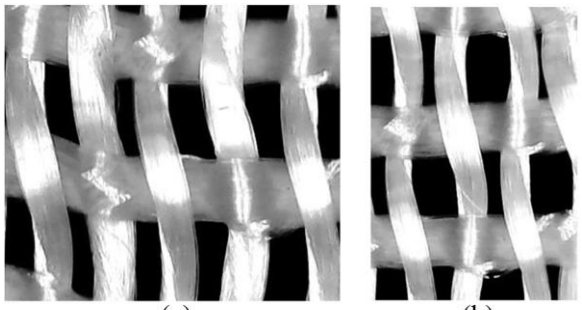

Figure 5-3 Two forms of yarn in auxetic woven fabric: (a) synclastic form; (b) symmetrical form

Associated to the porosity analysis above, AF and NF together with a pure polyurethane fabric specimen (PUF) were conducted for their air permeability. Each sample was tested three times at different levels of pressure and the average data of air permeability with applied pressures ranging from 200 to 300 Pa is shown in Figure 5-4. For different levels of pressure, the air permeability of PUF fabric was the highest, followed by that of the AF and NF. Compared with AF and PUF fabric, NF displays the lowest air permeability because the deformation of the pore areas under pressure was restricted by the polyamide filament in the parallel structure of the yarn. In contrast, PUF was fully elastic, and when pressure was applied it would be pushed

open without external restriction, and therefore demonstrated the highest air permeability. Due to the helical structure of the auxetic yarns, AF fabric deformed relatively easily until the moment when the stiffer ply became straightened. Considering both air permeability and porosity of AF, it is seen that the air permeability of AF fabric could be made different with control, and therefore would have potentials for filtrations. Based on the results of HAYs, it could be seen that the porosity of the AF fabric may be changed by adjusting the helical angles in the yarn.

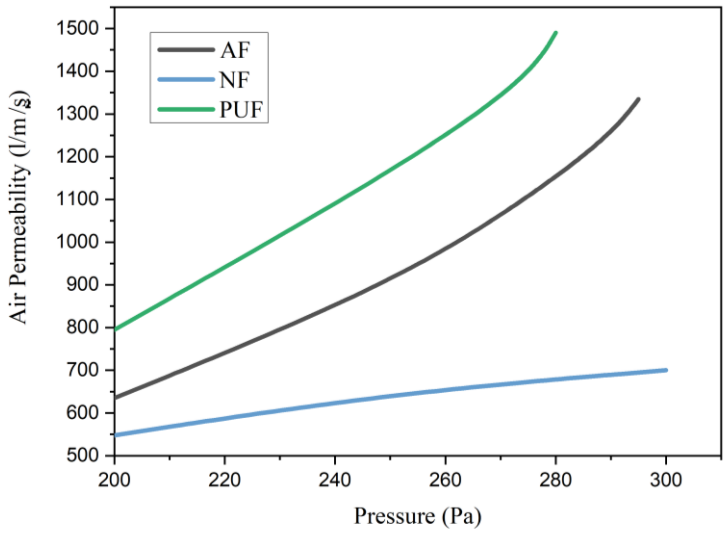

Figure 5-4 Air permeability of AF, NF and PUF

5.2.2 Auxetic fabrics with different float length

With the same testing method of the pore area, auxetic fabrics SWF-5 and DWF-5 were measured along the weft direction as the auxetic yarns were applied to the weft direction only. The fabrics SWF-5 and DWF-5 represent two variables of weave structure, plain weave and 2/2 warp rib weave respectively. Figure 5-5 demonstrates the porosity of them under different levels of longitudinal strain. It is noted that DWF-5 has a higher porosity than that of SWF-5 and the difference is increased with the increasing strain. This phenomenon occurred because the weave structure restricted the deformation of auxetic yarns and the outer contour diameter of the yarn became larger under tension rather than the solid yarn. The porosity of these two fabrics was overlapped from longitudinal strain 0 to 15% because the crimped auxetic yarns need to be straightened until the stiff ply of HAY could bear the tensile loading. After the

auxetic yarn started to be deformed, the plain weave structure restricted the deformation of the yarn under tension because it offered more interlacement than the 2/2 warp rib structure, as shown in Figure 5-6. The open area of DWF-5 exhibited around 61.5% higher than SWF-5 at 35% of longitudinal strain. Due to the 2/2 warp rib structure of DWF-5, the auxetic yarns were bundled by every two threads and they were deformed together with the same helical direction under the tensile loading, which resulted in the larger area of each open pore. Thus, with the same fabric density and other structural parameters of the yarn, weave structure constructing longer float length leads to higher porosity of the fabric.

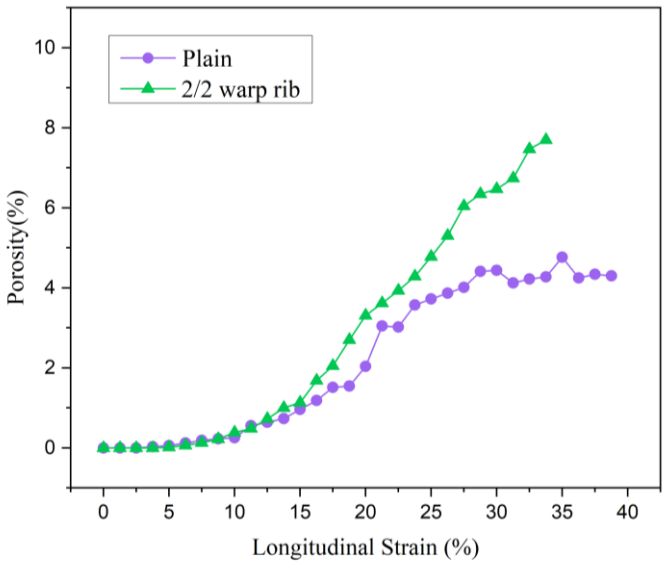

Figure 5-5 Porosity of SWF-5 (plain weave) and DWF-5 (2/2 warp rib weave) during tensile test

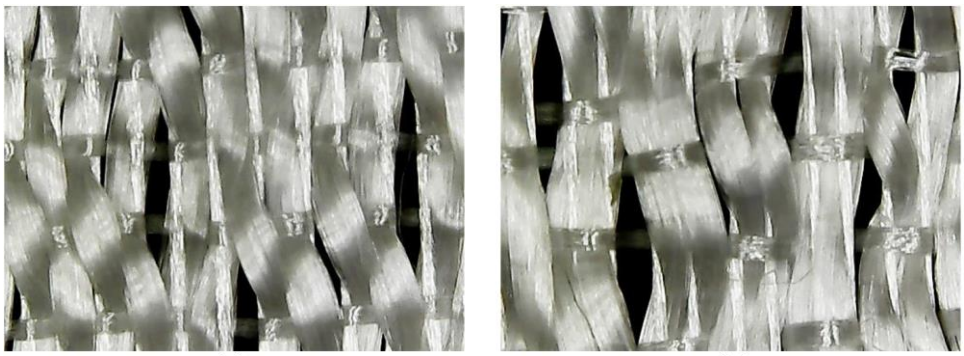

Figure 5-6 Pore area of auxetic woven fabrics under tension: (a) plain (SWF-5); (b) 2/2 warp rib (DWF-5)

5.2.3 Auxetic fabrics constructed by different HAY

Meanwhile, the porosity of SWF-1, SWF-4, SWF-5 and SWF-7 were compared with different HAYs used in them, as illustrated in Figure 5-7. When the fabrics were stretched in the weft direction, SWF-1 showed larger porosity and extension than SWF-4, followed by SWF-5 and SWF-7. This phenomenon may come from the helical angles of the auxetic yarn within the fabric. A higher helical angle of the yarn resulted in more open area of the fabric because there were more wraps with the same length of the yarn. The maximum porosity of the SWF-1, SWF-4, SWF-5 and SWF-7 can be achieved as around 11.4%, 10.2%, 7.5% and 1.62% corresponded to the helical angles of 38.96°, 34.03°, 28.2° and 19.94°, respectively. Thus, it is noted that higher helical angles of the yarn lead to larger porosity of the woven fabric.

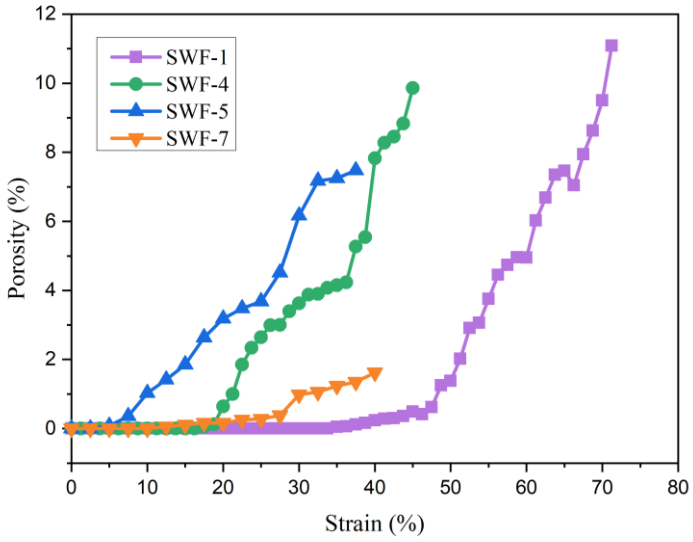

Figure 5-7 Porosity of auxetic fabrics SWF-1, SWF-4, SWF-5 and SWF-7

Based on the investigation, it was found that the porosity is an interesting performance index for the auxetic fabrics, but this will not be pursued further in this research due to the time limit and this will be proposed as part of the future work.

5.3 Impact property

5.3.1 Auxetic fabrics versus non-auxetic fabrics

Low velocity impact testing was carried out for auxetic fabric (AF) and non-auxetic fabric (NF) and single layer fabrics were prepared and used as the testing samples. Figure 5-8 shows the energy and the load of AF and NF against the fabric deflection, with the impact speed being 1.5 m/s. The result shows that NF received an 18% higher

resistant load than AF during the impact test and AF displayed a 20% larger deflection than NF. Experiments also led to the finding that during an impact event, AF absorbed more energy than NF because of its higher extensibility, as shown in Figure 5-8.

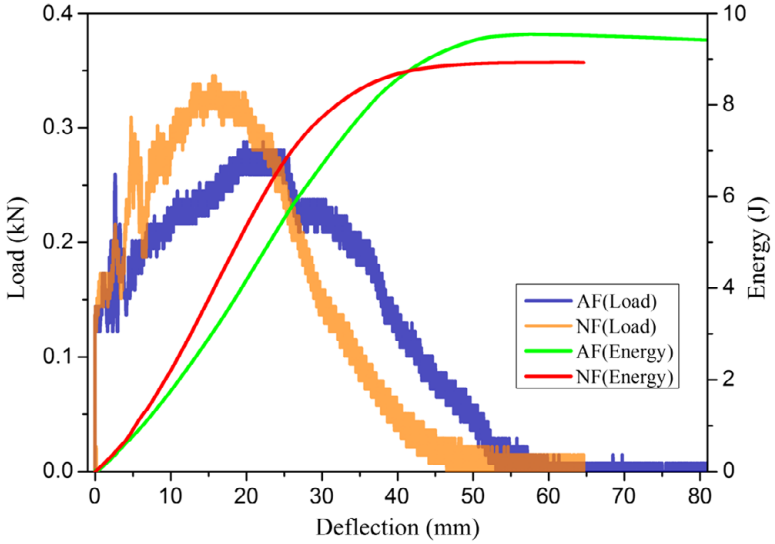

Figure 5-8 Impact properties of auxetic fabric (AF) and non-auxetic fabric (NF)

5.3.2 Auxetic fabrics with different impact level

Figure 5-9 shows the load and the energy of auxetic fabric (AF) with the impact speed of 1 m/s, 1.5 m/s and 2 m/s, respectively. It was found that the maximum load of AF is around 0.3 kN. As for the speed of 1 m/s, the tested fabric is not broken and the highest load is less than 0.2 kN, meaning that the fabric could withstand more loads and energy. The surface of the fabric after impact is shown in Figure 5-10 (a). It is obvious that the polyamide yarn is a little loose and located below the polyurethane due to its low elasticity. At the speed of 1.5 m/s, the polyamide yarn, which is the wrap filament of the auxetic yarn, is broken. The appearance of the fabric surface is shown in Figure 5-10 (b). The deflection of AF is slightly higher than the first one. At the impact speed of 2 m/s, the fabric is totally broken, and this situation is shown in Figure 5-10 (c). It is noted from Figure 5-9 that after the failure of the polyamide ply, the polyurethane ply became load bearing and the second peaks in load and energy appeared. In Figure 5-9 (a), the load of AF with the speed of 2 m/s declines sharply at the deflection of 30 mm. Then, it rises slowly and arrives to another peak of the load which is 0.1 kN. Unlike the tensile properties of auxetic fabrics, the polyamide yarn bears the force at first from the deflection of 0–30 mm until it is broken, and the polyurethane bears the force from the deflection of 30–120 mm. In Figure 5-9 (b), the

total energy absorption is higher with the increasing speed of impact. This could provide a good reference for the impact applications.

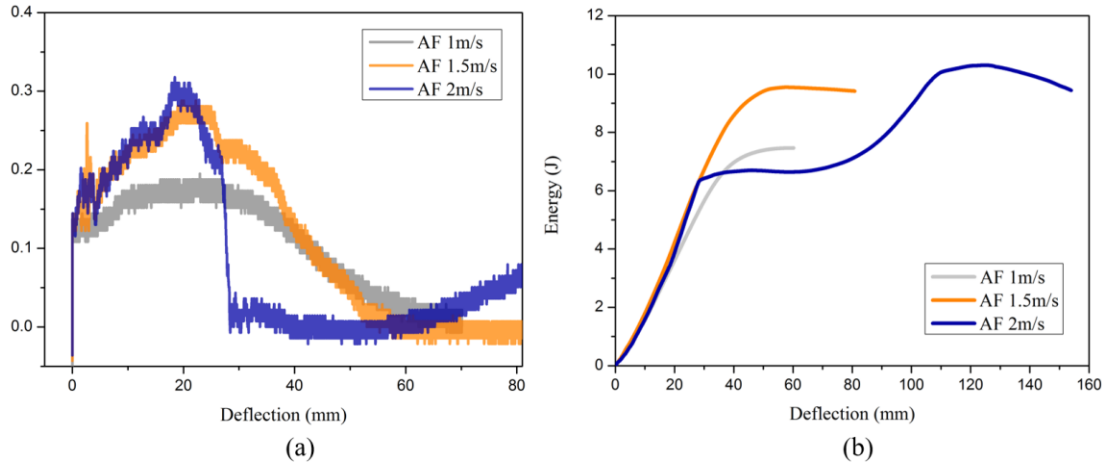

Figure 5-9 Impact properties of auxetic fabric (AF) with different speeds: (a) load; (b) energy

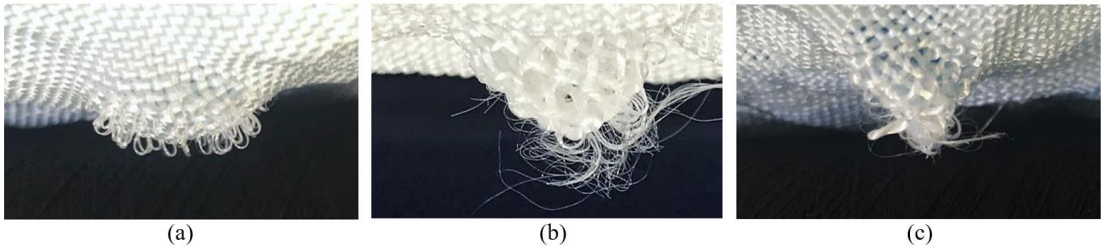

Figure 5-10 Surface of auxetic fabric (AF) after impact testing: (a) 1m/s; (b) 1.5 m/s; (c) 2m/s

5.4 Phenomenon of the auxetic woven fabric

The Poisson's ratio was calculated from the data obtained from the tensile testing. Figure 5-11 demonstrates the Poisson's ratio of AF in the warp and weft directions, corresponding to the tension applied in the weft and warp directions, respectively. The dimensional changes of the fabric were measured at every timed interval by Digimizer software and the maximum negative Poisson's ratio of AF is -0.052 in the weft direction and -0.025 in the warp direction, respectively.

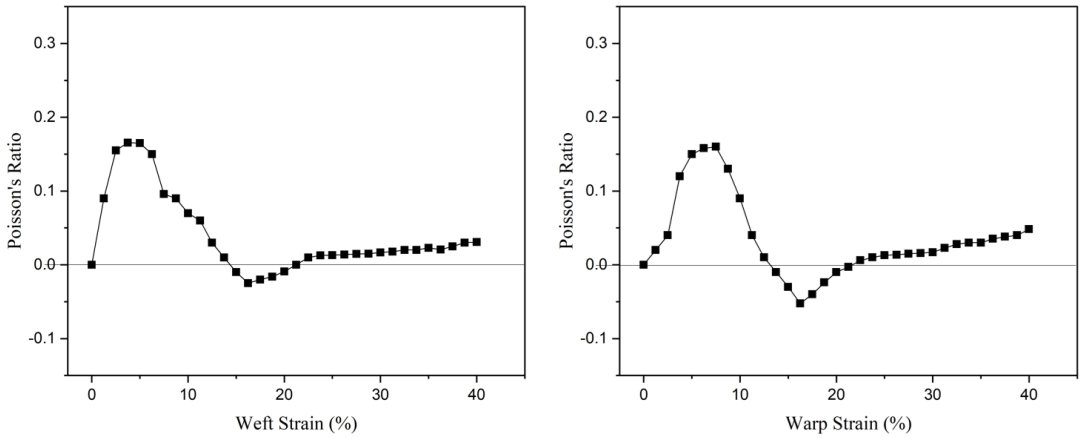

(a) (b)

Figure 5-11 Poisson's ratio of AF: (a) in the warp (longitudinal) direction; (b) in the weft (transverse) direction

The auxetic behaviour of the woven fabric is much smaller than that of the auxetic yarns. This can be explained by the crimp interchange. When the woven fabric is loaded in the warp (say) direction, the crimp in warp yarn is reduced and that forces the crimp in the weft yarn to increase, resulting in narrowing down of the fabric in the weft direction. When the fabric density is high, the auxetic yarns would be pushed with each other, but the expansion of the fabric may still be minimal because of yarn deformation in the transverse direction and the crimp interchange as described earlier. If the fabric density is low, the deformed auxetic yarn would not influence the fabric dimension because increase in the outer contour diameter of the yarn is still smaller than the gap between two adjacent yarns. Because of all these, it could be deduced that the auxetic behaviour of woven fabrics could not be expected purely based on dimensional changes. Also, it is suggested that the majority of the auxetic behaviour of the fabric would be demonstrated in other aspects rather than fabric dimension.

5.5 Summary

In this Chapter, auxetic woven fabrics with helical and parallel yarn structures were created for characterisation. Parameters of the fabrics have been analysed on mechanical properties including tensile property, porosity and air permeability as well as impact property. The Poisson's ratios of the fabric in dimensional changes were also examined. According to the experimental results, the following summaries are drawn.

(1) Auxetic woven fabric made of HAYs in both weft and warp directions has been manufactured and evaluated, the auxetic behaviour of which is found not significantly obvious with maximum NPRs of AF being -0.052 in the weft direction and -0.025 in the warp direction, much smaller than that of the auxetic yarn. Thus, the woven fabrics should not be expected to be auxetic in the plane directions but in other aspects which will be discussed in the next Chapter.

(2) Increased fabric porosity was observed in the auxetic fabric compared to the non-auxetic fabric because of the deformation of the helical yarns, and the permeability can be controlled by adopting different helical angles of the yarn. This indicates special applications for fluid filtration.

(3) Impact tests revealed that one layer of auxetic fabric has higher energy absorption than that of non-auxetic fabric under the same impact conditions. This calls for further investigation for special applications.

In summary, a comparison between such auxetic fabric (helical structure of the yarns) and the non-auxetic fabric (parallel structure of the yarn) has not been investigated so far in the existing literature. The results revealed that the structure of the HAYs influence the tensile property, porosity and impact property of the woven fabric. It was found that the 2D woven fabric would not demonstrate significant auxeticity in the plane directions. Although an auxetic behaviour was reported in some of the literature, there should be more methods to explore and provide an effective auxeticity.

Chapter 6 Factors Influencing Poisson's Ratio of Auxetic Woven Fabrics

6.1 Introduction

Based on the experimental results in the previous Chapter, the auxetic behaviour of woven fabrics need to be further investigated and the key factors for weaving the fabrics need to be identified systematically by using the combination of experiments and numerical simulation. In this Chapter, different types of woven fabrics are compared and the key factors influencing Poisson's ratio are discussed including the HAY arrangements, fabric density, helical angles of the HAY, thickness of the HAY, weave structures, warp yarn types and loading directions. The auxeticity of the fabrics was measured in the thickness direction and in the warp and weft directions.

6.2 HAY arrangements

In this Section, three types of HAY arrangements are generated, which are in-phase, out-of-phase and hybrid phase. To investigate the influencing factors on Poisson's ratio, the other parameters of the fabric were set to remain the same and the structural details of the fabrics are listed in Table 6-1. The fabrics F-P1, F-P2 and F-P3 are classified as the fabric type A as the auxetic yarns were woven in the weft direction only. The fabrics F-P1', F-P2' and F-P3' are seen as the fabric type B and they are featured by auxetic yarns being woven in both warp and weft directions. The Poisson's ratio of each fabric sample is measured in both thickness and warp directions. In order to assess the performance of the two types of fabrics, the uniaxial weft directional test was carried out for fabric type A, whereas the biaxial directional test was used for fabric type B.

Table 6-1 Auxetic woven fabrics with different HAY arrangements

Fabric type	Fabric code	Variable parameters								
		Yarn arrangement	Fabric density (threads/cm)	Helical angle of HAY (°)	Vertical thickness of HAY (mm)	Weave structure	Warp yarn type			Loading direction
							Modulus (MPa)	PR*	Vertical thickness (mm)	
A	F-P1 (F-A28)	In-phase	5×10	28	0.56	Plain	1850	0.42	0.11	Uniaxial-weft direction
	F-P2	Out-of-phase								

	F-P3	Hybrid phase								
B	F-P1’	In-phase	5×10	28	0.56	Plain	HAY(Y-A28)			Biaxial
	F-P2’	Out-of-phase								
	F-P3’	Hybrid phase								

6.2.1 Fabric type A

6.2.1.1 In-phase arrangement

In-phase arrangement of auxetic yarns was created in the woven fabric model and the HAYs were applied in the weft direction of the fabric, coded as F-P1, as shown in Figure 6-1. After the tensile test in the weft direction, the Poisson’s ratios of the fabric measured in the thickness direction and the warp direction are drawn in Figure 6-2. It can be seen that the deformation of the woven fabric is similar to that of the auxetic yarn. In the case of F-P1 measured in the thickness direction, when the fabric was stretched under tensile loading, the HAY started to be deformed and the two plies of the HAY were helically twisted together, leading to the decreased cross section of the HAY and the positive Poisson’s ratio of the fabric until around 5% of strain. Then, from the strain 5% to 17%, the soft core ply of the HAY became more helical and the stiff wrap ply turned into straighten in the centre of the HAY, resulting in the decreased Poisson’s ratio of the fabric from positive to negative. During the stretching, the deformation of the fabric thickness was much slower than that of the corresponding HAY due to the restriction of the warp yarns. The maximum negative Poisson’s ratio of the woven fabric (F-P1) in the thickness direction was achieved as -1.35 at around 17% of strain. After the fabric reached to the maximum thickness, further loading made the fabric thinner again and the value of the Poisson’s ratio was increased from negative to positive under the strain around 20% to 43%. In the case of F-P1 measured in the warp direction, the length of the fabric in the warp direction was reduced initially and then expanded from 2.5% to 17% of strain, demonstrating the maximum negative Poisson’s ratio of -0.35. Then, from strain 17% to 43%, the Poisson’s ratio of the fabric was gradually increased until reached the positive value of 0.2. It was found that the auxetic behaviour of F-P1 was mainly demonstrated by the fabric thickness rather than the fabric dimension.

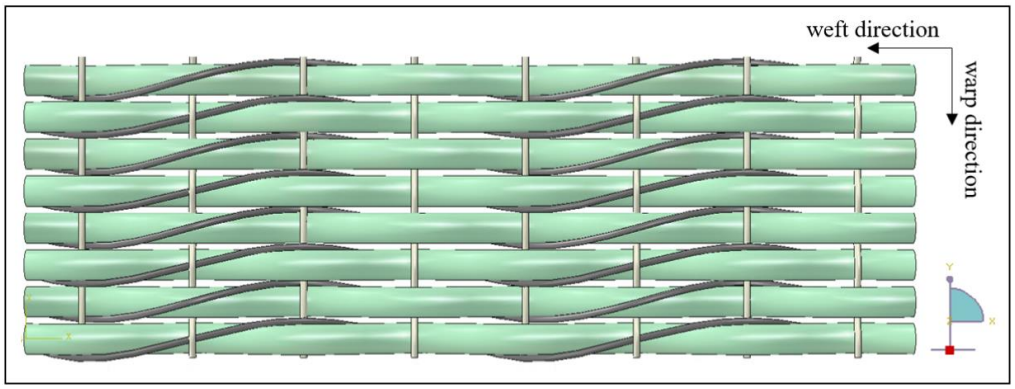

Figure 6-1 In-phase arrangement in the weft direction of the fabric (F-P1)

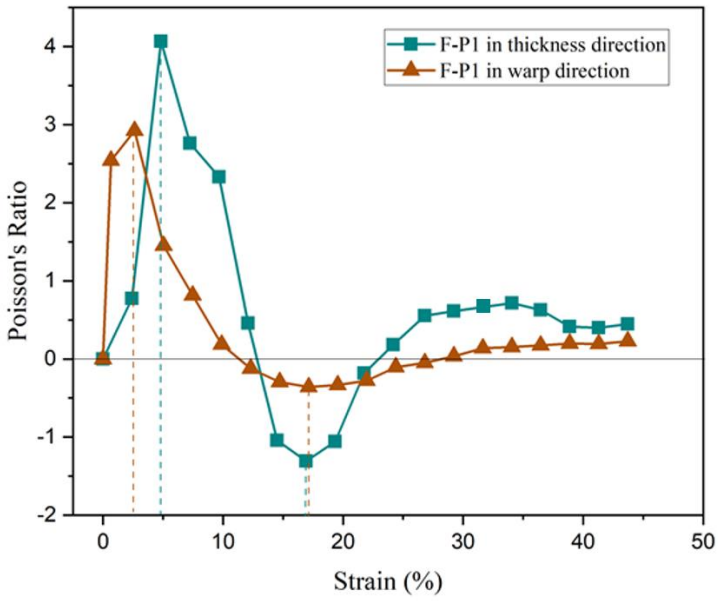

Figure 6-2 Poisson's ratio of the woven fabric (F-P1)

6.2.1.2 Out-of-phase arrangement

In Figure 6-3, the out-of-phase arrangement of the HAYs were applied to the weft direction of the woven fabric, coded as F-P2. Compared to the deformation of the fabric measured in the warp direction, the auxetic behaviour of F-P2 in thickness direction was more obvious, exhibiting maximum negative Poisson's ratio of -0.85 at around 15% of strain, as illustrated in Figure 6-4. The values of F-P2 measured in the warp direction illustrated a steadily trend that demonstrated maximum negative Poisson's ratio of -0.63 at the same strain level above. It was noted that the shrinkage and expansion of the fabric can clearly be observed in the thickness direction rather

than the warp direction of F-P2 even if this phenomenon was not as obvious as in the case of F-P1.

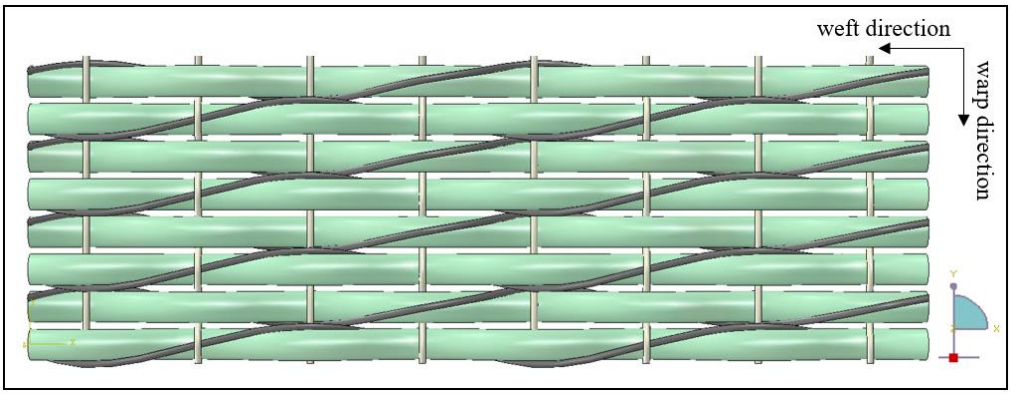

Figure 6-3 Out-of-phase arrangement in the weft direction of the fabric (F-P2)

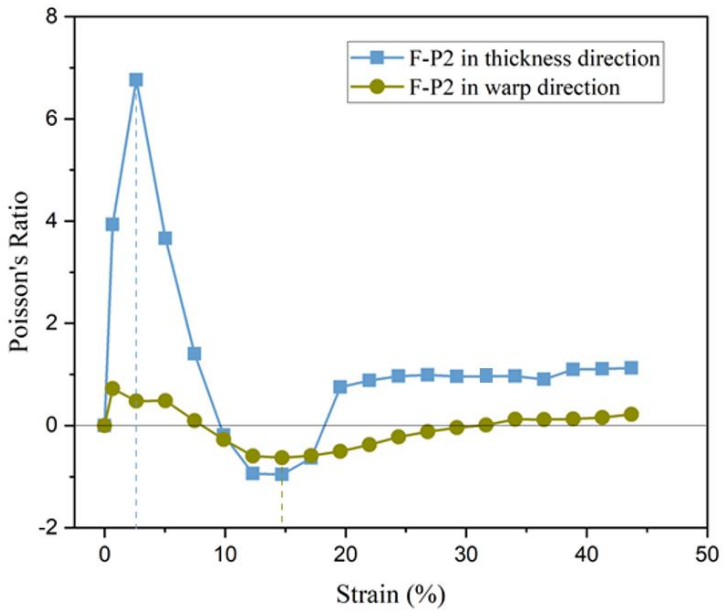

Figure 6-4 Poisson's ratio of the woven fabric (F-P2)

6.2.1.3 Hybrid phase arrangement

In reality, the yarns in the woven fabric are most likely to be random and the hybrid phase arrangements of the HAYs may have endless possibilities, so the middle situation between the in-phase and out-of-phase arrangements was simulated in the fabric model as the representative type of the hybrid phase arrangement shown in Figure 6-5, coded as F-P3. After the comparison between F-P3 measured in the thickness and warp directions, it was found that the highest auxetic behaviour is generated at 17% of strain and the minimum Poisson's ratio value of F-P3 in the

thickness direction and the warp direction are -0.92 and -0.51, respectively, as illustrated in Figure 6-6. An interesting phenomenon was observed that the negative Poisson's ratio of the fabric is shown from 10% to 36% of strain in the warp direction, whereas the negative value is generated in the thickness direction at the strain 13% to 21%. This can be explained that the woven auxetic yarns need to be decrimped and deformed at the same time. The fabric will be thinner when the decrimping level is higher than the auxetic extruded level.

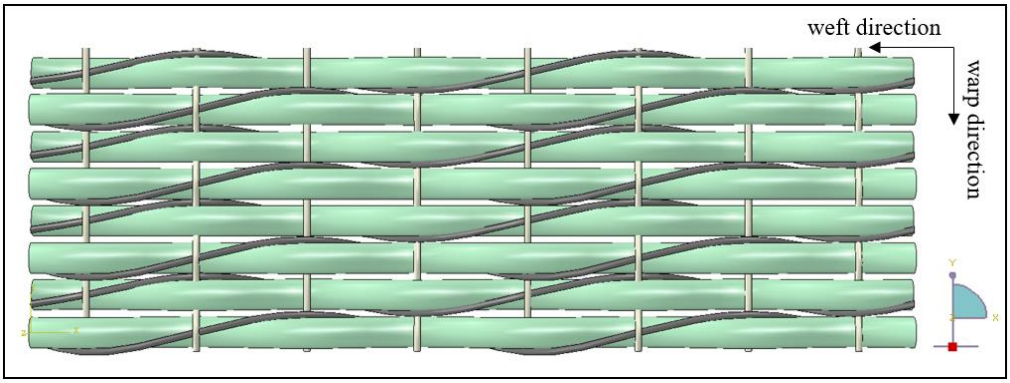

Figure 6-5 Woven fabric model (F-P3) with hybrid phase arrangement of HAYs

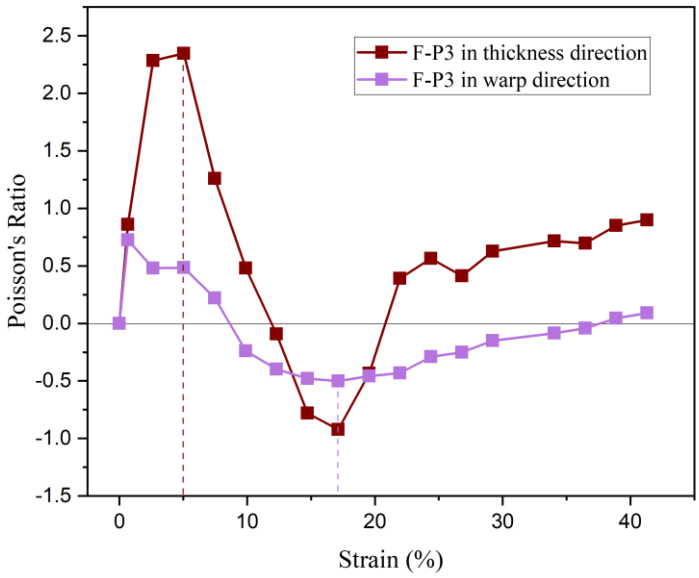

Figure 6-6 Poisson's ratio of woven fabric (F-P3) made of HAY with the hybrid phase arrangement

6.2.1.4 Discussion

Based on the results of fabric type A, the auxeticity was discussed in the aspects of thickness direction and warp direction, respectively. It was found that the in-phase arrangement generated a higher auxetic behaviour in the thickness direction, followed by the hybrid phase and out-of-phase arrangements. However, the in-phase arrangement showed 44% less auxeticity than out-of-phase arrangement in the warp direction and the value of hybrid phase arrangement was in the middle, as illustrated in Figure 6-7. The reason can be explained as follows.

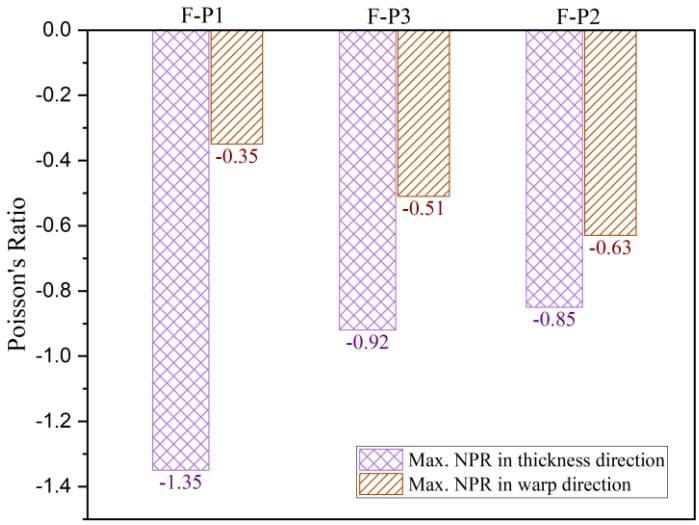

Figure 6-7 Minimum Poisson's ratios of woven fabrics F-P1 (in-phase), F-P2 (out-of-phase) and F-P3 (hybrid phase)

In the aspect of warp direction, when the fabric is stretched in the weft direction, the in-phase arranged yarns have less contact and physically nesting with each other shown in Figure 6-8, resulting in a smaller NPR value in the warp direction. In the situation of out-of-phase arrangement, if the material is rigid enough, the yarns will push the structure out, leading to higher auxetic behaviour of the fabric in the warp direction. Even if the yarn materials are compressible and the yarn configuration can be deformed very easily which can absorb the intended changes of the fabric, the out-of-phase arrangement shows higher auxeticity than the in-phase arrangement. In the aspect of thickness direction, the in-phase arranged yarns are deformed with the same helical path, forcing the extruded yarns to be out-of-plane at the same direction. It was found that the weft yarns shown in Figure 6-9 (a) bear more force from the in-phase

arranged yarns than that shown in Figure 6-9 (b) with out-of-phase arranged yarns at the same strain of 17%. It was observed that the in-phase arranged yarns have higher out-of-plane extrusion than the out-of-phase arranged yarns. In Figure 6-9 (b), the out-of-phase arranged yarns are pushed each other out and the expansion of the fabric in the thickness direction is absorbed by the increased area of the adjacent yarns in the warp direction. Therefore, the in-phase arrangement of the HAYs demonstrates higher auxetic behaviour of the fabric in the thickness direction than the out-of-phase arrangement. Another reason may come from the fabric density. If the fabric density is low, the yarns will be more open when the fabric is stretched. Despite the increased thickness of the auxetic yarns, the auxeticity is mainly happened in warp/weft direction rather than thickness direction. If the fabric density is high, the yarns will be more touch with each other and there will be a lot of squeeze, giving higher thickness of the fabric. As shown in Figure 6-10 (a), the in-phased arranged yarns are squeezed at 14% of strain and then nesting with each other at 17% of strain. In this Section, the weft density is 10 threads/cm and a lower weft density will be investigated in Section 6.3, finding out the auxetic behaviour of the fabric when the auxetic yans are not contacted with each other. In the situation of out-of-phase arrangement shown in Figure 6-10 (c), although there is a squeeze between the HAYs, the out-of-plane extrusion of the fabric is restricted by the contact of adjacent HAYs and the deformation of them is absorbed by material itself. Hence, the out-of-phase arrangement shows less auxeticity in fabric thickness.

In summary, by adopting the HAYs in the weft direction only, the auxeticity of the fabric is less significant in the warp direction. The auxetic behaviour of the fabric in the thickness direction can be maximised by using in-phase arrangement of the HAYs. The out-of-phase arrangement of the auxetic yarns can enlarge the auxeticity of the fabric in the warp direction.

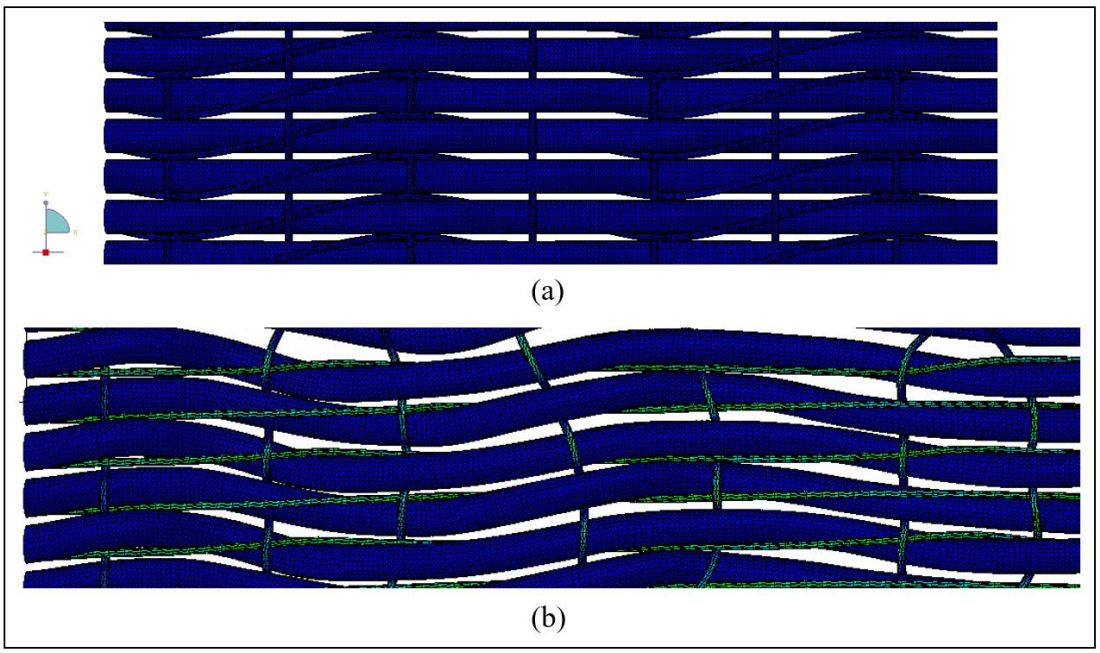

Figure 6-8 Deformation of in-phase arrangements of HAYs in the weft direction: (a) without tension; (b) under 17% of strain

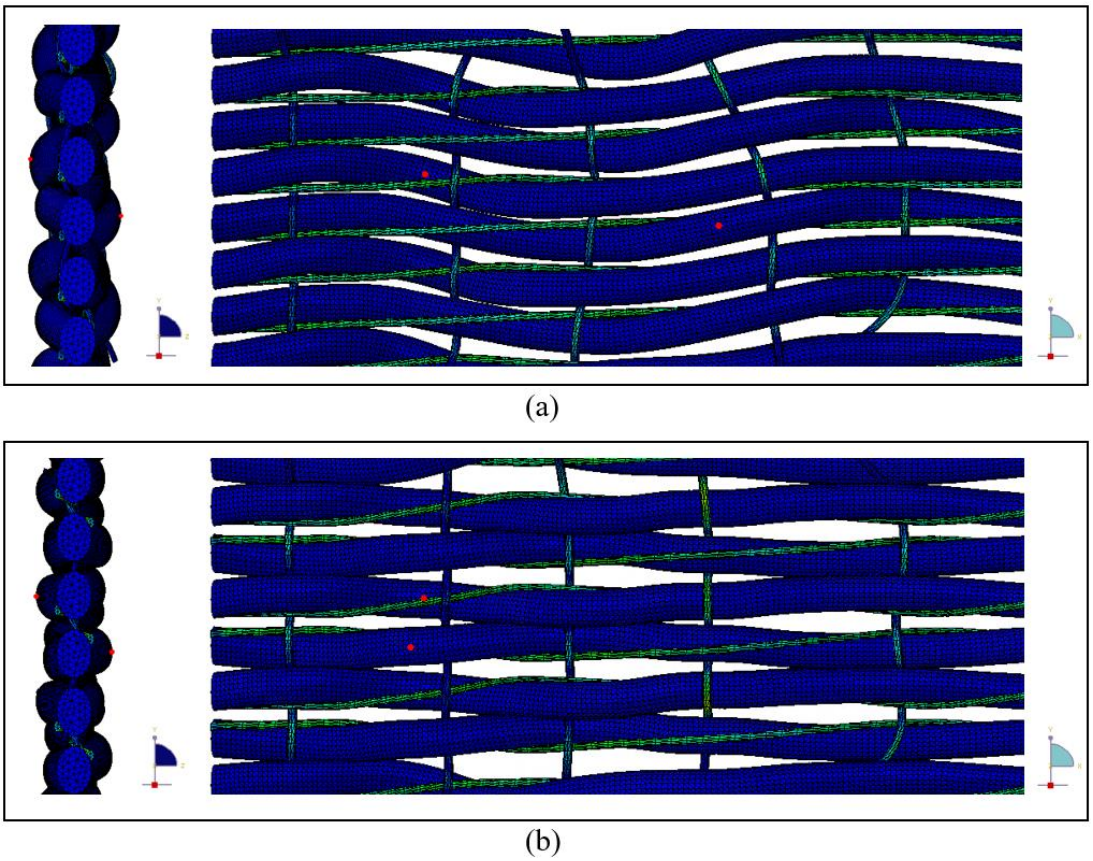

Figure 6-9 Auxetic fabrics at the same strain of 17%: (a) F-P1 (In-phase); (b) F-P2 (out-of-phase)

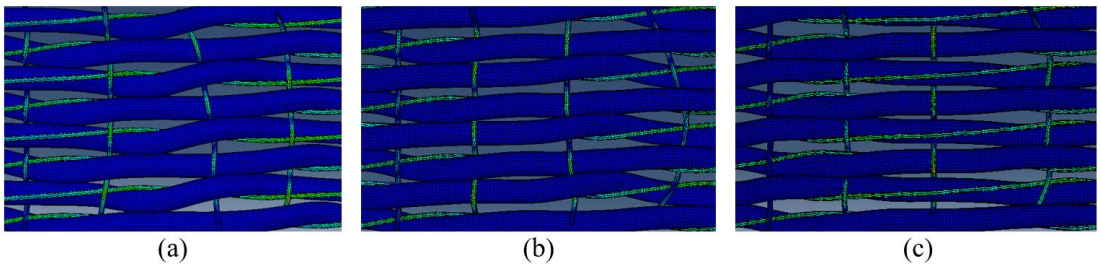

Figure 6-10 Squeezed HAYs in the fabric at 14% of strain: (a) in-phase; (b) hybrid phase; (c) out-of-phase

6.2.2 Fabric type B

6.2.2.1 In-phase arrangement

Another type of fabric was generated by arranging in-phase auxetic yarns in both warp and weft directions, coded as F-P1', as shown in Figure 6-11. The biaxial loading was applied to the fabric model, so the HAYs in both directions would contribute to the auxetic behaviour of the fabric. It was found that the minimum biaxial strain ratio of F-P1' was achieved as -0.62 in the thickness direction at around 18% of strain shown in Figure 6-12, which was smaller than that of F-P1 due to the different warp yarns used in F-P1'. It should be pointed out that thicker warp yarns result in higher crimping level of the weft yarns, leading to higher initial thickness of the fabric. When the fabric is stretched, the auxetic yarns need to be decrimped at first and start to be auxetic afterwards. Thus, the out-of-plane auxetic behaviour of the fabric is eaten by involving HAYs in both warp and weft directions due to the compressibility of the yarn materials, decrimping effect and increased gap between adjacent yarns. When F-P1' measured in the warp direction, the minimum biaxial strain ratio was achieved as -0.99 at around 20% of strain, which indicated that the decrimping of the yarns is not effectively influenced on fabric dimension. Therefore, the auxetic behaviour of F-P1' mainly comes from the warp direction of the fabric rather than the thickness direction of it.

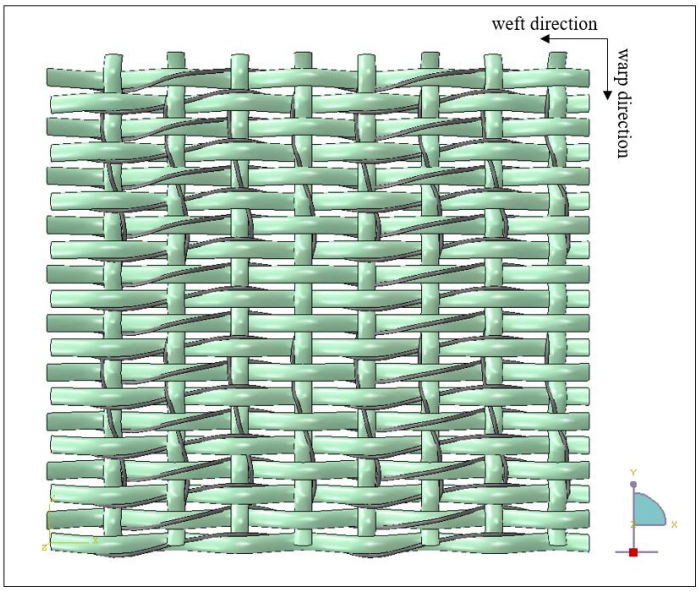

Figure 6-11 Woven fabric model (F-P1') with in-phase arrangement of HAYs

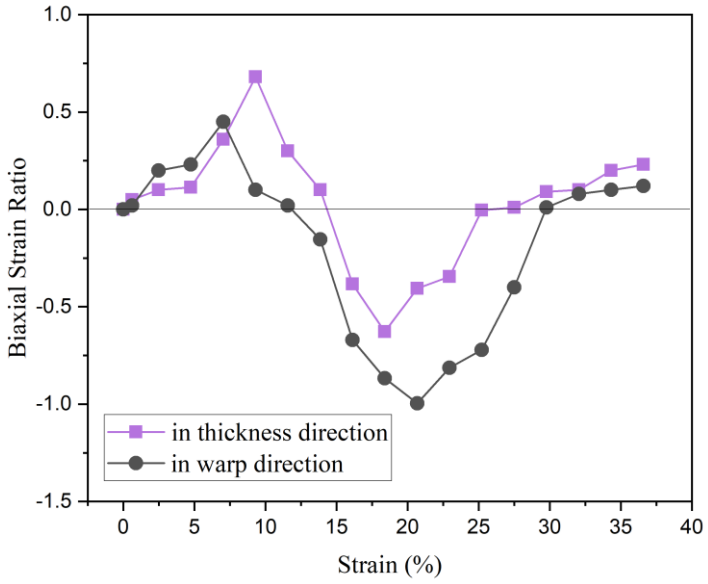

Figure 6-12 Biaxial strain ratio of F-P1'

6.2.2.2 Out-of-phase arrangement

Meanwhile, woven fabric model with out-of-phase arrangement of HAYs in the weft direction was generated, keeping the in-phase arrangement of HAYs in the warp direction, as shown in Figure 6-13 (a). Under the biaxial loading, the symmetric deformation of the yarns was demonstrated in the weft direction from 16% of strain and the minimum biaxial strain ratios in thickness direction and warp direction were

achieved as -0.35 and -1.17 shown in Figure 6-13 (b) and (c), respectively. It can be seen that the auxeticity of the fabric in the warp direction is more obvious as the adjacent weft yarn pushes each other, exhibiting higher in-plane expansion of the fabric. The biaxial strain ratio of the fabric in thickness direction and in warp direction are shown in Figure 6-14.

When the auxetic yarns are out-of-phase in both warp and weft directions as shown in Figure 6-15 (a), the minimum biaxial strain ratio generated is positive 0.56, in fabric thickness, but exhibited as negative -0.76 at the same strain of 18%, as shown in Figure 6-15 (b) and (c), respectively. It was confirmed that the auxetic behaviour of the fabric mainly generates in fabric dimension when the HAYs are woven in both warp and weft directions.

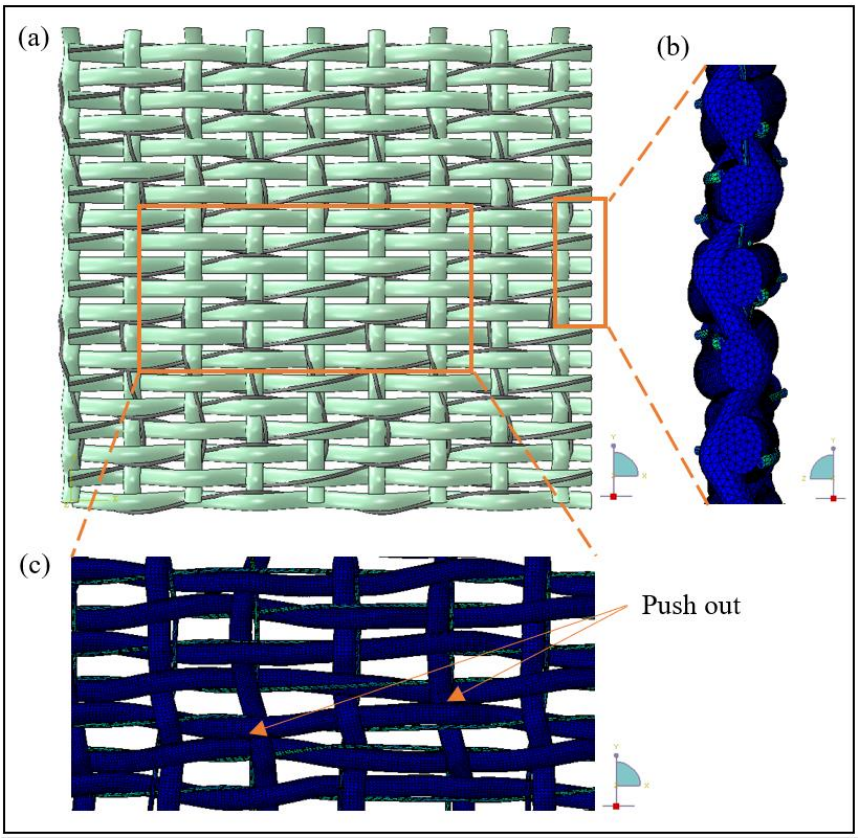

Figure 6-13 Woven fabric model (F-P2') with out-of-phase arrangement of HAYs in the weft direction: (a) fabric model without tension; (b) fabric thickness at 18% of strain; (c) fabric dimension at 18% of strain

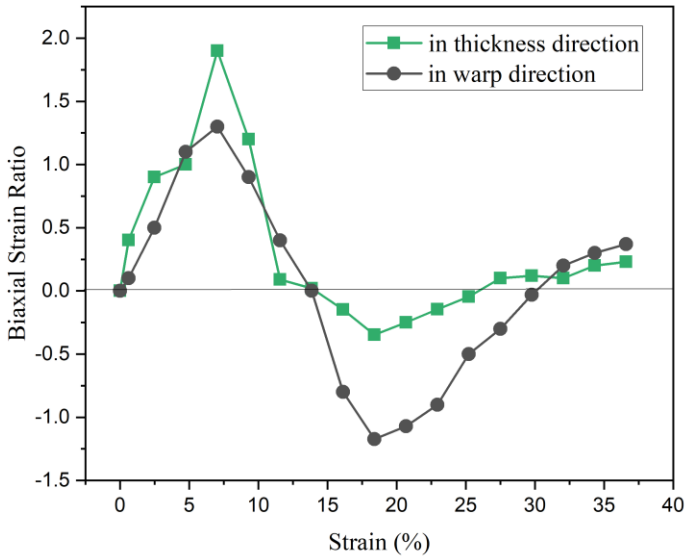

Figure 6-14 Biaxial strain ratio of F-P2’

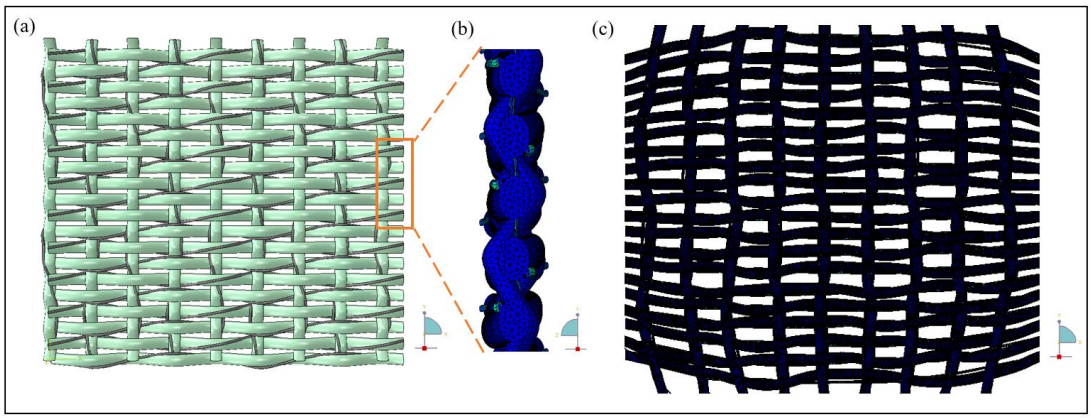

Figure 6-15 Out-of-phase arrangement of HAYs in both warp and weft directions: (a) without tension; (b) fabric thickness at 18% of strain; (c) fabric dimension at 18% of strain

6.2.2.3 Hybrid phase arrangement

Figure 6-16 shows the fabric model with hybrid phase arrangement of HAYs in the weft direction, coded as F-P3’, containing the same structural parameters of F-P1’ and F-P2’. It was found that the minimum biaxial strain ratios of the fabric in the thickness direction and the warp direction are -0.45 and -1.06, respectively, as illustrated in Figure 6-17. This also confirmed that F-P3’ shows less auxeticity than F-P3 in fabric thickness but higher auxetic behaviour in fabric dimension due to the involvement of auxetic yarns in the warp direction.

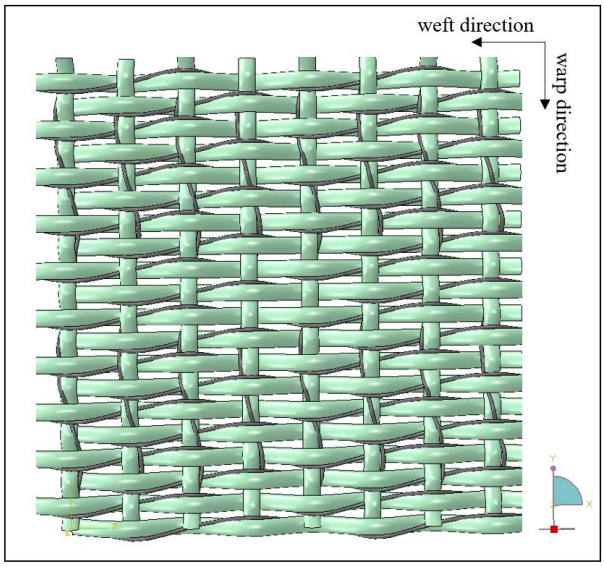

Figure 6-16 Woven fabric model (F-P3') with hybrid phase arrangement of HAYs in the weft direction

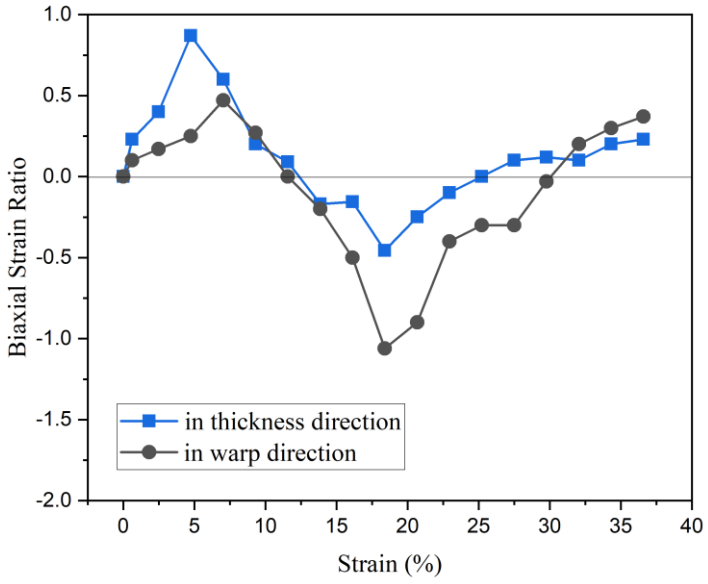

Figure 6-17 Biaxial strain ratio of F-P3'

6.2.2.4 Discussion

When the HAYs applied in both warp and weft directions of the fabric (Fabric type B), the minimum biaxial strain ratios of F-P1', F-P2' and F-P3' are compared in Figure 6-18. Similar to the results of fabric type A, the in-phase arrangement of the HAYs generates a higher auxetic behaviour than the out-of-phase arranged yarns of the fabric in the thickness direction, and the results of the hybrid phase arrangement are in the

middle. In the aspect of warp direction, out-of-phase arranged yarns in the fabric demonstrate around 15% higher auxeticity than in-phase arranged yarns due to the yarns having more contact and pushing each other. The auxeticity of fabric type B in the warp direction exhibits overall higher value than that in the thickness direction, in contrast to the results of fabric type A. This can be explained by the involvement of the HAYs in both directions, decrimping effect and the compressibility of the yarn materials. Therefore, when the fabric is stretched, the deformation of the HAYs in both warp and weft directions is mainly transferred to the in-plane auxeticity rather than out-of-plane. In the aspect of thickness direction, the in-phase arranged yarns are deformed and pushed the weft yarns out, leading to the higher auxetic behaviour of the fabric, as shown in Figure 6-19 (a). As indicated in fabric type A, the in-phase arranged yarns extruded with the same helical path and the weft yarns undertook more force, leading to higher out-of-plane auxeticity of the fabric. In contrast, the out-of-phase arranged yarns cannot push the weft yarns out at the same strain of 18%, as shown in Figure 6-19 (b). Therefore, the in-phase arrangement generates higher auxeticity of the fabric than out-of-phase arrangement in the thickness direction.

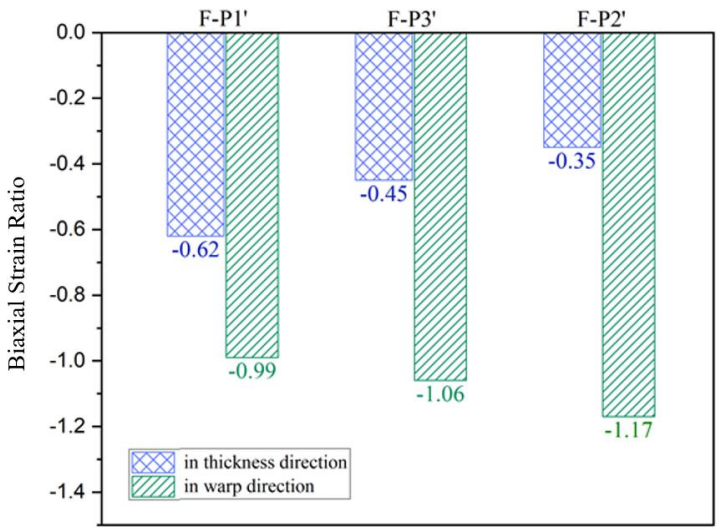

Figure 6-18 Minimum biaxial strain ratios of fabric type B (F-P1', F-P2', F-P3') with different yarn arrangements

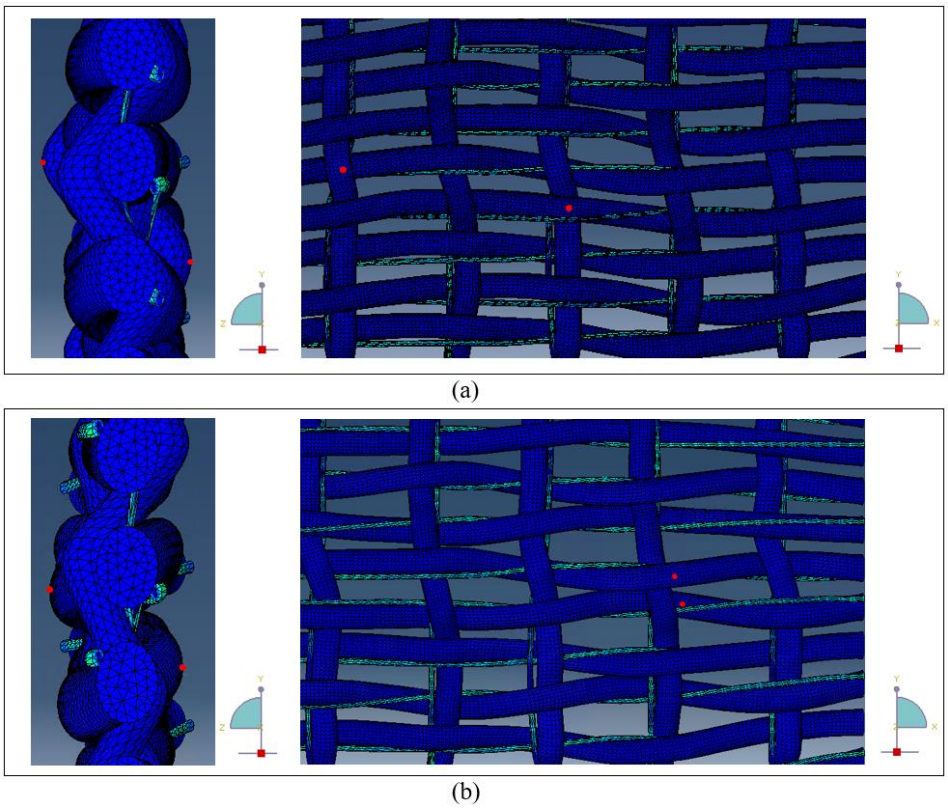

Figure 6-19 Deformation of auxetic woven fabrics at 18% of strain: (a) in-phase arrangement (F-P1'); (b) out-of-phase arrangement (F-P2')

In summary, the in-plane auxeticity of the fabric is more obvious by weaving the HAYs in both warp and weft directions. In-phase arrangement of the HAYs exhibits higher auxeticity of the fabric in the thickness direction and out-of-phase arrangement of the auxetic yarns generates higher auxetic behaviour in the warp direction. Based on the results of fabric type A and type B, it was also found that the tightness of the fabric could affect the out-of-plane auxeticity of the fabric and this will be discussed in Section 6.3. Also, the two types of fabric corresponding to the uniaxial and biaxial loading have some interesting influence on auxeticity, which will be investigated detailly in Section 6.8.

6.3 Fabric density

Based on the findings in HAY arrangements, the auxeticity could highly depend on the density of the fabric. In this Section, the fabric was considered in the situation of the auxetic yarns applied in the weft direction only. Then, the weft density of auxetic fabric model was set as 6 threads/cm and 8 threads/cm, compared to the fabric with

10 threads/cm weft density corresponding to the fabric above in Section 6.2.1. Three types of fabric densities were investigated with three types of yarn arrangements as well and the details are shown in Table 6-2.

Table 6-2 Auxetic woven fabrics with different fabric densities

Fabric code	Variable parameters								
	Yarn arrangement	Fabric density (threads /cm)	Helical angle of HAY (°)	Vertical thickness of HAY (mm)	Weave structure	Warp yarn type			Loading direction
						Modulus (MPa)	PR*	Vertical thickness (mm)	
F-N1	In-phase	5×6	28	0.56	Plain	1850	0.42	0.11	Uniaxial
F-N2	Out-of-phase								
F-N3	Hybrid phase								
F-N4	In-phase	5×8	28	0.56	Plain	1850	0.42	0.11	Uniaxial
F-N5	Out-of-phase								
F-N6	Hybrid phase								
F-P1 (F-A28)	In-phase	5×10	28	0.56	Plain	1850	0.42	0.11	Uniaxial
F-P2	Out-of-phase								
F-P3	Hybrid phase								

The maximum negative Poisson's ratio of each fabric in the thickness and warp directions is illustrated in Figure 6-20. It was found that the auxeticity of the fabric in the warp direction is decreased with the decreasing weft density because the yarns are more open and they have less contact with each other. An interesting phenomenon was observed that the fabric containing out-of-phase arranged yarns exhibits higher auxetic behaviour in the thickness direction with the reduced weft density from 10 threads/cm to 6 threads/cm, in contrast to the fabric involving in-phase arranged yarns. This is because the auxetic yarns are less restricted to be out-of-plane when they have less contact with each other during the deformation. In the situation of 10 threads/cm, the auxetic yarns in the fabric are squeezed at 14% of strain for in-phase, hybrid phase and out-of-phase arrangements, as shown in Figure 6-21 (a). With the increased tensile loading in the weft direction, the in-phase arranged yarns are nested with each other at 17% of strain but the out-of-phase arranged yarns are squeezed in a great extent shown in Figure 6-21 (b), leading to higher strain in the thickness direction for out-of-phase arrangement. In the situation of 8 threads/cm, the auxetic yarns in the fabric are less contacted with each other, as shown in Figure 6-22. Similar to the weft density of

10 threads/cm, the in-phase arranged yarns are squeezed at 14% of strain and they are nested at 17% of strain, whereas the out-of-phase and hybrid phase arranged yarns are both squeezed from 14% to 17% of stain. In the situation of 6 threads/cm, the auxetic yarns are not contacted with each other from 14% to 17% of strain, as shown in Figure 6-23. Thus, the out-of-phase arranged yarns are more freely to be deformed and the auxeticity of the fabric in the thickness direction is increased with the decreasing weft density. The auxetic behaviour of the fabric containing in-phase arranged yarns is always higher in the thickness direction than that of the out-of-phase and hybrid phase arranged yarns because the lowest Poisson's ratio value exhibits at 14% of strain for in-phase arrangement and that generates at 17% of strain for out-of-phase and hybrid phase arrangements. Although the strain in the thickness direction of out-of-phase arrangement is little higher than that of the in-phase arrangement with the decreasing weft density, the negative Poisson's ratio is lower for out-of-phase arrangement due to it having higher strain in the weft direction of the fabric.

Therefore, less contact of the adjacent auxetic yarns result in lower auxetic behaviour of the fabric in the warp direction. The auxetic behaviour of the fabric in the thickness direction is higher with decreasing weft density for out-of-phase arrangement due to less contact area and friction between the auxetic yarns, in contrast to the fabric having in-phased yarn arrangement.

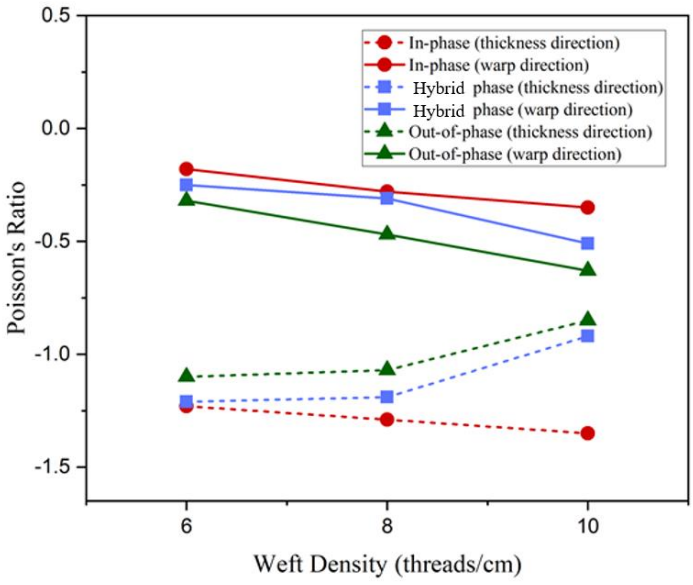

Figure 6-20 Maximum negative Poisson's ratio of the fabric with different densities

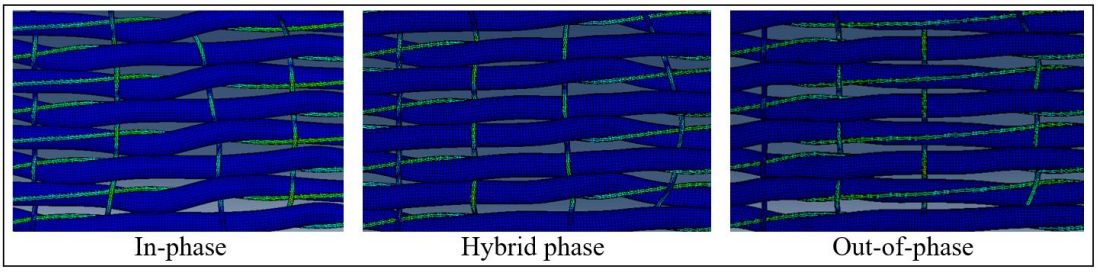

(a)

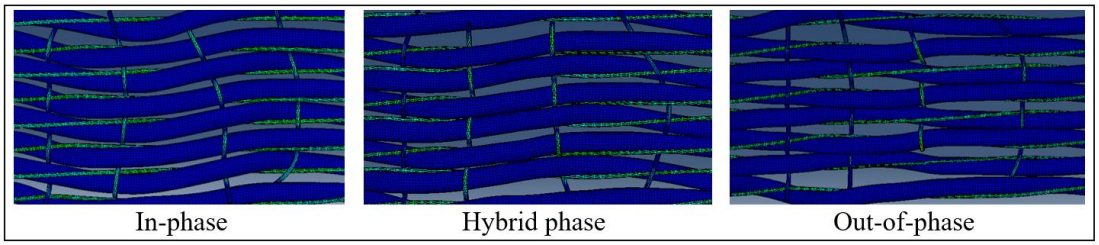

(b)

Figure 6-21 Auxetic fabrics with 10 threads/cm of weft density: (a) at 14% of strain; (b) at 17% of strain

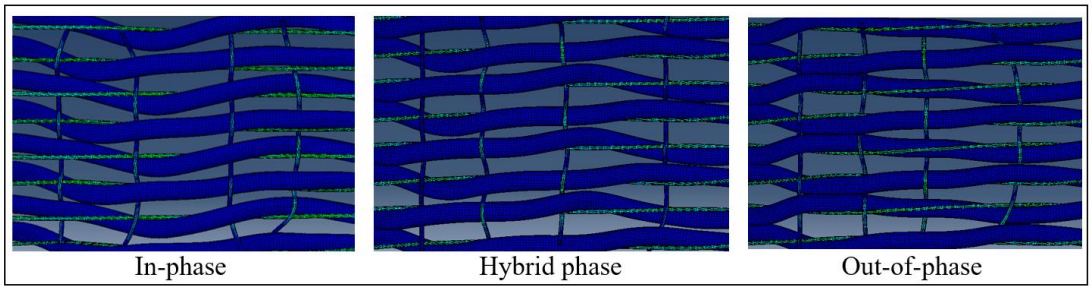

(a)

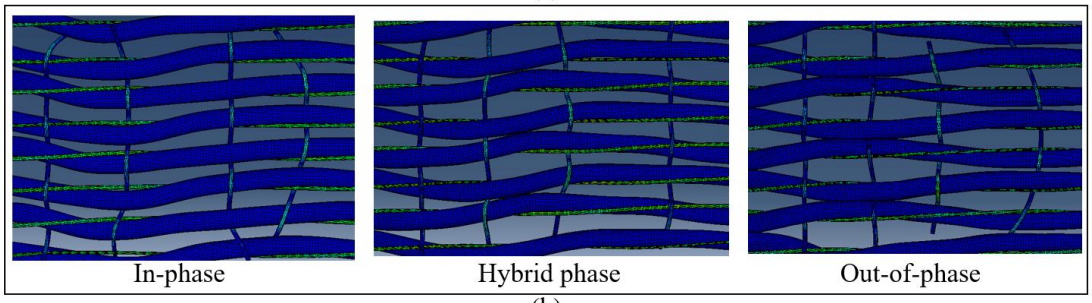

(b)

Figure 6-22 Auxetic fabrics with 8 threads/cm of weft density: (a) at 14% of strain; (b) at 17% of strain

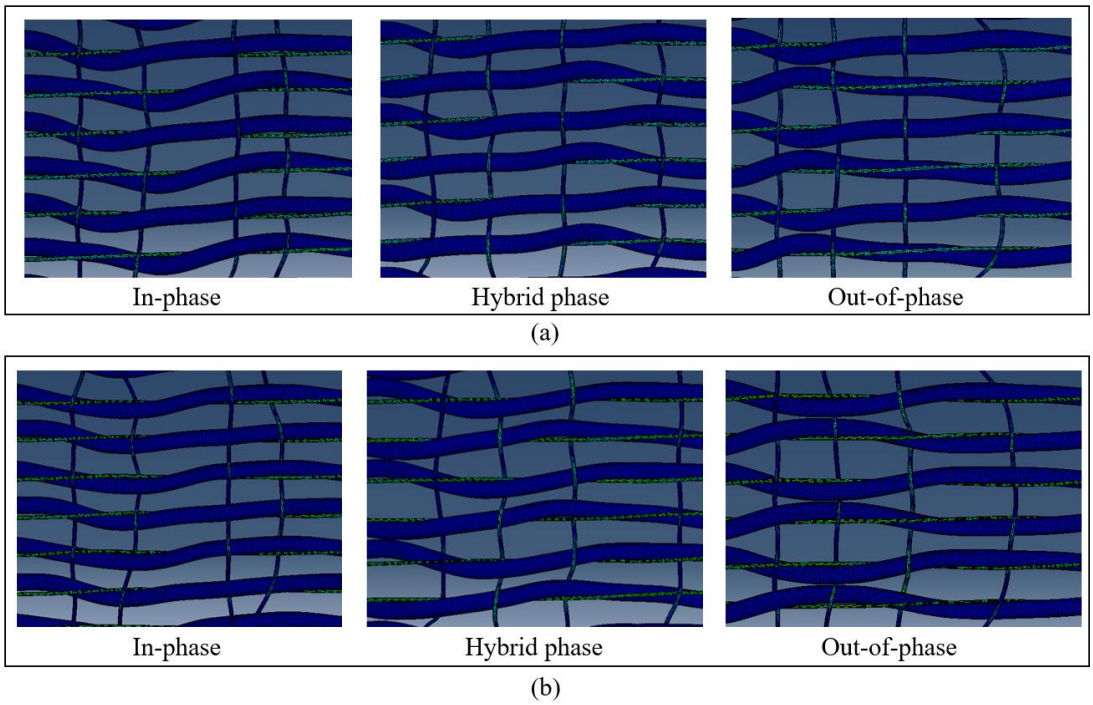

Figure 6-23 Auxetic fabrics with 6 threads/cm of weft density: (a) at 14% of strain; (b) at 17% of strain

6.4 Helical angles of the HAY

Four types of auxetic yarns with different helical angles from 20˚ to 39˚ were selected for making woven fabrics, coded as SWF-1, SWF-4, SWF-5 and SWF-7, respectively, accompanying with the corresponded fabric model F-A39, F-A34, F-A28 and F-A20 shown in Figure 6-24. The maximum negative Poisson's ratios of those fabrics were illustrated in Figure 6-25, compared with the results of FE simulation and the selected yarns. In Figure 6-25, the maximum negative Poisson's ratio of the yarn is overall higher than that of the corresponding fabric. When the helical angle is set as 20˚, the auxetic behaviour the fabric in experiments is around 41% smaller than that of the corresponding yarn. However, when the helical angle is reached to 39˚, the maximum negative Poisson's ratio of the fabric is -0.3, exhibiting a 28% lower value of the corresponding yarn. This can be explained that a higher angle of the HAY deforms at a larger tensile strain and the auxetic yarns are restricted by the warp yarns within the fabric during the stretching. Also, there exist interaction between the adjacent yarns. The auxetic behaviour of the fabric is increased from value -0.3 to -3.32 with the decreasing helical angles of the HAYs. The trends of the maximum negative Poisson's ratio are similar between the yarns and the fabrics. Thus, the auxetic effect of the

woven fabrics can be inherited from the auxetic yarns and the negative values are mainly demonstrated in the thickness direction of the fabric rather than the warp direction of the fabric. Combined the results of experiments and the FE simulation, lower helical angles of the auxetic yarn result in higher auxetic behaviour of the fabric and the loss of the auxeticity is decreased when the helical angle is smaller.

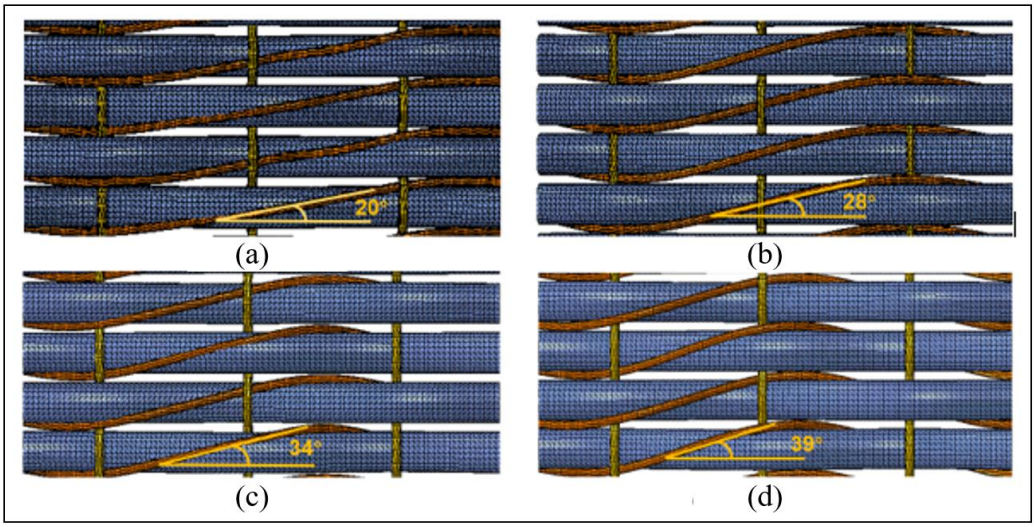

Figure 6-24 Woven fabric models containing different helical angles of HAYs: (a) F-A20; (b) F-A28; (c) F-A34; (d) F-A39

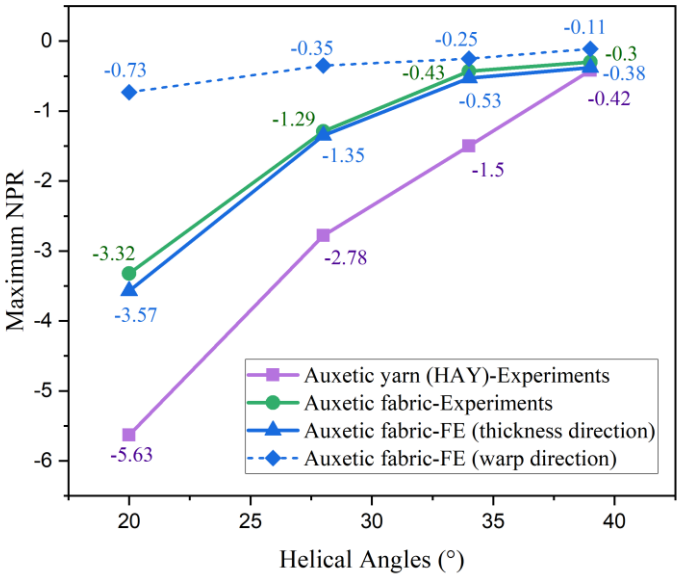

Figure 6-25 Maximum negative Poisson's ratio between auxetic fabrics and corresponding yarns with different helical angles

6.5 Thickness of the HAY

Based on the validated fabric model, the FE method was used for analysing the effect on thickness of the auxetic yarn. In this Section, the auxetic yarns are applied in the weft direction of the fabric only. Five different thickness of the weft yarn were involved for the plain woven fabrics including 0.28mm, 0.56 mm, 0.84mm, 1.12mm and 1.4mm, corresponding to the fabric code of F-T1, F-T2, F-T3, F-T4 and F-T5, respectively. Other parameters of the fabric were kept the same, including yarn arrangement, fabric density, helical angle of the HAY, weave structure, warp yarn type and loading direction, as shown in Table 6-3. The vertical thickness of the HAY in the fabric is smaller than that of the original HAY because the cross section of the yarns is deformed as a elliptic shape after weaving and the thickness of the fabric is mainly contributed by the vertical diameter of the HAY. Therefore, the variable parameter of the fabric for yarn thickness is presented by the vertical thickness of the HAY.

Table 6-3 Parameters of woven fabrics with different thickness of HAYs

Fabric code	Variable parameters								
	Yarn arrangement	Fabric density (threads/cm)	Helical angle of HAY (°)	Vertical thickness of HAY (mm)	Weave structure	Warp yarn type			Loading direction
						Modulus (MPa)	PR*	Vertical thickness (mm)	
F-T1	In-phase	5×5	28	0.28	Plain	1850	0.42	0.11	Uniaxial
F-T2 (F-A28)				0.56					
F-T3				0.84					
F-T4				1.12					
F-T5				1.4					

Figure 6-26 demonstrates the maximum negative Poisson's ratio of the fabrics in thickness direction and warp direction. It is obvious that the fabric shows a higher auxetic effect with decreasing thickness of the auxetic yarn because the contact area between the warp and weft yarns is larger when the fabric produced by thicker auxetic yarns. In addition, the thicker weft yarn shows less auxeticity because the core ply of the auxetic yarn is too soft and it is cut into the wrap ply under tension. Therefore, thicker auxetic yarn leads to lower auxetic effect of the fabric and this can provide a reference for researchers to select suitable yarn dimension for their fabric production.

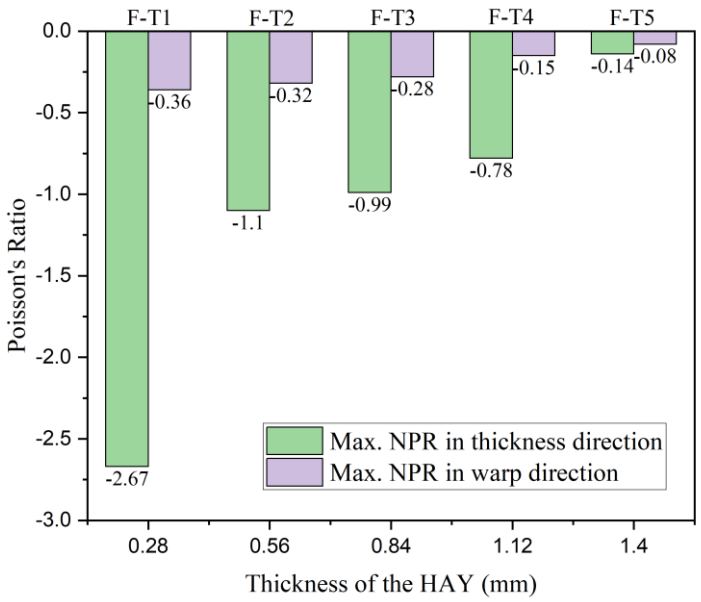

Figure 6-26 Maximum negative Poisson's ratio of the fabrics with different thickness of the yarn

6.6 Weave structures

Three types of weave structures were created in ABAQUS 2019 software, including plain, 2/2 warp rib and 3/3 warp rib, coded as F-W1, F-W2 and F-W3, respectively. The fabric models were considered in the situation of auxetic yarns applied in the weft direction. To investigate the effect of weave structure, other parameters of the fabric were kept the same including in-phase yarn arrangement, 5×10 threads/cm of fabric density, 28˚ angle and 0.56 mm thickness of the HAY, warp yarn type and loading direction. Figure 6-27 shows the changes of Poisson's ratio of the three types of woven fabrics in the thickness direction. It can be seen that the trend of the fabric deformation is similar to the yarn deformation. When the tensile loading applied to the weft direction of the fabric model, the thickness of the fabric is decreased, demonstrating positive Poisson's ratio from strain 0 to 5%. Then the soft core ply of the HAY in the fabric starts to be extruded as a helical shape, leading to the expansion of the fabric in the thickness direction and the Poisson's ratio is decreased from positive to negative. After the thickness of the fabric reaches to the maximum value, further loading makes the fabric thinner and the Poisson's ratio is close to zero again. In Figure 6-27, F-W3 shows a higher auxetic effect compared with F-W1 and F-W2, exhibiting the

maximum negative Poisson's ratio of -1.85, because the structure of F-W3 displays a longer float length and there are fewer weft yarns restricted by the warp yarns. In Figure 6-28, it is obvious that the thickness of the fabric is enlarged as the auxetic yarns increased and the yarns in F-W3 are extruded out-of-plane by every three weft threads at around 15% of strain compared to F-W1 and F-W2. During the stretching, the auxetic yarns have more freedom to be deformed with 3/3 warp rib structure of the fabric and the thickness of the fabric is able to expand in a great extent. Thus, the weave structure with longer float length to the auxetic yarns results in higher auxetic behaviour of the woven fabric.

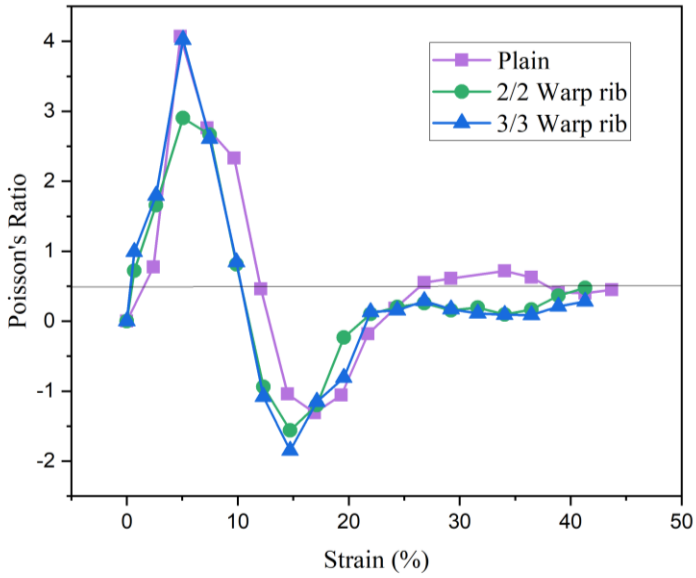

Figure 6-27 Poisson's ratios of plain (F-W1), 2/2 warp rib (F-W2) and 3/3 warp rib (F-W3) in thickness direction

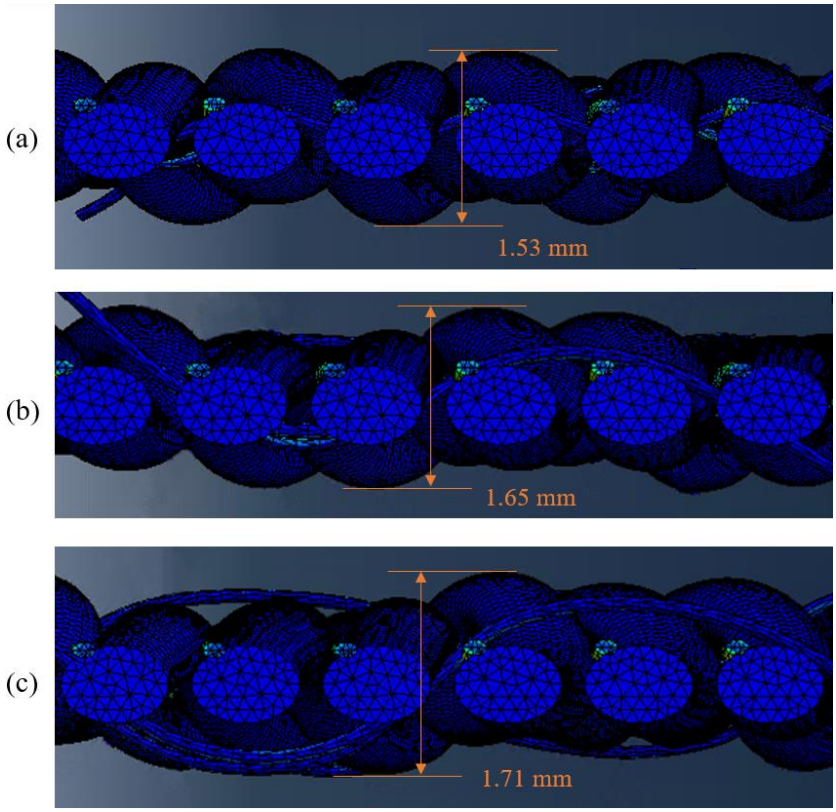

Figure 6-28 Deformation of fabric thickness at 15% of strain: (a) plain (F-W1); (b) 2/2 warp rib (F-W2); (3) 3/3 warp rib (F-W3)

6.7 Warp yarn types

In this Section, the woven fabric was considered by constructing auxetic yarns in the weft direction and non-auxetic yarns in the warp direction. It was noted that the deformation of the auxetic yarn under uniaxial tensile loading could highly affected by the properties of the warp yarn. Therefore, the key parameters of the warp yarn was investigated, including tensile modulus, Poisson's ratio and the dimension of thickness.

6.7.1 Tensile modulus and Poisson's ratio

To investigate the effect of the warp yarn, other parameters of the auxetic woven fabric were kept constant. The maximum negative Poisson's ratio of the fabric in thickness and warp directions was illustrated in Figure 6-29. It was found that the auxeticity of the fabric in thickness direction is higher than that in the warp direction. Firstly, for the changes of tensile modulus of the warp yarn, the Poisson's ratio was set as 0.42 corresponding to the PA 6,6 yarn in experiments. Five tensile moduli of the warp were tried in the FE model including 1000MPa, 1850 MPa, 3000 MPa, 4000 MPa and 5000

MPa, respectively. The results demonstrate that the auxetic behaviour is more obvious with the decreasing tensile modulus of the warp yarn, as shown in Figure 6-29 (a). Because when the warp yarn is softer, the auxetic yarn will easily be deformed during the stretching and the restriction between the warp and weft yarns are smaller as well. Then, five different Poisson's ratios were tried from 0.3 to 0.48 in the same FE model with 1850 MPa tensile modulus of the warp yarn. It can be seen that the fabric shows the lowest auxetic effect when the Poisson's ratio reached to 0.42, as illustrated in Figure 6-29 (b). It reveals that the closer Poisson's ratio value between the warp and the wrap ply of the HAY, the lower auxeticity of the woven fabric. From the Poisson's ratio of 0.3 to 0.42, the maximum negative Poisson's ratio of the fabric is decreased slowly, whereas from the value of 0.42 to 0.48, the gradient of the value is higher. This indicated that the fabric is more sensitive between the Poisson's ratio from 0.42 to 0.48 and the results also provide the possibilities of the warp yarn selection for making auxetic woven fabrics.

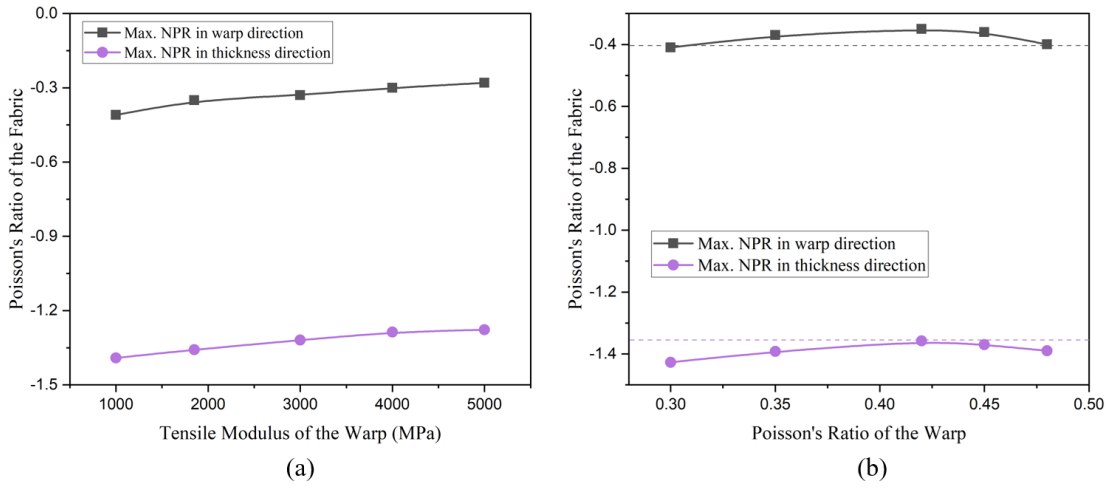

Figure 6-29 Maximum negative Poisson's ratio of the fabric: (a) tensile modulus of the warp; (b) Poisson's ratio of the warp

6.7.2 Thickness of the warp yarn

Thickness of the warp yarn is another key factor which can influence the Poisson's ratio of the woven fabric. By keeping the same aspect ratio of the yarn and fabric structure, the thickness of the warp yarn was set as 0.11 mm, 0.22 mm, 0.33 mm and 0.44 mm, respectively, as shown in Figure 6-30. It was found that thicker warp yarn results in higher crimp level of the weft yarn. In Figure 6-31, the auxetic behaviour of

the fabric is found to be smaller as the thickness of the warp yarn increased. This can be explained by the interlacement of the woven fabric, that the warp yarn restricts the fabric deformation when it becomes thicker. Also, the crimp level of the auxetic yarn in the fabric is higher with the increasing thickness of the warp yarn, leading to a larger initial thickness and lower auxeticity of the fabric. By changing the thickness of the warp yarn, it was found that the fluctuation of Poisson's ratio in the thickness direction is higher than that in the warp direction. This indicated that the out-of-plane auxeticity of the fabric is influenced by the thickness of the warp yarn in a great extent.

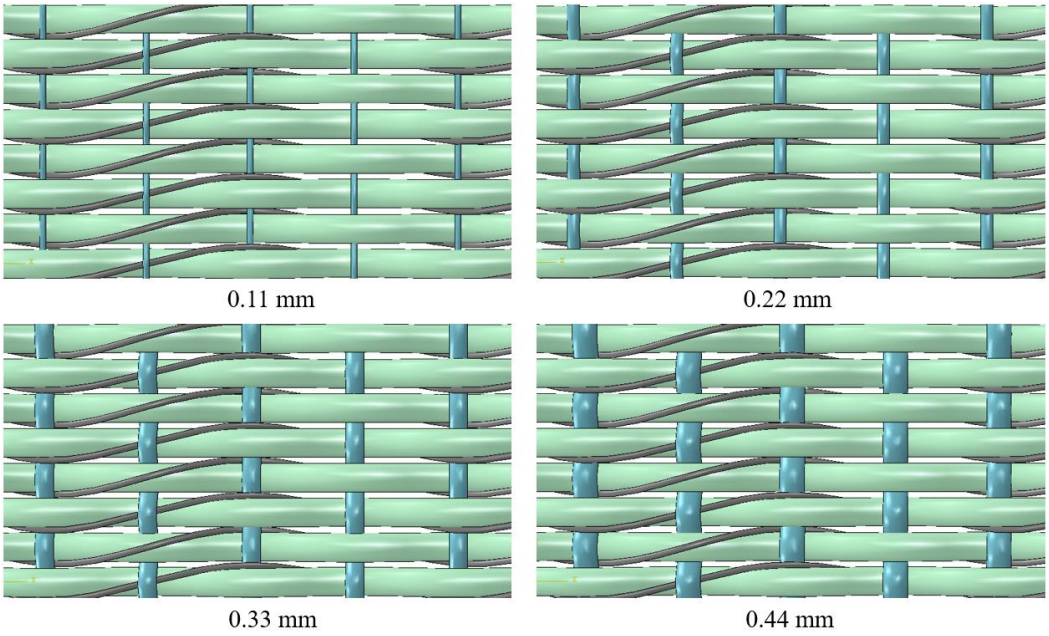

Figure 6-30 Fabric models with different warp yarn thickness

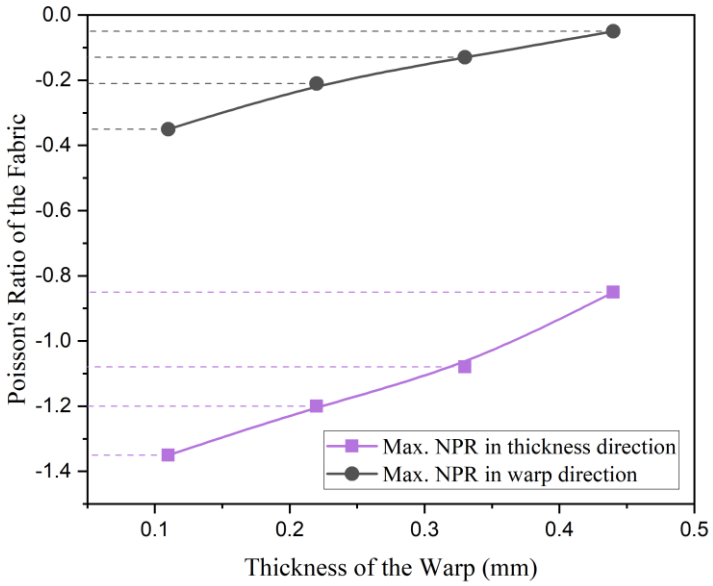

Figure 6-31 Maximum negative Poisson's ratio of the fabrics with different thickness of the warp yarn

6.8 Loading directions

In this Section, the auxetic yarns were applied in both warp and weft directions of the woven fabric model, keeping the yarn dimension, fabric density and weave structure as the constant parameters, as summarised in Table 6-4. Then, four types of uniaxial loading and two types of biaxial loading are investigated as follows.

Table 6-4 Parameters of woven fabrics with different loading directions

Test code	Variable parameters						
	Yarn arrangement	Fabric density (threads /cm)	Helical angle of HAY (°)	Vertical thickness of HAY (mm)	Weave structure	Warp yarn type	Loading direction
F-D1	In-phase	5×10	28	0.56	Plain	HAY (Y-A28)	Uniaxial-weft1
F-D2							Uniaxial-weft2
F-D3							Uniaxial-warp1
F-D4							Uniaxial-warp2
F-D5	In-phase	5×10	28	0.56	Plain	HAY (Y-A28)	Biaxial (Approach 1)
F-D6 (F-P1')							Biaxial (Approach 2)

6.8.1 Uniaxial loading

There are four types approach for uniaxial loading. The first approach is to set fixed edge on the left edge of the fabric and to apply tensile loading on the right edge of the

fabric with the speed of 1 mm/s corresponding to the experiments of the tensile test, as illustrated in Figure 6-32. By using the first approach, the fabric was coded as F-D1. It was found that the thickness of F-D1 becomes smaller initially from 1.54mm to 1.48 mm at the strain of 0 to 7%. Then, the fabric is thicker until it reaches to the strain of 18%. After that, further loading makes the fabric thinner again, as shown in Figure 6-33. The maximum negative Poisson's ratio of F-D1 in the thickness direction is achieved as -0.58 which is smaller than the auxetic behaviour of the fabric in the warp direction containing the maximum negative Poisson's ratio of -0.7 due to the involvement of the auxetic yarns in both directions. Although the differential of auxetic behaviour in thickness and warp directions is not obvious, it can be confirmed that the small negative Poisson's ratio value comes from the warp yarn thickness. As mentioned the factor of warp yarn type in Section 6.7, thicker warp yarn results in lower auxetic behaviour of the fabric. Herein, the warp and weft yarns are set as the same dimension. When the yarn woven into a fabric, the crimp level of the yarn is higher than before in the case of F-F1 based on the same fabric density, which results in a higher initial thickness of the wove fabric. It was found that by using the first approach of uniaxial loading, the auxetic yarns are deformed from the right side to the left side, so the unevenly deformation of the yarns result in lower auxeticity of the fabric either in the thickness direction or in the warp direction.

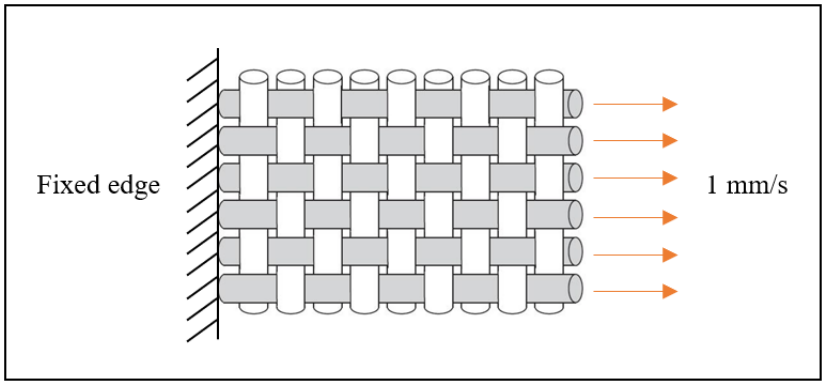

Figure 6-32 Uniaxial loading-weft 1 (F-D1)

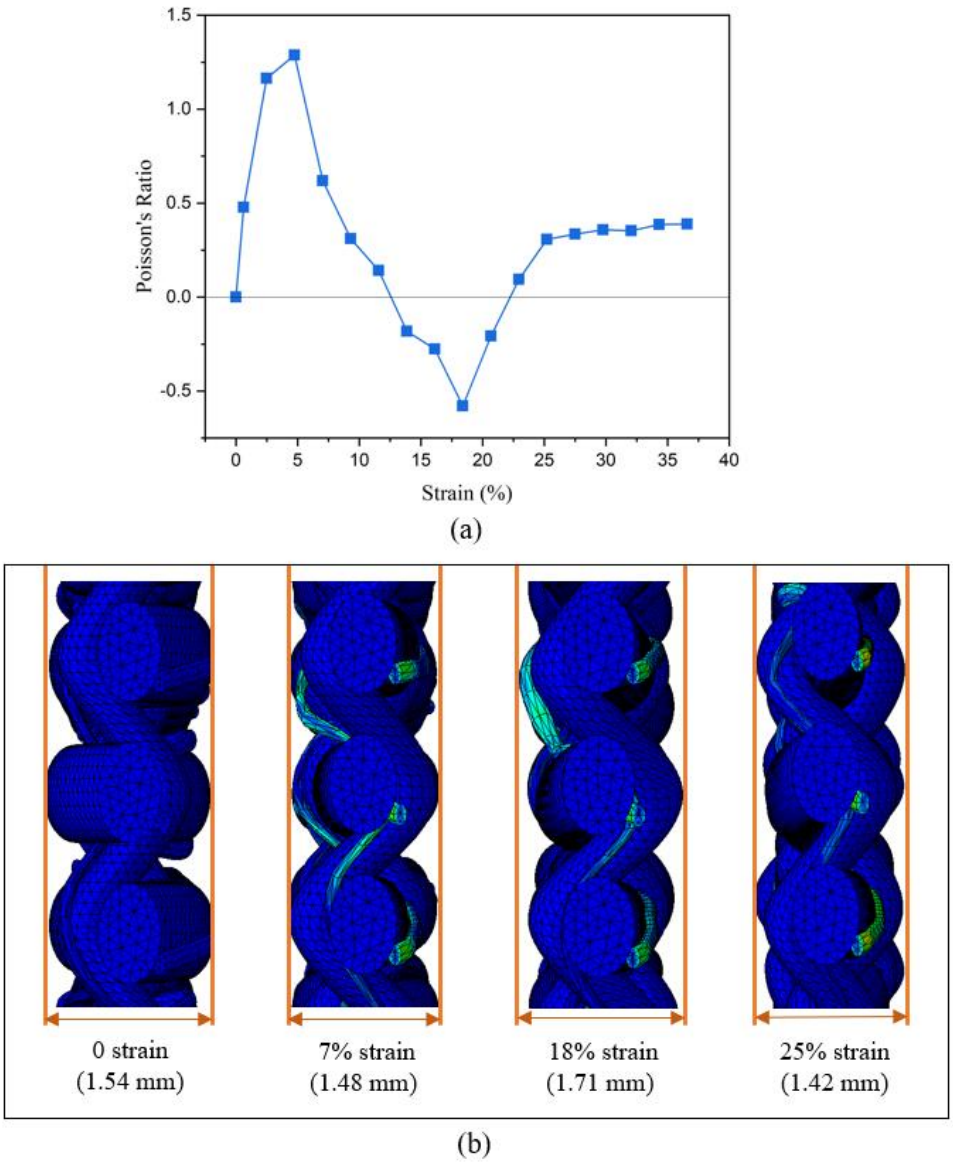

Figure 6-33 Thickness of the fabric (F-D1) under tension by adopting approach 1: (a) strain versus Poisson's ratio; (b) image captured at the specific strain

The second approach of uniaxial loading is illustrated in Figure 6-34. As shown, the tensile loading is applied to both left and right sides of the edge with the speed of 0.5 mm/s, so the overall extension of the fabric is the same as the first approach. By using the second approach, the fabric was coded as F-D2 and it can be found that the maximum negative Poisson's ratio of F-D2 is higher than that of F-D1, exhibiting the value around -0.8 in the thickness direction, as shown in Figure 6-35. This can be explained by the fact that the auxetic yarns are more uniformly stretched in the weft direction, leading to higher auxetic behaviour of the fabric. As shown in Figure 6-36, two red points are marked, representing the measured location where the maximum

thickness of the fabric at 18% of strain. It can be seen that the maximum thickness of F-D2 comes from the warp yarn, that is, the weft yarn pushes the warp yarn out to achieve the largest thickness under tension. In contrast, the maximum thickness of F-D1 is contributed by the weft yarn at the same strain by using the first approach. Even though the overall expansion of the fabric in thickness direction reaches the same value of 1.71 mm by using the two approaches, the maximum thickness of F-D2 exhibits at a lower strain, resulting in a lower Poisson's ratio value afterwards.

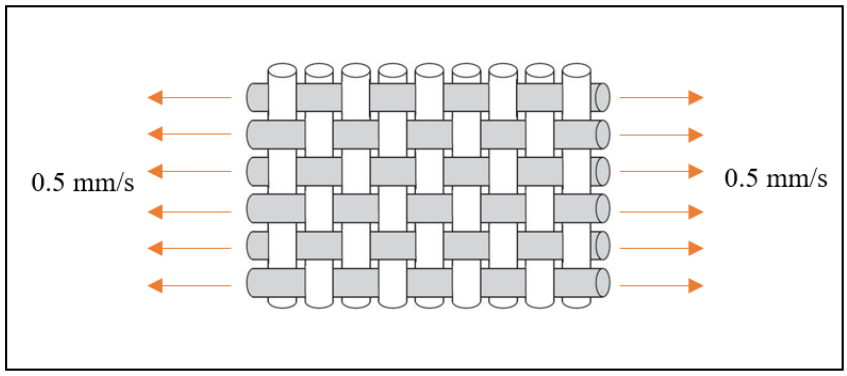

Figure 6-34 Uniaxial loading-weft 2 (F-D2)

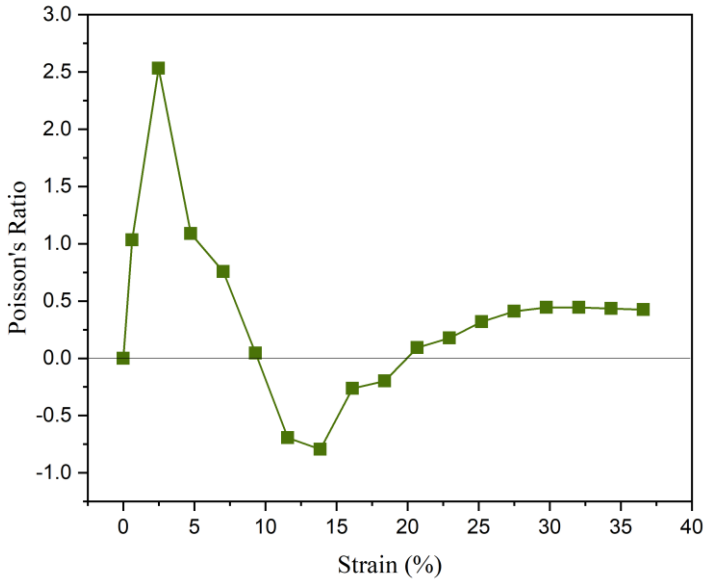

Figure 6-35 Poisson's ratio of F-D2

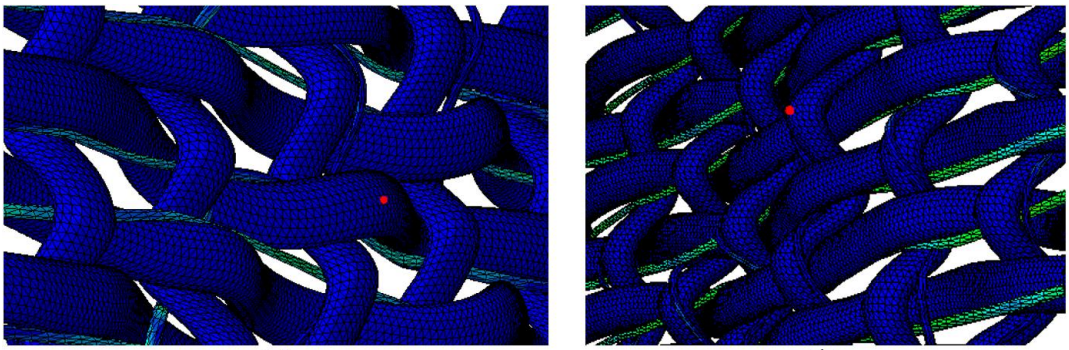

Figure 6-36 Comparison of measured points on fabric surface: (a) uniaxial loading-weft 1 (F-D1); (b) uniaxial loading-weft 2 (F-D2)

The third approach is to set tensile loading in the warp direction of the fabric with one side of fixed edge and another side of 1mm/s stretching, as shown in Figure 6-37. By adopting the third approach, the fabric was coded as F-D3 and the maximum negative Poisson' ratio was found to be -0.56 in the thickness direction and -0.06 in the weft direction. The auxetic behaviour of F-D3 is overall lower than that of F-D1 and F-D2 because the weft density is two times larger than the warp density, leading to more open area of the adjacent warp yarns. Therefore, the auxeticity of the fabric in the weft direction is not obvious.

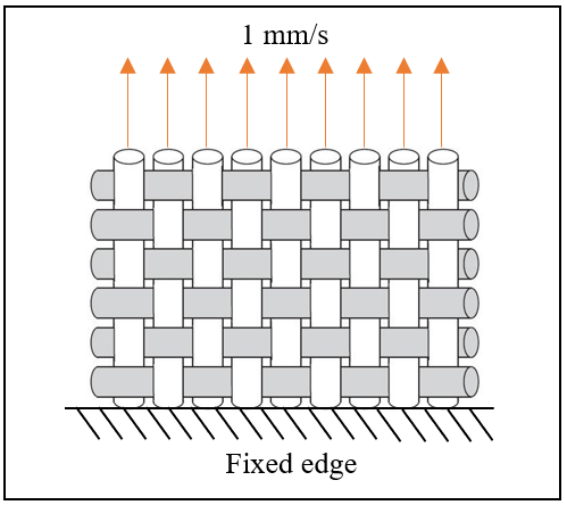

Figure 6-37 Uniaxial loading-warp 1 (F-D3)

The last approach of uniaxial loading is shown in Figure 6-38. The tensile loading is applied to the both sides of the edge in the warp direction with the speed of 0.5 mm/s, corresponding to the same interval strain of the third approach above. The fabric was coded as F-D4. Similar to the comparison between F-D1 and F-D2, F-D4 generates evenly deformation of the auxetic yarns and demonstrates higher auxetic behaviour of

the fabric compared to F-D3. The maximum negative Poisson's ratio of F-D4 is achieved as -1.09 in the thickness direction and -0.09 in the weft direction at around 30% of strain because more weft yarns are pushed out with the increased dimension of the warp yarns, as shown in Figure 6-39. For the weft direction, F-D4 should be narrowed with the increasing strain in the warp direction, resulting in positive Poisson's ratio of the fabric as shown in Figure 6-40. However, the deformation of the fabric is measured by the first warp yarn to the last warp yarn, so the negative Poisson's ratio value is generated with low auxeticity.

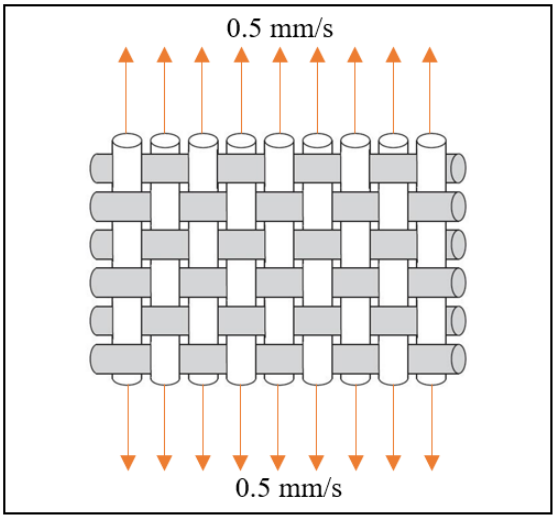

Figure 6-38 Uniaxial loading-warp 2 (F-D4)

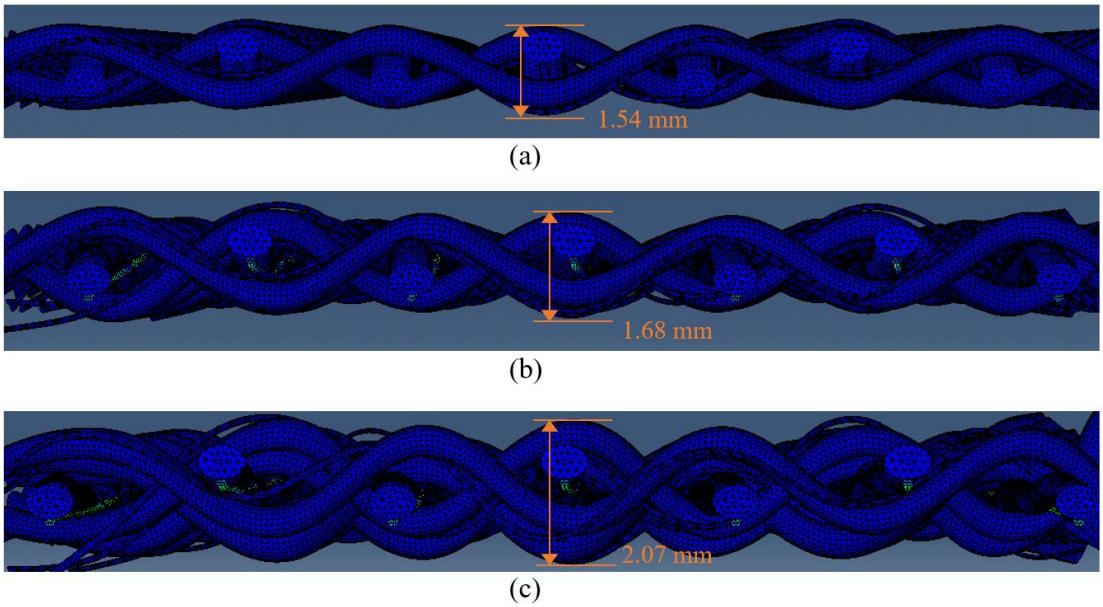

Figure 6-39 Deformation of F-D4 in the thickness direction: (a) initial state; (b) 20% of strain; (c) 30% of strain

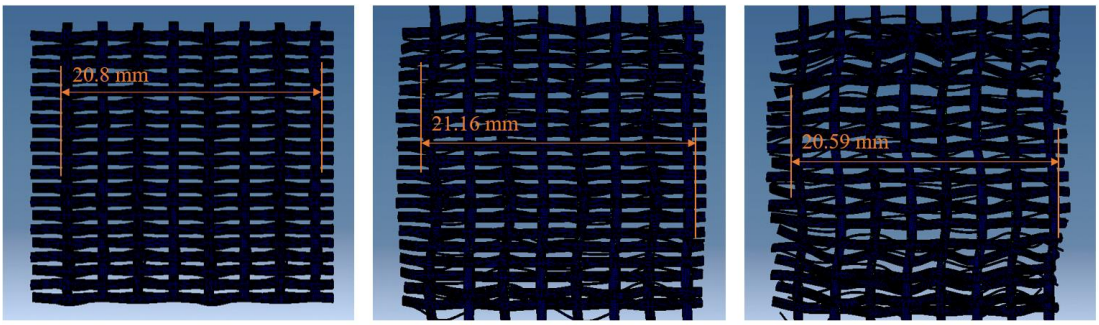

Figure 6-40 Deformation of F-D4 in the weft direction: (a) initial state; (b) 20% of strain; (c) 30% of strain

6.8.2 Biaxial loading

Two types of approach are applied to the biaxial loading of the fabric. The first approach is illustrated in Figure 6-41 where the tensile loading is applied to the up and right sides of the edge with the speed of 1 mm/s, and such loading method is coded as F-D5. It was found that the minimum biaxial strain ratio of the fabric exhibits as -0.7 in the thickness direction at 11% of strain, which is much earlier than the fabric (F-D1) by using the first approach of uniaxial loading (≈14% strain). Because of the involvement of the biaxial loading, the auxetic yarns in both warp and weft directions are deformed and they are pushed out from 9% of strain, as show in Figure 6-42, leading to the negative biaxial strain ratio of the fabric. Even if the auxetic behaviour of the fabric using the biaxial loading comes from the deformation of the warp and weft yarns, the auxetic behaviour of F-D5 is smaller than F-D2 because the compressibility of the warp yarns reduce the auxeticity of fabric and the gap between the adjacent yarns becomes bigger, leading to the less out-of-plane extrusion of the fabric.

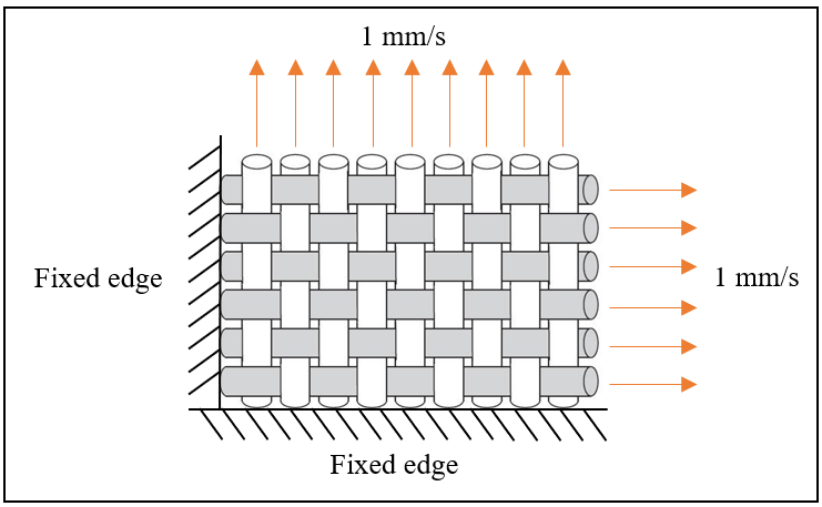

Figure 6-41 Biaxial loading: Approach 1 (F-D5)

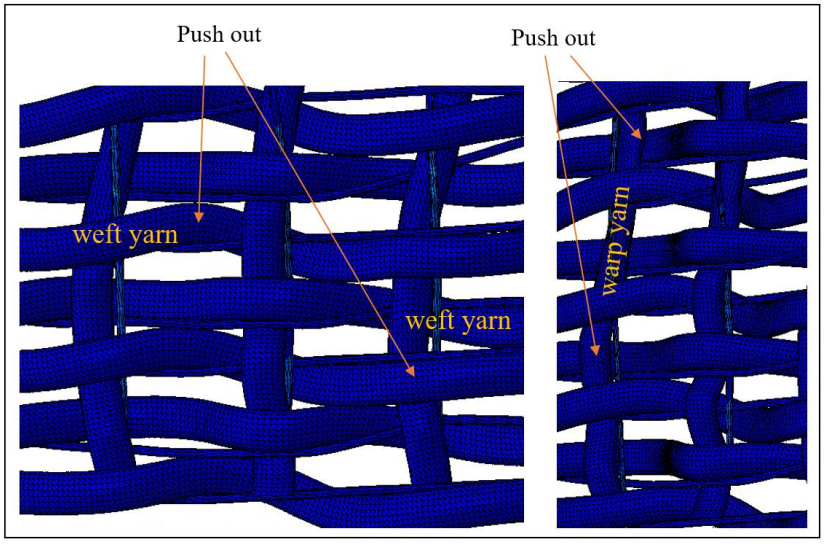

Figure 6-42 Deformation of F-D5 at 9% of strain

Another approach is to apply the tensile loading in both four sides of the fabric, coded as F-D6, with the speed of 0.5 mm/s, so the overall extension of the fabric is the same as F-D5, as illustrated in Figure 6-43. It was found that the maximum thickness of F-D6 reaches to around 1.73 mm which is higher than that of F-D5 and the minimum biaxial strain ratio is exhibited as -0.62 at around 18% of strain. Ideally, if the fabric stretched on four sides, the deformation of the fabric is more even and the auxetic yarns in both warp and weft directions are contributed to the expansion of the fabric, leading to the doubled auxetic behaviour of the fabric. However, F-D6 generates 11% less auxetic behaviour than F-D5 and 22.5% less auxeticity than F-D2 in the thickness direction. This can be explained by the fact that the solid yarn materials are compressible during the stretching and the out-of-plane auxetic behaviour of the fabric

is eaten by the decrimped and compressed yarns, even if the outer contour diameter of the auxetic yarns become larger. Therefore, the auxeticity of F-D6 is reduced in the thickness direction.

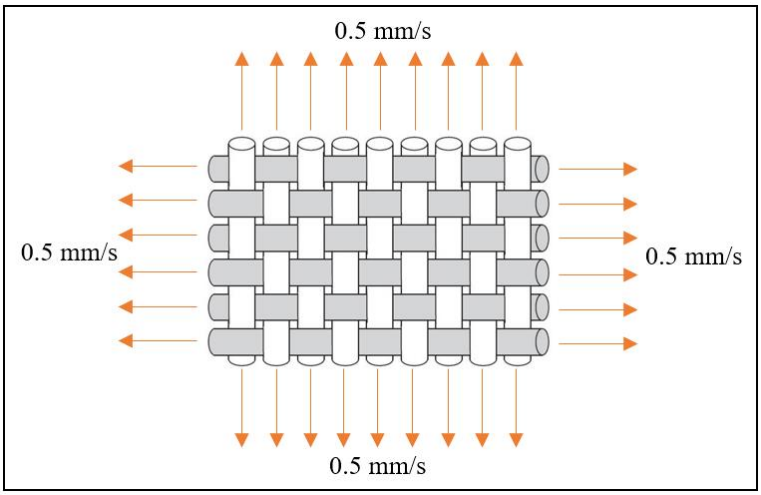

Figure 6-43 Biaxial loading: Approach 2 (F-D6)

6.8.3 Discussion

Six loading approaches were investigated and the auxetic behaviour of the fabric was generated in the thickness direction and the warp and weft directions, and the results are shown in Figure 6-44. Under the uniaxial loading in the weft direction, F-D2 demonstrates a higher auxetic behaviour compared to F-D1 shown in Figure 6-44 (a) due to the application of more uniform stress to the auxetic yarns in the fabric, leading to more obvious increase in thickness. By providing evenly tension of the auxetic yarns, the auxetic behaviour of the fabric in the thickness direction is not increased under the biaxial loading, as shown in Figure 6-44 (c). The value of the ratio is reduced from -0.7 to -0.62 because the compressibility of the solid yarn, enlarged gaps between the adjacent yarns and decrimping effect absorb the auxeticity of the fabric in the thickness direction. Compared to the stretching in the weft direction, the maximum negative Poisson's ratio of the fabric under uniaxial loading in the warp direction is illustrated in Figure 6-44 (b). The auxetic behaviour in the weft direction is much lower than in the warp direction as a result of low warp density of the fabric. This is also shown by adopting biaxial loading in Figure 6-44 (c) that the biaxial strain ratio of the fabric in the weft direction is higher than in the warp direction. Based on the findings above, the auxetic behaviour of the fabric can be enlarged under uniaxial

loading with uniformly stretching either in fabric thickness or fabric dimension. The auxeticity of the fabric in the thickness direction is increased when stretching evenly along the direction with low thread density. Biaxial loading with evenly stretching on both four sides of the fabric can slightly increase the auxeticity in both warp and weft directions, but it reduces the auxetic behaviour in the thickness direction.

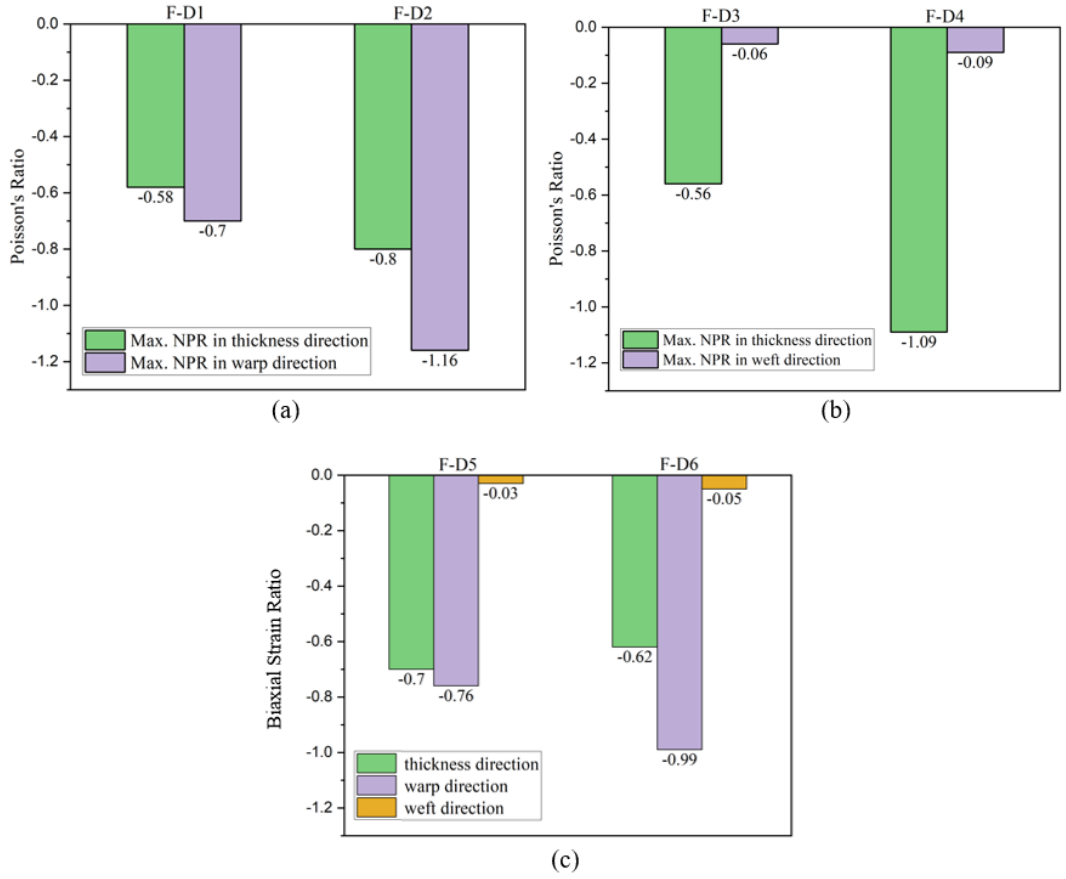

Figure 6-44 Minimum ratios of woven fabrics: (a) F-D1 and F-D2; (b) F-D3 and F-D4; (c) F-D5 and F-D6

6.9 Summary

The manufacture of woven fabrics made from helical auxetic yarns and their geometric models were introduced and discussed. The key factors influencing the Poisson's ratio, including HAY arrangements, fabric density, helical angles of the HAY, thickness of the HAY, weave structures and loading directions, were investigated leading to the establishment of the following understanding.

(1) In the case of auxetic yarns woven in the weft direction only, the auxeticity of the woven fabric is found more effectively in the thickness direction, whereas in the warp and weft directions are minimum. In-phase arrangement of the HAYs with higher

fabric density, lower helical angle of the HAY, thinner HAY, longer float length of the weave structure, lower tensile modulus and thickness of the warp yarn can improve the auxeticity of the wove fabric.

(2) In the case of auxetic yarns woven in both warp and weft directions, the auxeticity is more obvious in the plane direction rather than in the thickness direction. Out-of-phase arranged HAYs can effectively improve the auxeticity of the fabric in the warp direction.

(3) Uniaxial loading with uniform tension of the two relative edges is able to maximise negative Poisson's ratio of the woven fabric.

In summary, an enhanced understanding of auxetic textile materials was established so that the fabric can be produced with auxeticity in the thickness direction and the plane directions, which has not been studied in the literature so far. The auxeticity of the woven fabric in the plane directions is negligible, but that in the thickness direction is notable. From the simulation and analysis, some of the key influential parameters are not summarised as a general principle, such as yarn arrangements and loading directions. However, the phenomenon of them can provide a clue for further experimental work.

Chapter 7 Conclusions and Future Work

7.1 Conclusions

The aim of this research is to establish understanding of the design principles and behaviour of auxetic yarns and woven fabrics. To achieve this aim, helical auxetic yarns and auxetic woven fabrics with various structural parameters were manufactured and evaluated, and finite element modelling were carried out for further parametric studies. The Poisson's ratio of the auxetic yarns was investigated based on three key parameters, i.e. the initial helical angle, yarn thickness and tensile moduli of the two plies. Tensile property, porosity and impact property of the developed woven fabrics were studied, in comparison to the non-auxetic fabrics made with the same fabric parameters. The auxetic behaviour of the woven fabric was considered in both thickness direction and the fabric plane direction, and the auxeticity was evaluated against seven influential factors. The main achievements of this research are included as follows.

7.1.1 Auxetic behaviour of the yarns

i. **The structural problem of the yarn has been overcome, which enabled the making of high-quality auxetic yarns with a wider range of machine settings.**

One pair roller system and two pairs roller system were used for producing the helical auxetic yarns and the yarns were manufactured with three feeding formats, including under feeding, equal feeding and over feeding. The auxetic yarns were examined under the Projectina microscope using 10× magnification and it was found that the over feeding format with 16.8 m/min of upper delivery speed could effectively improve the wrapping quality of the yarn. Thus, the over feeding format was adopted for producing the yarn when the twisting speed was lower than 3500 rpm and the stable yarn were developed with a wider range of lowest helical angle from 34˚ to 14˚.

ii. **For given materials and diameter ratio of the two plies, there exists an optimal helical angle that makes the yarn more auxetic. Higher tensile modulus ratio of the wrap ply to the core ply result in higher auxetic behaviour of the yarn.**

Based on the investigation of initial helical angle and tensile modulus of the two plies, it was found that the maximum negative Poisson's ratio of the yarn was increased from -0.42 to -9.6 with the decreasing helical angle from 39˚ to 14˚ in experiments and this trend was also proved by the FE simulation. The auxetic behaviour of the yarn was more obvious with the increasing tensile modulus of the wrap ply from 500 MPa to 4000 MPa and decreasing tensile modulus of the core ply from 120 MPa to 15 MPa. This provides a reference for choosing the best ply material for the highest auxeticity.

iii. **A concave relationship between the Poisson's ratio and diameter ratio of the core ply to the wrap ply is discovered. The auxeticity of the yarn cannot be increased with the increasing thickness of the core ply after a specific value of diameter ratio.**

Based on the investigation of diameter ratio experimentally and numerically, the Poisson's ratio of the yarn was decreased from 0.37 to -2.63 corresponding to the diameter ratio from 1:1 to 4:1. After the diameter ratio of the core ply to the wrap ply reached to 4:1, the Poisson's ratio of the yarn was increased from -2.63 to -1.44, which could provide a reference for making helical auxetic yarns.

iv. **Accurate predictions on yarn auxeticity are supported by experiments and geometric calculations.**

By using the FE simulation, a theoretical modelling of the yarn structure has been done and the relationship between the Poisson's ratio and different parameters was established. In order to have a higher auxeticity, the absolute value of negative Poisson's ratio could be increased to over 20 for the yarn when the helical angle is further reduced. Also, the gradient becomes higher which revealed that the yarn becomes more sensitive when the angle is smaller.

7.1.2 Properties of auxetic woven fabrics

i. **The auxeticity in fabric plane directions is negligible but the auxeticity in the thickness direction is notable with maximum NPR of -3.32.**

Experimental work shows the auxeticity in fabric plane directions is insignificant, showing the maximum NPR is -0.052 in the weft direction and -0.025 in the warp direction. In simulation, the fabric density plays a roll in affecting the NPR. Based on the model which only involved limited number of warp and weft yarns, the NPR is

larger when the fabric is stretched along the denser direction, demonstrating a maximum NPR up to -1.16. When the tensile loading is applied along the lower density direction, the NPR is small with a value of -0.09. The simulation is the extended work for investigating auxeticity in the fabric plane directions and further FE revealed the influence on the warp and weft densities. This is the first time to point out that using auxetic yarns for making the fabric may not achieve obvious auxeticity in the plane directions. Any effort to achieve noticeable auxeticity using the current approach would not lead to significant auxetic behaviour. However, the fabric NPR is notable in the thickness direction with a maximum value of -3.32 in experiments.

ii. The NPR of auxetic fabrics increases as the yarn helical angle decreases.

Based on the experimental work on yarn helical angles, the auxetic behaviour of the fabric was also increased with the decreasing helical angle from 39˚ to 20˚ and the loss of the auxeticity between HAYs and fabrics was reduced when the helical angle was smaller. This phenomenon was also proved by using the FE simulation.

iii. Auxetic fabrics show superior porosity and energy absorption than non-auxetic fabrics.

From the tensile test results, it can be found that the auxetic fabric exhibited a low initial modulus and a high extension compared to the non-auxetic fabric. The pore area measurements and air permeability tests showed that the porosity of auxetic fabric was around 3 times as large as that of non-auxetic fabric just when the fabrics started to fail. The pore area of the auxetic fabric can be made different with control, and therefore would have potentials for filtrations.

iv. The influence of weave structures shows that the longer float length contributes to higher auxetic behaviour of the fabric.

From the discussion of weave structures, three types of weave structures were compared including plain, 2/2 warp rib and 3/3 warp rib. It was found that 3/3 warp rib structure generates higher auxetic behaviour with a maximum NPR of -1.85 because the long float length in the structure was able to provide more freedom of the auxetic yarns and they can be pushed out-of-plane in a great extent.

In conclusion, the auxetic behaviour of the yarns and woven fabrics is improved by adjusting different influencing factors, and the results indicated that there is a

possibility for achieving higher NPRs according to the theoretical principles, suitable materials and structures. That points out the way forward on potential applications.

7.2 Limitation

In this research, the design principles and behaviour of auxetic yarns and woven fabrics have been studied and several limitations also have been found as follows:

- The auxetic behaviour of the yarns cannot be fully transferred to the woven fabric due to the interlacement of the weave structure. The negative Poisson's ratio of the fabric in the thickness direction is shown within a small range of strain under tension which is lower than 10%. This indicates that the auxeticity of the fabric can only be demonstrated at a specific tensile strain.
- It is hard to arrange every auxetic yarns in-phase or out-of-phase in weaving process, even though the in-phase arranged HAYs provides the best auxeticity of the fabric based on FE simulation.
- Some of the factorial investigations are based on FE simulation and the experimental verification is still required.
- The produced auxetic woven fabrics have not been used for any products to explore the applications in real life.

7.3 Future work

According to the research and discussions above, the development of auxetic yarns and woven fabrics can be extended in the future as described as follows:

- Based on the investigation of helical angles, it was found that the auxeticity increases as the helical angle decreases and there is no auxeticity when the angle is 0. It would be theoretically interesting to find out where the turning point of the angle is and to carry out a fully parametric study.
- Based on the investigation of porosity, it would be interesting to further explore the performance of auxetic fabrics with different pore areas experimentally and numerically.
- From the mechanical properties of auxetic woven fabric, multi-layers of the fabric could be developed to improve the impact resistance by adopting the same design principle.

- It was found that the auxeticity of the fabric is restricted by the interlacement of the weave structure. Therefore, a composite can be developed by arranging the auxetic yarns in multi-layers without any interlacement, which might help to increase the auxetic behaviour of the fabric.
- The engineering design and characterisation of auxetic woven fabrics are suggested to use in functional garments to show their benefits on different occasions.

References

1. Lim T-C. Auxetic materials and structures: Springer; 2015.
2. Greaves GN, Greer A, Lakes RS, Rouxel T. Poisson's ratio and modern materials. Nature materials. 2011;10(11):823-37.
3. Hu H, Zhang M, Liu Y. Auxetic textiles: Woodhead Publishing; 2019.
4. Evans KE, Nkansah M, Hutchinson I, Rogers S. Molecular network design. Nature. 1991;353(6340):124-.
5. Voigt W. Bestimmung der Elasticitätsconstanten für das chlorsaure Natron. Annalen der Physik. 1893;285(8):719-23.
6. ME PSNS, Teja GSRC, Krishna CAS, Rao BKD, Aravind AA, Rao BL. Modeling and Analysis of Structures with Negative Poisson's Ratio. International Journal of Engineering Research & Technology (IJERT). 2020;9(03).
7. Lakes R. Foam structures with a negative Poisson's ratio. Science. 1987;235:1038-41.
8. Novak N, Vesenjak M, Ren Z. Auxetic cellular materials-a review. Strojniški vestnik-Journal of Mechanical Engineering. 2016;62(9):485-93.
9. Evans KE, Alderson A. Auxetic materials: functional materials and structures from lateral thinking! Advanced materials. 2000;12(9):617-28.
10. McMullan PJ, Kumar S, Griffin AC. Textile fibres engineered from molecular auxetic polymers. National Textile Center Annual Report. 2004.
11. Alderson K, Alderson A, Smart G, Simkins V, Davies P. Auxetic polypropylene fibres: Part 1-Manufacture and characterisation. Plastics, Rubber and Composites. 2002;31(8):344-9.
12. Simkins V, Alderson A, Davies P, Alderson K. Single fibre pullout tests on auxetic polymeric fibres. Journal of materials science. 2005;40(16):4355-64.
13. Ravirala N, Alderson KL, Davies PJ, Simkins VR, Alderson A. Negative Poisson's ratio polyester fibers. Textile research journal. 2006;76(7):540-6.
14. Wright J, Sloan M, Evans K. Tensile properties of helical auxetic structures: a numerical study. Journal of Applied Physics. 2010;108(4):044905.
15. Sloan M, Wright J, Evans K. The helical auxetic yarn–a novel structure for composites and textiles; geometry, manufacture and mechanical properties. Mechanics of Materials. 2011;43(9):476-86.
16. Miller W, Hook P, Smith CW, Wang X, Evans KE. The manufacture and characterisation of a novel, low modulus, negative Poisson's ratio composite. Composites Science and Technology. 2009;69(5):651-5.
17. Hu H, Wang Z, Liu S. Development of auxetic fabrics using flat knitting technology. Textile Research Journal. 2011;81(14):1493-502.
18. Ge Z, Hu H. Innovative three-dimensional fabric structure with negative Poisson's ratio for composite reinforcement. Textile Research Journal. 2013;83(5):543-50.
19. Wang Z, Hu H. 3 D auxetic warp‐knitted spacer fabrics. physica status solidi (b). 2014;251(2):281-8.
20. Alderson A, Alderson K, Chirima G, Ravirala N, Zied K. The in-plane linear elastic constants and out-of-plane bending of 3-coordinated ligament and cylinder-ligament honeycombs. Composites Science and Technology. 2010;70(7):1034-41.
21. Alderson A, Alderson K. Expanding materials and applications: exploiting auxetic textiles. Technical textiles international. 2005;14(6):29-34.

22. Zhang G, Ghita O, Evans KE. The fabrication and mechanical properties of a novel 3-component auxetic structure for composites. Composites Science and Technology. 2015;117:257-67.
23. Ge Z, Hu H, Liu S. A novel plied yarn structure with negative Poisson's ratio. The Journal of The Textile Institute. 2016;107(5):578-88.
24. Liu S, Pan X, Zheng D, Du Z, Liu G, Yang S. Study on the structure formation and heat treatment of helical auxetic complex yarn. Textile Research Journal. 2019;89(6):1003-12.
25. Gao Y, Chen X, Studd R. Experimental and numerical study of helical auxetic yarns. Textile Research Journal. 2020;91(11-12):0040517520977194.
26. Prawoto Y. Seeing auxetic materials from the mechanics point of view: a structural review on the negative Poisson's ratio. Computational Materials Science. 2012;58:140-53.
27. Alderson A. A triumph of lateral thought. Chemistry & Industry. 1999;17:384-91.
28. Alderson A, Alderson K. Auxetic materials. Proceedings of the Institution of Mechanical Engineers, Part G: Journal of Aerospace Engineering. 2007;221(4):565-75.
29. Baughman RH, Shacklette JM, Zakhidov AA, Stafström S. Negative Poisson's ratios as a common feature of cubic metals. Nature. 1998;392(6674):362-5.
30. Avellaneda M, Swart PJ. Calculating the performance of 1–3 piezoelectric composites for hydrophone applications: an effective medium approach. The Journal of the Acoustical Society of America. 1998;103(3):1449-67.
31. Friis E, Lakes R, Park J. Negative Poisson's ratio polymeric and metallic foams. Journal of Materials Science. 1988;23(12):4406-14.
32. Nakamura M. Fundamental properties of intermetallic compounds. MRS Bulletin. 1995;20(8):33-9.
33. Kim K-W, Kim D-M. Contact pressure of non-pneumatic tires with auxetic spokes. Journal of the Korean Society for Aeronautical & Space Sciences. 2011;39(8):719-24.
34. Sripada S, Unsworth J, Krishnamurty M, Ng Y. PZT/polymer composites for medical ultrasound. Materials research bulletin. 1996;31(6):731-9.
35. Liu Y, Hu H. A review on auxetic structures and polymeric materials. Scientific Research and Essays. 2010;5(10):1052-63.
36. Foster L, Peketi P, Allen T, Senior T, Duncan O, Alderson A. Application of auxetic foam in sports helmets. Applied Sciences. 2018;8(3):354.
37. Smithers R. Origami-inspired clothing range that grows with your child wins Dyson award The Guardian2017 [Available from: https://www.theguardian.com/environment/2017/sep/07/origami-inspired-clothing-range-that-grows-with-your-child-wins-dyson-award?CMP=Share_AndroidApp_Outlook.
38. Hasan K. Study of bi-stretch woven fabrics with negative poisson's ratio. 2021.
39. Sanami M, Ravirala N, Alderson K, Alderson A. Auxetic materials for sports applications. Procedia Engineering. 2014;72:453-8.
40. Konaković M, Crane K, Deng B, Bouaziz S, Piker D, Pauly M. Beyond developable: computational design and fabrication with auxetic materials. ACM Transactions on Graphics (TOG). 2016;35(4):1-11.
41. Tibbits S. Active matter: MIT Press; 2017.

42. Cross TM, Hoffer KW, Jones DP, Kirschner PB, Langvin E, Meschter JC. Auxetic structures and footwear with soles having auxetic structures. Google Patents; 2016.
43. Wang Z, Hu H. Auxetic materials and their potential applications in textiles. Textile Research Journal. 2014;84(15):1600-11.
44. Alderson K, Webber R, Kettle A, Evans K. Novel fabrication route for auxetic polyethylene. Part 1. Processing and microstructure. Polymer Engineering & Science. 2005;45(4):568-78.
45. Papadopoulou A, Laucks J, Tibbits S. Auxetic materials in design and architecture. Nature Reviews Materials. 2017;2(12):1-3.
46. Toronjo A. Articles of apparel including auxetic materials. Google Patents; 2017.
47. Santulli C, Langella C. Study and development of concepts of auxetic structures in bio-inspired design. International Journal of Sustainable Design. 2016;3(1):20-37.
48. Grima JN, Evans KE. Auxetic behavior from rotating squares. 2000.
49. Grima JN, Gatt R. Perforated sheets exhibiting negative Poisson's ratios. Advanced engineering materials. 2010;12(6):460-4.
50. Lakes R. Deformation mechanisms in negative Poisson's ratio materials: structural aspects. Journal of materials science. 1991;26(9):2287-92.
51. Alderson A, Evans K. Modelling concurrent deformation mechanisms in auxetic microporous polymers. Journal of materials science. 1997;32(11):2797-809.
52. Hook P. Auxetic mechanisms, structures & materials: Ph. D. thesis, School of Engineering and Computer Science, University of Exeter; 2003.
53. Grima JN, Ravirala N, Galea R, Ellul B, Attard D, Gatt R, et al. Modelling and testing of a foldable macrostructure exhibiting auxetic behaviour. physica status solidi (b). 2011;248(1):117-22.
54. Gibson LJ, Ashby MF, Schajer G, Robertson C. The mechanics of two-dimensional cellular materials. Proceedings of the Royal Society of London A Mathematical and Physical Sciences. 1982;382(1782):25-42.
55. Masters I, Evans K. Models for the elastic deformation of honeycombs. Composite structures. 1996;35(4):403-22.
56. Carneiro VH, Meireles J, Puga H. Auxetic materials—A review. Materials Science-Poland. 2013;31(4):561-71.
57. Larsen UD, Signund O, Bouwsta S. Design and fabrication of compliant micromechanisms and structures with negative Poisson's ratio. Journal of microelectromechanical systems. 1997;6(2):99-106.
58. Grima JN, Gatt R, Alderson A, Evans K. On the potential of connected stars as auxetic systems. Molecular Simulation. 2005;31(13):925-35.
59. Smith CW, Grima J, Evans K. A novel mechanism for generating auxetic behaviour in reticulated foams: missing rib foam model. Acta materialia. 2000;48(17):4349-56.
60. Gaspar N, Ren X, Smith CW, Grima J, Evans KE. Novel honeycombs with auxetic behaviour. Acta Materialia. 2005;53(8):2439-45.
61. Dolla WJS, Fricke BA, Becker BR. Structural and drug diffusion models of conventional and auxetic drug-eluting stents. 2007.
62. Saxena KK, Das R, Calius EP. Three decades of auxetics research− materials with negative Poisson's ratio: a review. Advanced Engineering Materials. 2016;18(11):1847-70.

63. Grima JN, Alderson A, Evans KE. Negative Poisson’s ratios from rotating rectangles. Comput Methods Sci Technol. 2004;10(2):137-45.
64. Grima JN, Farrugia PS, Gatt R, Attard D. On the auxetic properties of rotating rhombi and parallelograms: A preliminary investigation. physica status solidi (b). 2008;245(3):521-9.
65. Grima JN, Evans KE. Auxetic behavior from rotating triangles. Journal of materials science. 2006;41(10):3193-6.
66. Grima JN, Gatt R, Ellul B, Chetcuti E. Auxetic behaviour in non-crystalline materials having star or triangular shaped perforations. Journal of Non-Crystalline Solids. 2010;356(37-40):1980-7.
67. Grima JN, Winczewski S, Mizzi L, Grech MC, Cauchi R, Gatt R, et al. Tailoring graphene to achieve negative Poisson's ratio properties. Advanced materials. 2015;27(8):1455-9.
68. Prall D, Lakes R. Properties of a chiral honeycomb with a Poisson's ratio of—1. International Journal of Mechanical Sciences. 1997;39(3):305-14.
69. Grima JN, Gatt R, Farrugia PS. On the properties of auxetic meta‐tetrachiral structures. physica status solidi (b). 2008;245(3):511-20.
70. Caddock B, Evans K. Microporous materials with negative Poisson's ratios. I. Microstructure and mechanical properties. Journal of Physics D: Applied Physics. 1989;22(12):1877.
71. He C, Liu P, McMullan PJ, Griffin AC. Toward molecular auxetics: Main chain liquid crystalline polymers consisting of laterally attached para‐quaterphenyls. physica status solidi (b). 2005;242(3):576-84.
72. Evans KE, Nkansah M, Hutchinson I. Auxetic foams: modelling negative Poisson's ratios. Acta metallurgica et materialia. 1994;42(4):1289-94.
73. Lakes R, Witt R. Making and characterizing negative Poisson's ratio materials. International Journal of Mechanical Engineering Education. 2002;30(1):50-8.
74. Rad MS, Prawoto Y, Ahmad Z. Analytical solution and finite element approach to the 3D re-entrant structures of auxetic materials. Mechanics of Materials. 2014;74:76-87.
75. Hengsbach S, Lantada AD. Direct laser writing of auxetic structures: present capabilities and challenges. Smart materials and structures. 2014;23(8):085033.
76. Ma Z-d. Three-dimensional auxetic structures and applications thereof. Google Patents; 2011.
77. Yang L, Harrysson O, West H, Cormier D. Mechanical properties of 3D re-entrant honeycomb auxetic structures realized via additive manufacturing. International Journal of Solids and Structures. 2015;69:475-90.
78. Wang Y, Wang L, Ma Z-d, Wang T. Parametric analysis of a cylindrical negative Poisson’s ratio structure. Smart Materials and Structures. 2016;25(3):035038.
79. Alderson A, Evans K. Rotation and dilation deformation mechanisms for auxetic behaviour in the α-cristobalite tetrahedral framework structure. Physics and Chemistry of Minerals. 2001;28(10):711-8.
80. Ha CS, Plesha ME, Lakes RS. Chiral three-dimensional lattices with tunable Poisson’s ratio. Smart Materials and Structures. 2016;25(5):054005.
81. Ha CS, Plesha ME, Lakes RS. Chiral three‐dimensional isotropic lattices with negative Poisson's ratio. physica status solidi (b). 2016;253(7):1243-51.

82. Huang HH, Wong BL, Chou YC. Design and properties of 3D-printed chiral auxetic metamaterials by reconfigurable connections. physica status solidi (b). 2016;253(8):1557-64.
83. Bouaziz O, Masse J, Allain S, Orgéas L, Latil P. Compression of crumpled aluminum thin foils and comparison with other cellular materials. Materials Science and Engineering: A. 2013;570:1-7.
84. Gao Y, Liu S, Wu M, Chen X, Studd R. Manufacture and Evaluation of Auxetic Yarns and Woven Fabrics. physica status solidi (b). 2020;257(10).
85. Jiang N, Hu H. A study of tubular braided structure with negative Poisson's ratio behavior. Textile Research Journal. 2018;88(24):2810-24.
86. Ng WS, Hu H. Woven Fabrics Made of Auxetic Plied Yarns. Polymers. 2018;10(2):226.
87. Yang W, Li Z-M, Shi W, Xie B-H, Yang M-B. Review on auxetic materials. Journal of materials science. 2004;39(10):3269-79.
88. Zhang W, Ma Z, Hu P. Mechanical properties of a cellular vehicle body structure with negative Poisson's ratio and enhanced strength. Journal of Reinforced Plastics and Composites. 2014;33(4):342-9.
89. Alderson A, Rasburn J, Evans K, Grima J. Auxetic polymeric filters display enhanced de-fouling and pressure compensation properties. Membrane Technology. 2001;2001(137):6-8.
90. Lakes R, Elms K. Indentability of conventional and negative Poisson's ratio foams. Journal of Composite Materials. 1993;27(12):1193-202.
91. Mohsenizadeh S, Alipour R, Rad MS, Nejad AF, Ahmad Z. Crashworthiness assessment of auxetic foam-filled tube under quasi-static axial loading. Materials & Design. 2015;88:258-68.
92. Imbalzano G, Tran P, Ngo TD, Lee PV. A numerical study of auxetic composite panels under blast loadings. Composite Structures. 2016;135:339-52.
93. Scarpa F, Bullough W, Lumley P. Trends in acoustic properties of iron particle seeded auxetic polyurethane foam. Proceedings of the Institution of Mechanical Engineers, Part C: Journal of Mechanical Engineering Science. 2004;218(2):241-4.
94. Yang S, Qi C, Wang D, Gao R, Hu H, Shu J. A comparative study of ballistic resistance of sandwich panels with aluminum foam and auxetic honeycomb cores. Advances in Mechanical Engineering. 2013;5:589216.
95. Hook P. Uses of auxetic fibres. USA Patent US. 2011;8:B2.
96. Darja R, Tatjana R, Alenka P-Č. Auxetic textiles. Acta Chimica Slovenica. 2014;60(4):715-23.
97. Zhou L, Zeng J, Jiang L, Hu H. Low-velocity impact properties of 3D auxetic textile composite. Journal of materials science. 2018;53(5):3899-914.
98. Alderson A, Rasburn J, Evans K. Mass transport properties of auxetic (negative Poisson's ratio) foams. physica status solidi (b). 2007;244(3):817-27.
99. Bezazi A, Boukharouba W, Scarpa F. Mechanical properties of auxetic carbon/epoxy composites: static and cyclic fatigue behaviour. physica status solidi (b). 2009;246(9):2102-10.
100. Donoghue J, Alderson K, Evans K. The fracture toughness of composite laminates with a negative Poisson's ratio. physica status solidi (b). 2009;246(9):2011-7.
101. Bhullar S, Wegner J, Mioduchowski A. Strain energy distribution in an auxetic plate with a crack. Journal of Engineering and Technology Research. 2010;2(7):118-26.

102. Love A. H. A treatise on the mathematical theory of elasticity. Cambridge: Cambridge University Press. 1944;1:952.
103. Garber A. Pyrolytic materials for thermal protection systems. Aerospace Eng. 1963;22:126-37.
104. Veronda D, Westmann R. Mechanical characterization of skin—finite deformations. Journal of biomechanics. 1970;3(1):111-24.
105. Gunton D, Saunders G. The Young's modulus and Poisson's ratio of arsenic, antimony and bismuth. Journal of Materials Science. 1972;7(9):1061-8.
106. Li Y. The anisotropic behavior of Poisson's ratio, Young's modulus, and shear modulus in hexagonal materials. physica status solidi (a). 1976;38(1):171-5.
107. Williams J, Lewis J. Properties and an anisotropic model of cancellous bone from the proximal tibial epiphysis. 1982.
108. Nur A, Simmons G. The effect of saturation on velocity in low porosity rocks. Earth and planetary science letters. 1969;7(2):183-93.
109. Homand-Etienne F, Houpert R, editors. Thermally induced microcracking in granites: characterization and analysis. International Journal of Rock Mechanics and Mining Sciences & Geomechanics Abstracts; 1989: Elsevier.
110. Critchley R, Corni I, Wharton JA, Walsh FC, Wood RJ, Stokes KR. A review of the manufacture, mechanical properties and potential applications of auxetic foams. physica status solidi (b). 2013;250(10):1963-82.
111. Lee T, Lakes R. Anisotropic polyurethane foam with Poisson'sratio greater than 1. Journal of materials science. 1997;32(9):2397-401.
112. Evans K, Caddock B. Microporous materials with negative Poisson's ratios. II. Mechanisms and interpretation. Journal of Physics D: Applied Physics. 1989;22(12):1883.
113. Alderson K, Evans K. The fabrication of microporous polyethylene having a negative Poisson's ratio. Polymer. 1992;33(20):4435-8.
114. Alderson K, Evans K. Strain-dependent behaviour of microporous polyethylene with a negative Poisson's ratio. Journal of materials science. 1993;28(15):4092-8.
115. Neale P, Alderson K, Pickles A, Evans K. Negative Poisson's ratio of microporous polyethylene in compression. Journal of materials science letters. 1993;12(19):1529-32.
116. Alderson K, Alderson A, Evans K. The interpretation of the strain-dependent Poisson's ratio in auxetic polyethylene. The Journal of Strain Analysis for Engineering Design. 1997;32(3):201-12.
117. Evans K, Alderson K. The static and dynamic moduli of auxetic microporous polyethylene. Journal of materials science letters. 1992;11(24):1721-4.
118. Pickles A, Webber R, Alderson K, Neale P, Evans K. The effect of the processing parameters on the fabrication of auxetic polyethylene. Journal of materials science. 1995;30(16):4059-68.
119. Alderson K, Kettle A, Neale P, Pickles A, Evans K. The effect of the processing parameters on the fabrication of auxetic polyethylene. Journal of materials science. 1995;30(16):4069-75.
120. Alderson K, Alderson A, Webber R, Evans K. Evidence for uniaxial drawing in the fibrillated microstructure of auxetic microporous polymers. Journal of materials science letters. 1998;17(16):1415-9.
121. Pickles A, Alderson K, Evans K. The effects of powder morphology on the processing of auxetic polypropylene (PP of negative Poisson's ratio). Polymer Engineering & Science. 1996;36(5):636-42.

122. Simkins V, Ravirala N, Davies P, Alderson A, Alderson K. An experimental study of thermal post-production processing of auxetic polypropylene fibres. physica status solidi (b). 2008;245(3):598-605.
123. Wang Y-C, Lakes R. Analytical parametric analysis of the contact problem of human buttocks and negative Poisson's ratio foam cushions. International Journal of Solids and Structures. 2002;39(18):4825-38.
124. Chan N, Evans K. Fabrication methods for auxetic foams. Journal of Materials Science. 1997;32(22):5945-53.
125. Grima JN, Attard D, Gatt R, Cassar RN. A novel process for the manufacture of auxetic foams and for their re-conversion to conventional form. Advanced Engineering Materials. 2009;11(7):533-5.
126. Bianchi M, Scarpa F, Banse M, Smith C. Novel generation of auxetic open cell foams for curved and arbitrary shapes. Acta Materialia. 2011;59(2):686-91.
127. Bianchi M, Frontoni S, Scarpa F, Smith C. Density change during the manufacturing process of PU–PE open cell auxetic foams. physica status solidi (b). 2011;248(1):30-8.
128. Duncan O, Shepherd T, Moroney C, Foster L, Venkatraman PD, Winwood K, et al. Review of auxetic materials for sports applications: Expanding options in comfort and protection. Applied Sciences. 2018;8(6):941.
129. Duncan O, Foster L, Senior T, Allen T, Alderson A. A comparison of novel and conventional fabrication methods for auxetic foams for sports safety applications. Procedia engineering. 2016;147:384-9.
130. Evans K, Ainsworth K. International Patent Publication no. WO91/01210. 1991.
131. Alderson K, Alderson A, Davies P, Smart G, Ravirala N, Simkins G. The effect of processing parameters on the mechanical properties of auxetic polymeric fibers. Journal of materials science. 2007;42(19):7991-8000.
132. Alderson K, Nazaré S, Alderson A. Large-scale extrusion of auxetic polypropylene fibre. physica status solidi (b). 2016;253(7):1279-87.
133. Ravirala N, Alderson A, Alderson K, Davies P. Expanding the range of auxetic polymeric products using a novel melt-spinning route. physica status solidi (b). 2005;242(3):653-64.
134. Hook P, Evans K. How do auxetic materials work. 2006.
135. Miller W, Ren Z, Smith C, Evans K. A negative Poisson's ratio carbon fibre composite using a negative Poisson's ratio yarn reinforcement. Composites Science and Technology. 2012;72(7):761-6.
136. Wright JR, Burns MK, James E, Sloan MR, Evans KE. On the design and characterisation of low-stiffness auxetic yarns and fabrics. Textile Research Journal. 2012;82(7):645-54.
137. Zhou M, Du ZQ, editors. Effects of structural parameters and performance on Poisson's ratio of auxetic yarn. Advanced Materials Research; 2013: Trans Tech Publ.
138. Bhattacharya S, Zhang G, Ghita O, Evans KE. The variation in Poisson's ratio caused by interactions between core and wrap in helical composite auxetic yarns. Composites science and technology. 2014;102:87-93.
139. Du Z, Zhou M, He L, Liu H. Study on negative Poisson's ratio of auxetic yarn under tension: Part 2–Experimental verification. Textile Research Journal. 2015;85(7):768-74.

140. Sibal A, Rawal A. Design strategy for auxetic dual helix yarn systems. Materials Letters. 2015;161:740-2.
141. Zhang G, Ghita O, Lin C, Evans KE. Varying the performance of helical auxetic yarns by altering component properties and geometry. Composite Structures. 2016;140:369-77.
142. Zhang G, Ghita OR, Evans KE. Dynamic thermo-mechanical and impact properties of helical auxetic yarns. Composites Part B: Engineering. 2016;99:494-505.
143. Zhang G, Ghita OR, Lin C, Evans KE. Large-scale manufacturing of helical auxetic yarns using a novel semi-coextrusion process. Textile Research Journal. 2018;88(22):2590-601.
144. Chen J, Du Z. Structural design and performance characterization of stable helical auxetic yarns based on the hollow-spindle covering system. Textile Research Journal. 2020;90(3-4):271-81.
145. Liu S, Pan X, Zheng D, Liu G, Du Z. The manufacture and characterization of auxetic, self-curling, and self-folding woven fabrics by helical auxetic yarns. Journal of Industrial Textiles. 2020;50(1):3-12.
146. McAfee J, Faisal NH. Parametric sensitivity analysis to maximise auxetic effect of polymeric fibre based helical yarn. Composite structures. 2017;162:1-12.
147. Du Z, Zhou M, Liu H, He L. Study on negative Poisson's ratio of auxetic yarn under tension: Part 1–Theoretical analysis. Textile Research Journal. 2015;85(5):487-98.
148. Ng WS, Hu H. Tensile and deformation behavior of auxetic plied yarns. physica status solidi (b). 2017;254(12):1600790.
149. Lim TC. Semi‐auxetic yarns. physica status solidi (b). 2014;251(2):273-80.
150. Jiang N, Hu H. Auxetic Yarn Made with Circular Braiding Technology. physica status solidi (b). 2019;256(1):1800168.
151. Monika V, Petra V. Auxetic woven fabrics—pores' parameters observation. Journal of Donghua University (English Edition). 2013(5):19.
152. Liu S, Pan X, Zheng D, Liu G, Du Z. The manufacture and characterization of auxetic, self-curling, and self-folding woven fabrics by helical auxetic yarns. Journal of Industrial Textiles. 2018:1528083718817559.
153. Nazir MU, Shaker K, Hussain R, Nawab Y. Performance of novel auxetic woven fabrics produced using Helical Auxetic Yarn. Materials Research Express. 2019;6(8):085703.
154. Lolaki A, Shanbeh M. Variation of Poisson's ratio of fabrics woven with helical composite auxetic weft yarns in relation to fabric structural parameters. Journal of Industrial Textiles. 2020;50(2):149-69.
155. Chen J, Du Z, Li T. Structural design and characterization of highly elastic woven fabric containing helical auxetic yarns. Textile Research Journal. 2020;90(7-8):809-23.
156. Ali M, Zeeshan M, Qadir MB, Riaz R, Ahmad S, Nawab Y, et al. Development and mechanical characterization of weave design based 2d woven auxetic fabrics for protective textiles. Fibers and Polymers. 2018;19(11):2431-8.
157. Ali M, Zeeshan M, Ahmed S, Qadir B, Nawab Y, Anjum AS, et al. Development and comfort characterization of 2d-woven auxetic fabric for wearable and medical textile applications. Clothing and Textiles Research Journal. 2018;36(3):199-214.
158. Zulifqar A, Hua T, Hu H. Development of uni-stretch woven fabrics with zero and negative Poisson's ratio. Textile Research Journal. 2018;88(18):2076-92.

159. Zulifqar A, Hu H. Development of bi-stretch auxetic woven fabrics based on re-entrant hexagonal geometry. physica status solidi (b). 2019;256(1):1800172.
160. Kamrul H, Zulifqar A, Hu H. Deformation behavior of auxetic woven fabric based on re-entrant hexagonal geometry in different tensile directions. Textile Research Journal. 2020;90(3-4):410-21.
161. Cao H, Zulifqar A, Hua T, Hu H. Bi-stretch auxetic woven fabrics based on foldable geometry. Textile Research Journal. 2019;89(13):2694-712.
162. Zulifqar A, Hu H. Geometrical analysis of bi-stretch auxetic woven fabric based on re-entrant hexagonal geometry. Textile Research Journal. 2019;89(21-22):4476-90.
163. Liu Y, Hu H, Lam JK, Liu S. Negative Poisson's ratio weft-knitted fabrics. Textile Research Journal. 2010;80(9):856-63.
164. Ugbolue SC, Kim YK, Warner SB, Fan Q, Yang C-L, Kyzymchuk O, et al. The formation and performance of auxetic textiles. Part I: theoretical and technical considerations. the Journal of the Textile Institute. 2010;101(7):660-7.
165. Alderson K, Alderson A, Anand S, Simkins V, Nazare S, Ravirala N. Auxetic warp knit textile structures. physica status solidi (b). 2012;249(7):1322-9.
166. Ma P, Chang Y, Jiang G. Design and fabrication of auxetic warp-knitted structures with a rotational hexagonal loop. Textile Research Journal. 2016;86(20):2151-7.
167. Ugbolue SC, Kim YK, Warner SB, Fan Q, Yang CL, Kyzymchuk O, et al. The formation and performance of auxetic textiles. Part II: geometry and structural properties. The Journal of the Textile Institute. 2011;102(5):424-33.
168. Verma P, Shofner ML, Lin A, Wagner KB, Griffin AC. Inducing out-of-plane auxetic behavior in needle-punched nonwovens. physica status solidi (b). 2015;252(7):1455-64.
169. Verma P, Shofner ML, Lin A, Wagner KB, Griffin AC. Induction of auxetic response in needle-punched nonwovens: Effects of temperature, pressure, and time. physica status solidi (b). 2016;253(7):1270-8.
170. Verma P, Smith CL, Griffin AC, Shofner ML. Wool nonwovens as candidates for commodity auxetic materials. Engineering Research Express. 2020;2(4):045034.
171. Bhullar SK, Ko J, Cho Y, Jun MB. Fabrication and characterization of nonwoven auxetic polymer stent. Polymer-Plastics Technology and Engineering. 2015;54(15):1553-9.
172. Dobnik Dubrovski P, Novak N, Borovinšek M, Vesenjak M, Ren Z. In-plane behavior of auxetic non-woven fabric based on rotating square unit geometry under tensile load. Polymers. 2019;11(6):1040.
173. Ahmed HI, Umair M, Nawab Y, Hamdani STA. Development of 3D auxetic structures using para-aramid and ultra-high molecular weight polyethylene yarns. The Journal of The Textile Institute. 2020:1-11.
174. Liu Y, Hu H. Compression property and air permeability of weft-knitted spacer fabrics. The Journal of the Textile Institute. 2011;102(4):366-72.
175. Liu Y, Hu H, Long H, Zhao L. Impact compressive behavior of warp-knitted spacer fabrics for protective applications. Textile Research Journal. 2012;82(8):773-88.
176. Liu Y, Hu H, Zhao L, Long H. Compression behavior of warp-knitted spacer fabrics for cushioning applications. Textile Research Journal. 2012;82(1):11-20.

177. Guo X, Long H, Zhao L. Investigation on the impact and compression-after-impact properties of warp-knitted spacer fabrics. Textile Research Journal. 2013;83(9):904-16.
178. Wang Z, Hu H, Xiao X. Deformation behaviors of three-dimensional auxetic spacer fabrics. Textile research journal. 2014;84(13):1361-72.
179. Wang Z, Hu H. A finite element analysis of an auxetic warp-knitted spacer fabric structure. Textile Research Journal. 2015;85(4):404-15.
180. Chen F, Hu H, Liu Y. Development of weft-knitted spacer fabrics with negative stiffness effect in a special range of compression displacement. Textile Research Journal. 2015;85(16):1720-31.
181. Chang Y, Ma P, Jiang G. Energy absorption property of warp-knitted spacer fabrics with negative Possion's ratio under low velocity impact. Composite Structures. 2017;182:471-7.
182. Rawal A, Kumar V, Saraswat H, Weerasinghe D, Wild K, Hietel D, et al. Creating three-dimensional (3D) fiber networks with out-of-plane auxetic behavior over large deformations. Journal of Materials Science. 2017;52(5):2534-48.
183. Wang Z, Hu H. Tensile and forming properties of auxetic warp-knitted spacer fabrics. Textile Research Journal. 2017;87(16):1925-37.
184. Chang Y, Ma P. Fabrication and property of auxetic warp-knitted spacer structures with mesh. Textile Research Journal. 2018;88(19):2206-13.
185. Chang Y, Ma P. Energy absorption and Poisson's ratio of warp-knitted spacer fabrics under uniaxial tension. Textile Research Journal. 2019;89(6):903-13.
186. Potluri P. Braiding. Wiley encyclopedia of composites. 2011:1-9.
187. Shen Y. Modeling of Tensile Properties of Woven Fabrics and Auxetic Braided Structures by Multi-Scale Finite Element Method 2013.
188. Shen Y, Adanur S. Mechanical analysis of the auxetic behavior of novel braided tubular structures by the finite element method. Textile Research Journal. 2019;89(23-24):5187-97.
189. Alderson K, Simkins V, Coenen V, Davies P, Alderson A, Evans K. How to make auxetic fibre reinforced composites. physica status solidi (b). 2005;242(3):509-18.
190. Herakovich CT. Composite laminates with negative through-the-thickness Poisson's ratios. Journal of Composite Materials. 1984;18(5):447-55.
191. Zhou L, Jiang L, Hu H. Auxetic composites made of 3D textile structure and polyurethane foam. physica status solidi (b). 2016;253(7):1331-41.
192. Ge Z, Hu H, Liu Y. A finite element analysis of a 3D auxetic textile structure for composite reinforcement. Smart materials and structures. 2013;22(8):084005.
193. Ge Z, Hu H. A theoretical analysis of deformation behavior of an innovative 3D auxetic textile structure. The Journal of The Textile Institute. 2015;106(1):101-9.
194. Liaqat M, Samad HA, Hamdani STA, Nawab Y. The development of novel auxetic woven structure for impact applications. The Journal of The Textile Institute. 2017;108(7):1264-70.
195. Yang S, Chalivendra V, Kim Y, editors. Impact behaviour of auxetic Kevlar®/epoxy composites. IOP Conference Series: Materials Science and Engineering; 2017: IOP Publishing.
196. Khan MI, Akram J, Umair M, Hamdani ST, Shaker K, Nawab Y, et al. Development of composites, reinforced by novel 3D woven orthogonal fabrics with enhanced auxeticity. Journal of Industrial Textiles. 2019;49(5):676-90.

197. Grimmelsmann N, Meissner H, Ehrmann A, editors. 3D printed auxetic forms on knitted fabrics for adjustable permeability and mechanical properties. IOP Conference Series: Materials Science and Engineering; 2016: IOP Publishing.
198. Steffens F, Oliveira FR, Mota C, Fangueiro R. High-performance composite with negative Poisson's ratio. Journal of Materials Research. 2017;32(18):3477-84.
199. Moshtaghian Z, Hasani H, Zarrebini M, Pourheidar Shirazi M. Development and auxetic characterization of 3D composites produced with newly-designed multi-cell flat-knitted spacer fabrics. Journal of Industrial Textiles. 2020:1528083720971696.
200. Xu W, Sun Y, Lin H, Wei C, Ma P, Xia F. Preparation of soft composite reinforced with auxetic warp-knitted spacer fabric for stab resistance. Textile Research Journal. 2020;90(3-4):323-32.
201. Steffens F, Oliveira FR, Fangueiro R. Energy absorption from composite reinforced with high performance auxetic textile structure. Journal of Composite Materials. 2021;55(7):1003-13.
202. Subramani P, Rana S, Oliveira DV, Fangueiro R, Xavier J. Development of novel auxetic structures based on braided composites. Materials & Design. 2014;61:286-95.
203. Sharma S, Kushawah D, Rawal A. Designing nonwoven auxetic metamaterials with spatially textured functionalities. Materials Letters. 2019;241:214-8.
204. Kwietniewski M, Miedzińska D, editors. Numerical analysis of Helical Auxetic Yarn elastomeric core tension. AIP Conference Proceedings; 2019: AIP Publishing LLC.
205. Zeng J, Cao H, Hu H. Finite element simulation of an auxetic plied yarn structure. Textile Research Journal. 2019;89(16):3394-400.
206. Liu S, Du Z, Liu G, Pan X, Li T. Study on the tensile behavior of helical auxetic yarns by modeling and mechanical analysis. The Journal of The Textile Institute. 2020:1-7.
207. Zeng J, Hu H. A theoretical analysis of deformation behavior of auxetic plied yarn structure. Smart Materials and Structures. 2018;27(7):075003.
208. Zhang G, Ghita OR, Lin C, Evans KE. Large-scale manufacturing of helical auxetic yarns using a novel semi-coextrusion process. Textile Research Journal. 2017:0040517517725125.
209. Ge Z, Hu H, Liu Y. Numerical analysis of deformation behavior of a 3D textile structure with negative Poisson's ratio under compression. Textile Research Journal. 2015;85(5):548-57.
210. Luan K, West A, DenHartog E, McCord M. Auxetic deformation of the weft-knitted Miura-ori fold. Textile Research Journal. 2020;90(5-6):617-30.
211. Kamrul H, Zulifqar A, Yang Y, Zhao S, Zhang M, Hu H. Geometrical analysis of auxetic woven fabrics based on foldable geometry. Textile Research Journal. 2021:00405175211008663.
212. ASTM D. 3822-07: Standard Test Method for Tensile Properties of Single Textile Fibers. ASTM International: West Conshohocken, PA. 2007.
213. Clark SD, Grant-Muller S, Chen H. Cleaning of matched license plate data. Transportation research record. 2002;1804(1):1-7.
214. Zahid B, Chen X. Development of a helmet test rig for continuously textile reinforced riot helmets. Int J Text Sci. 2013;2(1):12-20.
215. Srinivas K. Abaqus – Tips and Tricks Vol 1: Advanses; 2017 [Available from: https://advanses.com/abaqus-tips-and-tricks-vol-1/.

216. Liu S, Du Z, Chen X, editors. A finite element analysis of auxetic behavior of complex yarns with negative Poisson′ s ratio. Proceedings of the 8th World Conference on 3D Fabrics and Their Applications; 2018.
217. Sadowski AJ, Rotter JM. Solid or shell finite elements to model thick cylindrical tubes and shells under global bending. International Journal of Mechanical Sciences. 2013;74:143-53.
218. Kim S, Kim H. A new metric of absolute percentage error for intermittent demand forecasts. International Journal of Forecasting. 2016;32(3):669-79.
219. Mouritz A. Fibre–polymer composites for aerospace structures and engines. Introduction to Aerospace Materials, 1st ed; Woodhead Publishing Ltd: Cambridge, UK. 2012:338-93.

Appendix 1

Calculation of helical angle of auxetic yarns

Due to the limitations of the spinning machine, the twisting speed can only be set as 500 rpm by every intervals and the delivery speed is set as 2.5 m/min. Then, the initial helical angle of the yarn can be calculated based on the mechanical model of Du et al. [147] which has been presented in the literature review. The results of table are shown as follow:

Table A-1: Calculated angle based on the twisting speed and delivery speed

	1000 rpm*	**1500 rpm**	**2000 rpm**	**2500 rpm**	**3000 rpm**	**3500 rpm**	**4000 rpm**	**4500 rpm**	**5000 rpm**
2.5 m/min	43.22	54.65	61.99	66.94	70.47	73.09	75.1	76.7	77.99
5 m/min	25.17	35.18	43.22	49.59	54.65	58.7	61.99	64.69	66.94
7.5 m/min	17.39	25.17	32.07	38.07	43.22	47.63	51.41	54.65	57.44
10 m/min	13.22	19.41	25.17	30.43	35.18	39.43	43.22	46.59	49.59
12.5 m/min	10.64	15.75	20.6	25.17	29.42	33.34	36.94	40.22	43.22
15 m/min	8.9	13.22	17.39	21.38	25.17	28.73	32.07	35.18	38.07
17.5 m/min	7.65	11.39	15.03	18.55	21.94	25.17	28.24	31.14	33.87
20 m/min	6.7	9.99	13.22	16.37	19.41	22.35	25.17	27.86	30.43

* rpm: rounds per minute